UNITED STATES ENVIRONMENTAL PROTECTION AGENCY
EPA New England
Office of Environmental Measurement & Evaluation
11 Technology Drive, North Chelmsford, MA 01863

MEMORANDUM

DATE: September 17, 2007 RFA No. 07309*

SUBJ: Approval of Hyperspectral Imagery QAPP

FROM: Arthur E. Clark, Chemist,
Quality Assurance Office (EQA)

TO: Al Basile, EPA Water Quality Branch, OEP (CWQ)

On August 28, 2007, we received the following quality assurance project plan:

Using Moored Arrays and Hyperspectral Aerial Imagery to Develop Nutrient Criteria for New Hampshire's Estuaries, by New Hampshire Estuaries Project Marine Program, University of New Hampshire, August 24, 2007.

I have reviewed the QAPP and found that it includes the necessary elements provided in our Agency guidance document, *EPA Requirements for Quality Assurance Project Plans* (EPA QA/R-5, March, 2001). I have signed a copy of the title page; it is enclosed. Please sign it and forward it to Phil Trowbridge of the NHEP. When everyone has signed it, please send me a photocopy for my files.

This approval covers the 2007 sampling season

- If minor changes occur, our office should be informed by email or letter, but approvals of such changes are not required.
- If major changes occur, a revised QAPP should be submitted for review and approval.

If you have any comments or questions, please contact me at any time. I may be reached by phone at (617)918-8374 and by fax at (617)918-8274.

* FOR QUALITY ASSURANCE TRACKING PURPOSES, PLEASE ADD THE FOLLOWING TRACKING NUMBER TO ALL CORRESPONDENCE RELATING TO THIS DOCUMENT: EPA RFA # 07309.

UNITED STATES ENVIRONMENTAL PROTECTION AGENCY
EPA New England
Office of Environmental Measurement & Evaluation
11 Technology Drive, North Chelmsford, MA 01863

MEMORANDUM

DATE: July 14, 2008 RFA No. 07309*

SUBJ: Approval of Hyperspectral Imagery QAPP Addendum

FROM: Arthur E. Clark, Chemist,
Quality Assurance Office (EQA)

TO: Al Basile, EPA Water Quality Branch, OEP (CWQ)

On September 17, 2007, we approved the following quality assurance project plan:

> *Using Moored Arrays and Hyperspectral Aerial Imagery to Develop Nutrient Criteria for New Hampshire's Estuaries,* by New Hampshire Estuaries Project Marine Program, University of New Hampshire, August 24, 2007.

On July 11, 2008, I received an addendum to the QAPP entitled *Hyperspectral Imageryfor Great Bay, NH,* July 11, 2008. It proposes to use the imagery already gathered to produce additional information. No new monitoring will occur. I find the addendum to be satisfactory.

If you have any comments or questions, please contact me at any time. I may be reached by phone at (617)918-8374 and by fax at (617)918-8274.
* FOR QUALITY ASSURANCE TRACKING PURPOSES, PLEASE ADD THE FOLLOWING TRACKING NUMBER TO ALL CORRESPONDENCE RELATING TO THIS DOCUMENT: EPA RFA # 07309.

cc: N. Conlon
M. Lataille
V. Perelli (DES)
G. Sotolongo
P. Trowbridge (NHEP)

USING MOORED ARRAYS AND HYPERSPECTRAL AERIAL IMAGERY TO DEVELOP NUTRIENT CRITERIA FOR NEW HAMPSHIRE'S ESTUARIES
Quality Assurance Project Plan

Prepared by

New Hampshire Estuaries Project
Marine Program
University of New Hampshire
Durham, NH 03824

August 24, 2007

Ru Morrison Project Manager	Date	Jennifer Hunter NHEP Program Manager	Date
Tom Gregory UNH Research Staff	Date	Phil Trowbridge NHEP QA Officer	Date
AJ Markow SpecTIR Project Manager	Date	Al Basile EPA Project Officer	Date
Jeff Merriam Laboratory QA Officer	Date	Arthur Clark EPA QA Project Officer	Date

A2 – Table of Contents

List of Appendices

A. Quality Assurance Plan for UNH Water Quality Analysis Laboratory
B. Specifications of the SpecTIR VNIR Sensor
C. Ocean Optics Protocols for Satellite Ocean Color Sensor Validation, Revision 4, Volume IV
D. Ocean Optics Protocols for Satellite Ocean Color Sensor Validation, Revision 4, Volume V
E. Standard Operating Procedures for LI-1400 Datalogger PAR Measurements
F. Field data sheet for station visits

List of Tables

List of Figures

A3 – Distribution List

Table 1 shows the individuals and their respective agency affiliations that will receive the approved QAPP, the QAPP revisions, and any amendments.

Table 1. QAPP Distribution List

QAPP Recipient Name	Project Role	Organization	Telephone number and Email address
Ru Morrison	Project Manager	UNH	Ru.morrison@unh.edu (603) 862-4354
Tom Gregory	UNH Research Staff	UNH	Tom.gregory@unh.edu (603) 862-4397
Mike Novak	UNH Research Staff	UNH	mnovak@cisunix.unh.edu (603) 862-1348
William Bernard	SpecTIR Program Manager	SpecTIR	WBernard@SpecTIR.com (410) 820-5591
AJ Markow	SpecTIR Project Manager	SpecTIR	775.329.6660 775.722.7701 (cell) ajmarkow@SpecTIR.hostpilot.com
Oliver Weatherbee	SpecTIR Project Staff	SpecTIR	Oweatherbee@spectir.com (410) 820-5592
Chris Joyce	SpecTIR Project Staff	SpecTIR	(702) 526-1322 (cell)
Jeff Merriam	Laboratory QA Officer	UNH	Jeff.merriam@unh.edu (603) 862-2341
Jennifer Hunter	NHEP Program Manager	NHEP	Jennifer.hunter@unh.edu (603) 862-3948
Phil Trowbridge	NHEP QA Project Officer	NHEP/ NHDES	ptrowbridge@des.state.nh.us (603) 271-8872 (603) 340-5220 (cell)
Arthur Clark	EPA QA Officer	EPA	Clark.arthur@epa.gov (617) 918-8374
Al Basile	EPA Project Officer	EPA	Basile.alfred@epa.gov (617) 918-1599
Jonathan Pennock	Water Quality Field Sampling	UNH	Jonathan.pennock@unh.edu (603) 862-2921
Steve Jones	Water Quality Field Sampling	UNH	shj@cisunix.unh.edu (603) 862-5124
Colin Edwards	Water Quality Field Sampling	UNH	(603) 862-5124
Jeremy LeClair	Water Quality Field Sampling	UNH	Jeremy.LeClair@unh.edu (603) 862-5136
Chris Nash	Water Quality Field Sampling	NHDES	cnash@des.state.nh.us (603) 559-1509 (603) 568-6741 (cell)

A4 – Project/Task Organization

The project will be completed by a partnership of the University of New Hampshire and the New Hampshire Estuaries Project with the assistance of subcontractors using funds from the US Environmental Protection Agency.

The University of New Hampshire will manage the field data collection and data analysis tasks for this project. Specifically, Ru Morrison of the UNH Coastal Observing Center will be the overall Project Manager and will oversee all data collection and data analysis activities. The UNH Coastal Observing Center, an IOOS pilot project funded through the NOAA Coastal Services Center, has deployed an instrumented buoy in Great Bay in 2005, 2006, and 2007. This group also conducts periodic cruises throughout the Great Bay system with flow-through instrument array to document spatial heterogeneity of water quality parameters. Field crews from the UNH Marine Program will be used to collect water quality samples in the estuary.

The NHEP will provide administrative and technical oversight for this project. The NHEP is part of EPA's National Estuary Program, and is coordinating the nutrient criteria development process through its Technical Advisory Committee, with the NHEP Coastal Scientist leading the work. The NHEP's latest "State of the Estuaries" report highlighted declines in eelgrass beds and increases in nitrogen concentrations in Great Bay (available at www.nhep.unh.edu). Jennifer Hunter, the NHEP Director, will be responsible for the contractual and fiscal aspects of the project. Phil Trowbridge, the NHEP Coastal Scientist, will act as the QA Project Officer and will ensure the quality of the data products produced.

Chris Nash of the NH Department of Environmental Services (DES) will also assist with field sampling activities.

Several subcontractors will assist UNH in the data collection efforts. Each subcontractor is listed below.

Hyperspectral imagery for the project will be provided by SpecTIR. AJ Markow will be the Project Manager for SpecTIR with program oversight provided by Willam Bernard and assistance from Oliver Weatherbee and Chris Joyce. SpecTIR is a small, privately owned business with headquarters in Reno, NV and another facility in Easton, MD. The company was founded in 1993, and has advanced from the design and production of hyperspectral instruments, to full remote sensing collection and exploitation services. SpecTIR's staff consists of spectral scientists, project managers, field and data collection personnel, and a data exploitation group.

The Water Quality Analysis Laboratory at UNH will conduct laboratory analyses of water samples. Jeff Merriam will be the UNH-WQAL Laboratory QA Officer and will be responsible for reviewing and revising laboratory-related elements of the QAPP.

Funding for the project will be provided by EPA (Region I) through a competitive 104(b)(3) grant. The EPA Project Officer will be Al Basile, who will be responsible for managing contract deliverables. Art Clark will be the EPA Project QA Officer. The EPA QA Project Officer will provide technical reviews of the QAPP and any QAPP addenda throughout the duration of the study and will be responsible for approving this Quality Assurance Project Plan.

Figure 1. Project organizational chart

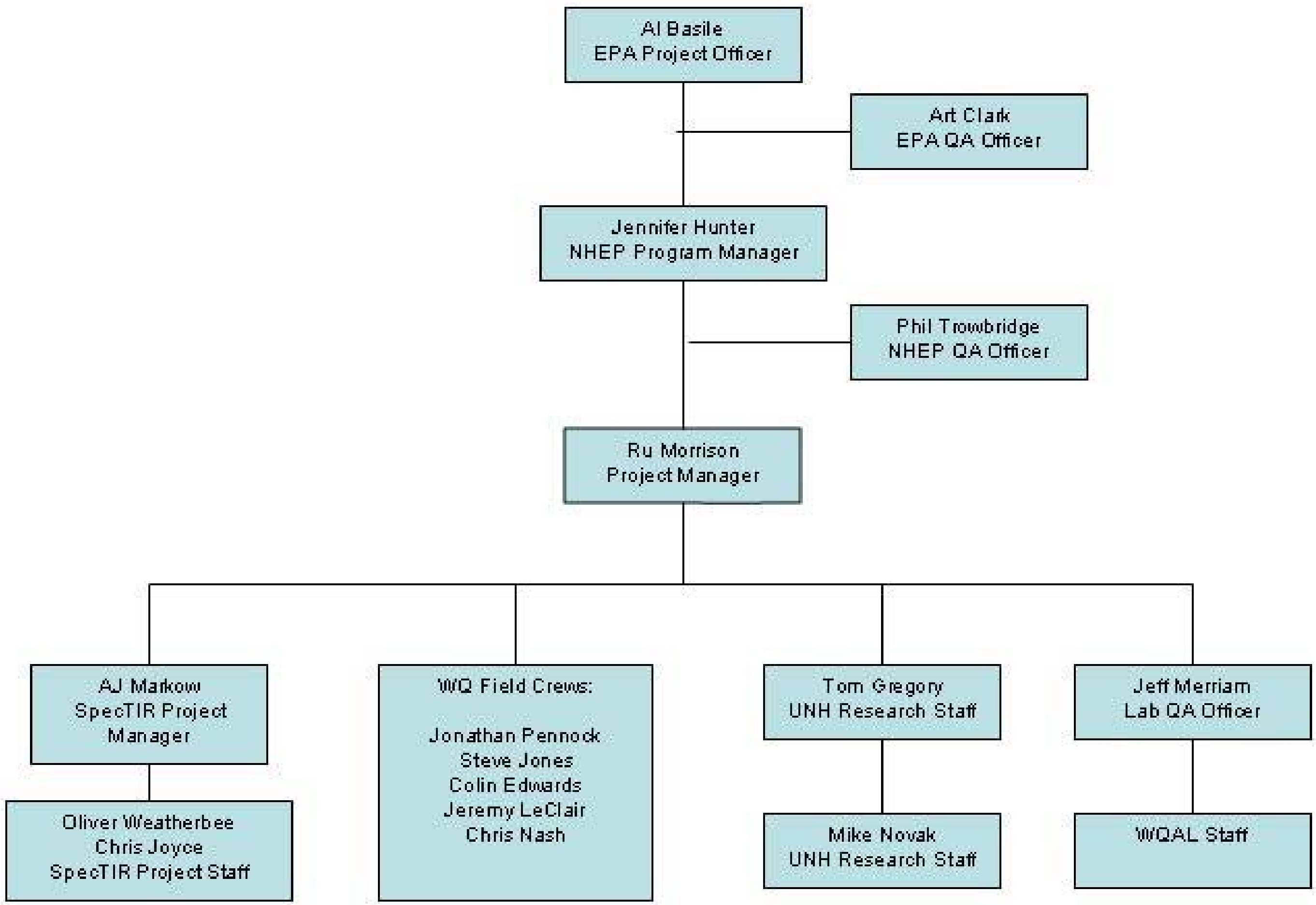

A5 – Problem Definition/Background

Problem Definition

Increasing nitrogen concentrations (Figure 2) and declining eelgrass beds in Great Bay (Figure 3) are clear indicators of impending problems for NH's estuaries (NHEP, 2006). The NH Department of Environmental Services (DES) is responsible for developing nutrient criteria for NH's estuaries. DES, in collaboration with the New Hampshire Estuaries Project (NHEP), began this process with the formation of a workgroup in 2005. The NHEP Coastal Scientist, a DES employee, is coordinating the work to undertake this process, with input from the workgroup. Information from the workgroup meetings is available at www.nhep.unh.edu/programs/nutrient.htm. This workgroup adopted eelgrass survival as the water quality target for nutrient criteria development for NH's estuaries.

Eelgrass survival is largely dependent on light availability. The NHEP Coastal Scientist has undertaken a review of the water clarity data for NH's estuaries. There are three important constituents in the optically complex coastal waters: phytoplankton, non-algal particulates, and colored dissolved organic matter (CDOM, IOCCG 2000). These constituents, by changing the Inherent Optical Properties (IOPS), affect water clarity or more precisely the magnitude of light attenuation, an Apparent Optical Property (AOP, see Mobley, 1994). Preliminary results indicate that CDOM is the major factor controlling water clarity. However, NHEP is not able to draw strong conclusions from these results because of significant datagaps and a large degree of spatial heterogeneity in NH's estuaries.

Therefore, the NHEP sought and received funding from the Environmental Protection Agency to support an instrumented buoy in Great Bay, which will be managed by the University of New Hampshire (UNH) Coastal Observing Center, to gather sufficient data to resolve uncertainties in relationships between parameters. Funding will also support coordinated collection of spatial data from aerial imagery and flow-through surveys to characterize spatial heterogeneity in water quality parameters. The goal of the research is to develop a scientifically defensible conceptual model of the relationships between water clarity and water quality parameters. The conceptual model will be the basis of nutrient criteria for NH's estuaries. A secondary goal of the project is to demonstrate the value of integrating buoy-based measurements with aerial imagery and flow-through surveys to map heterogeneity in water quality parameters within estuarine and near-coastal systems.

The expected outputs for this project are results of research which supports development of environmental results-based nutrient criteria for estuaries, specifically:

A) A single or multi-variate model between the light attenuation coefficient and concentrations of CDOM, turbidity/suspended solids, and chlorophyll-a for the Great Bay system which can be used to develop numeric nutrient criteria;

B) Maps of the distribution of CDOM, turbidity, and chlorophyll-a (and light attenuation using the model described above) on at least two different days for the entire Great Bay system; and

C) A calibrated light availability model for the Great Bay system.

All three of the outputs will support the expected outcome of developing numeric nutrient criteria for water clarity and, therefore, the protection of eelgrass beds. Eelgrass is a critical estuarine habitat. The protection of this habitat would benefit all users of the estuary: fish, waterfowl, and humans.

Presentations of the plans for the studies and the results of the research will be made to the NHEP Technical Advisory Committee, which is serving as the advisory group to DES on the process of developing nutrient criteria.

Progress toward achieving these outputs will be documented in one interim and one final report to EPA. The desired outcome will be achieved when NHEP makes a recommendation to the Water Quality Standards Advisory Committee for a water clarity based water quality criterion for NH's estuaries.

The project will be completed in the Great Bay estuarine system of NH and Maine. This area encompasses the Great Bay, Little Bay, Piscataqua River and some or all of the tidal portions of the Winnicut, Squamscott, Lamprey, Oyster, Bellamy, Cocheco and Salmon Falls Rivers (Figure 4). Approximately 40 square kilometers of estuarine waters will be part of the study area.

Figure 2: Dissolved inorganic nitrogen concentrations in Great Bay (NHEP, 2006)

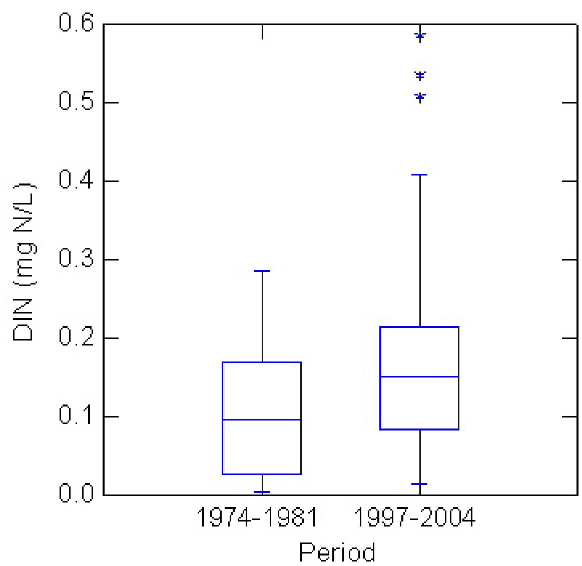

Figure 3: Eelgrass cover and biomass in Great Bay (NHEP, 2006)

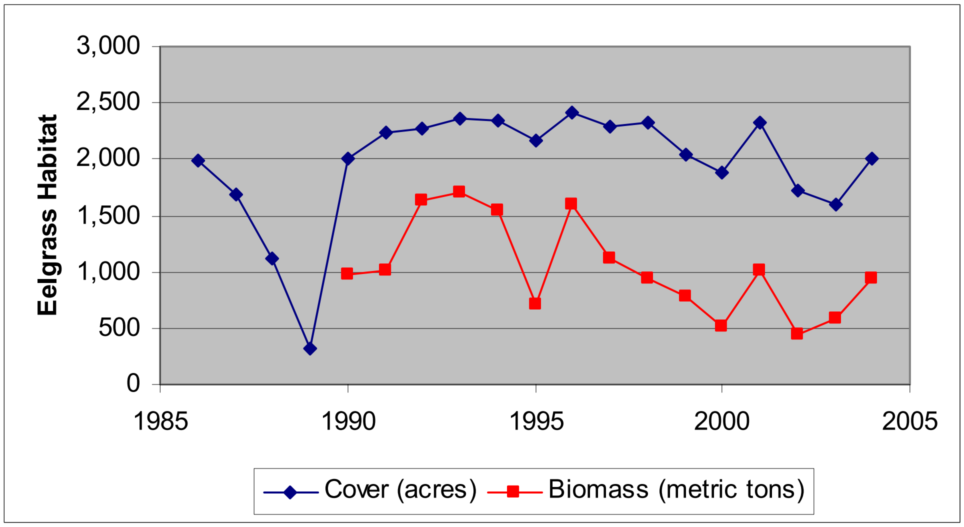

Figure 4: Study Area

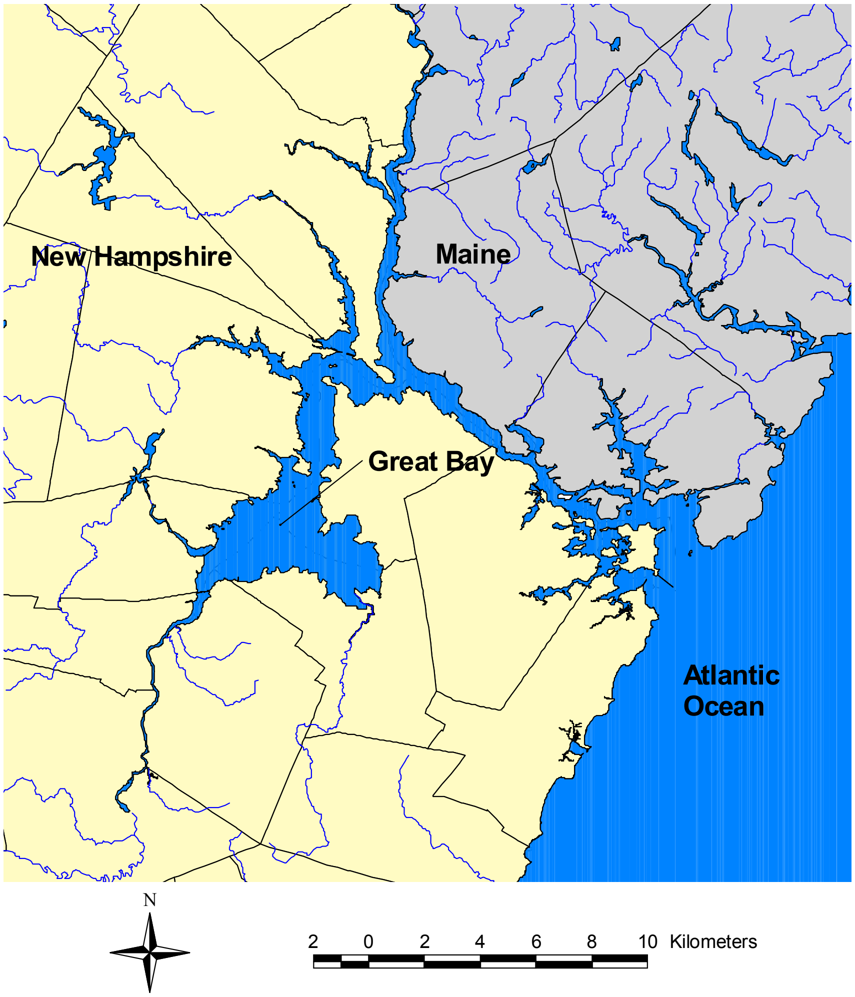

A6 – Project/Task Description

The project will consist of three parts.

For the first task of the project, UNH Coastal Observing Center will redeploy a moored buoy in Great Bay (Figure 5) with appropriate sensors for measuring the hyperspectral light field including attenuation coefficients and the remote sensing reflectance, as well as CDOM, turbidity, chlorophyll-a, nitrate, and other physico-chemical parameters (http://www.cooa.unh.edu/buoydata/buoy.jsp). These parameters will be measured in-situ on a 30 minute time step. The large volume of data on all the parameters related to light attenuation, collected over a broad range of environmental and optical conditions, will make it possible to derive a statistically significant relationship to predict water clarity from water quality parameters (Output A).

Figure 5: Buoy and sampling locations within the Great Bay Estuary

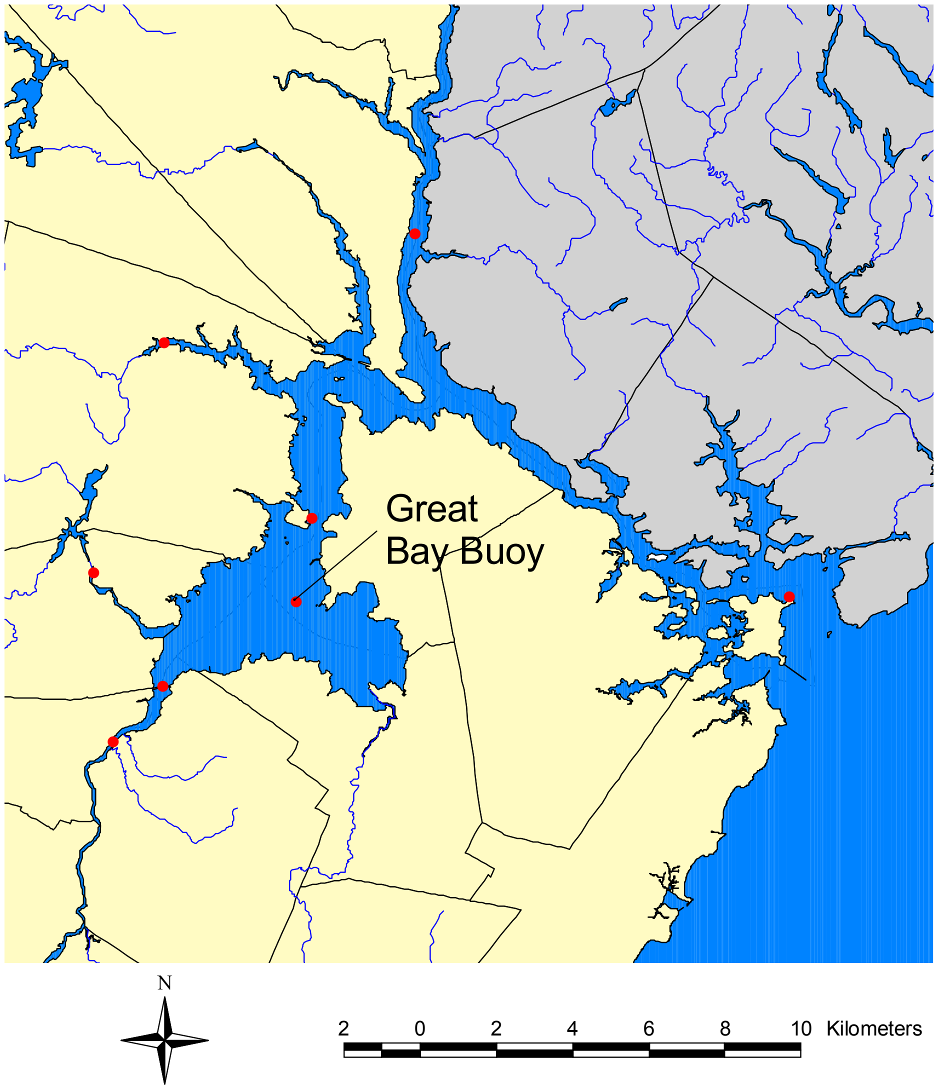

For the second task of the project, the NHEP will arrange for at least two overflights to collect hyperspectral imagery of the entire Great Bay system. The overflights will be conducted by SpecTIR (www.SpecTIR.com). SpecTIR proposes an airborne data collection with the VNIR sensor with a spatial resolution of 2.5 meters for the area of interest (Figure 6, in red), and a nominal spectral resolution of 10nm or 64 spectral channels from approximately 430 nm to 1000 nm. The delivered product will consist of calibrated radiance and geographic lookup tables with navigation. Navigation will be performed with high speed airborne DGPS integrated with a laser ring gyro. Personnel in the company have more than 10 years in the planning of hyperspectral flights and the collection/processing of airborne hyperspectral data. Specifications for the SpecTIR VNIR sensor are appended to this workplan.

Figure 6: Area for hyperspectral imagery collection (shown in red)

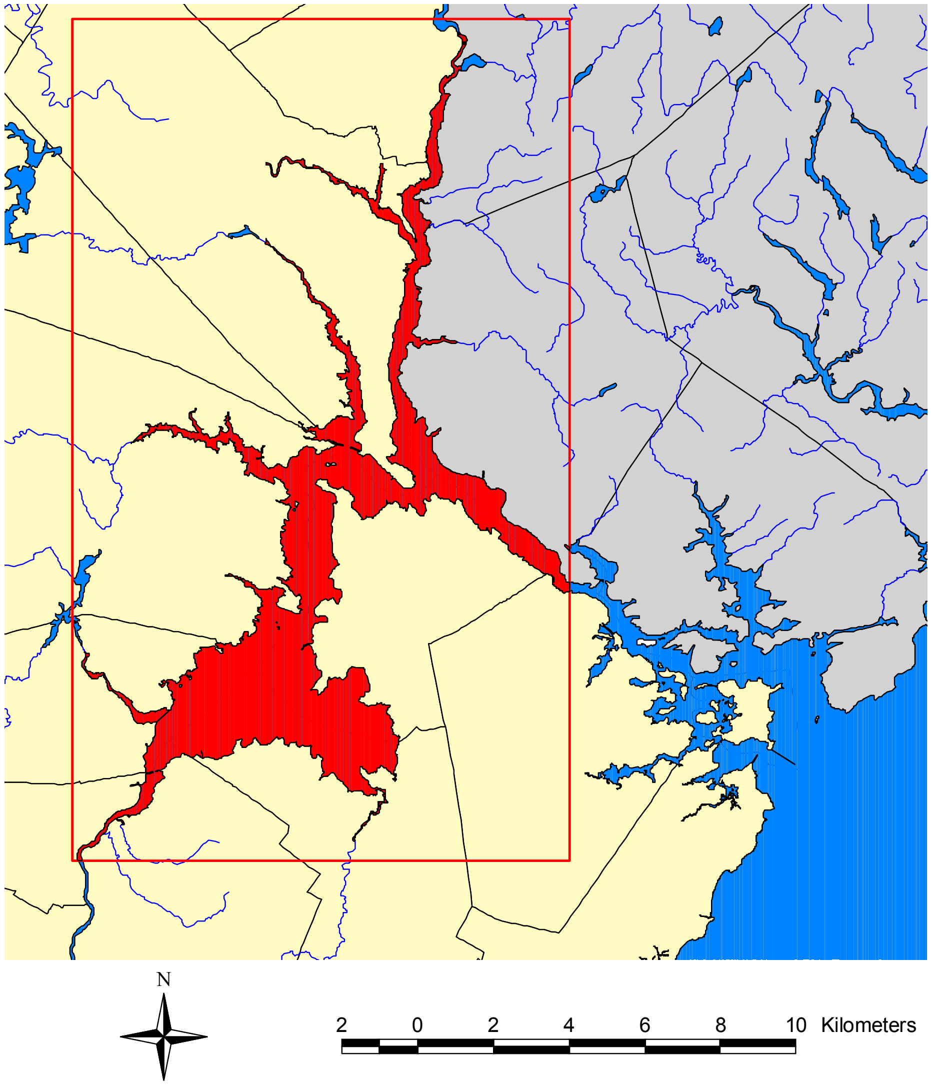

The overflights will be coordinated with times of buoy operation, grab sample collection and flow-through surveys to ground truth the imagery. Field sampling and buoy operation will be completed by the UNH Coastal Observing Center and the UNH Marine Program. The flow-through transects will continuously measure water temperature, salinity, chlorophyll-a, and colored dissolved organic matter. Grab samples will be analyzed for physico-chemical parameters, dissolved nutrients, chlorophyll-a, total suspended solids, CDOM, and water clarity (measured in the field). A custom profiling package will measure the vertical distribution of the IOPs with a hyperspectral attenuation-absorption meter and nine channel backscattering meter (ACS and BB-9 WetLABS Inc). Laboratory based measurements of absorption spectra for the optically important constituents from discrete water samples will help with the interpretation and validation of profiler measurements (Mitchell et al, 2000). The combination of in-situ moored measurements, flow-through measurements, and grab samples will be used to ground truth the aerial imagery.

After calibrating the hyperspectral imagery with the ground truth measurements, the UNH Coastal Observing Center will analyze the imagery to map the distributions of chlorophyll-a, CDOM, particulates, and benthic light availability throughout the system (Output B). The combination of aerial imagery and

ground truth measurements has been proven to be effective at producing accurate maps of water quality parameters (Sugumaran et al., 2005) and submerged aquatic vegetation (Dierssen et al, 2003).

For the third task of the study, UNH Coastal Observing Center will apply a multi-spectral radiative transfer model (Hydrolight, Sequoia Inc.) to the Great Bay to predict light availability to eelgrass under different water quality conditions. The model will be customized to Great Bay conditions using the information from the first part of the study. By comparing the model output to the measured light availability, UNH will be able to verify consistency with optical theory (Output C).

Finally, this project has been designed to meet many of the aims and goals of the Integrated Ocean Observing System (IOOS) by facilitating the use of observing system measurements by those involved in managing the state's coastal water. Funding for the initial development and deployment of the Great Bay Coastal Buoy was derived from an IOOS pilot project from the NOAA Coastal Services Center to the Coastal Observing Center at UNH.

The specific tasks and schedule for this project are listed below.

1. Prepare quality assurance project plan – due one month after receipt of award.

This report will document the methods to be used for the study and the quality assurance procedures. The plan will be approved by project partners and EPA Region I.

2. Purchase sensor equipment and deploy buoy – due by 7/15/07

UNH Coastal Observing Center will purchase, with separate funds, a junction box and other equipment needed to measure hyperspectral light intensity at two depths in the water and one location in the air. The buoy will be deployed in the middle of Great Bay at approximately 43.0715 degrees N latitude and 70.8677 degrees W longitude (Figure 4).

3. Obtain hyperspectral aerial imagery – due by 10/31/07

SpecTIR will obtain hyperspectral band imagery for the study area on two different dates between 7/15/07 and 10/31/07.

4. Collect water quality data from flow-through surveys and grab samples – due by 10/31/07

UNH Coastal Observing Center will measure water quality parameters along transects using a flow-through sampling device on the same date as the hyperspectral aerial imagery. UNH Marine Program will collect grab samples for water quality parameters at seven stations and operate six in-situ datasondes on the same date as well (Figure 4). These data will be used for ground truthing the aerial imagery.

5. Present preliminary results to nutrient criteria work group – due by 12/31/07

NHEP will present the preliminary results of the project to the nutrient criteria workgroup during the fall of 2007. The group will provide feedback on the results and guidance for additional analysis.

6. Interim status report – due 12/31/07

The NHEP will prepare a report to EPA on the status of the project. The interim status report will summarize the field data collection activities that occurred in 2007 and will note any discrepancies from the QAPP.

7. Final report – due 6/30/08

The final report will contain the planned outputs for the project (listed below), conclusions and recommendations.

Planned Outputs

A) A single or multi-variate model between the light attenuation coefficient and concentrations of CDOM, turbidity/suspended solids, and chlorophyll-a for the Great Bay system which can be used to develop numeric nutrient criteria;

B) Maps of the distribution of CDOM, turbidity, and chlorophyll-a (and light attenuation using the model described above) on at least two different days for the entire Great Bay system; and

C) A calibrated light availability model for the Great Bay system.

8. Present results to nutrient criteria work group – due by 6/30/08

NHEP will present the results of the project to the nutrient criteria workgroup during the spring of 2008.

9. Recommendation to the Water Quality Standards Advisory Committee – due 12/31/08

The nutrient criteria workgroup (staffed by DES) will prepare a white paper to present its recommendations to the WQSAC.

A7 – Quality Objectives and Criteria

The specific data quality objectives that will be used to determine the quality of the measurements for the study are listed in Table 2.

Table 2: Data quality objectives

Parameter	Condition	QC Sample and/or Activity Used to Assess Measurement Performance	Data Quality Objective
Activity #1: Buoy sensor measurements	Precision	Field replicate measurements with an independently calibrated meter or grab samples	RPD ≤ 30 %
	Accuracy	Calibration check with known standards	Calibrations are performed on schedule.
	Completeness	Data completeness check by QA Officer	80% of planned measurements must be collected.
Activity #2: Hyperspectral imagery	Accuracy-irradiance	Calibration with a NIST traceable spectral radiance	RPD ≤ 5 %
	Accuracy-position	Comparison of imagery to USGS digital orthophoto quads	+/-6 meters for imagery collected from 3,800 m altitude
Activity #3: Flow through survey measurements	Precision	Field replicate measurements with grab samples collected along flow through transect	RPD ≤ 30 %
	Accuracy	Calibration check with known standards	Calibrations are performed on schedule.
	Completeness	Data completeness check by QA Officer	80% of planned measurements must be collected.
Activity #4: Grab samples for laboratory analysis	Precision-field	Field replicate	RPD ≤ 30 %
	Precision-lab	Laboratory replicates	RPD ≤ 10 %
	Accuracy-lab	Independent calibration verification samples	Calibrations are performed on schedule.
	Completeness	Data completeness check by QA Officer	80% of planned measurements must be collected.
All Parameters	Representativeness	The sampling stations will be situated within the study area. Grab samples and hyperspectral imagery will be collected during the index period of 7/1/07 to 10/31/07. Grab samples will be collected within 1 hour of the flight time. Flow through transects will be completed within 2 hours of the flight time.	
	Comparability	Data comparability will be achieved primarily through the use of standardized methods from past studies and the scientific literature.	

A8 – Special Training/Certification

Data will be collected by trained, professional staff at UNH and SpecTIR. Each agency will be responsible for training staff working under the supervision of the Project Officers before any field work is conducted.

Table 3: Special Personnel Training Requirements

Project function	Description of Training	Training Provided by	Training Provided to	Deadline for Training	Location of Training Records
Study design	Sampling process design from section B1	Project Manager	UNH Research Staff and SpecTIR Project Officers	8/24/07	Documentation will be on file at NHEP
Water quality field procedures	Field measurement procedures in sections B2 through B9 and related appendices	Project Manager	Field crews	8/24/07	Documentation will be on file at NHEP

A9 – Documents and Records

QA Project Plan: The NHEP QA Officer will be responsible for maintaining the approved QA Project Plan and for distributing the latest version of the plan to all parties on the distribution list (Table 1). A copy of the approved plan will be on file at the NHEP offices in Durham, NH.

Interim Report: The NHEP QA Officer will prepare a report to EPA on the status of the project by 12/31/07. The interim status report will summarize the field data collection activities that occurred in 2007 and will note any discrepancies from the QAPP.

Final Report: The Project Manager will prepare a final report to EPA by 6/30/08. The final report will contain the planned outputs for the project (listed below), conclusions and recommendations.

Planned Outputs

- A single or multi-variate model between the light attenuation coefficient and concentrations of CDOM, turbidity/suspended solids, and chlorophyll-a for the Great Bay system which can be used to develop numeric nutrient criteria;
- Maps of the distribution of CDOM, turbidity, and chlorophyll-a (and light attenuation using the model described above) on at least two different days for the entire Great Bay system; and
- A calibrated light availability model for the Great Bay system.

Archiving: Water quality data from the study will be permanently archived in the DES Environmental Monitoring Database (EMD) with all relevant metadata. Hyperspectral imagery data will be permanently archived in the NH GIS repository, GRANIT, with all relevant metadata. The QAPP, interim report, and final report will be kept on file at the NHEP for a minimum of 10 years after the publication date of the final report. All data from the project will be made available to the public through the EMD and GRANIT, which are publicly accessible.

Turnaround times for laboratories are specified in section B4.

B1 – Sampling Process Design

Data for this study will be collected through four activities: (1) Near continuous buoy observations; (2) Low altitude aerial surveys for hyperspectral imagery; (3) Near continuous flow-through surveys of water quality; and (4) Point measurements with field sensors and grab samples. The parameters for the study are shown in Table 4. The rationale for the sampling efforts is described in Section A6. The sample process design for each of the activities is described in the following sections.

Table 4: List of Parameters

Parameter	Measurement Type	Priority
Light attenuation, backscatter, and irradiance at various wavelengths	Near continuous buoy observations (Act #1) Measurements with field sensors (Act #4)	Critical
Chlorophyll-a	Near continuous buoy observations (Act #1) Near continuous flow-through obs. (Act #3) Grab sample and laboratory analysis (Act #4)	Critical
Colored Dissolved Organic Matter (CDOM)	Near continuous buoy observations (Act #1) Near continuous flow-through obs. (Act #3) Grab sample and laboratory analysis (Act #4)	Critical
Turbidity	Near continuous buoy observations (Act #1) Near continuous flow-through obs. (Act #3) Measurements with field sensors (Act #4)	Critical
Total Suspended Solids	Grab sample and laboratory analysis (Act #4)	Critical
Hyperspectral imagery	Low altitude aerial survey (Act #2)	Critical
Water Temperature	Near continuous buoy observations (Act #1) Near continuous flow-through obs. (Act #3) Measurements with field sensors (Act #4)	For information only
Salinity	Near continuous buoy observations (Act #1) Near continuous flow-through obs. (Act #3) Measurements with field sensors (Act #4)	For information only
Nutrients (i.e., nitrate+nitrite, orthophosphate)	Near continuous buoy observations (Act #1) Grab sample and laboratory analysis (Act #4)	For information only

Sample Process Design for Activity #1: Near Continuous Buoy Observations

The stations for this activity are listed on Table 5. The Activity #1 stations will be monitored continuously from 4/1/07 to 12/15/07 for several water quality parameters. The water quality parameters to be measured by each buoy are listed in Table 6.

Table 5: Sampling Station Summary for Activity #1

Station ID	Description	Latitude (DD MM.MMM)	Longitude (DD MM.MMM)
Great Bay Coastal Buoy	Central Great Bay	43.0715	-70.8677

Table 6: Sample Process Design for Field Measurements for Activity #1

Station ID	Parameters	Sampling Period and Frequency	Responsible Agency
Great Bay Coastal Buoy	Water Temperature Salinity Chlorophyll-a CDOM Turbidity Light Attenuation Nitrate	4/1/07 – 12/15/07 Every 30 minutes	UNH Coastal Observing Center

Sample Process Design for Activity #2: Hyperspectral imagery collection

On two dates between 7/1/07 and 10/31/07, hyperspectral imagery will be collected across the study area. Details regarding the hyperspectral imagery will be presented in section B2. The overflights will be conducted by SpecTIR (www.SpecTIR.com). The flights will be conducted within 2 hours of either low or high tide at Adams Point (preferably one flight at high tide and one flight at low tide). Flights will be conducted during the morning or afternoon to avoid sun glint. For each flight, the target altitude and speed will be 12,500 feet (3,800 meters) at 160 knots, respectively. Imagery over the entire study area will be collected during a 1.5 hour period. Imagery will be collected from the estuarine area within the area shown in Figure 6.

Sample Process Design for Activity #3: Near Continuous Flow Through Surveys

Two flow through surveys will conducted in the study area between 7/1/07 and 10/31/07. The surveys will coincide with the date of hyperspectral imagery collection. The flow through surveys will cover Great Bay and Little Bay during the overflights in order to document optical properties in the water near and directly above eelgrass beds.

The flow through surveys collect data on temperature, salinity, chlorophyll-a, turbidity, CDOM, light absorption and attenuation and backscatter and from sensors deployed on a moving boat. Water is brought through the hull and flows through all the instruments which are on deck. The sensor measurements are recorded every at variable sampling rates most commonly on the order of 1 Hz and are georeferenced using dGPS. The result is a spatial dataset of water quality measurements along a transect. The transects in Great Bay and Little Bay will be criss-crossed to make a matrix of water quality measurements covering a majority of the estuarine area.

Sample Process Design for Activity #4: Point measurements with field sensors and grab samples

During the two days of aerial data collection, point measurements of water quality will be collected at stations throughout the study area (Table 7, Figure 7). Grab samples will be analyzed for physico-chemical parameters, dissolved nutrients, chlorophyll-a, total suspended solids, CDOM, and water clarity. At some of the stations, a custom profiling package will measure the vertical distribution of the IOPs with a hyperspectral attenuation-absorption meter and nine channel backscattering meter (ACS and BB-9 WetLABS Inc). Laboratory based measurements of absorption spectra for the optically important constituents from discrete water samples will help with the interpretation and validation of profiler measurements (Mitchell et al, 2000).

On each sampling date, samples for each parameter will be collected during 21 station visits (Table 8). Field replicate replicate samples will be collected at station GRBGB and GRBAP by the UNH Coastal Observing Center.

Table 7: Sampling Station Summary for Activity #4

Station ID	Description	Latitude (DD.DDDD)	Longitude (DD.DDDD)
GRBGB	Central Great Bay	43.0722	-70.8694
GRBSQ	Mouth of Squamscott River	43.0417	-70.9222
GRBLR	Lamprey River	43.0800	-70.9344
GRBOR	Oyster River	43.1340	-70.9110
GRBAP	Great Bay at Adams Point	43.0919	-70.8636
GRBCL	Squamscott River at Chapman’s Landing	43.0394	-70.9283
GRBSF	Salmon Falls River	43.2142	-70.8172
NH-0049A	Oyster River	43.1270	-70.8805
NH-0052A	Bellamy River	43.1340	-70.8470
NH-0057A	Upper Piscataqua River	43.1589	-70.8302
NH-0058A	Cocheco River	43.1950	-70.8580
NH-0062A	Salmon Falls River	43.1970	-70.8210
GB4A	Great Bay in channel leading to the Squamscott River	43.0695	-70.8819
GB16	Great Bay in channel leading to the Winnicut River	43.0600	-70.8559
NH00-0035A	Great Bay in northwestern eelgrass beds	43.0786	-70.8831
NH01-0026A	Great Bay in southern eelgrass beds	43.0620	-70.8890
NH00-0027B	Great Bay in southeastern eelgrass beds	43.0639	-70.8590
NH-0070A	Great Bay in northeastern eelgrass beds	43.0769	-70.8653
NH04-0245C	Upper Little Bay	43.10894	-70.85962
NH04-0235C	Entrance to Great Bay near Furber Strait	43.0844	-70.86374

Figure 7: Sampling Stations for Activity #4

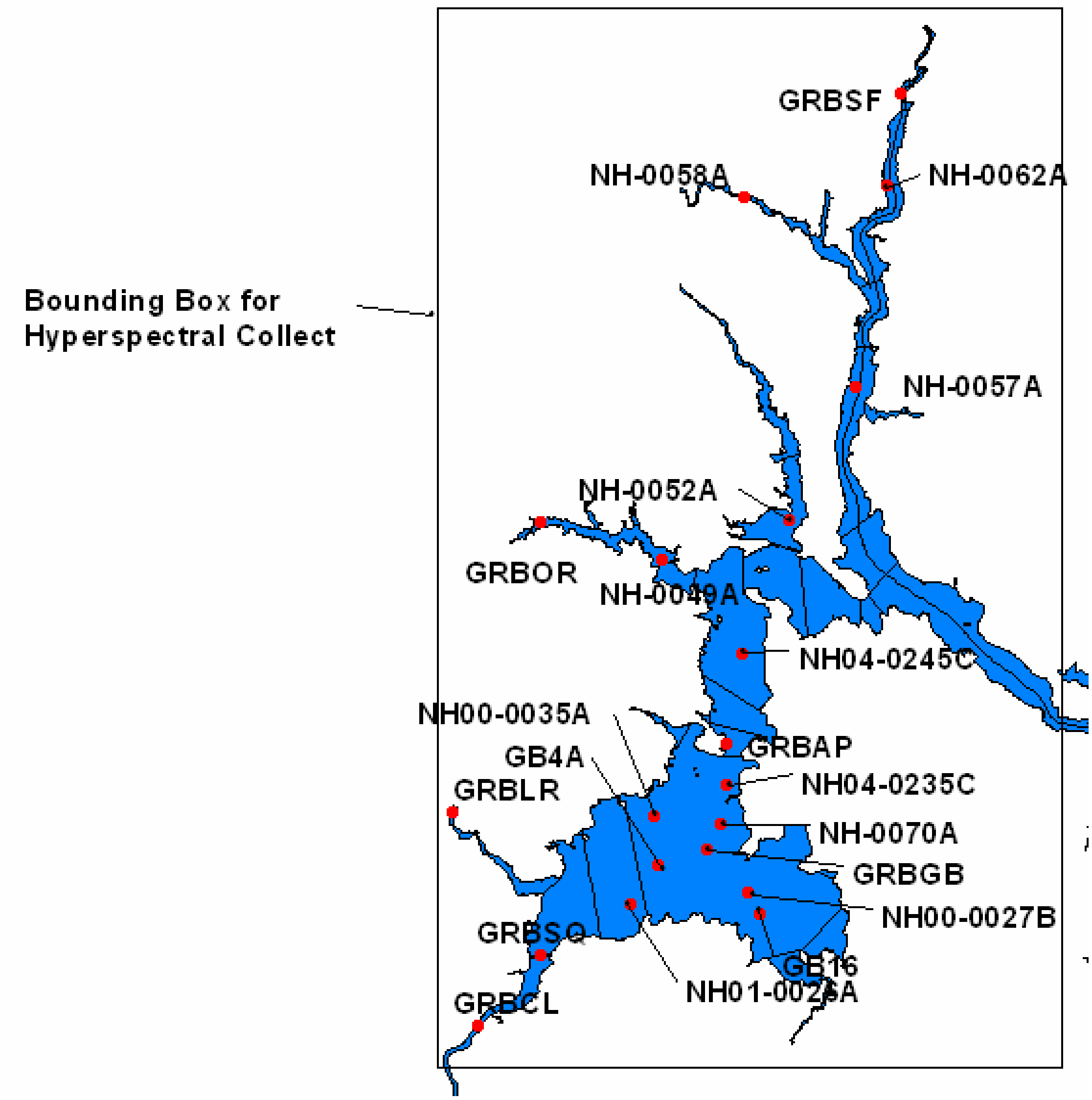

Table 8: Sample Process Design for Field Measurements for Activity #3

Station ID	Parameters	Sampling Period and Frequency	Responsible Agency
GRBGB GRBSQ GRBLR GRBCL GRBAP	Water Temperature* Salinity* Light Attenuation* Chlorophyll-a CDOM TSS Absorption spectra Nitrate+nitrite Orthophosphate	One sample or field measurement on each date of hyperspectral imagery collection *field measurement	UNH/GBNERR System Wide Monitoring Program
GRBOR NH-0049A NH-0052A	Water Temperature* Salinity* Light Attenuation* Chlorophyll-a CDOM TSS Absorption spectra Nitrate+nitrite Orthophosphate	One sample or field measurement on each date of hyperspectral imagery collection *field measurement	UNH National Coastal Assessment Program
NH-0057A NH-0058A NH-0062A GRBSF	Water Temperature* Salinity* Chlorophyll-a CDOM TSS Absorption spectra Nitrate+nitrite Orthophosphate	One sample or field measurement on each date of hyperspectral imagery collection *field measurement	DES Shellfish Program
GRBGB (+field rep) GRBAP (+field rep) GB4A GB16 NH00-0035A NH01-0026A NH00-0027B NH04-0245C NH04-0235C NH-0070A	Water Temperature* Salinity* Light attenuation* Turbidity* Upwelling and downwelling irradiance* Chlorophyll-a CDOM TSS Absorption spectra Nitrate+nitrite Orthophosphate	One sample or field measurement on each date of hyperspectral imagery collection *field measurement	UNH Coastal Observing Center

Procedure for Responding to Non-Standard Situations

The sample process design outlined in this section should be followed. However, in the event of a non-standard situation in which the sample process designs cannot be followed, the field sampling staff of any agency should contact the Project Manager for direction on how to proceed. Possible responses to non-standard situations include: Relocating sampling stations, altering sampling schedules, and modifying the sampling design.

B2 – Sampling Methods

Water sampling for Activities #1, #3 and #4 will be conducted using three approaches: (1) Continuous measurements with *in-situ* sensors and dataloggers; (2) Instantaneous measurements with hand-held sensors; and (3) Grab samples. Hyperspectral imagery will be collected from low-altitude aerial surveys. These approaches have been successfully used for past studies.

Sampling Methods for Activity #1: Near Continuous Buoy Observations

Water quality parameters are measured by in-situ sensors on a deployed buoy:

Temperature and Salinity are measured using a Sea-Bird MicroCAT C-T Model SBE 37-SIP (http://www.seabird.com/products/spec_sheets/37sipdata.htm).

CDOM is measured using a WET Labs ECO FLCDS open path fluorometer (http://www.wetlabs.com/products/eflcombo/fl.htm).

Chlorophyll-a is measured using a WET Labs ECO FLNTUS open path fluorometer (http://www.wetlabs.com/products/eflcombo/fl.htm).

Turbidity is measured using a WET Labs ECO FLNTUS open path fluorometer (http://www.wetlabs.com/products/eflcombo/fl.htm).

Nitrate is measured using a Satlantic ISUS (http://www.satlantic.com/details.asp?ID=11&CategoryID=2&SubCategoryID=0).

Light levels are measured at the surface and at 1 and 2 m below the surface using Satlantic HyOCR sensors. From these measurements light attenuation can be calculated.

(http://www.satlantic.com/details.asp?ID=9&CategoryID=1&SubCategoryID=0)

Sampling Methods for Activity #2: Hyperspectral imagery collection

SpecTIR proposes an airborne data collection with the VNIR sensor with a spatial resolution of 2.5 meters with 30% sidelap for the area of interest. The imagery will have a nominal spectral resolution of 10nm or 64 spectral channels from approximately 430 nm to 1000 nm. The delivered product will consist of calibrated radiance and geographic lookup tables with navigation. Navigation will be performed with high speed airborne DGPS integrated with a laser ring gyro. Specifications for the SpecTIR VNIR sensor are listed in Appendix B. The planned flight lines are shown in Figure 8.

Sampling Methods for Activity #3: Near Continuous Flow Through Surveys

Continuous along-track measurements of a number of physical and bio-optical properties are logged on the same computer with the geolocation and time information from a GPS unit.

Conductivity and temperature is measured with a Seabird SBE45 thermosalinograph

(http://www.seabird.com/products/spec_sheets/45data.htm)

CDOM and chlorophyll-a are measured using two WetLABS WETStar fluorometers

(http://www.wetlabs.com/products/pub/specsheets/wsxssg.pdf)

Beam attenuation is measured with a WetLABS C-Star transmissometer (Turbidity)

(http://www.wetlabs.com/products/pub/specsheets/cstarssi.pdf)

Light absorption and attenuation is measured at 9 wavelengths with a WetLABS ac-9

(http://www.wetlabs.com/products/pub/specsheets/ac9sse.pdf)

Optical backscattering is measured at three visible wavelengths with a WetLABS ECO bb3

http://www.wetlabs.com/products/pub/specsheets/triplestsse.pdf

Sampling Methods for Activity #4: Point measurements with field sensors and grab samples

Grab samples for chlorophyll-a, TSS, CDOM and absorption spectra will be collected, handled, and stored according the Ocean Optics Protocols (Appendix C and D).

Grab samples for nutrients (nitrate+nitrite, orthophosphate) will be collected, handled, and stored according the WQAL QAPP (Appendix A, Section III).

Field measurements of temperature and salinity will be made with YSI 30 or similar unit.

Field measurements of light attenuation will follow the Ocean Optics Protocols (Appendix C) or, for the GBNERR and NCA field crews, following the UNH Marine Program SOP (Appendix E).

The field data sheet to be used by field crews is attached as Appendix F.

Profiles of inherent optical properties will be made with a custom profiling package (WetLABS, Inc.). This contains a variety of instruments that are powered by two rechargeable waterproof batteries and the data is logged with a WetLABS DH-8 (http://www.wetlabs.com/products/pub/specsheets/dh4sse.pdf).

Conductivity, temperature and pressure with a Seabird Fastcat 49

(http://www.seabird.com/products/spec_sheets/49data.htm)

Chlorophyll-a and CDOM fluorescence with a WetLABS ECO-triplet fluorometer

(http://www.wetlabs.com/products/pub/specsheets/flssu.pdf)

Optical backscatter is measured at 9 wavelengths with a WetLABS BB-9

Absorption and attenuation is measured at over 80 wavelengths with a WetLABS acs

(http://www.wetlabs.com/products/pub/specsheets/acsssc.pdf)

Vertical profiles of the light field, both upwelling radiance and downwelling irradiance, at approximately 150 wavelengths between 350 and 850 nm will be measured using a Hyperpro-II (Satlantic Inc, http://www.satlantic.com/documents/419671_Specifications.pdf).

Procedure for Responding to Non-Standard Situations

The methods outlined in this section should be followed. However, in the event of a non-standard situation in which the methods cannot be followed, the field sampling staff of any agency should contact the Project Manager for direction on how to proceed.

Figure 8: Flight lines for hyperspectral imagery collect

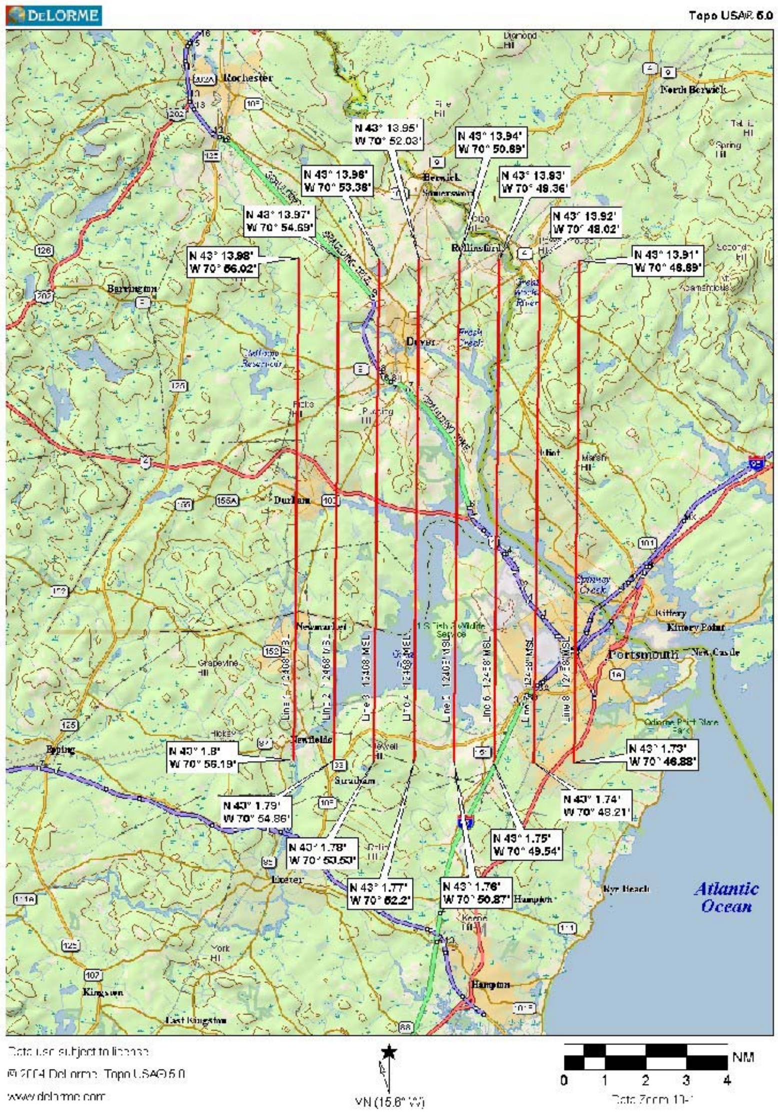

B3 – Sample Handling and Custody

Field sampling crews will deliver grab samples to the Project Manager at Jackson Estuarine Laboratory. The Project Manager will process the samples at JEL. All the samples from each date for the UNH WQAL will be delivered to WQAL together to avoid confusion and lost samples. The sample handling protocols are provided in Appendices A, C and D.

Chain of custody forms will not be used. Each sample will be clearly labeled with the station ID, date and time of collection, and the initials of the sampler.

B4 – Analytical Methods

Grab samples for chlorophyll-a, CDOM, TSS and absorption spectra will be analyzed in the UNH Jackson Estuarine Laboratory, Durham, NH. Protocols for analysis are provided in Appendices C and D.

Grab samples for dissolved nutrients will be analyzed by the UNH Water Quality Analysis Laboratory, Durham NH. The Quality Assurance Plan for this laboratory is attached as Appendix A.

The analytical methods for each parameter are listed in Table 9.

A laboratory turn-around time of 30 days is needed for the sample analyses in order to meet grant contract deadlines.

The UNH Laboratory QA Officer will be responsible for responding to all non-standard situations pertaining to the WQAL laboratory analyses. The Project Manager will be responsible for responding to non-standard situations at the Jackson Estuarine Laboratory.

Table 9. Method Reference

Parameter	Method	Laboratory
Chlorophyll-a	See Appendix D	JEL
CDOM	See Appendix C	JEL
TSS	SM17 2540 D (EPA Method 160.2)	JEL
Absorption spectra	See Appendix C	JEL
Nitrogen, NO2 + NO3	EPA Method 353.3	WQAL
Phosphorus, PO4	EPA Method 365.2	WQAL

B5 – Quality Control

The quality control tests for this study and the frequency at which they will be performed are listed in Table 10. The acceptance criteria for each test are listed on Table 2. Quality control will be achieved through frequent cleaning and maintenance of sensors (see section B6), at least annual recalibration of sensors, comparison of field replicate samples, and traditional laboratory QC samples.

Preliminary laboratory and field data will be reviewed by the UNH Research Staff. Results that do not meet the data quality objectives from Section A7 will be flagged as needing corrective action. The corrective action taken will range from rejection of data to adjustment of values with new calibration values.

After the field sampling is complete, the NHEP Project QA Officer will conduct a data completeness check for valid data in the EMD. The data quality objectives for data completeness are provided in Section A7. The NHEP Project QA Officer will also compile all of the quality control results for each parameter (listed in Table 10) and determine the percentage of quality control samples that met the data quality objectives. If this percentage falls below 80%, the NHEP Project QA Officer will investigate the possibility of systematic error in the measurements.

Table 10: Quality Control Test Frequency

Parameter	Condition	QC Sample and/or Activity Used to Assess Measurement Performance	Frequency

Parameter	Condition	QC Sample and/or Activity Used to Assess Measurement Performance	Frequency
Activity #1: Buoy sensor measurements	Precision	Field replicate measurements with an independently calibrated meter or grab samples	Weekly
	Accuracy	Calibration check with known standards	Twice per year
	Completeness	Data completeness check by QA Officer	Once at the end of the project (6/30/08)
Activity #2: Hyperspectral imagery	Accuracy-irradiance	Calibration with a NIST traceable spectral radiance	Before and after each deployment
	Accuracy-position	Comparison of imagery to USGS digital orthophoto quads	For each imagery dataset
Activity #3: Flow through survey measurements	Precision	Field replicate measurements with grab samples collected along flow through transect	Each sampling date (5 stations)
	Accuracy	Calibration check with known standards	Yearly
	Completeness	Data completeness check by QA Officer	Once at the end of the project (6/30/08)
Activity #4: Grab samples for laboratory analysis	Precision-field	Field replicate	Every 10th measurement
	Precision-lab	Laboratory replicates	Every 10th sample
	Accuracy-lab	Independent calibration verification samples	Yearly for spectrophotometers, 2 times per year for fluorometer
	Completeness	Data completeness check by QA Officer	Once at the end of the project (6/30/08)

The definitions of precision and accuracy are provided below.

Precision

Precision is the degree of agreement among repeated measurements of the same characteristic (parameter) under the same or similar conditions. Precision is calculated for field and laboratory measurements through measurement replicates (instrumental variability), and is calculated for each sampling day. For field replicates, the measure of precision will be a parameter-specific relative percent difference (RPD) as derived from equation 1, below.

(1)

$$RPD = \frac{|x_1 - x_2|}{\frac{x_1 + x_2}{2}} \times 100 \ \%$$

where x_1 is the original sample concentration
x_2 is the replicate sample concentration

Accuracy

Accuracy is the extent of the agreement between an observed value (sample result) and the true value of the parameter being measured. Accuracy limits of laboratory analyses are defined through independent

calibration verifications and continuing calibration verifications of laboratory control samples. The measurement of accuracy will be the percent recovery of spiked compound from a matrix spiked duplicate sample using the following equation:

$$R = \frac{(x_1 - x_{2)}}{m} \times 100\%$$

where R is the percent recovery (%)
x_1 is the lab fortified sample concentration
x_2 is the original sample concentration
m is the amount of chloride added to the fortified sample

Accuracy measurements using standard reference materials will be evaluated using relative percent difference, which was discussed in the preceding paragraph.

Boresight Calibration

In order to ensure the optimal translation of the INS positional data to the image, the INS and camera must be boresighted. To achieve this, SpecTIR has established a boresight calibration site south of the Stead, NV airport. As control, 6 inch orthophotography and matching 2 foot contour data was obtained from Washoe County. The positional accuracy of the orthophotography is 9 inches.

Completeness

Data completeness is the percent of planned samples that were actually collected.

B6 – Instrument/Equipment Testing, Inspection, Maintenance

Sensors on deployed dataloggers will be inspected for possible debris or fouling, and cleaned as necessary prior to calibration and re-deployment. The following anti-fouling, maintenance and calibration measures will be used for the sensors.

Temperature and Salinity

Antifouling

The conductivity cell in the SBE37-SIP is equipped with two plugs containing tributyl tin (TBT) which are designed to eliminate or retard biological activity. Previous deployments have demonstrated the effectiveness of this system for at least several months.

Instrument Maintenance and Calibration

The instrument is sent to Sea-Bird for maintenance and calibration after each deployment period.

CDOM

Antifouling

The ECO fluorometers are equipped with copper plating surrounding the fluorometer window. The fluorometers were purchased with the optional bio-wiper assembly which is a copper and rubber wiper that is designed to keep the window clean by covering it when not in use and by wiping it clean each time the instrument is powered. To further mitigate fouling, the instrument housing is wrapped in copper tape prior to deployment.

Instrument Maintenance and Calibration

The instrument is sent to WET Labs for maintenance and calibration after each deployment period.

<u>Chlorophyll-a</u>

Antifouling
The ECO fluorometers are equipped with copper plating surrounding the fluorometer window. The fluorometers were purchased with the optional bio-wiper assembly which is a copper and rubber wiper that is designed to keep the window clean by covering it when not in use and by wiping it clean each time the instrument is powered. To further mitigate fouling, the instrument housing is wrapped in copper tape prior to deployment.

Instrument Maintenance and Calibration
The instrument is sent to WET Labs for maintenance and calibration after each deployment period.

<u>Turbidity</u>

Antifouling
The ECO fluorometers are equipped with copper plating surrounding the fluorometer window. The fluorometers were purchased with the optional bio-wiper assembly which is a copper and rubber wiper that is designed to keep the window clean by covering it when not in use and by wiping it clean each time the instrument is powered. To further mitigate fouling, the instrument housing is wrapped in copper tape prior to deployment.

Instrument Maintenance and Calibration
The instrument is sent to WET Labs for maintenance and calibration after each deployment period.

<u>Nitrate</u>

Antifouling
The ISUS is equipped with a measurement probe housing consisting of copper mesh and 20 μm Nitex screen.

Instrument Maintenance and Calibration
The ISUS is sent to Satlantic for maintenance and calibration at the end of each deployment year, usually in December. The probe housing is removed and cleaned during regular maintenance dives. A range of nitrate concentrations is analyzed in the laboratory before and after each deployment period. Instrument response (slope) and offset (blank) are checked by this method.

Sensors for hyperspectral imagery collection will be calibrated and serviced as follows:

<u>Radiometric and Spectral Calibration</u>

Radiometric calibration is achieved through the use of a Labsphere USS-2000-V uniform source. This 20-inch diameter integrating sphere is equipped with three internal 45-watt and one 75 watt externally mounted halogen light sources. Each lamp is powered by separate DC regulated constant current power supplies and the addition of a variable attenuator, provides even more precise control of light levels. Luminance output is variable from 0 to 4000 foot-lamberts and measured uniformity is > 98% over the entire 8-inch exit port. This sphere carries a NIST traceable spectral radiance calibration from 400nm to 2500nm at a sampling interval of 10nm.

The resultant calibration allows SpecTIR to provide data that is within +/- 5% of absolute radiance.

Wavelength calibration is generated and monitored through a characterized Mercury-Argon (HgAr) emmision lamp source. HgAr lamps are a common spectral calibration source for spectrometers and provides several fine distinct emission lines in both the VNIR and SWIR spectral domain allowing for accurate wavelength mapping. During processing, flight data QA/QC procedures rely on well documented atmospheric features such as the Oxygen fraunhaufer line at 760nm to ensure that accurate wavelength mapping is maintained.

Navigation and Boresighting

SpecTIR's instruments incorporate 3-ring laser gyro based Inertial Navigation Systems (INS) to provide for the accurate georeferencing of the data. The IMU is coupled with a 12-channel GPS system which utilizes Omnistar HP realtime differential corrections to feed the tightly coupled Kalman filter of the INS. The capabilities of this navigation system are as stated:

Position Accuracy:	0.10 m CEP
Velocity Accuracy:	0.02 m/s
Pitch Accuracy:	0.015 deg RMS
Roll Accuracy:	0.015 deg RMS
Azimuth Accuracy:	0.05 deg RMS
Data Rate:	100Hz

In order to ensure the optimal translation of the INS positional data to the image, the INS and camera must be boresighted. To achieve this, SpecTIR has established a boresight calibration site south of the Stead, NV airport. As control, 6 inch orthophotography and matching 2 foot contour data was obtained from Washoe County. The positional accuracy of the orthophotography is 9 inches.

In order to provide orthocorrected hyperspectral imagery, SpecTIR has the entire 10m resolution NED DEM database for the continental United States. If improved accuracies are required, client provided DEMs from such sources as Lidar can be incorporated into the processing stream.

During processing, georeferencing performance is assessed based upon USGS 1m DOQQ imagery.

The Project Manager will be responsible for maintaining spare parts and supplies for the field sensors and dataloggers for this project.

B7 – Instrument/Equipment Calibration and Frequency

Instrument calibration frequency is described in section B6.

B8 – Inspection/Acceptance Requirements for Supplies and Consumables

The sample bottles will be visually inspected immediately prior to the collection of the sample to determine the presence of damage (e.g., cracks) or contamination (e.g., dirt or other particulate matter within the container). The sample bottles will be accepted for use if damage and contamination are not visible or otherwise apparent. Similarly, the calibration reagents will be visually inspected for

discoloration or other indicator of poor quality or contamination. The reagents will be accepted for use if discoloration or other indicator is not observed. The Project Manager is responsible for the inspections.

B9 – Non-direct Measurements

UNH will use data from the following non-direct sources as part of this study.

Table 11: Non-Direct Data Sources for this Study

Type of Data	Original Use	Relevance	Acceptance Criteria	Limitations
Physico-chemical observations from GBNERR in-situ sensors (available at: http://cdmo.baruch.sc.edu/QueryPages/data_metadata_select.cfm)	The Great Bay National Estuarine Research Reserve operates six observation buoys in the study area. At each station, water depth, temperature, salinity, dissolved oxygen, pH and turbidity are recorded every 30 minutes. The data are collected as part of a national monitoring program.	Physico-chemical observations may be helpful in ground-truthing the hyperspectral imagery.	The data from the in-situ sensors are quality assured by UNH. Only data points that pass the UNH QA review will be used for this study. The accuracy of the temperature, salinity and turbidity sensors are +/-0.15 deg C, +/-1%, and +/-5%, respectively.	None

B10 – Data Management

The laboratory data will be transmitted to the Project Manager as Microsoft Excel spreadsheets. After QA checks, the data will be permanently archived in the DES Environmental Monitoring Database with all relevant metadata.

Hyperspectral imagery data will be permanently archived in the NH GIS repository, GRANIT, with all relevant metadata.

Data from the buoy will be transmitted to the shore station at JEL using wireless telemetry. The shore station routinely copies this data to a server Morse Hall on the UNH Durham campus and archives the data at JEL. Where appropriate raw count data is converted to calibrated engineering units on this server and both raw and converted data are archived. This server is backed up daily. In a final step the converted data is combined averaged for each 10 minute activity period and combined with appropriate metadata providing an initial dataset for each deployment. After each deployment a final QA step involving ancillary measurements made at the buoy, such as grab samples, allows the data to be finalized. This information, data and metadata from the buoy, will be permanently archived in the NH EMD.

Data from the flow through system is initially stored on a laptop computer on board the boat. At the end of each day this is uploaded to a server in Morse Hall on the UNH Durham campus. Where appropriate raw count data is converted to calibrated engineering units and both raw and converted data are archived. Typically flow through data undergoes QA checks and is averaged within a 20 second timestep. This data with appropriate metadata will be permanently archived at the NH DES EMD.

All data from the project will be made available to the public through the EMD and GRANIT, which are publicly accessible.

C1 – Assessments and Response Actions

In order to determine that field sampling, field analysis and laboratory activities are occurring as planned, field staff and laboratory personnel shall meet after the first sampling event to discuss the methods being employed and to review the quality assurance samples. At this time all concerns regarding the sampling protocols and analysis techniques shall be addressed and any changes deemed necessary shall be made to ensure consistency and quality of subsequent sampling. Assessment frequencies and responsible personnel are shown in the following table.

Table 12: Project Assessment Table

Assessment Type	Frequency	Person responsible for performing assessment	Person responsible for responding to assessment findings	Person responsible for monitoring effectiveness of corrective actions
Field sampling audit (effectiveness of grab sample collection)	Once after first sampling day	Ru Morrison Project Manager	Ru Morrison Project Manager	Ru Morrison Project Manager
Field analytical audit (effectiveness of field sensor operations)	Once after first sampling day	Ru Morrison Project Manager	Ru Morrison Project Manager	Ru Morrison Project Manager
UNH JEL Fixed Lab Audit	Weekly	Ru Morrison Project Manager	Ru Morrison Project Manager	Ru Morrison Project Manager
UNH WQAL Fixed Lab Audit	Weekly	Jeff Merriam Lab QA/QC Officer	Jeff Merriam Lab QA/QC Officer	Jeff Merriam Lab QA/QC Officer
Data Quality Audit	Once at end of project (6/30/08)	Phil Trowbridge NHEP QA Officer	Phil Trowbridge NHEP QA Officer	Phil Trowbridge NHEP QA Officer

Based on EPA-NE Worksheet #27b.

Field Sampling Audit: QAPP deviations and project deficiencies determined during the field sampling assessment will be evaluated for source of deviation and corrected with verbal communications in the field and documented in field log books. Any necessary written/structural changes will be made through a revision of the SOP for that activity (and this QAPP). Field sampling activities will be monitored to determine compliance.

Field Analytical Audit: QAPP deviations and project deficiencies determined during the field analytical assessment will be evaluated for source of deviation and corrected with verbal communications in the field and documented in field log books. Any necessary written/structural changes will be made through a revision of the SOP for that activity (and this QAPP). Field analytical activities will be monitored to determine compliance.

Fixed Laboratory Audit: QAPP deviations and project deficiencies determined during the fixed laboratory assessments will be addressed immediately. Replicates and critical range tables will be checked with data to determine if sources of error exist. Any deviations in results will be addressed in both written and verbal formats, and future sampling will be monitored to verify that compliance is reached.

Data Quality Audit: The NHEP Project QA Officer will review the quality assurance reports provided by each of the agencies. Non-conformances with this QAPP will be compiled. The NHEP Project QA Officer will be responsible for responding to any systemic non-conformances.

C2 – Reports to Management

The reports to management for this project are listed in Table 13.

Table 13: List of Reports to Management

Type of Report	Preparer	Recipient	Schedule
Interim Project Status Report	Project Manager	QAPP distribution list	12/31/07
Data Quality Audit	NHEP QA Officer	QAPP distribution list	6/30/08
Final Report	Project Manager	QAPP Distribution List NHEP Technical Advisory Committee Public via NHEP website	6/30/08

D1 – Data Review, Verification and Validation

The Project Manager will review all monitoring results and evaluate QC requirements for usability in obtaining the objectives of the project based on the criteria established in Section A7.

There are no project-specific algorithms or calculations required to generate definitive water quality data.

D2 – Verification and Validation Procedures

The NHEP QA Officer will be responsible for ensuring that data meet the QC requirements in Section A7. The NHEP QA Officer will prepare a memo for the Project Manager which describes the data submittal, any non-conformances with the QAPP, and any data that did not pass the QC requirements. The Project Manager will undertake any of the following corrective actions, as necessary, if unacceptable results exist.

1. Incomplete data: Omissions from logs, notebooks and worksheets place the entire analysis in question. The Project Manager will consult with the field crews and the NHEP QA Officer to determine an appropriate response. Incomplete field sampling data may require re-sampling of the questionable location.

2. Conflicting or poor quality data: When results do not meet the prescribed quality control (QC) goals, the available data will be reviewed by the Project Manager and the NHEP QA Officer. Upon examination, all or some of the following actions may be applied:
    a. Systems audit for analyte in question,
    b. Determination of matrix interference,
    c. Re-sampling of the questionable sample,
    d. Reconsideration of acceptable limits with statements explaining the results of the action/rationale taken,
    e. Rejection of data and exclusion from the report with written explanation, and/or
    f. Rejection of the entire sample/site location with recommendation for relocation of sample site or reconsideration of results.

If the Project Manager determines that any data are invalid, the invalid results will be flagged as "Not Valid" in the EMD in order to communicate this determination to all data users or deleted from the dataset altogether.

D3 – Reconciliation with User Requirements

If the project objectives from Section A7 are met, the user requirements have been met. If the project objectives have not been met, corrective action as discussed in D2 will be taken by the Project Manager. The overall reconciliation with user requirements will be documented in the technical memorandum written after the conclusion of the project.

References

Dierssen HM et al (2003) Ocean color remote sensing of seagrass and bathymetry in the Bahamas Banks by high-resolution airborne imagery. *Limnol. Oceanogr.,* 48(1, part 2), 2003, 444–455

IOCCG (2000) Remote Sensing of Ocean Color in Coastal, and Other Optically-Complex Waters. International Ocean Color Coordinating Group, Report #3. Edited by Shubha Sathyendranath, pp. 140. Available at: http://www.ioccg.org/reports_ioccg.html

Mitchell, B. G. et al (2000) Determination of spectral absorption coefficients of particles, dissolved material and phytoplankton for discrete water samples. *In* G. S. Fargion and J. L. Mueller [eds.], Ocean optics protocols for satellite ocean color sensor validation, revision 2, NASA Technical Memoradum, 2000-209966. NASA.

Mobley, C. D. (1994) Light and water: radiative transfer in natural waters. Academic Press, Inc.

NHEP (2004) Monitoring Plan. New Hampshire Estuaries Project, University of New Hampshire, Durham, NH. June 30, 2004. Available at: www.nhep.unh.edu/resources/pdf/nhepmonitoringplan-nhep-04.pdf

NHEP (2006) State of the Estuaries Report. New Hampshire Estuaries Project, University of New Hampshire, Durham, NH. June 30, 2004. Available at: www.nhep.unh.edu/resources/pdf/2006_state_of_the-nhep-06.pdf

Sugumaran R et al (2005) Hyperspectral Remote Sensing and Geographical Information Systems Tools to Assess Water Quality in Coastal Areas and Shallow Inland Lakes. University of Northern Iowa and NASA Kennedy Space Center, Iowa Space Grant Final Technical Report. January 2005. Available at: cosmos.ssol.iastate.edu/isgc/RES_INF/VRR2004/Sugu-COOP.pdf

UNH (2006) June 2006 Great Bay Sampling Report. UNH Coastal Ocean Observing Center, University of New Hampshire, Durham, NH. Available at: http://ccg.sr.unh.edu/pdf/June_2006_Great_Bay_Sampling_Report.pdf

UNH (2005) Great Bay Sampling Methods. UNH Coastal Ocean Observing Center, University of New Hampshire, Durham, NH. Available at: http://ccg.sr.unh.edu/pdf/Great_Bay_Methods_Report.pdf

Appendix A

QAPP for the Water Quality Analysis Lab at the University of New Hampshire, Department of Natural Resources, Durham, NH.

I. Laboratory Organization and Responsibility

Dr. William H. McDowell - Director

Jeffrey Merriam – Lab Manager/QA manager. Mr. Merriam supervises all activities in the lab. His responsibilities include data processing and review (QA review), database management, protocol development and upkeep, training of new users, instrument maintenance and repair, and sample analysis.

Jody Potter – Lab Technician. Mr. Potter's responsibilities include sample analysis, logging of incoming samples, sample preparation (filtering when appropriate), daily instrument inspection and minor maintenance.

All analyses are completed by Jody Potter or Jeffrey Merriam, and all data from each sample analysis batch (generally 40-55 samples) is reviewed by Jeffrey Merriam for QC compliance. All users are trained by the lab manager and must demonstrate (through close supervision and inspection) proficiency with the analytical instrumentation used and required laboratory procedures.

II. Standard Operating Procedures

Standard Operating Procedures for all instruments and methods are kept in a 3-ring binder in the laboratory, and are stored electronically on the Lab manager's computer. The electronic versions are password protected. SOPs are reviewed annually, or as changes are required due to new instrumentation or method development.

III. Field Sampling Protocols

Sample collection procedures are generally left up to the sample originators, however we recommend the guidelines described below, and provide our field filtering protocol on request.

All samples are filtered in the field through 0.7 um precombusted (5+ hours at 450 C) glass fiber filters (e.g. Whatman GF/F). Samples are collected in acid-washed 60-mL HDPE bottles. We prefer plastic to glass as our preservative technique is to freeze. Sample containers are rinsed 3 times with filtered sample, and the bottle is filled with filtered sample. Samples are stored in the dark and as cool as possible until they can be frozen. Samples must be frozen within 8 hours of sample collection. Once frozen, samples can be stored indefinitely (Avanzino and Kennedy, 1993), although they are typically analyzed within a few months.

After collection and freezing, samples are either hand delivered to the lab, or are shipped via an over-night carrier. Samples arriving in the lab are inspected for frozen contents, broken caps, cracked bottles, illegible labels, etc. Any pertinent information is entered into a password protected database (MS Access).

We do not require chain of custody paperwork unless a specific project requires it. If a project requires chain of custody, forms are provided by the specific project's manager.

IV. Laboratory Sample Handling Procedures

Samples are given a unique 5-digit code. This code and sample information including name, collection date, time (if applicable), project name, collector, logger, the

date received at the WQAL, sample type (e.g. groundwater, surface water, soil solution) and any other miscellaneous information, are entered into a password protected database. From this point through the completion of all analyses, we use the log number to track samples. Log numbers are used on sample run queues, spreadsheets, and when importing concentrations and run information into the database

After samples are logged into the WQAL, they are stored frozen in dedicated sample freezers located in the laboratory. Samples from different projects are kept separated in cardboard box-tops, or in plastic bags. Samples that may pose a contamination threat (based on the source or presumed concentration range) are further isolated by multiple plastic bags, or isolation in separate freezer space. This is typically not an issue as we primarily deal with uncontaminated samples.

We do not pay special attention to holding time of samples, as frozen samples are stable indefinitely (Avanzino and Kennedy, 1993). However, we do keep track of the date samples arrive at the WQAL, and can report holding times if necessary. After samples are analyzed they are returned to the project's manager for safe keeping or they are held for a period of time at the WQAL to allow necessary review and analysis of the data by the interested parties (not from a laboratory QC sense, but from a project specific viewpoint). Once the data is analyzed by the project's manager(s), the samples are returned or disposed of, based on the preference of the project's manager.

Chain of custody is only implemented when required by a specific project. This is usually only when it's required by the funding agency, or if the samples could be the basis for an enforcement action.

Samples that arrive unfrozen, with cracked bottles/caps, or with loose caps, are noted in the database and are not analyzed. These samples are disposed of to prevent accidental analysis. The sample originator is notified (generally via e-mail) of which samples were removed from the sample analysis stream. Similarly, if while in the possession of the WQAL, a sample bottle is broken or improperly stored (e.g. not frozen), the sample is removed and the sample originator is notified.

V. Calibration procedures for chemistry

Calibration curves are generally linear, and are made up of 4-7 points. A full calibration is performed at the beginning of each run (a run is generally 40-60 samples) with a reduced calibration (3-5 points) performed at the end of the run. Occasionally calibration data is best fit with a quadratic equation, and this is used if it best describes the data within a specific run.

Standards are made from reagent grade chemicals (typically JT Baker) that have been dried and are stored in a dessicator. Working stock solutions are labeled with the content description, concentration, initials of the maker, and the date the stock solution was made. Generally stock solutions are kept less than one week; however some stocks (Br, Na, Cl, C for DOC) can be stored for several months. Standard solutions are kept for less than one week from the date they were made. Stocks and standards are stored tightly covered, in a dark refrigerator.

Control charts are prepared and printed every few months. However data from each run are looked at within days of analyses. Calibration curves, Laboratory Duplicates, Lab Fortified Blanks (LFB), Lab Fortified Sample Matrices (LFM) and Lab

Reagent Blanks (LRB) are reviewed and are checked against known concentrations (where applicable) to ensure QC criteria are met for each run of samples.

VI. Data Reduction, validation, reporting and verification

Data reduction and validation are performed in a spreadsheet (MS Excel). The Raw data page of the spreadsheet lists the date of analysis, user, analysis performed, project, any issues or problems noted with the instrument on that date, and the sample queue and the raw data exported from the instruments. Most raw data is exported as an area or an absorbance value. A second page (typically named “Calculations”) is added to the spreadsheet where known concentrations of standards, check standards and reference solutions are added. The calibration curve(s) is calculated and the concentrations are calculated on this page. Calculated concentrations for all standards, LFB, LFM and IPC are compared to the “known” or prepared values. If these are acceptably close (+/- 10% of the “known”) no further changes to the calculated concentrations are made. If there is evidence of drift in the response of the instrument during a run, we try to correct for the drift using the responses from the front end calibration curve and the set of standards analyzed at the end of the run. All reference solutions and replicates must meet certain QC criteria (described below) for a run to be accepted.

Data are then exported to the WQAL database. Exported information includes the unique 5-digit code, calculated concentration, the analysis date, the user, the filename the raw data and calculations are saved in, and any notes from the run regarding the specific sample. Data are sent to sample originators upon completion of all requested sample analyses and following review by the WQAL lab manager. Generally the data include

the 5-digit code, the sample name, collection date, and concentrations, in row-column format. Any information entered into the database can be included upon request. Data transfer is typically via e-mail or electronic medium (CD or floppy disk).

All data corrections are handled by the lab manager. Corrections to data already entered into the database are very infrequent. Typically they involve reanalysis of a sample. In this case, the old data is deleted from the database, and the new value is imported, along with a note indicating that it was re-analyzed, the dates of initial and secondary analysis and the reason for the correction.

Hand written or computer printed run sheets are saved for each run and filed, based on the project and the analysis. Spreadsheet files with raw data and calculations are stored electronically by analysis and date. Information in the database allows easy cross-reference and access from individual samples to the raw data and the runsheets. This provides a complete data trail from sample log-in to completion of analysis.

VII. Quality Control

All analyses conducted at the WQAL follow approved or widely accepted methods (Table 1).

Quality Control Samples (QCS) (from Ultra Scientific) are analyzed periodically (approximately every 20 samples) in each sample analysis batch to assure accuracy. The response/unit concentration is also used to monitor day-to-day variation in instrument performance. A difference from the certified concentration of more than 10% requires further investigation of that run. A difference greater than 15% is failure (unless the average of the two samples is less than 10X the MDL), and results in re-analysis of the

entire sample queue, unless there is a very reasonable and supported explanation for the inconsistency. Table 2 lists historical average % recoveries. At least 2 QCS are analyzed on each run.

Standards and reagents are prepared from reagent grade chemicals (typically JT Baker) or from pre-made stock solutions. All glassware is acid washed (10% HCl) and rinsed 6 times with ultra pure-low DOC water (18.2 mega-ohm). All analyses (except CHN) use multi-point calibration curves (4-7) points, which are analyzed at the beginning and the end of each run. A Laboratory Reagent Blank (LRB), Laboratory Fortified Blank (LFB) (a standard run as a sample) and Laboratory Duplicate are analyzed every 10 to 15 samples during each run. At least one Laboratory Fortified Sample Matrix (LFM) is analyzed during each run to insure that sample matrices do not affect method analysis efficiency. Field Duplicates are not required by our lab, and are the responsibility of the specific project's manager.

Laboratory Duplicates must fall within 15% relative percent difference (RPD = abs(dup1-dup2)/average of dup1 and dup 2). A difference greater than 10% requires further investigation of the sample run. A difference greater than 15% is failure (unless the average of the two samples is less than 10X the MDL), and results in re-analysis of the entire sample queue, unless there is a very reasonable and supported explanation for the inconsistency. Long-term averages for relative % difference are included in Table 2.

LFM must show 85% to 115% recovery. A recovery <90% or > 110% requires further investigation of the sample run. A recovery <85% or >115% is failure (unless the sample is less than 10X the MDL), and results in re-analysis of the entire sample queue,

unless there is a very reasonable and supported explanation for the inconsistency. Long-term averages for % recovery are included in Table 2.

Method Detection Limits are calculated at least twice per year, or whenever major changes to instrumentation or methods occur. Table 2 lists most recently measured MDL values.

VIII. Schedule of Internal Audits

Internal audits are not routinely performed, however, review of QC charts, and tables are done at least quarterly by the lab manager.

IX. Preventive maintenance procedures and schedules

The laboratory manager, Jeff Merriam, has 10 years of experience and is highly experienced with all laboratory equipment used within the WQAL. The laboratory manager conducts all maintenance and inspection of equipment based on manufacturer requirements and specifications.

Each day an instrument is used, it receives a general inspection for obvious problems (e.g. worn tubing, syringe plunger tips, leaks). The instruments are used frequently and data is inspected within a few days of sample analysis. This allows instrument (or user) malfunctions to be caught quickly, and corrected as needed.

Each day's run is recorded in the instrument's run log, with the date, the user, the number of injections (standards, samples, and QC samples), the project, and other notes of interests. Maintenance, routine or otherwise, is recorded in the instrument run log, and

includes the date, the person doing the maintenance, what was fixed, and any other notes of interest.

X. Corrective Action Contingencies

Jeffrey Merriam is responsible for all QC checks and performs or supervises all maintenance and troubleshooting. When unacceptable results are obtained (based on within sample analysis batch QC checks) the data from the run are NOT imported into the database. The cause of the problem is determined and corrected, and the samples are re-analyzed. Problems are recorded in the sample queue's data spreadsheet, or on the handwritten runsheet associated with the run. Corrective actions (instrument maintenance and troubleshooting) are documented in each instrument's run log.

XI. Record Keeping Procedures

Protocols, Instrument Logs, QC charts, databases and all raw data files are kept on the lab manager's computer. These are backed up weekly, with the back up stored off site. The computer is password protected, and is only used by the lab manager. Protocols and the sample database are also password protected. Handwritten run sheets are stored in a filing cabinet in the lab. Instrument run and maintenance logs are combined with the QC data to form one large Excel file where instrument performance can easily be compared to instrument repair and the number of analyses, etc. This file is also stored on the lab manager's computer and is password protected.

All information pertinent to a sample is stored in the sample database. From this database we can easily determine the date of analysis and the location of the raw data file

if further review is necessary. The amount of information provided to sample originators is dependent on what is required by the project or funding agencies.

Table 1. List of standard operating procedures and description of analyses done at the Water Quality Analysis Laboratory.

Standard Operating Procedure	Analysis	Instrument Used	Description	Protocol Latest Revision	EPA method or other reference
Ion Chromatography Protocol for Anions and Cations Protocol	Anions and Cations	Ion Chromatograph Ion Chromatograph	Anions via ion chromatography w/ suppressed conductivity. Cations via ion chromatography and conductivity	June 11, 2002	Anions EPA #300.1
Dissolved Organic Carbon Protocol	DOC	Shimadzu TOC 5000 with autosampler	High Temperature Catalytic Oxidation (HTCO)	June 25, 2002	EPA 415.1
Total Dissolved Nitrogen Protocol	TDN	Shimadzu TOC 5000 coupled with an Antek 720 N detector	HTCO with chemiluminescent N detection	June 25, 2002	Merriam et al, 1996
DOC and TDN combined Protocol	DOC and TDN	Shimadzu TOC-V with TNM nitrogen module	HTCO with chemiluminescent N detection	June 25, 2002	EPA 415.1 and Merriam et al, 1996
Lachat QuikChem AE Protocol	Nitrate/Nitrite colorimetric NO_3/NO_2	Lachat QuikChem AE	Automated Cd-Cu reduction	June 25, 2002	EPA 353.2
	Ammonium colorimetric NH_4	Lachat QuikChem AE	Automated Phenate	June 25, 2002	EPA 350.1
	Soluble reactive Phosphorous colorimetric PO_4	Lachat QuikChem AE	Automated Ascorbic acid	June 25, 2002	EPA 365
Acid Washing Protocol	Glass and plastic-ware cleaning		10% HCl rinse and 6 rinses with DDW	June 25, 2002	
Field Filtering Protocol	Sample prep		3-times rinse with filtered sample	June 25, 2002	

Table 2. Detection limits, acceptable ranges, and recent historical averages for QC samples at the Water Quality Analysis Lab.

[1] Detection limit based on user experience and previous analysis (not statistically calculated). [2] Method Detection Limit (MDL) is the minimum concentration of a substance that can be measured and reported with 99% confidence that the analyte concentration is greater than zero.

Analyte	Units	Typical Range	Regression Type	# of Cal. Points	Detection Limit [1]	MDL [2]	Lab Duplicate % Relative Difference	Limit	LFM % recovery	Limit +/-	IPC % recovery	Limit +/-
SiO_2	mg SiO2/L	0 – 40	Linear	4-7	0.3		3.5	15.0	92.8	15.0		
PO_4	µg P/L	0 – 200	Linear	4-7	2 – 3	1.5	7.8	15.0	95.5	15.0	93.7	15.0
NH_4	µg N/L	0 – 200	Linear	4-7	2 – 3	1.5	7.1	15.0	103.9	15.0	95.0	15.0
NO_3 FIA	mg N/L	0 – 10	Linear	4-7	0.05	0.003	4.6	15.0	100.9	15.0	102.6	15.0
Na^+	mg Na/L	0 – 15	Quadratic	4-7	0.1		0.9	15.0			112.7	
K^+	mg K/L	0 – 7	Quadratic	4-7	0.05		10.4	15.0			97.8	
Mg^{2+}	mg Mg/L	0 – 7	Quadratic	4-7	0.1		4.5	15.0			89.7	
Ca^{2+}	mg Ca/L	0 – 10	Quadratic	4-7	0.1		4.0	15.0			98.2	
Cl^-	mg Cl/L	0 – 15	Quadratic	4-7	0.2	0.02	1.6	15.0			92.7	
NO_3^-	mg N/L	0 – 3	Quadratic	4-7	0.002	0.002	0.3	15.0			96.3	
SO_4^{2-}	mg S/L	0 – 8	Quadratic	4-7	0.1	0.04	2.2	15.0			86.5	
TDN	mg N/L	0 – 10	Linear	4-7	0.1	0.029	7.8	15.0	100.3	15.0	102.1	15.0
DOC	mg C/L	0 – 20	Linear	4-7	0.1	0.048	4.9	15.0	100.5	15.0	97.0	15.0

References

Avanzino R.J. and V.C. Kennedy, 1993. Long-term frozen storage of stream water samples for dissolved orthophosphate, nitrate plus nitrite, and ammonia analysis. *Water Resources Research*, 29(10) 3357-3362.

Merriam, J.L, W.H. McDowell, W.S. Currie, 1996. A high-temperature catalytic oxidation technique for determining total dissolved nitrogen. *Soil Science Society of America Journal*, 60(4) 1050-1055.

Appendix B

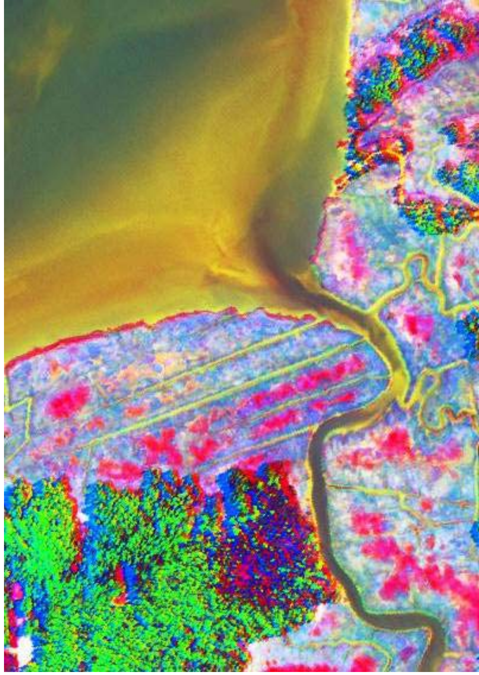

SpecTIR VNIR Sensor

Sensor head	Typical specifications			
Spectrograph	High efficiency imaging spectrograph. Smile and keystone < 2 microns. F/2.4			
Spectral range	400 – 990 nm			
Spectral resolution	2.3 – 20 nm*			
Slit width	30 microns			
# of spectral bands	1 – 256*			
Operating modes	Hyperspectral and multispectral			
Spectral sampling : bands	2.3nm : 256	4.6nm : 128	9.2nm : 64	18.4nm : 32
Image rate	4 – 100 Hz*			
Spatial swath (pixels)	960 pixels			
Fore optics options				
Focal length	23 mm	18.5 mm	9 mm	
FOV	29.9 degrees	37.7 degrees	63 degrees	
IFOV	0.029 degrees	0.037 degrees	0.062 degrees	
Swath width	0.53 x altitude	0.68 x altitude	1.22 x altitude	
Ground resolution @ 1,000 m altitude	0.52 m	0.67 m	1.2 m	
Camera	Progressive scan CCD camera			
Output	12 bits digital			
Integration time	Selectable independent of image rate			
Shutter	Electromechanical shutter for dark background registration, user controllable by software.			

*User selectable on the fly

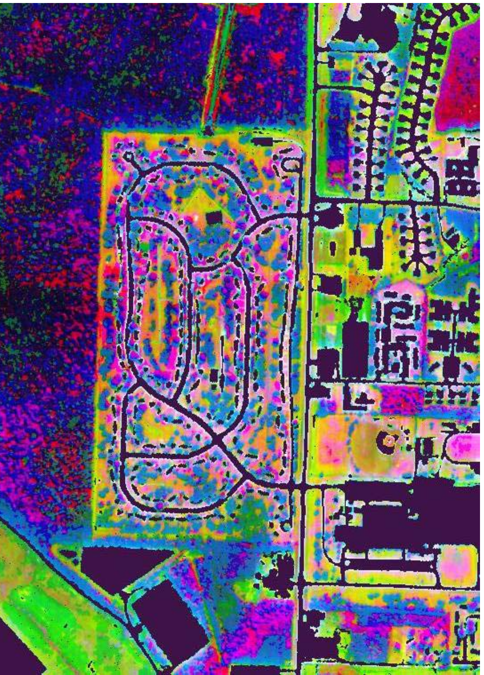

1320 Freeport Blvd.
Suite 106
Sparks, NV 89431
(775) 329-6660
FAX (775) 329-6668
Conrad@SpecTIR.com

8626 Brooks Drive
Suite 103
Easton, MD 21601
(410) 820-5001
www.spectir.com
WBernard@SpecTIR.com

WWW.SpecTIR.com

Appendix C

NASA/TM-2003-211621/Rev4-Vol.IV

Ocean Optics Protocols For Satellite Ocean Color Sensor Validation, Revision 4, Volume IV:

Inherent Optical Properties: Instruments, Characterizations, Field Measurements and Data Analysis Protocols

James L. Mueller, Giulietta S. Fargion and Charles R. McClain, Editors

Scott Pegau, J.Ronald V. Zaneveld, B. Gregg Mitchell, James L. Mueller, Mati Kahru, John Wieland and Malgorzat Stramska, Authors

National Aeronautical and
Space administration

Goddard Space Flight Space Center
Greenbelt, Maryland 20771

May 2002

NASA/TM-2003-211621/Rev4-Vol.IV

Ocean Optics Protocols For Satellite Ocean Color Sensor Validation, Revision 4, Volume IV:

Inherent Optical Properties: Instruments, Characterizations, Field Measurements and Data Analysis Protocols

J. L. Mueller
CHORS, San Diego State University, San Diego, California
Giulietta S. Fargion
Science ApplicationsInternational Corp., Beltsville, Maryland
Charles R. McClain
NASA Goddard Space Flight Center, Greenbelt, Maryland
Scott Pegau and J. Ronald V. Zaneveld
COAS, Oregon State University, Corvallis
B. Gregg Mitchell, Mati Kahru, John Wieland and Malgorzat Stramska
Scripps Institution of Oceanography, University of California San Diego, California

National Aeronautical and
Space administration

Goddard Space Flight Space Center
Greenbelt, Maryland 20771

May 2003

Preface

This document stipulates protocols for measuring bio-optical and radiometric data for the Sensor Intercomparison and Merger for Biological and Interdisciplinary Oceanic Studies (SIMBIOS) Project activities and algorithm development. The document is organized into 7 separate volumes as:

Ocean Optics Protocols for Satellite Ocean Color Sensor Validation, Revision 4

Volume I: Introduction, Background and Conventions
Volume II: Instrument Specifications, Characterization and Calibration
Volume III: Radiometric Measurements and Data Analysis Methods
Volume IV: Inherent Optical Properties: Instruments, Characterization, Field Measurements and Data Analysis Protocols
Volume V: Biogeochemical and Bio-Optical Measurements and Data Analysis Methods
Volume VI: Special Topics in Ocean Optics Protocols

The earlier version of *Ocean Optics Protocols for Satellite Ocean Color Sensor Validation*, *Revision 3* (Mueller and Fargion 2002, Volumes 1 and 2) is entirely superseded by the seven Volumes of Revision 4 listed above.

The new multi-volume format for publishing the ocean optics protocols is intended to allow timely future revisions to be made reflecting important evolution of instruments and methods in some areas, without reissuing the entire document. Over the years, as existing protocols were revised, or expanded for clarification, and new protocol topics were added, the ocean optics protocol document has grown from 45pp (Mueller and Austin 1992) to 308pp in Revision 3 (Mueller and Fargion 2002). This rate of growth continues in Revision 4. The writing and editorial tasks needed to publish each revised version of the protocol manual as a single document has become progressively more difficult as its size increases. Chapters that change but little, must nevertheless be rewritten for each revision to reflect relatively minor changes in, *e.g*., cross-referencing and to maintain self-contained consistency in the protocol manual. More critically, as it grows bigger, the book becomes more difficult to use by its intended audience. A massive new protocol manual is difficult for a reader to peruse thoroughly enough to stay current with and apply important new material and revisions it may contain. Many people simply find it too time consuming to keep up with changing protocols presented in this format - which may explain why some relatively recent technical reports and journal articles cite Mueller and Austin (1995), rather than the then current, more correct protocol document. It is hoped that the new format will improve community access to current protocols by stabilizing those volumes and chapters that do not change significantly over periods of several years, and introducing most new major revisions as new chapters to be added to an existing volume without revision of its previous contents.

The relationships between the Revision 4 chapters of each protocol volume and those of Revision 3 (Mueller and Fargion 2002), and the topics new chapters, are briefly summarized below:

Volume I: This volume covers perspectives on ocean color research and validation (Chapter 1), fundamental definitions, terminology, relationships and conventions used throughout the protocol document (Chapter 2), requirements for specific *in situ* observations (Chapter 3), and general protocols for field measurements, metadata, logbooks, sampling strategies, and data archival (Chapter 4). Chapters 1, 2 and 3 of Volume I correspond directly to Chapters 1, 2 and 3 of Revision 3 with no substantive changes. Two new variables, Particulate Organic Carbon (POC) and Particle Size Distribution (PSD) have been added to Tables 3.1 and 3.2 and the related discussion in Section 3.4; protocols covering these measurements will be added in a subsequent revision to Volume V (see below). Chapter 4 of Volume I combines material from Chapter 9 of Revision 3 with a brief summary of SeaBASS policy and archival requirements (detailed SeaBASS information in Chapter 18 and Appendix B of Revision 3 has been separated from the optics protocols).

Volume II: The chapters of this volume review instrument performance characteristics required for *in situ* observations to support validation (Chapter 1), detailed instrument specifications and underlying rationale (Chapter 2) and protocols for instrument calibration and characterization standards and methods (Chapters 3 through 5). Chapters 1 through 5 of Volume II correspond directly to Revision 3 chapters 4 through 8, respectively, with only minor modifications.

Volume III: The chapters of this volume briefly review methods used in the field to make the *in situ* radiometric measurements for ocean color validation, together with methods of analyzing the data (Chapter 1), detailed measurement and data analysis protocols for in-water radiometric profiles (Chapter 2), above water measurements of remote sensing reflectance (Chapter III-3), determinations of exact normalized water-leaving radiance (Chapter 4), and atmospheric radiometric measurements to determine aerosol optical thickness and sky radiance distributions (Chapter 5). Chapter 1 is adapted from relevant portions of Chapter 9 in Revision 3. Chapter 2 of Volume III corresponds to Chapter 10 of Revision 3, and Chapters 3 through 5 to Revision 3 Chapters 12 through 14, respectively. Aside from reorganization, there are no changes in the protocols presented in this volume.

Volume IV: This volume includes a chapter reviewing the scope of inherent optical properties (IOP) measurements (Chapter 1), followed by 4 chapters giving detailed calibration, measurement and analysis protocols for the beam attenuation coefficient (Chapter 2), the volume absorption coefficient measured *in situ* (Chapter 3), laboratory measurements of the volume absorption coefficients from discrete filtered seawater samples (Chapter 4), and *in situ* measurements of the volume scattering function, including determinations of the backscattering coefficient (Chapter 5). Chapter 4 of Volume IV is a slightly revised version of Chapter 15 in Revision 3, while the remaining chapters of this volume are entirely new contributions to the ocean optics protocols. These new chapters may be significantly revised in the future, given the rapidly developing state-of-the-art in IOP measurement instruments and methods.

Volume V: The overview chapter (Chapter 1) briefly reviews biogeochemical and bio-optical measurements, and points to literature covering methods for measuring these variables; some of the material in this overview is drawn from Chapter 9 of Revision 3. Detailed protocols for HPLC measurement of phytoplankton pigment concentrations are given in Chapter 2, which differs from Chapter 16 of Revision 3 only by its specification of a new solvent program. Chapter 3 gives protocols for Fluorometric measurement of chlorophyll *a* concentration, and is not significantly changed from Chapter 17of Revision 3. New chapters covering protocols for measuring, Phycoerythrin concentrations, Particle Size Distribution (PSD) and Particulate Organic Carbon (POC) concentrations are likely future additions to this volume.

Volume VI: This volume gathers chapters covering more specialized topics in the ocean optics protocols. Chapter 1 introduces these special topics in the context of the overall protocols. Chapter 2 is a reformatted, but otherwise unchanged, version of Chapter 11 in Revision 3 describing specialized protocols used for radiometric measurements associated with the Marine Optical Buoy (MOBY) ocean color vicarious calibration observatory. The remaining chapters are new in Revision 4 and cover protocols for radiometric and bio-optical measurements from moored and drifting buoys (Chapter 3), ocean color measurements from aircraft (Chapter 4), and methods and results using LASER sources for stray-light characterization and correction of the MOBY spectrographs (Chapter 5). In the next few years, it is likely that most new additions to the protocols will appear as chapters added to this volume.

Volume VI: also collects appendices of useful information. Appendix A is an updated version of Appendix A in Revision 3 summarizing characteristics of past, present and future satellite ocean color missions. Appendix B is the List of Acronyms used in the report and is an updated version of Appenix C in Revision 3. Similarly, Appendix C, the list of Frequently Used Symbols, is an updated version of Appendix D from Rev. 3. The SeaBASS file format information given in Appendix B of Revision 3 has been removed from the protocols and is promulgated separately by the SIMBIOS Project.

In the Revision 4 multi-volume format of the ocean optics protocols, Volumes I, II and III are unlikely to require significant changes for several years. The chapters of Volume IV may require near term revisions to reflect the rapidly evolving state-of-the-art in measurements of inherent optical properties, particularly concerning instruments and methods for measuring the Volume Scattering Function of seawater. It is anticipated that new chapters will be also be added to Volumes V and VI in Revision 5 (2003).

This technical report is not meant as a substitute for scientific literature. Instead, it will provide a ready and responsive vehicle for the multitude of technical reports issued by an operational Project. The contributions are published as submitted, after only minor editing to correct obvious grammatical or clerical errors.

Table of Contents

Chapter 1

Inherent Optical Property Measurement Concepts: Physical Principles and Instruments

Scott Pegau[1], J. Ronald V. Zaneveld[1] and James L. Mueller[2]

[1] *College of Oceanographic and Atmospheric Sciences, Oregon State University, Corvallis*

[2] *Center for Hydro-Optics and Remote Sensing, San Diego State University, California*

1.1 INTRODUCTION

The Inherent Optical Properties (IOP) of a medium, which describe absorption and scattering interactions that modify a vector light field propagating through it, are defined in Vol. I, Ch. 2, Sect. 2.4 of this protocol document. Geometric conventions and notation underlying definitions of, and relationships between IOP and radiative transfer in the medium are described in Section 2.2 of Vol. I, Ch. 2. The roles of the IOP in radiative transfer descriptions and models of light propagation in the sea are also introduced in Vol. I, Ch. 2, and appear elsewhere in many of the Volumes and Chapters of this protocol document.

The chapters of this volume (Vol. IV) describe the conceptual background, instrument characteristics, and methods of calibration, field measurements and data analysis for determining the IOP of seawater. The scope of this protocol volume is limited to practical methods for using commercially available instruments[1] to determine the IOP identified in Vol. I, Chapter 3 (Table 3.1) of *Ocean Optics Protocols for Satellite Ocean Color Sensor Validation, Rev. 4*. The scope of the present volume does not include applications of measured IOP to aspects of ocean color sensor validation that are described elsewhere in the document. The role of IOP in the determination of *Exact Normalized Water-Leaving Radiance* $L_{\mathrm{WN}}^{\mathrm{ex}}(\lambda)$ as a function of wavelength λ, for example, is discussed in Vol. III, Chapter 4.

In this chapter we extend the IOP definitions and relationships of Vol. I, Ch. 2 to develop the theoretical and mathematical bases for practical instrument concepts and methods for measuring IOP in seawater. Instruments will be described to measure, *in situ* at depth *z*, the beam attenuation coefficient $c(z,\lambda)$, the volume absorption coefficient $a(z,\lambda)$, and the volume scattering function (VSF) $\beta(z,\lambda,\psi)$ at one or more scattering angles ψ. Spectrophotometric laboratory methods are also described in detail for determining absorption coefficients from filtered, discrete water samples. Methods of data analysis are described to determine, from combinations of these measurements, the volume scattering coefficient $b(z,\lambda)$ and backscattering coefficient $b_{\mathrm{b}}(z,\lambda)$.

We do not consider instrument concepts or methods for measuring either fluorescence, or Raman scattering, in Vol. IV. Even though the Raman and fluorescence cross-sections of water, suspended particles and dissolved materials are also IOP of seawater, ***only elastic scattering processes*** are considered in this volume.

In the remainder of Vol. IV, we will ordinarily omit the explicit notation identifying IOP variables as functions of depth *z* in the water column. This is partly a desire for simplifying the notation, but the more important motive is to avoid confusing global coordinates (geographic location and vertical depth in the water column) with local coordinates (optical axes and normal planes) used to describe photon-matter interactions and measurement concepts.

---

[1] Certain commercial equipment, instruments, or materials are identified in this chapter to foster understanding. Such identification does not imply recommendation, or endorsement, by the National Aeronautics and Space Administration, nor does it imply that the materials or equipment identified are necessarily the best available for the purpose.

1.2 ABSORPTION AND SCATTERING PROPERTIES OF WATER, PARTICLES AND DISSOLVED SUBSTANCES

Because the IOP are additive (Vol. I, Ch. 2, Sect. 2.4), the absorption and scattering properties of natural water consists of the sums of these IOP of pure water, suspended particles, dissolved substances and turbulence. It is very difficult to experimentally determine the absorption of pure water in the laboratory, due principally to the difficulty of making and maintaining pure water during the course of an experiment. Nevertheless, there have been several successful experiments (several are cited below), over the past few decades, and the spectral absorption and scattering coefficients of pure water are reasonably well known. Using this information, several types of IOP instruments are calibrated by measuring their responses using pure water as an "optical standard". Thus, the calibrated responses of these instruments in field measurements represent the IOP of particles and dissolved material, independent of water. IOP.

From another perspective, the general characteristics of absorption and scattering properties vary spectrally, and in the case of scattering angularly, between the different optically important constituents of seawater. The contrast in angular distribution characteristics of scattering by water and by particles can be an important element of instrument design concepts.

Absorption by Pure Water

The spectral values recommended in Vol. I, Ch. 2 (Sect. 2.4) for the volume absorption coefficients of pure water, $a_W(\lambda)$ m^{-1}, are those of Sogandares and Fry (1997) for wavelengths between 340 nm and 380 nm, Pope and Fry (1997) for wavelengths between 380 nm and 700 nm, and Smith and Baker (1981) for wavelengths between 700 nm and 800 nm. Here, for wavelengths > 700 nm we recommend values calculated by Van Zee *et al*. (2002) from the imaginary part of the refractive indices for pure water measured by Kou *et al*. (1993). The composite $a_w(\lambda)$ spectrum derived from these sources is listed in Table 1.1, together with the linear temperature dependency $\frac{\partial a_w(\lambda)}{\partial T}$ $\left[\mathrm{m^{-1}\,{}^\circ C}\right]$ reported by Pegau and Zaneveld (1993) and Pegau *et al*. (1997).

Absorption by Suspended Particulates and Colored Dissolved Organic Material (CDOM)

Variations in the spectral absorption of natural waters result directly from variantions in the concentrations and chemical compositions of material substances distributed within the water volume. These absorbing materials may be present in seawater either in suspended particulates, such as pigment-bearing phytoplankton, or as solutes (*i.e.* CDOM). Fig. 1.1a illustrates qualitative comparisons between the absorption spectrum of pure water, $a_w(\lambda)$ (Table 1.1), a non-dimensional *Chl*-specific absorption spectrum of phytoplankton pigment concentration, $a^*_{chl}(\lambda)$ (Prieur and Sathyendranath 1981), and a typically exponential absorption spectrum of CDOM $a_g(\lambda)$ (Bricaud *et al*. 1981). The amplitude of each absorption spectrum in Fig. 1.1a is arbitrarily scaled to illustrate the characteristic difference in shapes between the constant water background absorption and two varying absorption components associated with *Chl* and CDOM concentrations. The unique shape and magnitude of the specific absorption spectrum for each individual constituent allows measured values of, *e.g.*, *Chl* and CDOM concentrations to be determined from measurements of $a(\lambda)$ at several appropriate wavelengths. The strong inverse depencence of remote sensing reflecance on $a(\lambda)$ (Vol. III, Ch. 4), together with the distinctive shape and magnitude characteristics of the constituents, similarly provides the physical basis for ocean color algorithms for determining their concentrations from satellite measurements of water leaving radiance at several wavelengths.

In Case 1 waters, it is often useful to assume (Gordon and Morel 1983; Morel and Maritorena 2001; Mobley and Sundman 2000) that particle absorption $a_p(\lambda)$ is dominated by phytoplankton pigments and may be expressed as a function of *Chl* concentration [mg m^{-3}] and a Chl-specific absorption spectrum $a^*_{chl}(\lambda)$ (Prieur and Sathyendranath 1981), and that CDOM concentration is correlated with *Chl* so that $a_g(\lambda)$ may also be calculated as

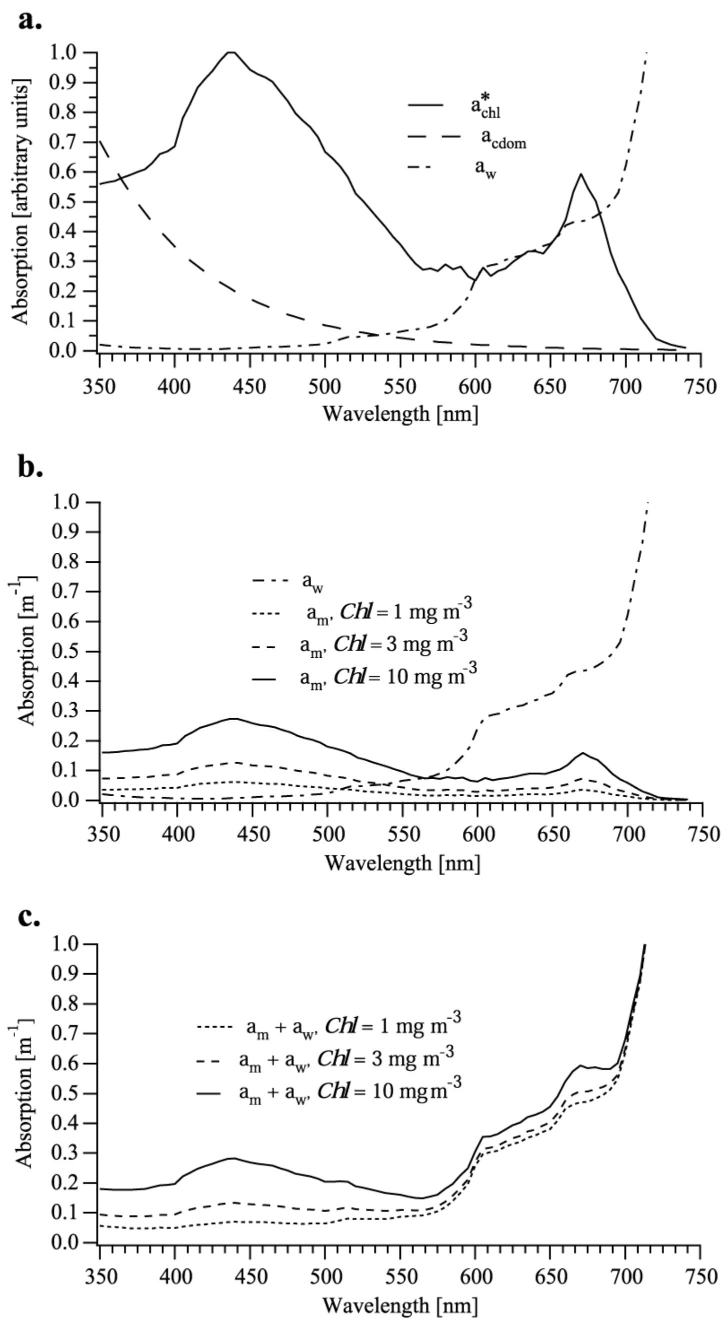

Fig. 1.1: Spectral variations of absorption in seawater. **a:** Qualitative comparison of the shapes of absorption spectra of pure water (Table 1.1), specific absorption by *Chl* (Prieur and Sathyendranath 1981), and CDOM as implemented in the HYDROLIGHT radiative transfer model (Mobley and Sundman 2000) described further by Morel and Maritorena (2001). **b:** Comparisons between $a_{\mathrm{w}}(\lambda)$, the absorption spectrum of pure water, and $a_{\mathrm{m}}(\lambda, Chl)$,the sum of absorption by suspended particles and CDOM for *Chl* concentrations of 1, 3 and 10 mg m^{-3}, following Mobley and Sundman (2000). An absorption meter calibrated relative to pure water would measure $a_{\mathrm{m}}(\lambda; Chl)$. **c:** The sums of pure water and "measured" absorption spectra from panel b.

Table 1.1: Volume absorption and scattering coefficients for pure water, $a_w(\lambda)$ and $b_w(\lambda)$, respectively. Values for $a_w(\lambda)$ are those of Sogandares and Fry (1997) [340 to 390 nm], Pope and Fry (1997) [400 to 700 nm], and Van Zee *et al*. (2002) as derived from Kou *et al*. (1993) [705 to 750 nm]. Alternative values of $b_w(\lambda)$ compared here are denoted (B) (Buitveld, *et al*. 1994) and (M) (Morel 1974). The linear temperature dependence of pure water absorption, $\frac{\partial a_w(\lambda)}{\partial T}$, is due to Pegau and Zaneveld (1993) and Pegau *et al*. (1997).

λ nm	a_w m^{-1}	$\frac{\partial a_w(\lambda)}{\partial T}$ m^{-1} °C	b_w m^{-1} (B)	b_w m^{-1} (M)	λ nm	a_w m^{-1}	$\frac{\partial a_w(\lambda)}{\partial T}$ m^{-1} °C	b_w m^{-1} (B)	b_w m^{-1} (M)	λ nm	a_w m^{-1}	$\frac{\partial a_w(\lambda)}{\partial T}$ m^{-1} °C	b_w m^{-1} (B)	b_w m^{-1} (M)
340	0.0325	0.0000	0.0104	0.0118	500	0.0242	0.0001	0.0021	0.0022	630	0.3184	0.0002	0.0008	0.0009
350	0.0204	0.0000	0.0092	0.0103	505	0.0300	0.0001	0.0020		635	0.3309	0.0000	0.0008	
360	0.0156	0.0000	0.0082	0.0091	510	0.0382	0.0002	0.0019	0.0020	640	0.3382	-0.0001	0.0008	0.0008
370	0.0114	0.0000	0.0073	0.0081	515	0.0462	0.0002	0.0018		645	0.3513	0.0000	0.0007	
380	0.0100	0.0000	0.0065	0.0072	520	0.0474	0.0002	0.0018	0.0019	650	0.3594	0.0001	0.0007	0.0007
390	0.0088	0.0000	0.0059	0.0065	525	0.0485	0.0002	0.0017		655	0.3852	0.0002	0.0007	
400	0.0070	0.0000	0.0053	0.0058	530	0.0505	0.0001	0.0017	0.0017	660	0.4212	0.0002	0.0007	0.0007
405	0.0060	0.0000	0.0050		535	0.0527	0.0001	0.0016		665	0.4311	0.0002	0.0006	
410	0.0056	0.0000	0.0048	0.0052	540	0.0551	0.0001	0.0015	0.0016	670	0.4346	0.0002	0.0006	0.0007
415	0.0052	0.0000	0.0045		545	0.0594	0.0001	0.0015		675	0.4390	0.0001	0.0006	
420	0.0054	0.0000	0.0043	0.0047	550	0.0654	0.0001	0.0014	0.0015	680	0.4524	0.0000	0.0006	0.0006
425	0.0061	0.0000	0.0041		555	0.0690	0.0001	0.0014		685	0.4690	-0.0001	0.0006	
430	0.0064	0.0000	0.0039	0.0042	560	0.0715	0.0001	0.0013	0.0014	690	0.4929	-0.0002	0.0006	0.0006
435	0.0069	0.0000	0.0037		565	0.0743	0.0001	0.0013		695	0.5305	-0.0001	0.0005	
440	0.0083	0.0000	0.0036	0.0038	570	0.0804	0.0001	0.0012	0.0013	700	0.6229	0.0002	0.0005	0.0005
445	0.0095	0.0000	0.0034		575	0.0890	0.0002	0.0012		705	0.7522	0.0007	0.0005	
450	0.0110	0.0000	0.0033	0.0035	580	0.1016	0.0003	0.0011	0.0012	710	0.8655	0.0016	0.0005	0.0005
455	0.0120	0.0000	0.0031		585	0.1235	0.0005	0.0011		715	1.0492	0.0029	0.0005	
460	0.0122	0.0000	0.0030	0.0031	590	0.1487	0.0006	0.0011	0.0011	720	1.2690	0.0045	0.0005	0.0005
465	0.0125	0.0000	0.0028		595	0.1818	0.0008	0.0010		725	1.5253	0.0065	0.0004	
470	0.0130	0.0000	0.0027	0.0029	600	0.2417	0.0010	0.0010	0.0011	730	1.9624	0.0087	0.0004	0.0005
475	0.0143	0.0000	0.0026		605	0.2795	0.0011	0.0010		735	2.5304	0.0108	0.0004	
480	0.0157	0.0000	0.0025	0.0026	610	0.2876	0.0011	0.0009	0.0010	740	2.7680	0.0122	0.0004	0.0004
485	0.0168	0.0000	0.0024		615	0.2916	0.0010	0.0009		745	2.8338	0.0119	0.0004	
490	0.0185	0.0000	0.0023	0.0024	620	0.3047	0.0008	0.0009	0.0009	750	2.8484	0.0106	0.0004	0.0004
495	0.0213	0.0001	0.0022		625	0.3135	0.0005	0.0008						

an exponential function of wavelength (Bricaud *et al*. 1981) scaled as a function of *Chl*. Fig. 1.1b shows the sum $a_{\mathrm{m}}(\lambda;Chl) = a_{\mathrm{p}}(\lambda;Chl) + a_{\mathrm{g}}(\lambda;Chl)$ calculated, for $Chl =$ 1, 3 and 10 mg m^{-3}, using this simple model, as implemented in one of the standard IOP spcification options within the HYDROLIGHT radiative transfer model (Mobley and Sundman 2000). The subscript "m" indicates that the spectra shown in Fig. 1.1b are those that would be measured by an instrument that was calibrated using pure water as a standard reference medium (Chapter 3). The absorption of pure water $a_{\mathrm{w}}(\lambda)$ is compared with $a_{\mathrm{m}}(\lambda;Chl)$ in Fig. 1.1b, and the corresponsding total absorption coefficient spectra $a(\lambda;Chl) = a_{\mathrm{w}}(\lambda) + a_{\mathrm{m}}(\lambda;Chl)$ are illustrated in Fig. 1.1c. The illustrated examples are admittedly an oversimplification, but they are adequate as a basis for considering the nature of IOP components of the signal measured by an absorption meter, or transmissometer, at individual wavelengths.

Scattering by Pure Water

The spectral values of the pure water volume scattering coefficient $b_{\mathrm{w}}(\lambda)$ recommended in Vol. I, Chapter 2 (Sect. 2.4) are those of Morel (1974), as reported by Smith and Baker (1981). Following Van Zee *et al*. (2002), however, we recommend here that preference be given to the $b_{\mathrm{w}}(\lambda)$ scales of Buiteveld, *et al*. (1994). Both scales are listed in Table 1.1 for comparison. The difference between the two scales is $\leq 0.0001\ \mathrm{m}^{-1}$ at wavelengths > 475 nm, increases to $\leq 0.0005\ \mathrm{m}^{-1}$ as wavelength decreases to 400 nm, and increases further to $\leq 0.0014\ \mathrm{m}^{-1}$ at 340 nm. In no instance does the difference closely approach the $0.005\ \mathrm{m}^{-1}$ measurement uncertainty of beam attenuation and absorption meters that are commercially available to date.

The angular distribution of the molecular scattering phase function $\tilde{\beta}_{\mathrm{w}}(\psi)$, as approximated with equation (2.29) [Vol. I, Ch. 2] , is illustrated in Fig. 1.2. The magnitude of $\tilde{\beta}_{\mathrm{w}}(\psi)$ represents the probability that a photon scattering interaction with a water molecule will redirect the photon path direction by an angle ψ measured from its original path. The shape of $\tilde{\beta}_{\mathrm{w}}(\psi)$ is sometimes referred to as "isotropic" in the literature, a characterization that is true only in that the function is axially symmetric and the probabilities of forward and backward scattering are equal.

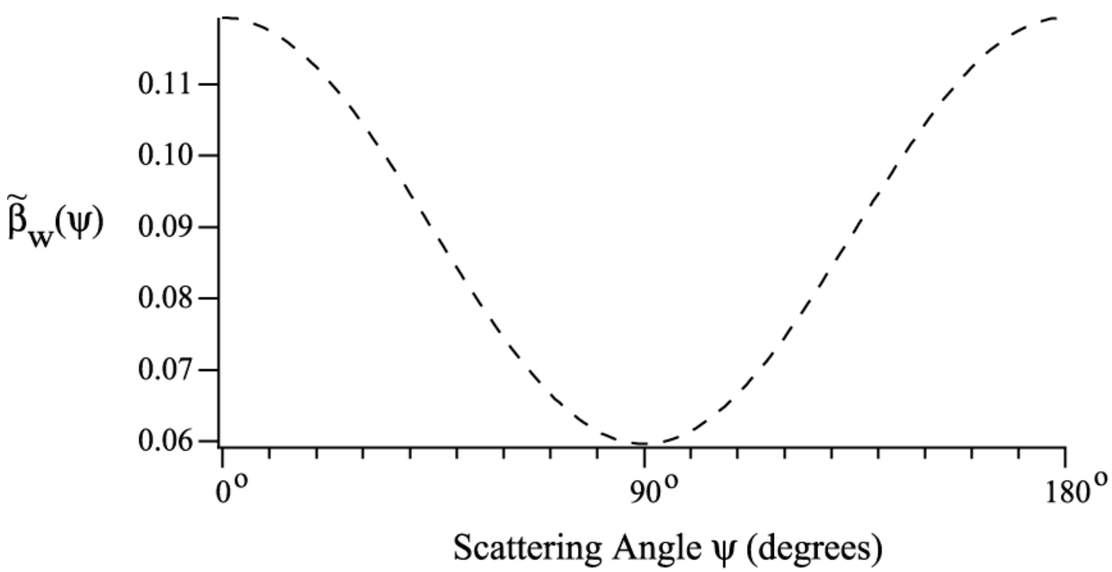

Fig. 1.2: The dashed curve represent the angular distribution of the scattering phase function for pure water, calculated using the approximate Rayleigh scattering model [equation (2.29) of Vol. I, Ch. 2].

Scattering by Particles

In many natural waters, the volume scattering coefficient for particles $b_p(\lambda)$ is comparable to, or larger than, that of pure water. Moreover, the shape of a particle scattering phase function $\tilde{\beta}_w(\lambda,\psi)$, an example of which is illustrated as the solid curve in Fig. 1.3, is strongly peaked - by several orders of magnitude - in the forward direction. The extreme contrast between the angular probability distributions of particulate and molecular scattering (the dashed curve in Fig. 1.3) are important factors that must be considered when designing transmissometers and scattering meters for use in the sea.

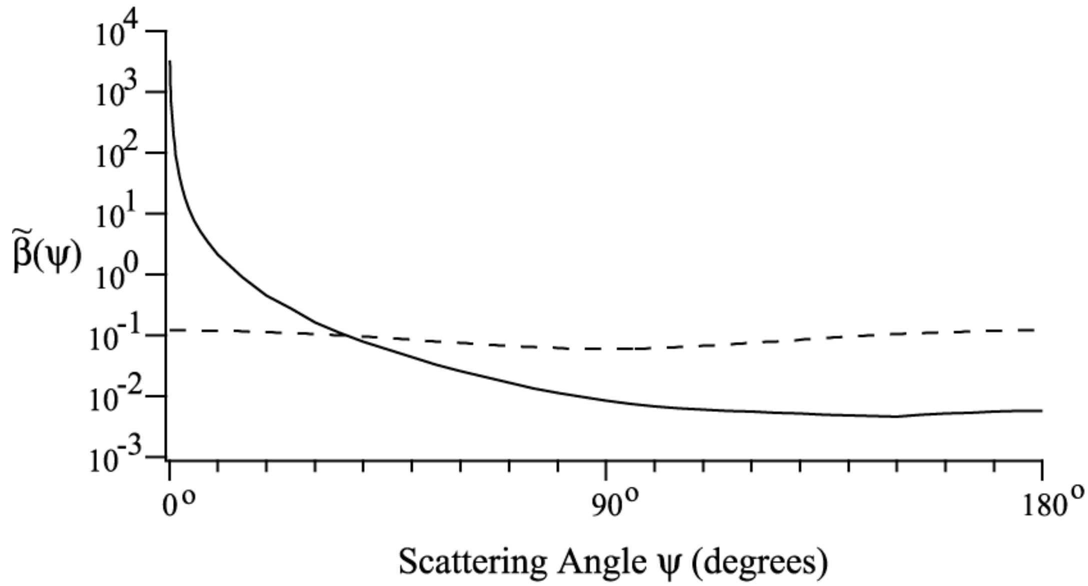

Fig. 1.3: The solid curve is an example of a measured scattering phase function for ocean water dominated by particle scattering (Petzold 1972; San Diego Harbor Stn. 2040). The dashed curve is the pure water phase function from Fig. 1.2, shown here for comparison.

Scattering by Turbulence

Random fluctuations in water density, induced by turbulence, act to steer photons through very small angles in the forward direction, and therefore, scattering by turbulence is also strongly peaked, by orders of magnitude, in the forward direction. Because turbulent fluctuations are completely random in space and time, the variance of photons scattered by turbulence at small angles is much greater than the variance associated with small angle scattering by particles (Bogucki *et al*. 1998)

1.3 RADIANT FLUX TRANSMISSION MEASUREMENT CONCEPTS

Geometry and Nomenclature

In Fig. 1.4 the origin of a local instrument coordinate system is placed at the exit aperture of a source of monochromatic radiant flux $\Phi_o(\lambda,0,0,0)$ $\left[\text{in } \mu\text{W nm}^{-1}\right]$[2] directed as a collimated beam along the positive z_m-axis (see also Fig. 2.2 in Vol. I, Ch. 2). The subscript "m" associated with the coordinate basis vectors $(\hat{\mathbf{x}}_m, \hat{\mathbf{y}}_m, \hat{\mathbf{z}}_m)$ in

[2] The choice of these units, rather than, *e.g.*, W m^{-1}, is customary in ocean color science and is used throughout these protocols.

Fig. 1.4 indicate that the local "measurement" coordinate frame is associated with a particular instrument concept, as distinguished from global coordinates defining positions and directions in the extended medium (*cf* Figs. 2.1 and 2.2 in Vol. I, Ch. 2). The local instrument coordinate framework is related to global coordinates by a translation and rotations that are arbitrary and need not be considered in the present context[3].

The direction associated with an optical path vector intersecting the transmitted beam axis (z_m-axis) is described by the angle pair (ψ, φ), where $0 \le \psi \le \pi$ is measured from the z_m-axis and $0 \le \varphi \le 2\pi$ is measured from the x_m-axis counterclockwise in the $x_m y_m$-plane. The variable r, with various subscripts, will denote geometric distance along any such optical path[4]. Directional radiant flux at distance r from a source, or from a scattering interaction site within the transmitted beam, is denoted $\Phi(\lambda, r, \psi, \varphi)$. In Fig. 1.4 for example, radiometric flux scattered into direction (ψ, φ) at position $\bar{\mathbf{x}}_S$ is denoted as $\Phi_S(\lambda, 0, \psi, \varphi)$, and the scattered flux transmitted in that direction to Detector 2, at position $\bar{\mathbf{x}}_D$, as $\Phi_S(\lambda, r_D, \psi, \varphi)$. Radiometric flux within the beam transmitted to a point on the z_m-axis at distance r from the source is denoted, $\Phi_T(\lambda, r, 0, \bullet)$, where the dot indicates that φ is indeterminate when $\psi = 0$ or $\psi = \pi$. In particular, the flux transmitted from the source to Detector 1 is $\Phi_T(\lambda, r_T, 0, \bullet)$.

Transmittance and Beam Attenuation

The shaded rectangle overlaid on the extended z_m-axis in Fig. 1.4 schematically illustrates a cylinder (of cross sectional area Δs) representing the collimated beam of radiant flux transmitted from the source to Detector 1. The gradient in shading represents the exponential decrease in $\Phi_T(\lambda, r, 0, \bullet)$ with increasing distance r, as photons interact with the medium and are absorbed and scattered out of the beam. During transmission over a path interval from r to $r + \Delta r$, the fraction of radiant flux absorbed in the volume $\Delta s \Delta r$ is ***spectral absorptance***, $A(\lambda)$ and the fraction of flux scattered out of the beam direction in that volume is ***spectral scatterance*** $B(\lambda)$ (see Vol. I, Chapter 2, Sect. 2.4).

One could envision superimposing a lightly shaded "cloud" on Fig. 1.4 to visualize scattered photons escaping from the beam in all directions, but this would not indicate the directional nature of the scattering losses. Instead, the scattering process is schematically illustrated in Fig. 1.4 as a mottled, shaded path of photons scattered in a particular direction (ψ, φ) at a single location $\bar{\mathbf{x}}_S$ in the beam[5]. At this on-axis location, $\bar{\mathbf{x}}_S$, similar beams could be drawn in any other direction to visually indicate scattered flux intensity and its subsequent transmittance and attenuation in the new direction. The same type of graphic could be drawn anywhere along the optical path, and if many were combined we'd generate the aforementioned "photon cloud" masking any indication of the vector nature of the scattered radiant field. Nevertheless, that mental construct is adequate for considering transmission measurement concepts. If the pathlength r_T is short enough that photons initially scattered out of the beam have a negligible chance of undergoing two (or more) additional scattering interactions that could return them to the beam, then it may be assumed that they will not be detected by Detector 1 (Fig. 1.4)[6].

---

[3] When the IOP are used in the context of a radiative transfer model, on the other hand, the translations and rotations relating local coordinates, used to describe scattering interactions (*e.g.* as at position $\bar{\mathbf{x}}_S$ .in Fig. 1.3), to global coordinates, describing locations and directions in the medium as whole, become critically important.

[4] See Footnote 2 in (Vol. 1, Chapter 2) regarding the usage of the variable *z* in Fig. 2.2 and Sect. 2.4 of that chapter. Here we have substituted the symbol *r* for the optical pathlength along the z-axis in Fig. 1.3 (compare with Fig. 2.2 of Vol. 1 Ch. 2).

[5] The transmission of the illustrated beam of scattered photons to Detector 2 will be further considered as a starting point in the discussion of scattering measurement concepts in Sect. 1.5 below.

[6] The question, "What pathlength limit is *'short enough'* to avoid multiply scattered photons from reaching a transmissometer's detector?" is considered in Chapter 2 of this Protocol Volume.

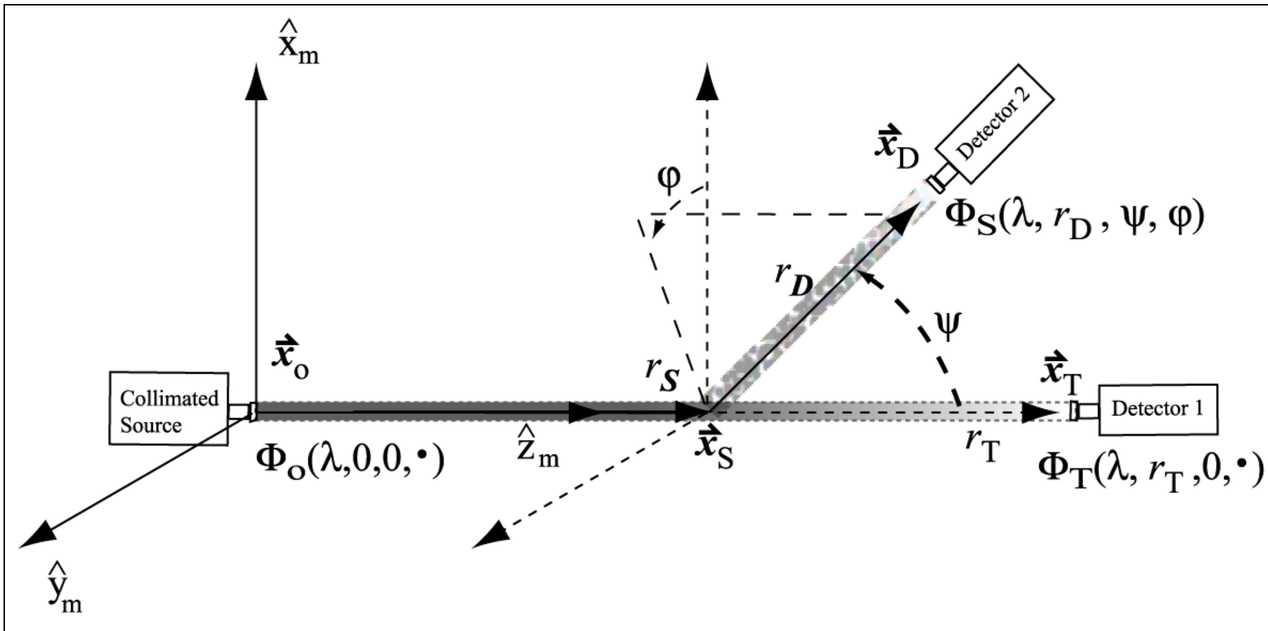

Figure 1.4: The local "Instrument Coordinate" framework describing optical beam transmission and scattering geometry. A collimated beam of radiometric flux $\Phi_o(\lambda,0,0,\bullet)$ is emitted from a source at the origin $\vec{x}_o$. The flux within the collimated beam, shown schematically as a gradient shaded rectangle extending along the z_m-axis to Detector 1, is reduced by scattering and absorption as it is transmitted along the z_m-axis, and a reduced flux $\Phi_T(\lambda,r_T,0,\bullet)$ is measured by Detector 1 at position $\vec{x}_T$. At the intermediate location $\vec{x}_S$, some fraction of the flux $\Phi_T(\lambda,r_S,0,\bullet)$ that reaches that location is scattered out of the beam into direction (ψ,φ). The directionally scattered flux $\Phi_S(\lambda,0,\psi,\varphi)$ is subsequently transmitted a distance r_D in that direction, with further losses due to scattering and absorption, and the reduced scattered flux $\Phi_S(\lambda,r_D,\psi,\varphi)$ is measured by Detector 2 at position $\vec{x}_D$. See text for further explanations.

The ***beam attenuation coefficient*** is defined in equations (2.16) through (2.18) of Vol. I, Chapter 2 (Sect. 2.4) as

$$c(\lambda) = a(\lambda) + b(\lambda), \text{ m}^{-1}, \tag{1.1}$$

where the ***volume absorption*** and ***scattering coefficients*** $a(\lambda)$ and $b(\lambda)$ are defined in terms of ***absorptance*** $A(\lambda)$ and ***scatterance*** $B(\lambda)$ in the limit of the optical pathlength Δr approaching zero as

$$a(\lambda) = \lim_{\Delta r \to 0} \frac{A(\lambda)}{\Delta r}, \text{ and } b(\lambda) = \lim_{\Delta r \to 0} \frac{B(\lambda)}{\Delta r}, \text{ m}^{-1}, \tag{1.2}$$

respectively. Equation (2.16) (Vol. I, Chapter 2) may be rearranged as

$$\lim_{\Delta r \to 0} \left\{ \frac{\Phi_T(\lambda) - \Phi_i(\lambda)}{\Phi_i(\lambda)\Delta r} \right\} = \lim_{\Delta r \to 0} \left\{ -\frac{A(\lambda) + B(\lambda)}{\Delta r} \right\}, \tag{1.3}$$

where Φ_i and Φ_T are incident and transmitted radiant fluxes, respectively. Equation (1.3) may be expressed in differential form as

$$\frac{d\Phi(\lambda)}{\Phi(\lambda,r)} = -c(\lambda)\,dr\,. \tag{1.4}$$

Integrating (1.4) over an optical pathlength r_T as

$$c(\lambda)\int_0^{r_T} dr = -\int_0^{r_T} \frac{d\Phi(\lambda)}{\Phi(\lambda, r)}, \tag{1.5}$$

we obtain the solution for the beam attenuation coefficient

$$c(\lambda) = \frac{\ln \Phi_o(\lambda, 0, 0, \bullet) - \ln \Phi_T(\lambda, r_T, 0, \bullet)}{r_T} = \frac{-\ln T(\lambda, r_T)}{r_T} \text{ m}^{-1}, \tag{1.6}$$

where we adopt the conventions and notations described above and in Fig. 1.4. In (1.6), ***transmittance*** $T(\lambda, r_T) \equiv \frac{\Phi_T(\lambda, r_T, 0, \bullet)}{\Phi_o(\lambda, 0, 0, \bullet)}$ is the fraction of radiant flux transmitted over the path distance r_T. Equation (1.6) is the fundamental equation by which the ***beam attenuation coefficient*** is determined from a measurement made with a ***transmissometer*** (Chapter 2 of this volume).

The attenuation of radiant flux transmitted over a short optical pathlength r_T in seawater may be determined using the *Beer-Lambert-Bouguer Law* [equation (2.41), Vol. I, Ch. 2], which here follows directly from (1.6) as

$$\Phi_T(\lambda, r_T, 0, \bullet) = \Phi_o(\lambda, 0, 0, \bullet) e^{-c(\lambda) r_T}. \tag{1.7}$$

1.4 ABSORPTION MEASUREMENT CONCEPTS

Reflecting Tube Absorption Meters

To determine the volume absorption coefficient $a(\lambda)$ with a source and detector pair arranged on a common axis (*e.g.* the source and Detector 1 in Fig. 1.4), the flux reaching the detector window Φ_K must include the sum of directly transmitted and scattered fluxes, *i.e.* $\Phi_K = \Phi_T + \Phi_B$. If the source and collector are equal in area and the water path between them (the shaded transmission path volume in Fig. 1.4) were enclosed in a perfectly reflecting tube, then all forward scattered photons would be redirected into the beam and reach the detector. For the present, we will postpone consideration of the flux loss due to backscattered photons and treat it as being negligible. Under this construct and assumption, equation (1.3) may be rewritten as

$$\lim_{\Delta r \to 0} \left\{ \frac{\Phi_T(\lambda) + \Phi_B(\lambda) - \Phi_i(\lambda)}{\Phi_i(\lambda) \Delta r} \right\} = -\lim_{\Delta r \to 0} \left\{ \frac{A(\lambda)}{\Delta r} \right\}, \tag{1.8}$$

expressed in differential form as

$$\frac{d\Phi_K(\lambda, r)}{\Phi(\lambda, r)} = -a(\lambda) dr, \tag{1.9}$$

and integrated over the path from 0 to r_T to obtain

$$a(\lambda) = \frac{\ln \Phi_o(\lambda, 0, 0, \bullet) - \ln \Phi_K(\lambda, r_T, 0, \bullet)}{r_T} = \frac{-\ln T_K(\lambda, r_T)}{r_T} \text{ m}^{-1}. \tag{1.10}$$

The reflecting tube method has been used to measure spectral absorption in the laboratory for many decades (James and Birge 1938). In recent years, this method has been adapted for use in the ocean (Zaneveld *et al*. 1992). Suitable instruments are now commercially available and are coming into general use within the oceanographic community. The best-known, commercially available example of this type of instrument is the “ac-9” manufactured by WET Labs Inc. of Philomath, OR. Protocols for calibrating and using reflecting tube absorption meters, and methods of data analysis are described in Chapter 3 of this volume, and in more specific detail for the ac-9 by Van Zee *et al*. (2002), which is available at (www.wetlabs.com).

Laboratory Methods for Determining Absorption Coefficients

Protocols in Chapter 4, by Mitchell *et al*., describe methods for filtering seawater to capture suspended particles on GF/F filters, and for measuring the absorption spectra of the particle-laden filters with a laboratory spectrophotometer. Methods are also described for extracting phytoplankton pigments from the filters, and measuring the residual absorption spectrum of particulate materials other than phytoplankton pigments. Finally, laboratory methods are also described for measuring the absorption spectrum of CDOM in filtered seawater samples. The material in this chapter derives from the results of recent experimental intercomparison workshops in which the authors participated, as well as from the published literature. Chapter 4 of this volume is a reformatted, but otherwise unchanged, version of Chapter 15 in Revision 3 to the ocean optics protocols (Mueller and Fargion 2002).

Absorption Determinations from Radiometric Measurements of Irradiance Flux Divergence

In situ spectral absorption coefficient profiles can also be measured with spectral radiometers conforming to the performance specifications listed in Vol. II, Chapter 2, if the radiometric package is extended to measure $E_d(z,\lambda)$ and $E_u(z,\lambda)$, as well as scalar irradiances $\overset{o}{E}_d(z,\lambda)$ and $\overset{o}{E}_u(z,\lambda)$. This combination may be approached either using hemispherical collectors to measure upwelling and downwelling hemispherical irradiances (Hojerslev 1975), or by using cosine collectors on one radiometer in tandem with spherical collectors on another radiometer. Given these irradiance components, spectral absorption is then computed using Gershun's equation (Gershun 1939) as

$$a(z,\lambda) = \vec{K}(z,\lambda)\frac{\vec{E}(z,\lambda)}{\overset{o}{E}(z,\lambda)}, \tag{1.11}$$

where $\vec{E}(z,\lambda) = E_d(z,\lambda) - E_u(z,\lambda)$ is vector irradiance, $\vec{K}(z,\lambda)$ is the vertical attenuation coefficient for vector irradiance, and scalar irradiance $\overset{o}{E}(z,\lambda) = \overset{o}{E}_d(z,\lambda) + \overset{o}{E}_u(z,\lambda)$ (see also Vol. I, Chapter 2).

Comparisons between absorption profiles measured using Gershun's equation with $\vec{E}(z,\lambda)$ and $\overset{o}{E}(z,\lambda)$ (scalar irradiance) data, and absorption profiles measured with a reflecting tube instrument, agreed within 8% (Pegau *et al*. 1994). This level of agreement is well within the calibration uncertainties of the particular prototype instruments used for that experiment, which were approximately 10% uncertainties in both the scalar irradiance radiometer and in the reflecting tube instrument. Less than 5% uncertainties in absorption are expected in future experiments, assuming the data are properly averaged to remove near-surface irradiance fluctuations caused by surface waves (Zaneveld *et al*. 2001). In very clear oligotrophic water, moreover, uncertainty in water absorption values may make it impossible to realize this level of relative agreement.

Other Methods of Measuring Absorption

There are several other measurement concepts that may be used to determine the absorption coefficient of seawater, however, none of them are currently useful for making routine measurements during daylight conditions at sea. One possible exception is the determination of absorption by inverting radiance distribution profiles measured using a camera system (Voss 1989), but at present, such camera systems are not commercially available[7]. In a similar method, absorption may be determined by inverting the radiative transfer equation for several measured moments of an axially symmetric radiance distribution in the asymptotic regime (Zaneveld and Pak 1972; Wells 1983) Other examples include the determination $a_w(\lambda)$ using an integrating cavity (Pope and Fry 1997), photothermal methods (Sogandares and Fry 1997), and differential optoacoustic spectroscopy (Voss and Trees 1987). Optoacoustic spectroscopy was also used to measure $a_p(\lambda)$ in phytoplankton cultures (Trees and Voss 1990). Absorption may also be determined from measurements of irradiance divergence from a submerged isotropic

[7] It would be advantageous were this situation to change in the future, as such camera systems are potentially even more useful for determining the Bidirectional Reflectance Distribution Function (BRDF) and Exact Normalized Water-Leaving Radiance (Vol. III, Ch. 4).

source (Maffione *et al*. 1993, and earlier references cited there). The present version of this volume does not address any of these methods.

1.5 SCATTERING MEASUREMENT CONCEPTS

Scattering Coefficient Determinations

There is no practical way to directly measure the volume scattering coefficient $b(\lambda)$. Given measurements of absorption and beam attenuation coefficients, however, the volume scattering coefficient may computed from (1.1) as $b(\lambda) = c(\lambda) - a(\lambda)$, m^{-1}. In practice it's not quite that simple, and several interrelated scattering and absorption corrections must be applied (Chapters 3 and 5 in this Volume). Alternatively, attempts have been made to calculate $b(\lambda)$ by integrating measurements of the VSF, *e.g.*, by Petzold (1972).

Volume Scattering Function Measurements

In Fig. 1.4, the combination of the source at $\vec{\mathbf{x}}_\mathrm{o}$, directional scattering at $\vec{\mathbf{x}}_\mathrm{S}$, and Detector 2 at location $\vec{\mathbf{x}}_\mathrm{D}$ schematically illustrate the conceptual elements of a scattering meter designed to measure the VSF $\beta(\lambda,\psi,\varphi)$. Collimated flux $\Phi_\mathrm{o}(\lambda,0,0,\bullet)$ is transmitted, in a beam of cross-sectional area A, from the source to $\vec{\mathbf{x}}_\mathrm{S}$ as

$$\Phi_\mathrm{T}(\lambda,r_\mathrm{S},0,\bullet) = \Phi_\mathrm{o}(\lambda,0,0,\bullet)e^{-c(\lambda)r_\mathrm{S}}. \tag{1.12}$$

The irradiance incident normal to the optical transmission axis at $\vec{\mathbf{x}}_\mathrm{S}$ is

$$E_\mathrm{i} = \frac{\Phi_\mathrm{T}(\lambda,r_\mathrm{S},0,\bullet)}{\mathrm{A}} = \frac{\Phi_\mathrm{o}(\lambda,0,0,\bullet)e^{-c(\lambda)r_\mathrm{S}}}{\mathrm{A}}. \tag{1.13}$$

At position $\vec{\mathbf{x}}_\mathrm{S}$, some of the incident radiant flux is scattered in direction (ψ,φ), into the solid angle field-of-view Ω_FOV of Detector 1, from the volume $V(\psi)$ defined by the intersection of the beam and detector field of view. The radiant intensity of the scattered flux is

$$I_\mathrm{S}(\lambda,\psi,\varphi) = \frac{\Phi_\mathrm{S}(\lambda,0,\psi,\varphi)}{\Omega_\mathrm{FOV}}, \tag{1.14}$$

and scattered flux reaching the detector is

$$\Phi_\mathrm{S}(\lambda,r_\mathrm{D},\psi,\varphi) = \Phi_\mathrm{S}(\lambda,0,\psi,\varphi)e^{-c(\lambda)r_\mathrm{D}}. \tag{1.15}$$

From equation (2.30) we may determine the VSF averaged over the working volume and solid angle FOV approximately as

$$\overline{\beta}(\lambda,\psi,\varphi) \cong \frac{I_\mathrm{S}(\lambda,0,\psi,\varphi)}{E_i V(\psi)}, \tag{1.16}$$

or by substituting from (1.12) through (1.13), directly in terms of source and detector fluxes as

$$\overline{\beta}(\lambda,\psi,\varphi) \cong \frac{\Phi_\mathrm{S}(\lambda,r_\mathrm{D},\psi,\varphi)\mathrm{A}}{\Phi_\mathrm{o}(\lambda,0,0,\bullet)V(\psi)\Omega_\mathrm{FOV}}e^{-c(\lambda)(r_\mathrm{S}-r_\mathrm{D})}. \tag{1.17}$$

One must know both $c(\lambda)$ and $\Phi_\mathrm{o}(\lambda,0,0,\bullet)$ to determine the VSF from (1.17). If the same detector were used at positions shown for detectors 1 and 2 in Fig. 1.4, following the method introduced by Kullenberg (1968), and if $r_\mathrm{D} = r_\mathrm{T} - r_\mathrm{S}$, we may substitute from (1.7) and determine the VSF from the two measured detector fluxes as

$$\overline{\beta}(\lambda,\psi,\varphi) \cong \frac{\Phi_\mathrm{S}(\lambda,r_\mathrm{D},\psi,\varphi)\mathrm{A}}{\Phi_\mathrm{T}(\lambda,r_\mathrm{T},0,\bullet)V(\psi)\Omega_\mathrm{FOV}}. \tag{1.18}$$

Equation (1.18) could be used to measure the VSF if the source and detector are well collimated, and there were no flux losses, or FOV distortions, associated with an instrument's optical assembly. For most scattering meters, however, the averaged VSF estimate $\overline{\beta}(\lambda,\psi,\varphi)$ is related to the true VSF $\beta(\lambda,\psi,\varphi)$ by a weighted integral

$$\overline{\beta}(\lambda,\psi,\varphi) = \int_0^{2\pi}\int_0^{\pi} \beta(\lambda,\psi,\varphi) W(\lambda,\psi,\varphi;c) \sin\psi d\psi d\varphi \,. \tag{1.19}$$

where the weighting function $W(\lambda,\psi,\varphi;c)$ accounts for instrumental factors including the divergence and uniformity of the source beam and detector angular response function, the working volume geometry, variations in attenuation of flux scattered to the detector from different volume elements, and optical reflection and absorption losses in the system. Practical methods for determining $W(\lambda,\psi,\varphi;c)$ are described in Chapter 5.

The VSF of ocean water is usually considered to be azimuthally symmetric about the transmission axis. Therefore, the VSF is usually reported as $\beta(\lambda,\psi)$, which is a function of the polar "scattering angle" alone. In terms of the VSF measurements as represented in (1.19), we have that

$$\overline{\beta}(\lambda,\psi) = \int_0^{2\pi} \overline{\beta}(\lambda,\psi,\varphi) d\varphi = 2\pi\overline{\beta}(\lambda,\psi,\varphi) \,. \tag{1.20}$$

Backscattering Coefficient Determination

The backscattering coefficient $b_{\mathrm{b}}(\lambda)$ [Vol. I, Ch. 2, equation (2.23)] is an important factor in the physical relationship between the IOP and remote sensing reflectance (Vol. III, Ch. 4, Sect. 4.3 and references cited therein). As is the case for the volume scattering coefficient $b(\lambda)$, there is no practical way to directly measure $b_{\mathrm{b}}(\lambda)$ in the sea. If that is true, then how can $b_{\mathrm{b}}(\lambda)$ be determined using the so-called "backscattering meters" in common use within the community? These instruments actually measure the VSF $\overline{\beta}(\lambda,\psi)$ at one angle ψ^*, or several angles $\psi_i^*, i = 1,2,\ldots,\mathrm{N}$, in the backward direction. For single angle VSF instruments, such as the HOBILABS HydroScat-series and WET Labs ECO-BB series , one uses the fact that most observed phase functions and modeled VSFs show a common crossover angle ψ^* at which $\overline{\beta}(\lambda,\psi^*) \propto b_{\mathrm{b}}(\lambda)$. An empirical linear equation is used to calculate $b_{\mathrm{b}}(\lambda)$ from $\overline{\beta}(\lambda,\psi^*)$; where the angle ψ^* is selected to minimize the uncertainty in $b_{\mathrm{b}}(\lambda)$ associated with a simulated uncertainty in $\tilde{\beta}_{\mathrm{P}}(\lambda,\psi)$ (Oishi 1990; Maffione and Dana; Boss and Pegau 2001). The approach used to determine $b_{\mathrm{b}}(\lambda)$ from measurements of $\overline{\beta}(\lambda,\psi_i,\varphi); i = 1,2,\ldots,\mathrm{N}$ angles, *e.g.* using a WET Labs VSF-3, is to fit a polynomial to the N+1 values $2\pi\overline{\beta}(\lambda,\psi_i,\varphi)\sin\psi_i$ derived from the N measurements and the endpoint $2\pi\beta(\lambda,\pi,\bullet)\sin\pi \equiv 0$ and integrate it from $\frac{\pi}{2}$ to π (following Beardsley and Zaneveld 1969).

REFERENCES

Beardsley, G.F. and J.R.V. Zaneveld, 1969: Theoretical dependence of the near-asymptotic apparent optical properties of sea water. *J. Opt. Soc. Amer*. 59: 373-377.

Boss, E. and W.S. Pegau, 2001: Relationship of light scattering at an angle in the backward direction to the backscattering coefficient. *Appl. Opt.,* **40:** 5503-5507.

Bogucki, D.J., J.A. Domaradzki, D. Stramski and J.R.V. Zaneveld, 1998. Comparison of near-forward light scattering on oceanic turbulence and particles. *Appl. Opt.*, **37(21):** 4669-4677.

Bricaud, A., A. Morel and L. Prieur, 1981. Absorption by dissolved organic matter of the sea (yellow substance) in the UV and visible domains. *Limnol Oceanogr,* **26(1):** 43-53.

Buiteveld, H., J.H.M. Hakvoort and M. Donze, 1994: The optical properties of pure water. *Ocean Optics XII*, SPIE Vol. 2258: 174-183.

Gordon, H.R. and A. Morel, 1983: *Remote Assessment of Ocean Color for Interpretation of Satellite Visible Imagery, a Review; Lecture Notes on Coastal and Estuarine Studies, Vol. 4*, Springer Verlag, New York, 114pp.

Gershun, A., 1939: The light field. *J. Math. Phys*. **18**: 51-151.

Hojerslev, N.K., 1975: A spectral light absorption meter for measurements in the sea. *Limnol. Oceanogr*., **20**: 1024-1034.

James, H.R., and E.A. Birge, 1938: A laboratory study of the absorption of light by lake waters. *Trans. Wis. Acad. Sci*., **31**: 1--154.

Kou, L., D. Labrie and P. Chylek, 1993: Refractive indices of water and ice in the 0.65 to 2.5 μm spectral range, *Appl. Opt.*, **32:** 3531-3540.

Kullenberg, G., 1968: Scattering of light by Sargasso Sea water, *Deep-Sea Res.*, **15:** 423-432.

Maffione, R.A. and D.R. Dana, 1997: Instruments and methods for measuring the backward-scattering coefficient of ocean waters. *Appl. Opt*. **36**: 6057-6067.

Maffione, R.A., K.J. Voss and R.C. Honey, 1993. Measurement of the spectral absorption coefficient in the ocean with an isotropic source. *Appl. Opt.*, **32(18):** 3273-3279.

Morel, A., 1974: Optical properties of pure water and pure sea water. In: *Optical Aspects of Oceanography*, N.G. Jerlov and E.S. Nielson, Eds., pp1-23.

Morel, A. and S. Maritorena, 2001. Bio-opical properties of oceanic waters: A reappraisal, *J. Geophys. Res.*, **106(C4):** 7163-7180.

Mueller, J.L. and G.S. Fargion,[Eds.], 2002: Ocean Optics Protocols for Satellite Ocean Color Sensor Validation, Revision 3. *NASA Tech. Memo. 2002-210004*, NASA Goddard Space Flight Center, Greenbelt, Maryland, 308pp.

Oishi, T., 1990. Significant relation between the backward scattering coefficient of sea water and the scatterance at 120 degrees. *Appl. Opt.*, **29(31):** 4658-4665.

Pegau, W.S. and J.R.V. Zaneveld, 1993: Temperature dependent absorption of water in the red and near infrared portions of the spectrum. *Limnol. Oceanogr*., **38**(1): 188-192.

Pegau, W.S., J.S. Cleveland, W. Doss, C.D. Kennedy, R.A. Maffione, J.L. Mueller, R. Stone, C.C. Trees, A.D. Weidemann, W.H. Wells, and J.R.V. Zaneveld, 1995: A comparison of methods for the measurement of the absorption coefficient in natural waters. *J. Geophys. Res.*, **100**(C7): 13,201-13,220.

Pegau, W.S., D. Gray and J.R.V. Zaneveld, 1997: Absorption and attenuation of visible and near-infrared light in water: dependence on temperature and salinity. Appl. Opt., **36**(24): 6035-6046.

Petzold, T.J., 1972. Volume scattering functions for selected ocean waters. Contract No. N62269-71-C-0676, UCSD, SIO Ref. 72-78.

Pope, R.M. and E.S. Fry. 1997: Absorption spectrum (380-700 nm) of pure water. II. Integrating cavity measurements. *Appl. Opt*. **36**: 8710-8723.

Prieur, L. and S. Sathyendranath, 1981. An optical classification of coastal and oceanic waters based on the specific spectral absorption curves of phytoplankton pigments, dissolved organic matter, and other particulate materials. *Limnol. Oceanogr.*, **26(4):** 671-689.

Smith, R.C. and K.S. Baker, 1981. Optical properties of the clearest natural waters (200-800 nm), *Appl Opt*. **20 (2):** 177-184.

Sogandares, F.M. and E.S. Fry, 1997. Absorption spectrum (340-640 nm) of pure water. I. Photothermal measurements. *Appl. Opt.*, **36(33):** 8699-8709.

Trees, C.C. and K.J. Voss, 1990. Optoacoustic spectroscopy and its application to molecular and particle absorption. *OCEAN OPTICS X*, SPIE **1302:** 149-156.

Voss, K.J., 1989: Use of the radiance distribution to measure the optical absorption coefficient in the ocean, *Limnol. Oceanogr.*, **34:** 1614-1622.

Van Zee, H., D. Hankins, and C. deLespinasse, 2002: *ac-9 Protocol Document (Revision F)*. WET Labs Inc., Philomath, OR, 41pp.

Wells, W.H., 1983: Techniques for measuring radiance in sea and air. *Appl. Opt.*, **22:** 2313-2321.

Zaneveld, J.R.V., E. Boss and A. Barnard, 2001. Influence of surface waves on measured and modeled irradiance profiles. Appl. Opt., **40**(9): 1442-1449.

Zaneveld, J.R.V., J.C. Kitchen, A. Bricaud, and C. Moore, 1992: Analysis of *in situ* spectral absorption meter data. *Ocean Optics XI,* G.D. Gilbert, Ed., SPIE, 1750, 187--200.

Zaneveld, J.R.V., and H. Pak, 1972. Some aspects of the axially symmetric submarine daylight field. *J. Geophys. Res*., **77(15):** 2677-2680.

Chapter 2

Beam Transmission and Attenuation Coefficients: Instruments, Characterization, Field Measurements and Data Analysis Protocols

Scott Pegau[1], J. Ronald V. Zaneveld[1] and James L. Mueller[2]

[1]*College of Oceanographic and Atmospheric Sciences, Oregon State University, Corvallis*

[2]*Center for Hydro-Optics and Remote Sensing, San Diego State University, California*

2.1 INTRODUCTION

Beam transmittance $T(\lambda, r_{\mathrm{T}})$ over an optical path of length r_{T} m, and the beam attenuation coefficient $c(\lambda)$ $\left[\mathrm{m}^{-1}\right]$, are introduced in Chapter 1 (Sect. 1.3). The two variables are related by equation (1.6). A ***beam transmissometer*** is an instrument that combines a source of collimated spectral radiant flux $\Phi_{\mathrm{o}}(\lambda, 0, 0, \bullet)$ and a co-aligned detector, to measure the flux $\Phi_{\mathrm{T}}(\lambda, r_{\mathrm{T}}, 0, \bullet)$ transmitted over distance r_{T}, to measure $T(\lambda, r_{\mathrm{T}})$ (Fig. 1.4 and related text in Sect. 1.3, Ch. 1). A beam transmissometer is also frequently called a ***beam attenuation meter***, or a ***c-meter***.

2.2 TRANSMISSOMETER DESIGN CHARACTERISTICS

In concept, a beam transmissometer is a relatively simple instrument to build, and the derived beam attenuation coefficient is needed in many optical studies of the sea. Therefore, instruments of this type have been in use for many years. While a great number of different transmissometer designs have appeared, most follow one of the two basic designs illustrated in Fig. 2.1.

Direct and Folded Path Transmissometers

Probably the most common transmissometer design uses a collimated light beam[8], with a source in one housing and a detector facing the source (Fig. 2.1, top panel). In such an ideal ***direct-path transmissometer***, either a white light, or a light emitting diode (LED), source is combined with a pinhole to provide a point source. A lens is inserted into the path to collimate the light beam, an interference filter is inserted to select the waveband of the measurement, and the light is passed into the water through a window. At the other end of the optical path, the light enters the detector assembly through another window and is focused by a lens. An aperture at the focal point removes off-axis scattered light, and the transmitted light falls on the detector. Although this instrument is conceptually simple, it is difficult to build. The alignment of components is critical, and something as simple as the filament in the source sagging as the instrument is moved can create significant apparent changes in the derived beam attenuation coefficient. Several commercial transmissometers[9] including, some laboratory

[8] Cylindrically limited beam, as opposed to collimated beam, transmissometers will be discussed later in this section.

[9] Certain commercial equipment, instruments, or materials are identified in this chapter to foster understanding. Such identification does not imply recommendation, or endorsement, by the National Aeronautics and Space Administration, nor does it imply that the materials or equipment identified are necessarily the best available for the purpose.

spectrophotometers, and the (former) SeaTech and WET Labs field instruments use this basic design. Design variations include the addition of a reference detector and placing the wavelength filter in the detector housing.

The folded pathlength design (Fig. 2.1, bottom panel) uses one or more reflectors to create a longer pathlength. The basic idea for this design can be attributed to Petterson (1934). Initial designs used plane mirrors to expand the pathlength (Wattenberg, 1938; Timofeeva, 1960). The introduction of prisms to separate the incident and reflected beam (Nikolayev and Zhil'tsov 1968; Petzold and Austin 1968) and of concave mirrors as the reflectors, have led to improved versions of this general design. An optical pathlength of 10 m was achieved by Jerlov (1957) by using multiple reflections between three concave mirrors. A currently available commercial instrument with a folded path is the HOBILabs c meter.

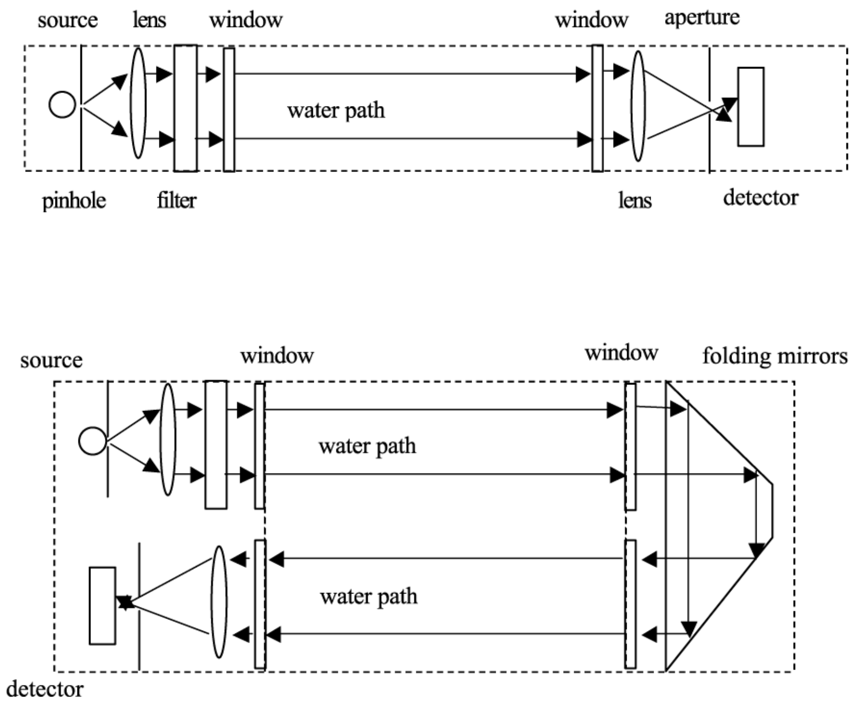

Fig. 2.1 Schematic illustrations of direct path (top panel) and folded path (bottom panel) beam transmissometers designs.

Other Types of Transmissometers

A ***variable pathlength transmissometer*** is probably the most desirable, and elusive, c-meter design concept. One desirable factor would be such an instrument's ability to adjust the pathlength to make it optimal for the measuring conditions (see *Pathlength Considerations*, below). More importantly, the variable pathlength instrument is self-calibrating. To understand this property of such an instrument, examine the basic equation (1.6) for transmissometer measurements. For any transmissometer measurement over pathlength r_i, the dark-corrected detector output $V_T(\lambda, r_i)$ is proportional to the flux reaching the detector window $\Phi_T(\lambda, r_i, 0, \bullet)$. If two transmissometer measurements are made using different path lengths, r_1 and r_2, the transmittance over the pathlength difference between the two measurements is simply

$$T(\lambda, r_2 - r_1) \equiv \frac{\Phi_T(\lambda, r_2, 0, \bullet)}{\Phi_T(\lambda, r_1, 0, \bullet)} = \frac{V_T(\lambda, r_2)}{V_T(\lambda, r_2)}, \tag{2.1}$$

and $c(\lambda)$ may be calculated from (1.6) with $r_T = r_2 - r_1$. The assumptions implicit in this calculation are that the beam attenuation coefficient is constant over the time and space extents of the measurements, and that the optical alignment and electronic properties of the instrument also are constant over time.

Barth *et al*. (1997) describe the design and application of a variable pathlength instrument for use in coastal waters. However, they also note that the errors in alignment made their instrument unsuitable for clear water applications. The requirement to exactly repeat the optical alignment at two distances is the most difficult aspect of building a variable pathlength instrument. Small changes in the alignment of the reference detector, or reflector will introduce large errors in the beam attenuation coefficient by causing the focal point of the beam to wander relative to the aperture in front of the detector. If biofouling exists, the spatial gradients in the fouling will cause $V_T(\lambda, r_i)$ to vary if the alignment is not perfect. Additionally, if the beam is not truly collimated, but instead has a slight divergence, the beam divergence will cause a different area of the detector window to be illuminated in each measurement, and any spatial gradients in the optical properties of the window will translate into errors in $c(\lambda)$.

Many laboratory ***benchtop spectrophotometers*** have a design very similar to a collimated beam transmissometer. A complication that arises when using laboratory spectrophotometers to measure beam attenuation is that much of the scattered light is kept in the sample by the total-internal-reflection at the glass-air interface. This makes it more likely that multiply scattered light will be received at the detector. This problem can be reduced by the addition of light baffles within the sample cuvette.

Source and Detector Characteristics

The transmittance ratio $\dfrac{\Phi_T(\lambda, r_T, 0, \bullet)}{\Phi_o(\lambda, 0, 0, \bullet)}$, *i.e.* the ratio of the flux transmitted to the detector window divided by the flux entering the water at the source window, must be known to compute $c(\lambda)$ from (1.6). A transmissometer does not actually measure either of these quantities. A transmissometer's detector output signal $V_D(\lambda)$ represents its response in the presence of flux $\Phi_D(\lambda)$, the part of $\Phi_T(\lambda, r_T, 0, \bullet)$ that arrives at the detector after passing through the instrument's detector assembly window and other optical elements (Fig. 2.1). Because of reflections and absorption during transmission through windows and other optical components, $\Phi_T(\lambda, r_T, 0, \bullet) > \Phi_D(\lambda)$, but assuming the optical throughput is linear, $\Phi_T(\lambda, r_T, 0, \bullet) \propto \Phi_D(\lambda)$. The detector's "dark" response $V_D^{dark}(\lambda)$ is any signal output that is present when the source is off and $\Phi_T(\lambda, r_i, 0, \bullet) = 0$. If the detector's electrical response is linear, $\Phi_D(\lambda) \propto \left[V_D(\lambda) - V_D^{dark}(\lambda)\right]$ and we may write

$$\Phi_T(\lambda, r_T, 0, \bullet) = C_D\left[V_D(\lambda) - V_D^{dark}(\lambda)\right], \text{ W nm}^{-1}, \tag{2.2}$$

where C_D is a constant, with units of $\left[\text{W nm}^{-1}\text{V}^{-1}\right]$, accounting for the combined effects of optical losses and the detector's flux responsivity.

A measure of the flux $\Phi_o(\lambda, 0_i, 0, \bullet)$ is still required if the transmission is to be determined. A beam splitter before the source window can be used to shunt a proportion of the source light to a reference detector to provide a measure of the flux being sent into the water. Because of losses associated with the source windows and beam splitter, the reference detector receives, and responds to, a flux proportional to $\Phi_o(\lambda, 0_i, 0, \bullet)$ and we have that

$$\Phi_o(\lambda, 0, 0, \bullet) = C_R\left[V_R(\lambda) - V_R^{dark}(\lambda)\right], \text{ W nm}^{-1}, \tag{2.3}$$

where $V_R(\lambda)$ and $V_R^{dark}(\lambda)$ are the reference detector response and ambient (dark) signals, respectively, and C_R is a second system response constant.

The transmittance may now be written as the ratio of (2.2) and (2.3)

$$T(\lambda, r_T) = \frac{\Phi_T(\lambda, r_T, 0, \bullet)}{\Phi_o(\lambda, 0, 0, \bullet)} = C_T \frac{\left[V_D(\lambda) - V_D^{dark}(\lambda)\right]}{\left[V_R(\lambda) - V_R^{dark}(\lambda)\right]}, \tag{2.4}$$

where $C_T = \dfrac{C_D}{C_R}$.

If the source output is constant, the constant $\left[V_R(\lambda) - V_R^{dark}(\lambda)\right]$ may be absorbed in C_T and (2.4) reduces to

$$T(\lambda, r_T) = \frac{\Phi_T(\lambda, r_T, 0, \bullet)}{\Phi_o(\lambda, 0, 0, \bullet)} = C_T\left[V_D(\lambda) - V_D^{dark}(\lambda)\right], \tag{2.5}$$

and there is no need to use a reference detector[10] output to calculate transmittance.

Depending on a transmissometer's design, we must determine the coefficient C_T in either (2.4) or (2.5). It is not practical to determine the system response constants based on first principles, because they are dependent on the optical component throughputs, the combined response(s) of the detector(s), and electronic circuits. Instead , a system's calibration constant C_T [dimensionless in (2.4), or in V^{-1} in (2.5)] is typically determined by measuring the instrument's output in a "standard" medium having a known beam attenuation coefficient $c_{STD}(\lambda)$. For oceanographic transmissometers, the "standard" medium is highly purified water (Sect. 2.3 below), and $c_{STD}(\lambda) = c_w(\lambda)$ (Ch. 1, Sect. 1.2).

Transmissometer Response Temperature Dependence

The source output, responsivity of the detector, and performance of other electronic components tend to be temperature dependent. This causes the calibration constants to be temperature dependent. Two approaches are used to remove the temperature dependence, 1) add compensating electronics that allow the voltage output to remain constant over a temperature range, or 2) measure the temperature of the instrument and determine the how the constants change with temperature. The first technique is used in many single-wavelength transmissometers, such as the Sea Tech and WET Labs transmissometers. The second approach is used in the WET Labs ac-9 spectral absorption and beam attenuation meter.

Spectral Characteristics

Many areas of research in ocean optics require knowledge of the spectral beam attenuation coefficient $c(\lambda)$ at more than one wavelength λ. Several c-meters have been built to provide this spectral information. Matlack (1974) used an instrument with a grating monochromator to measure $c(\lambda)$ in the wavelength range from 385 nm to 565 nm. Using a pair of circular wedge interference filters, Lundgren (1975) was able to measure the beam attenuation coefficient at wavelengths between 340 nm and 730 nm. More recent transmissometers that use a monochromator as the detector include the one described by Barth *et al*. (1997), and the WET Labs Histar. Another design for obtaining the spectral beam attenuation coefficient utilizes several interference filters mounted in a wheel that rotates them through the beam. Examples of filter-wheel c-meter designs include the VLST (Petzold and Austin 1968) and the WET Labs ac-9 (Moore *et al*. 1992; Van Zee *et al*. 2002).

Beam Geometry, Detector Acceptance Angle and Scattered Light

Real transmissometers do not have perfectly collimated sources or detectors. Unlike the idealized detector concept of Fig. 1.4 (Ch. 1, Sect. 1.3), a detector with a finite acceptance angle, or Field of View (FOV) ψ_{FOV}, detects photons that are singly scattered in the range $0 < \psi \le \psi_{FOV}$. Therefore, the flux $\Phi_T^M(\lambda, r_T, 0, \bullet)$ arriving at a

[10] A reference detector may be used in a feedback circuit to stabilize an LED source. However, the reference detector signal is not usually included in the instrument's data output stream in constant source output designs of this type.

transmissometer's detector assembly window and subsequently measured (see above) exceeds the true flux directly transmitted along the path direction $\psi \equiv 0$ according to

$$\Phi_{\mathrm{T}}^{\mathrm{M}}\left(\lambda, r_{\mathrm{T}}, 0, \bullet\right) = \Phi_{\mathrm{T}}\left(\lambda, r_{\mathrm{T}}, 0, \bullet\right) + 2\pi \int_{0}^{\psi_{\mathrm{FOV}}} \beta\left(\lambda, \psi, \varphi\right) \sin\psi d\psi \,, \tag{2.6}$$

where $\beta(\lambda, \psi, \varphi)$ is the volume scattering function (VSF) (Ch. 1, Sect. 1.5). In other words, because a transmissometer measures a portion of the forward scattered light, its measurement overestimates the transmittance $T(\lambda, r_{\mathrm{T}})$ and underestimates the beam attenuation coefficient calculated with equation (1.6). The acceptance angle, and thus the scattering error, is dependent on the optical elements of the instrument. There is no standard specified for transmissometer acceptance angle, and each manufacturer may use a different one for each particular instrument design. Therefore, were the transmittance of a homogeneous water volume to be measured a number of perfectly calibrated beam attenuation meters from HOBILabs, WET Labs, or Sea Tech, for example, each instrument model would yield a slightly different $c(\lambda)$, because of its different acceptance angle. These differences also depend on the shape of VSF.

These considerations lead to two questions. What is the best detector acceptance angle choice for a transmissometer design? What method should be used to correct the beam attenuation measurements for scattered light acceptance?

The first question appears to have a simple answer. The above discussion and equation (2.8) would seem to imply that the smaller the acceptance angle, the better the measurement. That may not be correct. One must further consider what is being measured when choosing the acceptance angle (Pegau *et al.* 1995), and particularly at very small angles, in the presence of near-forward scattering. Density fluctuations due to natural, or instrument related, turbulence steer the beam into random fluctuations and increase the apparent beam attenuation coefficient (Bogucki *et al.* 1998) independently from ordinary molecular and particle scattering processes (Ch. 1, Sect. 1.5). How might this phenomenon affect a particular application of the measurement? Were a person interested in inverting the spectral beam attenuation coefficient to determine particle properties, they wouldn't want a beam attenuation meter that is very sensitive to scattering by turbulence. For active LIDAR imaging systems, on the other hand, it may be important to know the transmittance effects due to very near forward scattering independent of the sources that may dominate the scattering process. From another perspective, the angular resolution of radiative transfer models tends to be larger than one degree, so fine angular resolution of the volume scattering coefficient and related beam attenuation coefficient is not needed for accurate model calculations (Mobley *et al*, 1993). For many such calculations it is preferable to smooth the highly forward peaked phase function (Fig. 1.3, Ch. 2) and decrease the beam attenuation coefficient accordingly. Gordon (1993) indicates that for irradiance level radiative transfer it is possible to completely disregard scattering in the first 15°, an angle much larger than the acceptance angles of transmissometers. Finally, from an engineering perspective, it is more difficult to build a stable transmissometer with a very small acceptance angle. Based on these considerations, most transmissometers are designed with an acceptance angle $\lesssim 1^{\circ}$.

The second question has been addressed by several investigators over the years (Gumprecht and Sliepcevich, 1953; Jones and Wills, 1956; Jerlov, 1957; Duntley, 1963; Voss and Austin, 1993). Voss and Austin (1993) examined the scattering error for both collimated beam and cylindrically limited instruments designs. They found that the percent error increases with increasing acceptance angle and with increasing $c(\lambda)$. The average error for a 670 nm transmissometer with a 1.0° acceptance angle is approximately 19%. However, accurate correction of an apparent $c_{\mathrm{M}}(\lambda)$ measured by that instrument would require knowing both the VSF $\beta(\lambda, \psi, \varphi)$ over the range $0 < \psi \le \psi_{\mathrm{FOV}}$, and the single scattering albedo $\omega_{\mathrm{o}}(\lambda) = \dfrac{b(\lambda)}{c(\lambda)}$ (Vol. I, Ch. 2, Sect. 2.4). To date, very few reliable measurements have been made of $\beta(\lambda, \psi, \varphi)$ at angles less than 1°. Given the extreme rate of increase in the magnitude of the VSF for particles $\beta_{\mathrm{p}}(\lambda, \psi, \varphi)$, and for turbulence, as $\psi \to 0$ (Ch. 1, Fig. 1.3), any estimate of its integrated value over the range $0 < \psi \le 1^{\circ}$ would be highly uncertain. That uncertainty would transmit directly into any $c(\lambda)$ correction algorithm attempting to account for the effects of the near-forward VSF.

The best approach to dealing with the effects of scattered light in measured beam attenuation coefficients may be that proposed by both Voss and Austin (1993) and Pegau *et al*. (1995). That is, do not try to apply any scattering corrections to the measured determination of $c(\lambda)$. Simply report the acceptance angle characteristics of the transmissometer used to make the measurements, and leave all considerations of how to handle scattering artifacts to the user of the data. Internal consistency of IOP is obtained by including light scattered up to a certain acceptance angle ψ_{FOV} in the beam attenuation coefficient, and not including it in the VSF. We may rerwrite (1.1), $c(\lambda) = a(\lambda) + b(\lambda)$, as

$$c(\lambda) = a(\lambda) + 2\pi \int_{\psi_{\mathrm{FOV}}}^{\pi} \beta(\lambda,\psi)\sin\psi d\psi + 2\pi \int_{0}^{\psi_{\mathrm{FOV}}} \beta(\lambda,\psi)\sin\psi d\psi ,$$

or,

$$c_{\mathrm{m}}(\lambda) = c(\lambda) - 2\pi \int_{0}^{\psi_{\mathrm{FOV}}} \beta(\lambda,\psi)\sin\psi d\psi = a(\lambda) + 2\pi \int_{\psi_{\mathrm{FOV}}}^{\pi} \beta(\lambda,\psi)\sin\psi d\psi = a(\lambda) + b_{\mathrm{m}}(\lambda)$$

where $c_{\mathrm{m}}(\lambda)$ and $b_{\mathrm{m}}(\lambda)$ are the measured beam attenuation and volume scattering coefficients, respectively.

In another design variant, the beam is cylindrically limited, rather than collimated. In the cylindrically limited light arrangement, the pinhole at the source is imaged on the receiver lens, and the receiver aperture is focused on the source lens. This design illuminates a large volume of water and uses more of the source light. No currently available commercial instruments use the cylindrically limited design, although at one point in history, transmissometers of this type were manufactured by Martek. The Visibility Laboratory Spectral Transmissometer (VLST) was a laboratory-built instrument using a cylindrically limited beam in a folded path configuration (Petzold and Austin 1968). Several copies of the VLST, built in the late 1970's, continued in use to measure $c(\lambda)$ until *circa* 1990.

Pathlength Considerations

One issue that must be addressed when designing a transmissometer is what the in-water pathlength should be. Scientifically, it is important to keep the pathlength long enough that the sample volume presents a statistical average of the surrounding water, and short enough that multiply scattered light is not incorporated into the beam. In most ocean waters, multiply scattered light is not in general a problem for the commercially available transmissometers. If scattered light leaves the beam then it will take two additional scattering events to get the light back into the beam and redirected towards the detector. The addition of baffles along the light path can nearly eliminate any possibility of multiply scattered light being detected in ordinary circumstance. In extremely turbid waters, however, the single scattering albedo is very large, and the volume scattering phase function $\tilde{\beta}(\lambda,\psi,\varphi)$ is extremely biased in the near forward direction (Fig. 1.3, Ch. 1). Under such conditions, if $r_{\mathrm{T}} > 3c(\lambda)^{-1}$ m , there is a significant probability that some fraction of scattered photons will undergo 3 or more successive small angle scattering events, re-enter the transmission path, and join the flux reaching the detector. The apparent beam attenuation coefficient will be artificially reduced if this occurs.

There are also engineering concerns associated with the optical pathlength. The path must be short enough that light reaches the detector; it would do no good to have an instrument with a pathlength $r_{\mathrm{T}} \approx 10c(\lambda)^{-1}$ m , because the transmitted signal would not be detectable. On the other hand, the pathlength must be long enough for attenuation to reduce the transmitted flux enough that the difference in incident and transmitted fluxes are large enough to be measurable. Longer pathlengths also reduce the relative uncertainty in the measurement of the pathlength r_{T} .

A pathlength in the range $c(\lambda)^{-1} \le r_{\mathrm{T}} \le 3c(\lambda)^{-1}$ is generally considered close to optimal. As electronics and sources have improved, however, instruments with pathlengths $r_{\mathrm{T}} < c(\lambda)^{-1}$ m have been shown to work well over a wide range of oceanic conditions.

Ambient Light Rejection in Open and Enclosed Path Transmissometers

The basic transmissometer designs (Fig. 2.1) do not physically reject all ambient sunlight, which could add to the measured flux. Enclosed path designs that place the optical path within a cell through which the water is pumped, such as the ac-9, have more physical blocking of ambient light, but are not totally immune to its effects. Some scheme must be developed to remove ambient light artifacts. A simple approach is to measure the signal with the source on and with the source off. The ambient signal with the source off is used as the dark reference for relating output signal to transmitted flux. The current generation of instruments use a more sophisticated, but similar, approach. The light source is rapidly modulated (chopped) and the detector output is phase locked to the modulation frequency, so that the transmitted flux is proportional to the amplitude of the alternating component of detector output. The key underlying assumption is that the natural light field varies slowly and is not part of the alternating signal. This approach may have difficulties when the ambient light also varies rapidly, such as with indoor lights that have a 60 Hz fluctuation, or near the ocean surface where waves may rapidly modulate the light field. Even with good electronic rejection of ambient light, it is wise to reduce the possible influence of ambient light by using baffles and careful positioning of the instrument.

2.3 CHARACTERIZATION and CALIBRATION OF BEAM TRANSMISSOMETERS

Calibration With Pure Water

As explained above, the calibration constant C_T for a transmissometer is determined by measuring its response to a "standard" medium having a known value of $c_{\mathrm{STD}}(\lambda)$. The optical "standard" medium commonly used to calibrate oceanographic transmissometers and absorption meters (Ch. 3) is pure water, so that $c_{\mathrm{STD}}(\lambda) = c_{\mathrm{w}}(\lambda) = a_{\mathrm{w}}(\lambda) + b_{\mathrm{w}}(\lambda)$. The recommended values of $a_{\mathrm{w}}(\lambda)$ and $b_{\mathrm{w}}(\lambda)$ are taken from Table 1.2, as explained in Ch. 1, Sect. 1.2.

Pure water of optical calibration grade is freshly prepared by methods described in Chapter 3. This difficult step is critical, because residual traces of particles and/or dissolved organic material introduce serious calibration offsets and relative uncertainties between calibrations. The pure water standard is introduced into the optical path by one of two methods:

1. An open path transmissometer must be thoroughly cleaned and rinsed in purified water, and then immersed in a test tank containing the pure water standard. Care must be taken to prevent bubbles from collecting on the instrument's optical windows. It is ordinarily not practical to carry out this calibration procedure at sea.
2. To calibrate an enclosed path instrument, a volume of the pure water standard is pumped through the flow-through measurement cell, as described in detail in Chapter 3 for the ac-9, as an example. Procedures to assure bubbles do not form within, or be introduced into, the flow-through measurement cell (Ch. 3) must be followed carefully. This pure-water calibration procedure can be carried out at sea, and it is recommended to do so daily, whenever possible.

In either case, after allowing suitable time for the instrument to warm up, the instrument signal outputs in response to flux transmitted in the pure water standard and dark (ambient) background, $V_{\mathrm{D,w}}(\lambda)$ and $V_{\mathrm{D,w}}^{\mathrm{dark}}(\lambda)$ [and if appropriate, also $V_{\mathrm{R,w}}(\lambda)$ and $V_{\mathrm{R,w}}^{\mathrm{dark}}(\lambda)$], are recorded over a several minute sampling period and averaged.

For pure water, the forward scattering is sufficiently small that the acceptance angle has little effect on the calibration. From equation (1.7) (Ch. 1), the transmittance of the pure water standard is $T_{\mathrm{w}}(\lambda, r_{\mathrm{T}}) = e^{-c_{\mathrm{w}}(\lambda) r_{\mathrm{T}}}$. For an instrument with a source reference detector we substitute from (2.4) to write

$$C_{\mathrm{T}}(\lambda) = T_{\mathrm{W}}(\lambda, r_{\mathrm{T}}) \frac{\left[V_{\mathrm{R,w}}(\lambda) - V_{\mathrm{R,w}}^{\mathrm{dark}}(\lambda)\right]}{\left[V_{\mathrm{D,w}}(\lambda) - V_{\mathrm{D,w}}^{\mathrm{dark}}(\lambda)\right]}, \tag{2.7}$$

or for an instrument with a constant source output we substitute from (2.5) to write

$$\mathrm{C_T}(\lambda)=\frac{T_{\mathrm{W}}(\lambda,r_{\mathrm{T}})}{\left[V_{\mathrm{D,w}}(\lambda)-V_{\mathrm{D,w}}^{\mathrm{dark}}(\lambda)\right]}, \qquad (2.8)$$

as appropriate.

By straightforward combinations of (1.6), (2.4) and (2.7) it is easy to show that for a transmissometer with a source reference detector,

$$\begin{aligned} T(\lambda,r_{\mathrm{T}})&=T_{\mathrm{W}}(\lambda,r_{\mathrm{T}})\frac{\left[V_{\mathrm{R,w}}(\lambda)-V_{\mathrm{R,w}}^{\mathrm{dark}}(\lambda)\right]\left[V_{\mathrm{D}}(\lambda)-V_{\mathrm{D}}^{\mathrm{dark}}(\lambda)\right]}{\left[V_{\mathrm{D,w}}(\lambda)-V_{\mathrm{D,w}}^{\mathrm{dark}}(\lambda)\right]\left[V_{\mathrm{R}}(\lambda)-V_{\mathrm{R}}^{\mathrm{dark}}(\lambda)\right]},\text{ and} \\ c(\lambda)-c_{\mathrm{w}}(\lambda)&=\frac{1}{r_{\mathrm{T}}}\ln\left\{\frac{\left[V_{\mathrm{R,w}}(\lambda)-V_{\mathrm{R,w}}^{\mathrm{dark}}(\lambda)\right]\left[V_{\mathrm{D}}(\lambda)-V_{\mathrm{D}}^{\mathrm{dark}}(\lambda)\right]}{\left[V_{\mathrm{D,w}}(\lambda)-V_{\mathrm{D,w}}^{\mathrm{dark}}(\lambda)\right]\left[V_{\mathrm{R}}(\lambda)-V_{\mathrm{R}}^{\mathrm{dark}}(\lambda)\right]}\right\} \end{aligned}, \qquad (2.9)$$

or combining (1.6), 2.(5) and (2.8) for a transmissometer with a constant source output

$$\begin{aligned} T(\lambda,r_{\mathrm{T}})&=T_{\mathrm{W}}(\lambda,r_{\mathrm{T}})\frac{\left[V_{\mathrm{D}}(\lambda)-V_{\mathrm{D}}^{\mathrm{dark}}(\lambda)\right]}{\left[V_{\mathrm{D,w}}(\lambda)-V_{\mathrm{D,w}}^{\mathrm{dark}}(\lambda)\right]},\text{ and} \\ c(\lambda)-c_{\mathrm{w}}(\lambda)&=\frac{-1}{r_{\mathrm{T}}}\ln\left\{\frac{\left[V_{\mathrm{D}}(\lambda)-V_{\mathrm{D}}^{\mathrm{dark}}(\lambda)\right]}{\left[V_{\mathrm{D,w}}(\lambda)-V_{\mathrm{D,w}}^{\mathrm{dark}}(\lambda)\right]}\right\}. \end{aligned} \qquad (2.10)$$

The essential calibration factors to be reported, therefore, are the detector response and ambient (dark) offset in pure water $V_{\mathrm{D,w}}(\lambda)$ and $V_{\mathrm{D,w}}^{\mathrm{dark}}(\lambda)$, and if a source reference detector is used also its response and ambient offset $V_{\mathrm{R,w}}(\lambda)$ and $V_{\mathrm{R,w}}^{\mathrm{dark}}(\lambda)$. The total beam attenuation coefficient $c(\lambda)$ may be easily determined by adding $c_{\mathrm{w}}(\lambda)$ from Table 1.1 (Ch. 1) to the difference calculated with equation (2.9) or (2.10).

An alternative approach to determining the total beam attenuation coefficient directly from the measured voltage response is to determine, from the pure water calibration, a calculated offset reference voltage $V_{\mathrm{ref}}(\lambda)$ and dark offset $V_{\mathrm{dark}}(\lambda)$ such that the total transmittance may be calculated directly as

$$T(\lambda,r_{\mathrm{T}})=\frac{\left[V_{\mathrm{D}}(\lambda)-V_{\mathrm{D,w}}^{\mathrm{dark}}(\lambda)\right]}{\left[V_{\mathrm{ref}}(\lambda)-V_{\mathrm{D,w}}^{\mathrm{dark}}(\lambda)\right]}, \qquad (2.11)$$

where it is assumed that $V_{\mathrm{D}}^{\mathrm{dark}}(\lambda)=V_{\mathrm{D,w}}^{\mathrm{dark}}(\lambda)$ varies very slowly over time and may be treated as an instrument constant. This approach is only used with transmissometers assumed to have a constant source output, examples of which include the former SeaTech red transmissometers. The value of $V_{\mathrm{ref}}(\lambda)$ is calculated by combining (2.11) with the transmittance relationship (2.10) as

$$T(\lambda,r_{\mathrm{T}})=T_{\mathrm{W}}(\lambda,r_{\mathrm{T}})\frac{\left[V_{\mathrm{D}}(\lambda)-V_{\mathrm{D}}^{\mathrm{dark}}(\lambda)\right]}{\left[V_{\mathrm{D,w}}(\lambda)-V_{\mathrm{D,w}}^{\mathrm{dark}}(\lambda)\right]}=\frac{\left[V_{\mathrm{D}}(\lambda)-V_{\mathrm{D,w}}^{\mathrm{dark}}(\lambda)\right]}{\left[V_{\mathrm{ref}}(\lambda)-V_{\mathrm{D,w}}^{\mathrm{dark}}(\lambda)\right]},$$

from which it easily follows that

$$V_{\mathrm{ref}}(\lambda)=\frac{V_{\mathrm{D,w}}(\lambda)-V_{\mathrm{D,w}}^{\mathrm{dark}}(\lambda)}{T_{\mathrm{W}}(\lambda,r_{\mathrm{T}})}+V_{\mathrm{D,w}}^{\mathrm{dark}}(\lambda),\ \mathrm{V}. \qquad (2.12)$$

The Sea Tech transmissometers were calibrated to read $c_{\mathrm{w}}(650)=0.364\ \mathrm{m}^{-1}$ in pure water. This representation and approach perhaps simplifies the determination of $c(\lambda)$ for the inexperienced user, but at the same time obscures the value of $c_{\mathrm{w}}(\lambda)$ used to determine the offset reference voltage.

Air "Calibrations"

The sensors output signal response $V_{\mathrm{D,air}}^{\mathrm{f}}$ and dark offset $V_{\mathrm{D,air}}^{\mathrm{dark,f}}$ are recorded in air by the manufacturer at the time of each factory water calibration. These values are typically reported with the calibration records, as "factory" air calibration and dark values (and thus the superscript "f"), to allow the user to periodically record "air calibration", or "air tracking" data as a check on instrument stability. Air tracking is primarily intended to be used to monitor offsets in the instrument's output due to changes in the optical system caused by shipping or mounting of the instrument to a cage or other deployment package. Air tracking can also be used to monitor instrument drift over extended periods of time. Historically, before the advent of pure water field calibrations, the air calibration was the only stability tracking method available.

Air tracking data is best obtained in the laboratory, where the environment is consistently clean and dry, preferably before and after each transmissometer deployment. Although air calibrations can be performed while in the field, it is at best, difficult to do them on a ship due to the moist environment. Readings in air may be significantly offset by small amounts of moisture either condensed on, or adsorbed in the windows.

Detailed protocols for carrying out air calibrations are provided for particular instruments by the manufacturer. In general terms, the protocols include instructions and methods for careful cleaning of optical surfaces, allowing time for exposed optical surfaces to dehydrate in a dry environment, and procedures to avoid or compensate for temperature increases when the instrument is operated in air.

User air calibration values can be used to adjust the pure water calibration and responses to correct for instrument drift as

$$V_{\mathrm{D,w}}^{\mathrm{adjusted}} = \frac{V_{\mathrm{D,air}} - V_{\mathrm{D,air}}^{\mathrm{dark}}}{V_{\mathrm{D,air}}^{\mathrm{f}} - V_{\mathrm{D,air}}^{\mathrm{dark,f}}} \left[V_{\mathrm{D,w}}^{\mathrm{f}} - V_{\mathrm{D,w}}^{\mathrm{dark,f}} \right], \tag{2.13}$$

and the adjusted pure water-response and dark values are substituted into (2.10) to calibrate field measurements. If the manufacturer instead provides a factory reference voltage for calibrating the instrument using equation (2.11), the adjusted pure water and dark values should be substituted in (2.12) to determine $V_{\mathrm{ref}}^{\mathrm{adjusted}}$. Air calibration adjustments of this type are usually recommended only for instruments with "constant" LED source output, such as the WET Labs C-Star, older SeaTech red transmissometers, and other similar instruments by different manufacturers. Field water calibrations are the recommended basis for correcting drifts in closed path, flow-through cell instrument, such as the ac-9.

Instrument Temperature Dependence

The change in a transmissometer's response and dark values are usually determined by measuring response variations, with the optical path in air, or in a dry, inert gas such as Nitrogen or Argon, as the instrument temperature is varied. The response and dark values at each internal instrument temperature (an ancillary measurement and data output needed for temperature corrections) are recorded, and reported either as a lookup table of correction factor and temperature pairs, or as the coefficients of a polynomial function of temperature that has been fit to the correction factors. Instruments that have a closed, flow-through optical cell are usually characterized in a water bath, the temperature of which is cycled over a range typically from 5 $^{\circ}$C to 30 $^{\circ}$C over the course of the experiment; to avoid condensation, the flow-through cell is usually filled with a dry, inert gas and sealed. The internal instrument temperatures are somewhat higher than the ambient temperature, due to heating by the electronic circuits and source. If this experiment is done with air in the optical path of an open-path transmissometer, *i.e.* in a temperature controlled chamber, some method must be used and documented to avoid artifacts due to condensation on the windows.

2.4 FIELD MEASUREMENT METHODS

The procedures for measuring *in situ* profiles, over depth *z*, of $c(z,\lambda)$ using constant output LED source transmissometers are straightforward. The instrument is connected into a data acquisition system and mounted on a profiling cage following the manufacturer's instructions. If the instrument has an analog output, the user must

ensure that the external analog-to-digital converter used to digitize the readings is calibrated in absolute units of V, since that is the basis on which the instrument has been calibrated.

The windows on the beam transmissometer must be cleaned with lens cleaner, or a mild detergent solution, and a soft cloth, or tissue, rinsed with distilled water, then rinsed with isopropyl alcohol and wiped dry. An approximate air calibration reading should be made before every cast to verify that the windows are clean. A transmissometer dark voltage should also be measured at this time. These on-deck air calibrations should be logged and compared to the more careful air calibrations done under dry laboratory conditions before and after each cruise (Section 2.3). If pre- and post-cruise air calibrations are significantly different, the time history should indicate whether the change occurred suddenly (*e.g.* a scratch in the window), or as a drift over time.

Each time an open-path transmissometer is placed into the water, care must be taken to assure that bubbles do not collect on the windows, particularly if the instrument is mounted in a vertical orientation.

Protocols covering methods for making field measurements with the ac-9 instrument are described in detail in Zee *et al*. (2002). Some critical aspects of these protocols are briefly reviewed in Chapter 3 to emphasize their importance.

2.5 DATA ANALYSIS METHODS

There are several generic steps needed to process and analyze a vertical profile of measured transmissometer data:

1. ***Merge the transmissometer data*** with externally measured ***depth*** and ***temperature data***. Assuming that the transmissometer does not have an internal, high-quality depth transducer, it is usually mounted together with a CTD to provide the depth and water temperature fields. If the transmissometer output data record does not include the internal instrument temperature measured by a built-in thermistor, external water temperature provides the basis for any temperature compensation adjustments that may be required.
2. Apply ***lag corrections*** to account for the time interval between when water enters the intake port and when it enters the beam-attenuation measurement optical path in a flow-through transmissometer.
3. Subtract the ***depth offset*** between the pressure transducer used to measure package depth and either

a. the intake port of a flow-through transmissometer, or

b. the midpoint of the optical path in an open path transmissometer.

4. ***Field calibration adjustments*** should be applied by the methods specified by the manufacturer of a particular instrument. In many cases this will involve entering the changes in an instrument calibration file used by the computer software that implements and applies (2.9) or (2.10) to calibrate the data.
   a. Pure water calibration results are the preferred source of these adjustments for flow-through instruments.
   b. Air calibration for tracking drift corrections should be applied using only data from calibrations carried out under dry laboratory conditions and showing insignificant variations between replicated calibrations. When the manufacturer represents the calibration coefficients in terms of a reference signal to be applied using (2.11), the corrected air calibration factor is computed using (2.13).
5. ***Instrument Internal Temperature Compensation*** factors should be applied in the manner specified by the manufacturer of a particular instrument.
6. *Compute transmittances* $T(\lambda, r_T)$, ***and beam attenuation coefficients*** $c(\lambda) - c_w(\lambda)$ offsets, ***relative to pure water*** using the appropriate combination of equations (2.9), (2.10), or (2.11) with (1.6) for the instrument type and output data.
7. ***Add pure water*** $c_w(\lambda)$, determined from Table 1.1, to $c(\lambda) - c_w(\lambda)$ to obtain the ***total beam attenuation coefficient*** $c(\lambda)$.

Detailed procedures required to carry out each of the above steps for particular instrument are typically provided by the manufacturer. WET Labs Inc., for example, provides both a User's Manual for it's *ac-9* absorption and beam attenuation coefficient meter, and a detailed ac-9 Protocol Manual (Van Zee *et al*. 2002); additional information from the latter document, regarding absorption and beam attenuation measurements, is outlined in Chapter 3.

Many of the steps listed above apply also when a transmissometer is installed and operated on a ship as a component of an along-track measurement system. The lengthy plumbing path in such a system introduces intake-to-measurement lags of up to several minutes, while a research vessel typically advances approximately one Km in 3 min. Therefore, accurate temporal and spatial co-registration of, *e.g.*, surface water temperature, chlorophyll a fluorescence, and $c(\lambda)$ requires accurate determination of the flow rate and lag time between a water volume's intake (usually in a ship's sea chest), passage through some debubbler apparatus, and its arrival in the measurement cell of each instrument.

REFERENCES

Barth, H., K. Grisard, K. Holtsch, R. Reuter, and U. Stute, 1997. Polycromatic transmissometer for *in situ* measurements of suspended particles and gelbstoff in water. *Appl. Opt.*, **36(30):** 7919-7928.

Bogucki, D.J., J.A. Domaradzki, D. Stramski and J.R.V. Zaneveld, 1998. Comparison of near-forward light scattering on oceanic turbulence and particles. *Appl. Opt.*, **37(21):** 4669-4677.

Duntley, S.Q., 1963. Light in the sea. J. Opt. Soc. Amer., 53(2): 214-233.

Gordon, H.R., 1993. Sensitivity of radiative transfer to small-angle scattering in the ocean: Quantitative assessment. *Appl. Opt*., **32(36):** 7505-7511.

Gumprecht, R.O. and C.M. Sliepcevich, 1953: scattering of light by large spherical particles, *J. Opt. Soc. Am.*, **57:** 90-94.

Jerlov, N.G., 1957: A transparency-meter for ocean water, *Tellus*, 9: 229-233.

Jones, D. and M.S. Wills, 1956: The attenuation of light in sea and estuarine waters in relation to the concentration of suspended solid matter, *J Mar. Biol. Assoc. U.K*., **35:** 431-444.

Kitchen, J.C., J.R.V. Zaneveld and H. Pak, 1982: Effect of particle size distribution and chlorophyll content on beam attenuation spectra. Applied Optics. **21**: 3913-3918.

Lundgren, B., 1975: Measurements in the Baltic with a spectral transmittance meter, *Univ. Copenhagen, Inst. Phys. Oceanogr. Rep.*, **30:** 28pp.

Matlack, D.E., 1974: Deep ocean optical measurements (DOM) report on North Atlantic, Caribbean, and Mediterranean cruises, *Tech. Rep. Naval Ordnance Lab.*, pp 1-103.

Moore, C., J.R.V. Zaneveld and J.C. Kitchen, 1992: Preliminary results from an *in situ* spectral absorption meter, *Ocean Optics XI*, *Proc. SPIE* **1750:** 330-337.

Mobley, C.D., and OTHERS, 1993. Comparison of numerical models for computing underwater light fields. *Appl. Opt.*, **32(36):** 7484-7504

Nikolayev, V.P. and A.A. Zhil'tsov, 1968: Simple photoelectric transparency meter, *Oceanology (U.S.S.R.)*, **8:** 428-432.

Pegau, W. S., J. R. V. Zaneveld, and K. J. Voss, 1995: Toward closure of the inherent optical properties of natural waters, *J. Geophys. Res.*, **100:** 13,193-13.

Pettersson, H., 1934: A transparency-meter for sea-water, Medd. Oceanogr. Inst. Gothenberg, Ser. B **4**.

Petzold, T. and R.W. Austin, 19686: An underwater transmissometer for ocean survey work, In: *Underwater Photo-optical Instrument Applications*, Proc. SPIE 12: 133-137.

Timofeeva, V.A., 1960: Instrument for determining the attenuation coefficient of directed light in the sea, *Sov. Oceanogr. 1962 Ser.*, **4:** 79-83.

Van Zee, H., D. Hankins, and C. deLespinasse, 2002: *ac-9 Protocol Document (Revision F)*. WET Labs Inc., Philomath, OR, 41pp.

Voss, K.J. and R.W. Austin, 1993. Beam-attenuation measurement error due to small-angle scattering acceptance. *J. Atmos. and Oceanic Tech*., **19(1):** 113-121

Wattenberg, H., 1938: Untersuchungen uber Durchsichtigkeit und Farbe des Seewassers, I. *Kieler Meeresforsch*., **2**.

Chapter 3

Volume Absorption Coefficients: Instruments, Characterization, Field Measurements and Data Analysis Protocols

Scott Pegau[1], J. Ronald V. Zaneveld[1] and James L. Mueller[2]

College of Oceanographic and Atmospheric Sciences, Oregon State University, Corvallis

[2]Center for Hydro-Optics and Remote Sensing, San Diego State University, California

3.1 INTRODUCTION

Concepts and methods for measuring the absorption coefficient $a(\lambda)$ of seawater are briefly reviewed in Chapter 1 (Sect. 1.4) of this Volume. Chapter 4 of this Volume is devoted to laboratory spectrophotometric methods of measuring absorption of particles and dissolved materials in filtered water samples. The present chapter focuses on commercially available instruments[11] that may be used from ships and moored platforms to practically measure $a(\lambda)$ in support of satellite validation activities. This first version of absorption protocols is particularly focused on instruments that fall under the "reflective tube" design concept briefly introduced in Sect. 1.4. However, the conceptual basis for determining absorption by measuring flux reflected from a diffuse target is also described later in this section. Expanded reviews of protocols using instruments based on other design concepts are deferred for possible consideration in future revisions to this volume.

Reflective Tube Absorption Meter Concepts

In Sect. 1.4 it was observed that to determine the absorption coefficient associated with transmission over an optical pathlength r_{T} (Fig. 1.4), it would be necessary to measure the sum of transmitted and scattered flux at the detector, $\Phi_{\mathrm{K}}(r_{\mathrm{T}}) = \Phi_{\mathrm{T}}(r_{\mathrm{T}}) + \Phi_{\mathrm{B}}(r_{\mathrm{T}})$. Neglecting backscattering, it was suggested that perhaps one might redirect all forward scattered flux to the detector using an *ideal reflective tube*, and determine the absorption coefficient as

$$a = \frac{-1}{r_{\mathrm{T}}} \ln\left(\frac{\Phi_{\mathrm{T}}(r_{\mathrm{T}}) + \Phi_{\mathrm{B}}(r_{\mathrm{T}})}{\Phi_{\mathrm{o}}(0)} \right). \tag{3.1}$$

Of course a perfectly reflecting tube cannot be realized in a real instrument. Nevertheless, because the scattering phase function of suspended particles in natural waters is strongly peaked in the forward direction (Fig. 1.3), it is possible to use this approach to retain more than approximately 85% of scattered photons in the beam reaching the detector of such an instrument. James and Birge (1938) built a laboratory version of such an instrument to measure absorption spectra of lake waters, and Zaneveld *et al*. (1992) introduced an instrument of this type for *in situ* absorption measurements. In essence, such an instrument is simply a poor transmissometer (Chapter 2) that fails to exclude all of the singly scattered photons from its beam transmittance measurement, and therefore, in its ideal realization would measure only losses due by absorption as per equations (1.9) and (1.10).

The transmittance, absorption, scattering and reflection interaction processes that occur in a real reflective tube absorption meter are illustrated schematically in Fig. 3.1. A source emits collimated flux with a cross sectional area slightly less that that of the reflective tube, and flux reaching the other end of the tube is measured by a detector that covers its entire cross-sectional area. Ray paths extending directly from the source to the detector indicate direct transmittance of flux. Ray paths that terminate within the water volume enclosed by the tube indicate absorbed flux.

---

[11] Certain commercial equipment, instruments, or materials are identified in this chapter to foster understanding. Such identification does not imply recommendation, or endorsement, by the National Aeronautics and Space Administration, nor does it imply that the materials or equipment identified are necessarily the best available for the purpose.

In natural waters a large fraction of scattered photons are only slightly deflected in the near forward direction (Fig. 1.3) and proceed directly to the large-area detector without encountering the tube walls. Ray paths with scattering angles large enough to encounter the water-quartz interface, where refraction and reflection take place; the refracted portion is transmitted to the outer quartz-air interface, where another refraction and reflection interaction occurs. For simplicity in this conceptual discussion, we do not consider multiple reflection and refractive transmittance interactions within the thin quartz layer. Ray paths containing a scattering angle less than the critical angle ψ_c associated with total internal reflection at the outer quartz-air interface, are totally reflected on each encounter with the tube wall and are transmitted to the detector over a slightly elongated path; for a quartz reflective tube, $\psi_c \cong 42°$, and thus the total internal reflectance represents a very large fraction of all flux scattered by particles (Fig. 1.3). Flux transmitted along ray paths with a scattering angle in the range $\psi_c < \psi < \frac{\pi}{2}$ undergoes partial transmittance losses $[1-\rho_g(\psi)]$ at each encounter with the reflectance tube, with the reflected portion continuing over a zig-zag path until either reaching the detector or disappearing due to attenuation by absorption and transmission losses in multiple encounters with the tube wall. Flux along ray paths containing a scattering angle $\psi \ge \frac{\pi}{2}$, *i.e.* backscattered flux, is lost from the forward transmittance altogether. Backscattering accounts for only a few percent of scattering by marine particulates (Fig. 1.3).

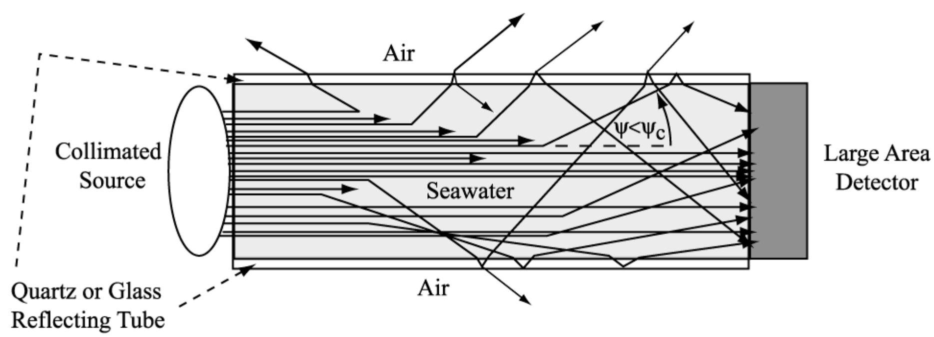

Figure 3.1: Schematic illustration of light interactions and transmission in a reflective tube absorption meter. Ray paths ending in the water represent absorption, and those extending directly from the source to detector represent beam transmittance. Other ray paths indicate scattering interactions: 1) backward scattered paths do not reach the detector, 2) paths with forward scattering at an angle less than the critical angle, *i.e.* $\psi \le \psi_c$, experience total internal reflection by the tube and reach the detector over an elongated optical path, and 3) forward scattered ray paths at angles in the range $\psi_c < \psi < \frac{\pi}{2}$ experience partial losses from the tube at the quartz-air interface, and may or may not reach the detector depending on whether the internally reflected path survives the absorption process.

In the single scattering approximation, the flux measured by the detector of a reflective tube absorption meter may be written

$$\begin{aligned}\Phi_m(r_T) = \Phi_T(r_T) + 2\pi\Phi_o(0)\int_0^{r_T}\int_0^{\psi_c}\beta(\psi)e^{-cr}e^{-a\frac{r_T-r}{\cos\psi}}\sin\psi d\psi dr + \\ 2\pi\Phi_o(0)\int_0^{r_T}\int_0^{\psi_c}\beta(\psi)e^{-cr}e^{-a\frac{r_T-r}{\cos\psi}}\left[\rho_g(\psi)\right]^{N(r_T-r)}\sin\psi d\psi dr\end{aligned}, \quad (3.2)$$

where $\rho_g(\psi)$ is net reflectance of the quartz tube beyond the critical angle, and the exponent $N(r_T - r;\psi)$ is the average number of wall reflections required for a ray path to reach the detector following a scattering event at

distance r and angle ψ. The first integral on the right-hand-side of (3.2) represents flux scattered at angles less than the critical over the optical path, and the second integral represents flux reaching the detector following scattering by angles greater than the critical angle. In either case, the pathlength to the detector from a scattering interaction at distance r is $\frac{r_T - r}{\cos\psi}$, and both types of scattered-reflected paths are attenuated by absorption over this elongated path. The second term also is reduced by incomplete reflectance in $N(r_T - r;\psi) \geq 1$ interactions with the reflective tube.

The measured absorption coefficient is therefore greater than the true absorption coefficient since

$$a_m = \frac{-1}{r_T}\ln\left(\frac{\Phi_m(r_T)}{\Phi_o(0)}\right) > a = \frac{-1}{r_T}\ln\left(\frac{\Phi_T(r_T)+\Phi_B(r_T)}{\Phi_o(0)}\right),$$

and the two may be related as

$$a_m = a + 2\pi\int_0^\pi W(\psi)\beta(\psi)\sin\psi d\psi, \tag{3.3}$$

where the weighting coefficients $W(\psi)$ account for the absorption and wall reflection losses in the two integral terms of (3.2) and for the exclusion of backscattering in the measured flux. In other words, the weighting coefficient $W(\psi)$ may be interpreted as the fraction of light that is scattered at angle ψ that does not reach the absorption detector; it may take values from 0, indicating all light scattered at that angle reaches the detector, to 1, indicating that none of the light reaches the detector. The uncertainty of absorption coefficients determined from measurements with a reflective tube instrument is largely determined by the uncertainty of the methods used to correct for the integrated scattering error (Zaneveld *et al*. 1994), which will be briefly summarized below in Sect. 3.4. The remaining sections of this chapter summarize protocols related to characterization, measurement and data analysis using the ac-9 reflective tube absorption meter.

Determination of Absorption by Measuring Flux Reflected from a Diffuse Reflectance Surface

Figure 3.2 illustrates an alternative proposed instrument concept for use in combination with a backscattering meter (Chapter 5) to determine $a(\lambda)$ *in situ*. A divergent source illuminates a diffusely reflecting target oriented parallel to the instrument's window at a fixed distance d_ρ. An instrument of this type, called the "**α-βeta**", is commercially available through HOBILABS, Inc.

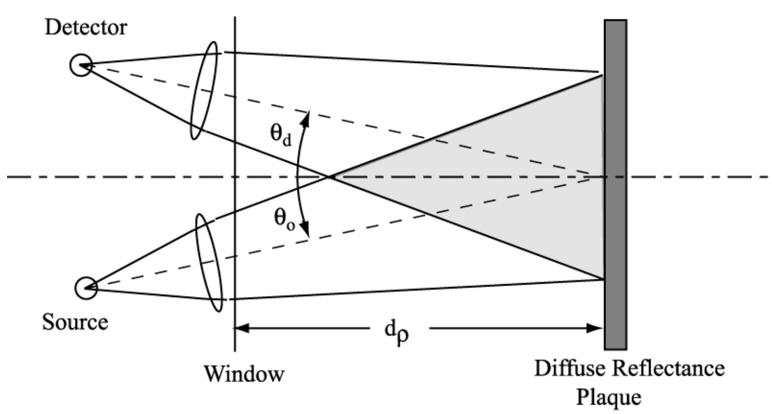

Figure 3.2: Conceptual schematic illustration of an instrument designed to determine the volume absorption coefficient by measuring diffuse reflectance from a plaque. The VSF at one or more angles must be independently and concurrently measured in this approach. See also Figure 5.1, and the related discussion of calibrating a VSF meter using a diffuse reflecting plaque in Section 5.3, in Chapter 5 of this Volume.

For simplicity in this conceptual discussion, we will assume: 1) that the source beam and detector FOV geometries are identical, 2) that the central viewing angles of each are equal, *i.e.* $\theta_o = \theta_d$ (Fig. 3.2), and 3) that the plaque's Bidirectional Reflectance Distribution Function (BRDF) is a constant $\frac{\rho}{\pi}$. The flux reaching the plaque from the source, including flux scattered in the near forward direction (up to ~15^o or so) as well as direct transmission, may be expressed as

$$\Phi_r = k_o \Phi_o \exp\left[-(a + \breve{b}_o)\overline{z}\right], \tag{3.4}$$

where k_o is a constant representing the optical characteristics (reflection and transmission losses, effective detector area, etc.) of the source, $\overline{z}$ is the mean effective pathlength for flux transmitted from the source window to the plaque, $\breve{b}_o = b - 2\pi \int_0^{\psi_f} \beta(\psi) \sin\psi d\psi$ is flux scattered beyond a forward scattering angle $\psi_f \lesssim 15°$ comparable to the beam geometric width. For typical particle phase functions, a very large fraction of singly scattered flux is confined within the forward 15^o cone. By similar reasoning, the flux reflected diffusely from the plaque and reaching the detector may be written as

$$\Phi_d = k_d \frac{\rho}{\pi} \Phi_r \exp\left[-(a + \breve{b}_d)\overline{z}\right] = k_d \frac{\rho}{\pi} k_o \Phi_o \exp\left[-(2a + \breve{b}_o + \breve{b}_d)\overline{z}\right], \tag{3.5}$$

where k_d is a constant accounting for the optical characteristics of the detector assembly, and $\breve{b}_d$ represents scattering losses at angles too large to be detected in a single scattering approximation, *i.e.* the counterpart for $\breve{b}_o$ for a diffuse source and the detector FOV. Equation (3.5) assumes further that the flux backscattered from the intersection volume of the source beam and detector FOV, the shaded conical region in Fig. 3.2, is negligibly small compared to the flux reflected from the plaque. At this point it may be appropriate for the reader to compare the similarities between the instrument concept illustrated Fig. 2.2 (Chapter 2) and the calibration geometry for determining the weighting function of a VSF, as illustrated in Fig. 5.1, and as described for a plaque reflectance measurement geometry at a fixed distance *z* as part of the VSF calibration described in Sect. 5.2 (Chapter 5 of this volume) and in Maffione and Dana (1997).

Following the approach used to determine the backscattering coefficient from a measurement $\beta(\psi^*)$ of the VSF at a single angle ψ^* in the backward direction (Chapter 5, Sect. 5.4), Dana, Maffione and Coenen (HOBILabs, Inc., personal comm., *circa* 2000) originally assumed that

$$\breve{b}_o + \breve{b}_d \cong \chi\beta(\psi^*), \tag{3.6}$$

where χ is an unknown constant. The "α-βeta" instrument designed and manufactured by HOBILabs combines a VSF meter (Chapter 5) to measure $\beta(140°)$ with a device conceptually similar to that illustrated in Fig. 3.2, mounted at opposite ends of a small cylinder.

If the source is regulated to emit constant flux, the system constants of the diffuse reflectance device may be collected as

$$k = F_d k_d \frac{\rho}{\pi} k_o \Phi_o, \tag{3.7}$$

where F_d is the detector assembly's signal responsivity to flux received at the instrument window in water, *i.e.* $F_d = \frac{V_d - V_d^{dark}}{\Phi_d}$. V_d and V_d^{dark} are the detector flux response and dark response signals, respectively.

Substituting (3.6) and (3.7) allows (3.5) to be rewritten in terms of the dark-corrected detector response $V_d - V_d^{dark}$ as

$$V_{\mathrm{d}} - V_{\mathrm{d}}^{\mathrm{dark}} = \mathrm{F_d}\Phi_{\mathrm{d}} = \mathrm{k}\exp\left\{-\left[2a + \chi\beta(\psi^*)\right]\overline{\mathrm{z}}\right\},$$

and taking the natural logarithm of both sides and rearranging yields

$$a = \frac{1}{2\overline{\mathrm{z}}}\left[\ln\left(\mathrm{k}\right) - \ln\left(V_{\mathrm{d}} - V_{\mathrm{d}}^{\mathrm{dark}}\right)\right] - \chi\beta\left(\psi^*\right). \tag{3.8}$$

Equation (3.7) contains one unknown variable, a, two measured variables $\left(V_{\mathrm{d}} - V_{\mathrm{d}}^{\mathrm{dark}}\right)$ and $\beta\left(\psi^*\right)$, and three unknown coefficients $\overline{\mathrm{z}}$ (the mean effective pathlength between the source, or detector, and reflectance target), k (an overall system optical characteristics constant), and χ (the scaling factor relating the VSF at one angle to the combined sum of backscattering plus forward scattering beyond ψ_{f} for the two optical paths).

The constant coefficients in (3.8) may be determined by placing the "α-βeta", or a similar instrument in pure water, and sequentially adding scattering and absorbing materials to increase a, b and $\beta(\psi)$ in $n = 1, 2, \ldots, \mathrm{N}$ increments spanning a suitable range of each variable. At each $n^{\underline{\text{th}}}$ incremental step, the reflectance detector response $V_{\mathrm{d}n}$ and VSF measurement $\beta_n\left(\psi^*\right)$ are recorded, together with the absorption coefficient $a_n\left(\lambda\right)$ measured using a WET Labs ac-9. It is convenient to define two new constants $\gamma = \frac{\ln\left(\mathrm{k}\right)}{2\overline{\mathrm{z}}}$ and $\vartheta = \frac{1}{2\overline{\mathrm{z}}}$, and express (3.8) in matrix form for the N sets of measurements as

$$\vec{\mathbf{a}} = \mathbf{X}\vec{\boldsymbol{\gamma}}, \tag{3.9}$$

where

$$\vec{\mathbf{a}} = \begin{bmatrix} a_1 \\ a_2 \\ \vdots \\ a_{\mathrm{N}} \end{bmatrix}, \quad \mathbf{X} = \begin{bmatrix} 1 & \ln(V_{\mathrm{d}1} - V_{\mathrm{d}}^{\mathrm{dark}}) & \beta_1\left(\psi^*\right) \\ 1 & \ln(V_{\mathrm{d}2} - V_{\mathrm{d}}^{\mathrm{dark}}) & \beta_2\left(\psi^*\right) \\ \vdots & \vdots & \vdots \\ 1 & \ln(V_{\mathrm{dN}} - V_{\mathrm{d}}^{\mathrm{dark}}) & \beta_{\mathrm{N}}\left(\psi^*\right) \end{bmatrix}, \text{ and } \vec{\boldsymbol{\gamma}} = \begin{bmatrix} \gamma \\ \vartheta \\ \chi \end{bmatrix}.$$

Multiplying both sides of (3.9) by $\mathbf{X}^{\mathbf{T}}$, the transpose of the matrix **X**, we obtain

$$\mathbf{X}^{\mathbf{T}}\vec{\mathbf{a}} = \left[\mathbf{X}^{\mathbf{T}}\mathbf{X}\right]\vec{\boldsymbol{\gamma}},$$

leading to the normalized least squares solution for the three coefficients as

$$\vec{\boldsymbol{\gamma}} = \left[\mathbf{X}^{\mathbf{T}}\mathbf{X}\right]^{-1}\mathbf{X}^{\mathbf{T}}\vec{\mathbf{a}}, \tag{3.10}$$

where $\left[\mathbf{X}^{\mathbf{T}}\mathbf{X}\right]^{-1}$ is the inverse of the 3 x 3 matrix $\left[\mathbf{X}^{\mathbf{T}}\mathbf{X}\right]$.

Having thus described the conceptual basis for determining the absorption coefficient from measurements with a HOBILabs "a-beta" instrument, or a similar instrument, time constraints on the publication schedule for this document preclude exploring more detailed protocols for its calibration and use, or the uncertainty budgets associated with this approach. These considerations must be deferred to a possible future revision to this protocol volume.

3.2 CHARACTERIZATION and CALIBRATION OF REFLECTIVE TUBE SPECTRAL ABSORPTION METERS

Perhaps the best-known version of a reflective tube absorption meter is the ac-9 manufactured by WET Labs, Inc. This instrument measures both the spectral beam attenuation coefficient $c\left(\lambda\right)$ in an enclosed flow-through non-reflective optical path, and the spectral volume absorption coefficient $a\left(\lambda\right)$ using parallel enclosed flow-through reflective tube optical paths, one of which (the absorption side) is a reflective tube (Fig. 3.1). Many aspects of the characterization, calibration, field measurements and data analysis protocols relating to this type of instrument were introduced in Chapter 2 and will not be repeated here. Moreover the manufacturer provides extremely detailed

protocols for calibrating and using this instrument, and for analyzing its data, both in the ac-9 User Manual, and in a detailed protocol manual (Van Zee *et al*. 2002), both of which are available online (www.wetlabs.com). Additional background information related to characterization, calibration and data analysis methods for this instrument may be found in Moore *et al*. (1992), Zaneveld *et al*. (1992) and Twardowski *et al*. (1999). Here we will briefly highlight critical aspects of the protocols that must be carefully followed to obtain accurate $a(\lambda)$ measurements using this, or a similar, instrument in the field. Many of these topics, as they relate to the beam transmissometer side of the instrument, have been discussed in Chapter 2 of this volume.

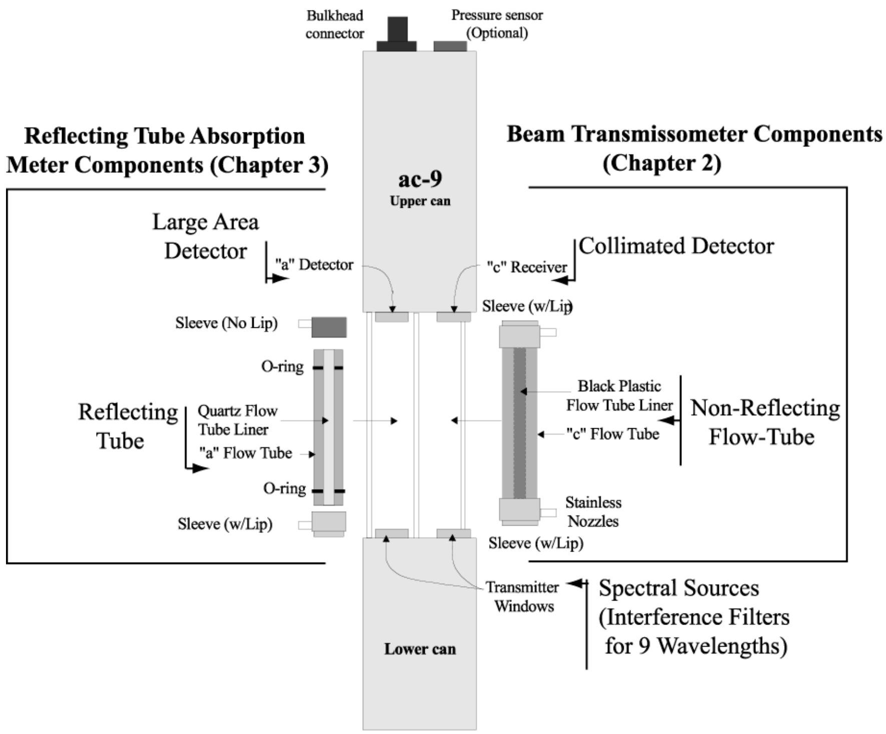

Fig. 3.3 Schematic illustration of the ac-9 beam attenuation and absorption meter (courtesy of WET Labs , Inc).

Pure Water Calibration

The procedure for using pure water to calibrate the reflective tube absorption meter side of an ac-9 is identical to that described in Chapter 2 (Sect. 2.4) for its flow-through beam-transmissometer side. The calibration equation for measured absorption a_{m} relative to pure water, corresponding to equation (2.9) for c, is

$$a_{\mathrm{m}}(\lambda)-a_{\mathrm{w}}(\lambda)=\frac{1}{r_{\mathrm{T}}}\ln\left\{\frac{\left[V_{\mathrm{R,w}}(\lambda)-V_{\mathrm{R,w}}^{\mathrm{dark}}(\lambda)\right]\left[V_{\mathrm{D}}(\lambda)-V_{\mathrm{D}}^{\mathrm{dark}}(\lambda)\right]}{\left[V_{\mathrm{D,w}}(\lambda)-V_{\mathrm{D,w}}^{\mathrm{dark}}(\lambda)\right]\left[V_{\mathrm{R}}(\lambda)-V_{\mathrm{R}}^{\mathrm{dark}}(\lambda)\right]}\right\}, \qquad (3.11)$$

where the signal notations on the right-hand-side are the same as those defined in Chapter 2, and pure water absorption values are listed in Table 1.1 of Chapter 1.

Pure Water Preparation

The methods for preparation of optical calibration grade pure water were not addressed in Chapter 2, and are included here.

To prepare pure water for instrument calibrations, the manufacture uses a commercial de-ionization system and filtration system. After primary de-ionization, the water is processed using a Barnstead, or equivalent, purification unit and stored in a large holding tank. To maintain purity, water in the holding tank should be re-circulated through a ultra-violet chamber and additional purification filters. Water for calibration is drawn through a 0.01-micron ultra-filter at the point of delivery. The circulating holding tank allows the highly reactive de-ionized water to equilibrate with the ambient conditions and the ultra-violet chamber prevents any biological contamination from entering the reservoir.

For field calibrations, one approach is to either purchase HPLC grade pure water, or produce it in the lab, and transport it to the ship, especially for short cruises. On some research vessels, a water deionization and purification system is permanently installed to support the scientific party. If so, care must be taken to insure that the filters are fresh and do not produce Colored Dissolved Organic Matter (CDOM) from decaying particles trapped in the filter. Alternatively, a portable system consisting of a commercial filtration unit, such as the Barnstead E-Pure or the Milli-Q Q-Pak treatment systems may be set up temporarily on the ship. The input water should be pre-filtered using a 1.5 µm commercial filter cartridge and an activated charcoal filter to increase the lifetime of the primary unit. Pure water should be produced in advance of the calibration and stored in a clean 20-liter polycarbonate carboy and be allowed to stand for approximately 12 hours to equilibrate with the ambient temperature and to remove bubbles.

To calibrate an ac-9, the carboy may be equipped with a cap having barb fittings to connect tubing to a pressurization unit that pushes water to the instrument (Fig. 3.4). The carboy is pressurized to approximately 10 psi using an oil free air pump, or a tank of dry nitrogen gas. The air supply tube inside the carboy should be kept above the water level to prevent the creation of bubbles when pressurizing the carboy, and the outlet tube should extend nearly to the bottom of the carboy. To connect the carboy to the ac-9, Teflon tubing is recommended, rather than Tygon tubing, which may contain plasticizers that can contaminate the water. The tubing from the carboy is connected to the bottom nozzle on the ac-9 flow tube. The tubing near the ac-9 inlet and outlet should be covered with black tape to avoid ambient light leaks into the optical path. A short piece of tubing with a valve is connected to the top nozzle on the flow tube, both to control water flow through the system, and to provide backpressure, which helps to keep gases in solution and prevents the formation of micro-bubbles. An optional 0.2-micron filter may be placed at the point of delivery.

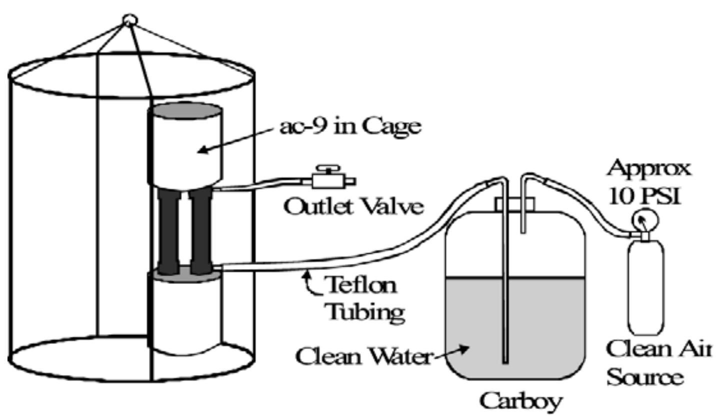

Fig. 3.4. Schematic illustration of a pure-water supply system for field calibrations of an ac-9.

Air "Calibrations"

This procedure is discussed adequately in Chapter 2.

3.3 MEASURING SPECTRAL ABSORPTION COEFFICIENTS WITH REFLECTIVE TUBE METERS

The ac-9 should be mounted in a profiling instrument cage following directions provided by the manufacturer (Van Zee *et al*. 2002). It is strongly recommended to mount a CTD data the same profiling package as an ac-9, and to develop a method for accurately merging the measurements from both instruments; combining the data streams from the two instruments in real time as part of the data acquisition system is the preferred approach, with a second choice being to time-tag both data records and merge the data on that basis. The basis of these recommendations is that water temperature and salinity data are essential for the corrections described below in Sect. 3.4.

To begin a cast, place the instrument package in the water before they are powered up. Then hold the package underwater near the surface allow approximately 5 min for the instruments to warm up, stabilize the electronics, and reduce the possibility that thermal shock may adversely affect the measurements. Monitor the instrument outputs and wait to begin profiling until the instrument stabilizes at the surface. If an absorption meter will not stabilize its readings after 5-10 minutes under these conditions, it is recommended that it be returned to the manufacturer for characterization of the problem and necessary repairs.

If possible place the instrument 10 to 20 meters below the surface to help purge bubbles. Purging bubbles is more difficult when making filtered measurements (see below). If you are not making filtered measurements the instruments will generally purge at the surface, but purging them below 10 m is still a good idea.

The reader is referred to Van Zee *et al*. (2002) for detailed recommendations concerning rates of descent during profiles using an ac-9.

After the instruments are brought on deck following a cast, they should be immediately rinsed, and the flow tubes flushed, with fresh water to mitigate corrosion. If the instrument will be on deck for more than 30 min between casts, the optics and flow tubes should be cleaned with Nannopure water and dried. At least once per day, while at sea, the optics and flow tubes should be cleaned with methanol, cleaned again using a mild detergent dissolved in Nannopure water, rinsed with Nannopure water, cleaned again with methanol, and finally dried. Use soft tissues, such as KimWipes, to gently clean and dry the optical surface, and be extremely careful to wipe them in a constant direction and to not scrub the optical surfaces.

When the instrument package is be stored on deck for a prolonged period between casts, cover it with a tarpaulin to protect the absorption meter from direct exposure to the sun. Excessive solar heating of the instrument may exceed the practical limits (5 ^{o}C to 30 ^{o}C) of internal temperature corrections for an ac-9, and thus invalidate its measurements until it has cooled sufficiently to restore normal operations.

Filtering the Water Intake Port of an ac-9 for Measurements of Absorption by CDOM and Particles

The absorption coefficient of dissolved material may be measured by attaching a 0.2 μm pore-size filter to the intake of an ac-9. The recommended practice is to locate the intake filter below the instrument at the bottom of the cage. Measurements in the filtered intake configuration are also very useful for testing the operational performance of ac-9; quality control procedures using dissolved measurements are discussed in Sect. 3.5.

Examples of suitable filters are the Gelman Suporcap 100 and Gelman Maxi-cap (0.2 μm) filters. These filters have high flow rates at low differential pressure and don't adsorb or leach materials. The outer housings of these commercial filter cartridges may be cut off to allow some flushing of the filter and increase the flow-rate. Make sure you don't handle the filter material, or lay a filter on the deck, where it can be exposed to oil and grease. Hose clamp the filter to the tubing and make sure any vents on the filter are closed. Before use, a filter should be either flushed for several minutes with DI water, or soaked several hours in DI water, to remove air pockets in the filter membrane. As a note of caution, never flush a filter in the reverse direction!

There are alternative ways to plumb the filters into the ac-9 instrument. The preferred arrangement is to filter the *a* and *c* sides separately using two filters and two pumps, so that each side is plumbed independently. This approach is expensive, however, and is not necessary for measuring the absorption by the dissolved component. For measurement of the absorption by dissolved materials, only one side needs to be filtered, because scattering by particles less than 0.2 μm in size is not detectable by an ac-9, and hence the filtered *a* and *c* measurements are equal. On the other hand, measurements with filters on intakes of both sides are useful for quality control tests (Sect. 3.5).

If possible replace the filter daily. If you choose to replace a filter less frequently, soak it in DI water during long breaks between profile measurements during a deployment. Record the date of each filter change in the cruise log.

Mixing of water within the filter cartridge will smear measurements of a vertical gradient in the absorption by dissolved materials, and an unfiltered instrument will detect a gradient in total absorption with better vertical resolution. In addition, the reduced flow rate through the filter will increase the time lag to approximately 4 to 6 sec, compared to 1.2 to 1.8 sec for unfiltered measurements. Moreover, the lag rate will gradually increase as a filter accumulates particles during its use. The preferred means of determining flow rate and lag corrections is to attach a flow-meter in-line into the supply or exhaust tubing. An indirect technique for estimating flow-rate related lag times is to match depths of changes in the $a(715)$ channel with depths of strong changes in water temperature; these changes are linked because absorption by water is temperature dependent in the near infrared (Sect. 3.4), and the time lag between matched changes can be derived from the depth separation and the profiler's rate of descent.

A combination of unfiltered and filtered ac-9 measurements can be used to derive particle absorption and attenuation coefficients, as well as absorption by CDOM. There are several combinations that can be used:

- From measurements using a single ac-9 with the *c* side filtered and the *a* side unfiltered, particle absorption can be obtained as $a_{\mathrm{p}}(\lambda) = a(\lambda) - a_{\mathrm{w}}(\lambda) - \left[c_{\mathrm{g}}(\lambda) - c_{\mathrm{w}}(\lambda)\right]$, where the measurements have been corrected using the methods described in 3.6 below. The subscript "g" is associated with CDOM, based on historical use of the term "gelbstoffe", or yellow-matter, as a pseudonym of CDOM.
- From measurements with two ac-9's, one filtered and one unfiltered, $a_{\mathrm{g}}(\lambda)$ is derived directly from the filtered measurements, after the corrections of Sect. 3.6, and $a_{\mathrm{p}}(\lambda) = a(\lambda) - a_{\mathrm{g}}(\lambda)$, where $a(\lambda)$ is derived from the unfiltered instrument and the pure water terms cancel. This approach may also be used with a single instrument by making successive casts, one with the filter attached and the second with the filter removed.
- Another alternative approach is to make successive casts with one instrument, filtering the a intake on one cast, and the c intake on the other. The filtered and unfiltered measurements from the two casts are combined as above.

The approach yielding the lowest instrumental uncertainty of the particulate absorption is to derive it from filtered and unfiltered measurements with the same instrument on successive casts. Calibration offsets, whether known or not, are identical in the filtered and unfiltered measurements on each side, and therefore, the offsets cancel when particle absorption is determined as the difference between the two measurements. On the other hand, potentially larger uncertainty may result from possible changes in the IOP profiles between casts, due to horizontal advection and/or vertical displacement of IOP features by internal waves.

3.6 DATA ANALYSIS METHODS

The initial steps in processing absorption measurements using an ac-9 reflective tube absorption meter are identical to those presented for processing beam transmissometer measurements in Chapter 2, Sect. 2.5 [substituting equation (3.11) for (2.9) in Step 4). This information will not be repeated here. Two additional analysis steps are necessary to obtain accurate absorption coefficients from combined ac-9, or similar instrument, measurements of $a_{\mathrm{m}}(\lambda)$ and $c_{\mathrm{m}}(\lambda)$: 1) corrections for water temperature and salinity induced offsets in water absorption and attenuation, and 2) corrections for scattering errors [equation (3.3)] in $a_{\mathrm{m}}(\lambda)$.

Temperature and Salinity Corrections

The absorption of pure water is dependent on water temperature T [$^{\mathrm{o}}$C] (Pegau and Zaneveld 1993) and the absorption coefficient of seawater is also dependent on its salinity S [PSU] (Pegau *et al.* 1997). These variations affect the measured coefficients of absorption $a_{\mathrm{m}}(\lambda)$ and attenuation $c_{\mathrm{m}}(\lambda)$ in the following ways:

1. The difference $(T - T_r)$ between the water temperature T during a measurement at sea and the temperature T_r of the pure water reference standard at the time the instrument was calibrated changes the water absorption "baseline" value $a_w(\lambda)$. This change affects $a_m(\lambda)$ and $c_m(\lambda)$ equally, because scattering by pure water is not significantly temperature dependent.
2. The absorption of seawater varies with salinity S, and of course $S = 0$ PSU for the pure water reference standard used to calibrate the ac-9. This additional shift in the water-absorption "baseline" also affects $a_m(\lambda)$ and $c_m(\lambda)$ equally.
3. The salinity dependent variations in the refractive index of seawater affect the transmission of the optical windows, and the effects are different for the windows of the absorption and beam transmission sides of the instrument. This effect may also vary slightly between instruments (Van Zee *et al*. 2002).
4. Therefore, separate coefficients $\frac{\partial a(\lambda)}{\partial S}$ and $\frac{\partial c(\lambda)}{\partial S}$ combine salinity dependent instrument characteristics and water-absorption variations (Pegau *et al*. 1997; Van Zee *et al*. 2002), and must be applied separately to correct to $a_m(\lambda)$ and $c_m(\lambda)$

The temperature and salinity corrections are applied to measured absorption as

$$a_m^{TS}(\lambda) = a_m(\lambda) - \frac{\partial a_w(\lambda)}{\partial T}(T - T_r) - \frac{\partial a(\lambda)}{\partial S} S, \tag{3.12}$$

and to measured beam attenuation as

$$c_m^{TS}(\lambda) = c_m(\lambda) - \frac{\partial a_w(\lambda)}{\partial T}(T - T_r) - \frac{\partial c(\lambda)}{\partial S} S. \tag{3.13}$$

The temperature dependence coefficients are listed in Table 1.1 (Pegau and Zaneveld 1993; Pegau *et al* 1997), and the salinity dependence coefficients are provided by the manufacturer (Van Zee *et al*. 2002). Temperature and salinity must be measured, using a CTD, concurrently with an ac-9 profile to apply these corrections using (3.12) and (3.13). Therefore, it is strongly recommended that the ac-9 be mounted on the same profiling package as an accurate CTD, and from this perspective, the priority of CTD measurements is higher than is implied in Table 3.1 (Vol. I, Chapter 3).

These corrections become directly significant only at red and near-infrared wavelengths (see Table 1.1). However, the methods of the next section depend on accurate values of $a_m^{TS}(\lambda_{NIR})$ and $c_m^{TS}(\lambda_{NIR})$ at a near-infrared reference wavelength $\lambda_{NIR} \approx 715$ nm to determine *scattering corrections* at all wavelengths. Moreover, the temperature correction in (3.12) must also be applied to laboratory spectrophotometric measurements of absorption by CDOM (Chapter 4), if the temperatures of the pure-water reference blank and filtered seawater sample differ significantly.

Scattering Corrections

The systematic scattering offsets between true absorption and absorption measured with a reflective tube instrument, as described in equations (3.2) and (3.3) and related text in Sect. 3.1, were evaluated by Zaneveld *et al*. (1994). They recommended a hierarchy of three alternative methods for correcting the scattering offsets to the temperature and salinity corrected measured absorption $a_m^{TS}(\lambda)$:

1. Subtract the measured absorption at a near infrared reference wavelength, *e.g.* $\lambda_{NIR} \approx 715$ nm for an ac-9, or $\lambda_{NIR} \approx 750$ nm for measurements with a laboratory spectrophotometer (Chapter 4). After first applying the *temperature and salinity* corrections using (3.12) and (3.13), assume that the $a(\lambda_{NIR}) - a_w(\lambda_{NIR}) \approx 0$ and that the entire measured signal at the reference wavelength is due to wavelength independent scattering errors, so that

$$a(\lambda) - a_w(\lambda) = a_m^{TS}(\lambda) - a_m^{TS}(\lambda_{NIR}). \tag{3.14}$$

The value of $a_{\mathrm{m}}^{TS}(\lambda_{\mathrm{NIR}})$ should be reported with the corrected absorption values when this method is used.

2. Assuming a wavelength-independent scattering phase function appropriate for the type of particulates in a given water mass, and a weighting function $W(\psi)$ based on instrument characteristics [see equation (3.3) and the preceding discussion in Sect. 1.1 above], estimate the scattering error as a fraction ε of the measured scattering coefficient, and subtract it from the measured absorption at each wavelength, *i.e.*

$$a(\lambda)-a_{\mathrm{w}}(\lambda)=a_{\mathrm{m}}^{TS}(\lambda)-\varepsilon\left[c_{\mathrm{m}}^{TS}(\lambda)-a_{\mathrm{m}}^{TS}(\lambda)\right]. \qquad (3.15)$$

   Based on analyses of field measurements, laboratory experiments using an ac-9, and theoretical calculations (Kirk 1992), the fraction ε varies from approximately 0.14 for predominately biological particles in the open ocean (Case 1 waters) and increases to approximately 0.18 in waters were scattering is dominated by suspended sediments (Case 2 waters). Note that although the scattering correction using (3.15) is not sensitive to temperature and salinity corrections at wavelengths < 650 nm, it is nevertheless strongly recommended that the temperature and salinity corrected values be used here as well - if for no other reason than facilitating quality control comparisons between corrections made by different methods.

3. Combine methods 1 and 2, and the assumptions underlying both methods, to use the ac-9 measurements at the reference wavelength to determine ε, so that (3.15) becomes

$$a(\lambda)-a_{\mathrm{w}}(\lambda)=a_{\mathrm{m}}^{TS}(\lambda)-\left[\frac{a_{\mathrm{m}}^{TS}(\lambda_{\mathrm{NIR}})}{c_{\mathrm{m}}^{TS}(\lambda_{\mathrm{NIR}})-a_{\mathrm{m}}^{TS}(\lambda_{\mathrm{NIR}})}\right]\left[c_{\mathrm{m}}^{TS}(\lambda)-a_{\mathrm{m}}^{TS}(\lambda)\right]. \qquad (3.16)$$

   The ac-9 instrument design constrains the scattering error fraction to $\varepsilon \geq 0.07$ (Kirk 1992), and although it is theoretically possible for ε to reach values exceeding 0.5, the authors have not encountered values greater than 0.35.

The choice of which method should be used to correct scattering errors in ac-9 absorption measurements depends largely on the combination of measured variables, the uncertainty of each measurements, and a judgment of how likely the assumption that $a(\lambda_{\mathrm{NIR}})-a_{\mathrm{w}}(\lambda_{\mathrm{NIR}})\approx 0$ is true in a given water mass.

1. It is strongly recommended to use Method 3 to apply the scattering correction, if all variables in (3.16) have been measured with acceptable uncertainty, and there is no reason to suspect that particle absorption is significant at the near-infrared reference wavelength λ_{NIR}.
2. Method 2 is recommended if both $a_{\mathrm{m}}^{TS}(\lambda)$ and $c_{\mathrm{m}}^{TS}(\lambda)$ are available at one or more visible wavelengths, but $a_{\mathrm{m}}^{TS}(\lambda_{\mathrm{NIR}})$ and $c_{\mathrm{m}}^{TS}(\lambda_{\mathrm{NIR}})$ either were not measured with acceptable uncertainties, or there is reason to suspect that $a(\lambda_{\mathrm{NIR}})-a_{\mathrm{w}}(\lambda_{\mathrm{NIR}})>0$.
3. Method 1 must be used if only $a_{\mathrm{m}}^{TS}(\lambda)$ and $a_{\mathrm{m}}^{TS}(\lambda_{\mathrm{NIR}})$ are measured, as for example, when a laboratory benchtop spectrophotometer is used to measure $a_{\mathrm{g}}(\lambda)$ in filtered water samples (Chapter 4). This situation might also occur if the *c* side data of an ac-9 were lost due to an electronic failure, or blockage of its flow-tube, and one wished to salvage the absorption profile measured with that instrument.

3.7 QUALITY CONTROL PROCEDURES

There are several quality assurance tests that can be made to check how well an ac-9 is operating.

When using intake filters for quality control measurements in tests of instrument performance, it is best to filter both sides of an ac-9. This can be done by filtering one side at a time, and doing multiple profiles, or by connecting a single filter and pump to both sides of the ac-9. When connecting to both sides using a single filter you are reducing an already low flow, which makes it more difficult to remove bubbles from the system, but it requires fewer casts to complete an instrument test. A degassing Y may be used on the outflow side of the combined plumbing arrangement to facilitate bubble removal.

The noise level in the measurements should be >0.005 m^{-1} at all channels. Measurements with noise exceeding this criterion indicate instruments with large measurement noise, a rough check of quality of the calibration, and pressure or temperature dependencies that may exist.

Assuming that there is no measurable scattering by particles that pass through the filter then the filtered a and c measurements should be equal, and departures >0.005 m^{-1} are symptoms of drift in pure water calibration offsets, or calibration errors due to optical impurity of the reference water.

Comparisons of profiles between successive down and up casts may help in separating suspected temperature effects from pressure dependencies. Evidence of hysteresis in different up and down profile responses to gradient features is symptomatic of a problem with an instrument's internal temperature compensation Care must be taken in this interpretation, however, because the upcast water intake is taken in the wake of the rising package and turbulence may also cause apparent hysteresis symptoms to appear in the measurements. Pressure effects should not have hysteresis.

If more than one ac-9 is available, it is useful to plumb both instruments in identical configurations (both with, or without an intake filter) on the same instrument and measure a quick sequence of comparative profiles to intercalibrate the instruments. The profile data from the two instruments should be compared only after each has been fully processed and corrected for temperature, salinity and scattering errors (Sect. 3.4). Discrepancies in this type of comparison cannot indicate which instrument is incorrect, but does provide a clear indication that the calibration of one, or both, is not correct.

REFERENCES

James, H.R., and E.A. Birge, 1938: A laboratory study of the absorption of light by lake waters. *Trans. Wis. Acad. Sci*., **31**: 1--154.

Kirk, J.T.O., 1992. Monte Carlo modeling of the performance of a reflective tube absorption meter. *Appl. Opt.* **31(30):** 6463-6468.

Moore, C., J.R.V. Zaneveld and J.C. Kitchen, 1992: Preliminary results from an *in situ* spectral absorption meter, *Ocean Optics XI*, *Proc. SPIE* **1750:** 330-337.

Maffione, R.A. and D.R. Dana, 1997: Instruments and methods for measuring the backward-scattering coefficient of ocean waters. *Appl. Opt.* **36:** 6057-6067.

Pegau, W.S. and J.R.V. Zaneveld, 1993: Temperature dependent absorption of water in the red and near infrared portions of the spectrum. *Limnol. Oceanogr*., **38**(1): 188-192.

Pegau, W.S., D. Gray and J.R.V. Zaneveld, 1997: Absorption and attenuation of visible and near-infrared light in water: dependence on temperature and salinity. Appl. Opt., **36**(24): 6035-6046.

Twardowski, M.S., J.M. Sullivan, P.L. Donaghay and J.R.V. Zaneveld. 1999: Microscale quantification of the absorption by dissolved and particulate material in coastal waters with an ac-9. *J. Atmos. Oceanic Tech.* **16**: 691-707.

Van Zee, H., D. Hankins, and C. deLespinasse, 2002: *ac-9 Protocol Document (Revision F)*. WET Labs Inc., Philomath, OR, 41pp.

Zaneveld, J.R.V., J.C. Kitchen, A. Bricaud, and C. Moore, 1992: Analysis of *in situ* spectral absorption meter data. *Ocean Optics XI,* G.D. Gilbert, Ed., SPIE, 1750, 187--200.

Zaneveld, J.R.V., J.C. Kitchen, and C. Moore, 1994: The scattering error correction of reflecting-tube absorption meters. *Ocean Optics XII, Proc. SPIE*, **2258**: 44-55.

Chapter 4

Determination of spectral absorption coefficients of particles, dissolved material and phytoplankton for discrete water samples

B. Greg Mitchell, Mati Kahru, John Wieland and Malgorzata Stramska
Scripps Institution of Oceanography, University of California San Diego, California

4.1 INTRODUCTION

The spectral absorption coefficient is one of the inherent optical properties that influence the reflectance of aquatic systems. The absorption coefficient $a(\lambda)$, in m^{-1}, at any point within a natural water body can be described in terms of the additive contribution of its components as

$$a(\lambda) = a_{\mathrm{w}}(\lambda) + a_{\mathrm{p}}(\lambda) + a_{\mathrm{g}}(\lambda),\ \mathrm{m}^{-1}, \tag{4.1}$$

where $a_{\mathrm{w}}(\lambda)$, $a_{\mathrm{p}}(\lambda)$ and $a_{\mathrm{g}}(\lambda)$ are the spectral absorption coefficients of water, particles, and soluble components, respectively. The spectral absorption coefficients of pure water adopted for the protocols are given in Table 1.1 (Ch. 1), and combine the results of Pope and Fry (1997), Sogandares and Fry (1997), Fry (2000) and Kou *et al*. (1993). The depth (z) dependence of the absorption coefficients is omitted for brevity. The particle absorption coefficient may be further decomposed as

$$a_{\mathrm{p}}(\lambda) = a_{\varphi}(\lambda) + a_{\mathrm{d}}(\lambda),\ \mathrm{m}^{-1}, \tag{4.2}$$

where $a_{\varphi}(\lambda)$ and $a_{\mathrm{d}}(\lambda)$ are the spectral absorption coefficients of phytoplankton, and de-pigmented particles, respectively. Laboratory methods are described for determining operational estimates of these fractions. It is conceptually possible to further separate $a_{\mathrm{d}}(\lambda)$ into absorption fractions due to de-pigmented organic and inorganic particles, but at present, there are no well established protocols for separately determining the absorption coefficient for inorganic particles.

To interpret aquatic spectral reflectance and better understand photochemical and photobiological processes in natural waters, it is essential to quantify the contributions of the individual constituents to the total absorption coefficients in the ultraviolet (UV) and visible region of the spectrum. The protocols presented here are based on the evolution, starting with articles by Kalle (1938) and Yentsch (1962), of methods for analyzing the absorption by soluble and particulate material in natural waters. Laboratory measurements and data analysis protocols are described for separating the total spectral absorption coefficient, $a(\lambda)$, into its components by spectrophotometric measurements of samples prepared from filtration of discrete water samples.

The spectral absorbance of the filters and filtrate from these samples, as measured in a spectrophotometer, are expressed in units of Optical Density (OD), defined as $OD(\lambda) = \mathrm{Log}_{10}\left[V_{\mathrm{o}}(\lambda)\right] - \mathrm{Log}_{10}\left[V_{\mathrm{t}}(\lambda)\right]$. $V_{\mathrm{o}}(\lambda)$ is the spectrometer response for spectral flux transmitted through the reference material and $V_{\mathrm{t}}(\lambda)$ is the response for spectral flux transmitted through the sample. For the methods presented here the reference is either a properly hydrated GF/F blank filter for particle absorption, or a clean quartz glass optical cuvette filled directly from a

purified water source for soluble material absorption. Note that OD is a dimensionless quantity. The use of base-10 logarithms in this context is a carryover from common practice in chemical spectroscopy and is the typical output of commercial spectrophotometers routinely used for these methods. Therefore, it is necessary to convert the OD measurements described in this chapter to the base-e representation of absorbance, *i.e.* to multiply OD by 2.303, to conform to the convention used throughout the ocean optics protocols. In general, these protocols are written assuming that the instrument that is used directly computes the optical density of the sample relative to the appropriate reference sample.

There has been considerable research to develop robust protocols that provide the most accurate estimates of absorption for various material fractions in natural waters. NASA-sponsored workshops were held at Scripps Institution of Oceanography and Bigelow Laboratory for Ocean Sciences to review absorption protocols, evaluate instrumentation, and define areas of consensus as well as areas of uncertainty that warrant further research (Mitchell *et al.* 2000).

The most widely used approach for estimating absorption by particulate matter in water samples involves analysis of the particles concentrated on filters (Yentsch, 1957). Absorption of phytoplankton suspensions determined using procedures that capture most of the forward scattered light (Shibata, 1958) can be related to the absorption measured on the filters to make quantitative corrections for the pathlength amplification effect (β) caused by the highly scattering filter medium (Duntley, 1942; Butler, 1962). The pathlength amplification parameter was symbolized as β by Kiefer and SooHoo (1982) following the nomenclature of Butler (1962). This symbol should not to be confused with the volume scattering coefficient $\beta(\lambda,\Psi)$ used in other chapters of this Technical Memorandum.

Kiefer and SooHoo (1982) reported a constant to scale the red peak of chlorophyll absorption for natural particles retained on GF/C filters to the diffuse absorption coefficients determined on suspensions by Kiefer *et al.* (1979). The diffuse absorption coefficient is double the value of the volume absorption coefficient of interest here (Preisendorfer, 1976). Mitchell and Kiefer (1984, 1988a) made direct estimates of volume absorption coefficients for phytoplankton suspensions and absorbance on glass fiber filters with the same particles to develop empirical equations that relate the amplification factor to the glass fiber sample optical density. This procedure is the basis of most laboratory methods for determining particle absorption in water samples.

Field applications of these quantitative estimates of $a_{\mathrm{p}}(\lambda)$ were reported by Mitchell and Kiefer (1984, 1988b) and Bricaud and Stramski (1990). More detailed empirical results to correct for pathlength amplification were reported by Mitchell (1990) for various filter types and diverse cultures coccoid cyanobacteria, nanochlorophytes, diatoms, chrysophytes and dinoflagellates with sizes ranging from 2 μm to 20 μm. Cleveland and Weidemann (1993) and Tassan and Ferrari (1995) found that the empirical relationships of Mitchell (1990) were consistent with similar types of phytoplankton, but Moore *et al.* (1995) reported large differences in the amplification factor for *Synechococcus sp*. (WH8103) and *Prochlorococcus marinus* that were about half the size of the smallest cells studied by Mitchell (1990). Similar results were obtained by Allali *et al*. (1997) for natural populations of the Equatorial Pacific dominated by picoplankton. For samples with substantial turbidity and scattering due to inorganic matter (coastal, shelf, coccolithophore blooms), methods to correct for resulting artifacts have been described by Tassan and Ferrari (1995a, 1995b). Table 4.1 provides a summary of various published results for pathlength amplification factors.

Separation of the particle fraction into phytoplankton and other components is of considerable ecological and biogeochemical interest. Early efforts to separate absorbing components for natural particles included treatment with organic solvents, UV radiation, and potassium permanganate (references can be found in Shifrin, 1988, and Bricaud and Stramski, 1990). The most widely used chemical method is based on methanol extraction (Kishino *et al.* 1985, 1986). A recent method consists of bleaching the phytoplankton pigments by sodium hypochlorite (Tassan and Ferrari, 1995a; Ferrari and Tassan, 1999). Spectral fluorescence methods to estimate the fraction of photosynthetically active absorption, if separate total particulate absorption has been determined, have been reported by Sosik and Mitchell, (1995).

Soluble absorption observations were described by Bricaud *et al*. (1981) for diverse ocean environments, including oligotrophic and eutrophic regions. Other field reports can be found in the references listed in more recent articles (Carder *et al*., 1989a, 1989b; Blough *et al*., 1993; Vodacek *et al*., 1996; Hoge *et al*., 1993; Nelson *et al*., 1998; D'Sa *et al*., 1999). Spectrophotometric measurement of absorption by dissolved materials is straightforward,

but has limits due to the very small signal for short pathlengths routinely employed (usually 10 cm), and to difficulties in maintaining quality control of purified water used as a reference.

This chapter defines protocols for the operational determinations of absorption coefficients for particulate and soluble matter in water samples. Methods are specified for separating particulate and soluble material by filtration, partitioning total particulate absorption into contributions by phytoplankton and de-pigmented particles (detritus), and corrections for pathlength amplification due to semi-diffuse transmittance of the filters. Recommendations are made based on widely accepted methods and processing procedures. NASA-sponsored workshops have confirmed various aspects of previously reported methods (Mitchell *et al*. 2000).

4.2 SAMPLE ACQUISITION

Water samples should be taken using Niskin (or similar) bottles at the site of, and simultaneously with, the surface in-water optical measurements, and at depth increments sufficient to resolve variability within at least the top optical depth. When possible, samples should be acquired at several depths distributed throughout the upper 300m of the water column (or in turbid water, up to seven diffuse attenuation depths for PAR irradiance, $\ln(E(0)/E(z))=7$), to provide a basis for relating the spectroscopic measurements of absorption to *in situ* profile measurements. Samples should be drawn immediately from the *in situ* sampling bottles into clean sampling bottles using clean silicon rubber or Tygon tubing or by directly filling the sample bottles from the Niskin bottle spigot. If Niskin bottles will not be sampled immediately, precautions must be taken to ensure large particles that settle are re-suspended. This can be done by transferring all water from the Niskin to a bottle or carboy larger than the total volume of the Niskin so that the entire water sample can be mixed (invert bottle numerous times to mix by turbulence), or by draining a small amount of water from the Niskin and manually inverting the entire Niskin prior to sub-sampling. Sample bottles should be kept cool (ideally near *in situ* temperatures), and dark prior to sample preparations. Preparations should be completed as soon as possible after sampling, but no later than several hours after the sample was acquired.

4.3 SPECTROPHOTOMETER CHARACTERISTICS AND CALIBRATION

A spectrophotometer used for absorption measurements following the protocols presented in this chapter must meet the following minimum performance specifications:

1. The unit's monochromator, or spectrograph, must yield a Full-Width at Half-Maximum (FWHM) bandwidth ≤ 4 nm. A larger FWHM bandwidth will not adequately resolve the red chlorophyll *a* absorption band.
2. The instrument's baseline spectrum characteristics, specified below, must be maintained over the range from 300 nm to 850 nm for measuring absorption by particles concentrated on filters, and from 250 nm to 850 nm for measuring absorption by dissolved materials.
3. For measuring absorption by particles concentrated on filters, baseline noise must be <0.01 OD, and noise <0.005 OD is strongly recommended.
4. For measuring absorption by dissolved materials, baseline noise must be <0.001 OD units, and noise <0.0005 OD is strongly recommended.
5. The instrument's baseline spectrum must be relatively flat over the wavelength range of interest and its shape and magnitude must be stable over time. Any tendencies for the spectral shape and magnitude of an instrument's baseline to drift must be well-behaved and slow enough that the rate of baseline drift may be characterized with an uncertainty less than the noise levels specified above. It is recommended to check the instrument baseline at intervals of 1 hr to 2 hr during an extended series of measurements.

Other desirable, but not absolutely essential, spectrophotometer features are variable slit width (to allow reducing the FWHM spectral resolution, when desired), automatic baseline corrections (the adequacy of which must nevertheless be verified), and automatic spectral calibration during instrument warm-up (using mercury emission lines supplied by an internal lamp source).

The spectral accuracy of the spectrometer should be verified by scanning a holmium oxide filter, with reference to an air-to-air baseline. This spectral calibration should be repeated each time the instrument is turned on, and at

the conclusion of a series of measurements. Alternatively, a spectrophotometer's spectral characteristics may be calibrated using an internal line source (*e.g.* a mercury lamp), if the instrument is so equipped, but independent checks with the holmium oxide filter are also strongly advised. A set of absorbance reference filter standards, of known OD, must be used to calibrate a spectrophotometer's responses over the range of OD associated with the samples to be measured. This calibration, together with instrument baseline spectrum determinations, should be repeated at intervals necessary to characterize (within the noise tolerances given above) any measurable drifts in the instrument baseline and/or OD response. Unless the investigator can confirm the stability of the instrument that is used, these calibration procedures should be repeated each time the spectrophotometer is turned on. As a minimum they should be performed at any time there is a change of lamp source, blocking filter, or other instrument setup characteristic that affects the optical response and on a regular basis during routine work.

The present version of these protocols is written assuming the use of a commercial dual-beam spectrophotometer, with the sample and reference targets illuminated by the collimated output of a grating monochromator. The protocols also apply, with minimal modifications, to measurements using a single-beam monochromator or otherwise similar optical configuration. Mitchell *et al*. (2000) report comparisons between OD measurements of a common set of GF/F filtered particle samples using several spectrophotometers of these types, as well as spectrophotometers based on very different optical configurations. For a diatom culture measured during the Scripps workshop, several commercial dual beam spectrophotometers estimated sample filter OD spectra consistently within 5 % (Figure 4.1). Some of the differently configured instruments were within 10 % of the selected reference dual-beam instrument but in some cases had limited spectral range either in the UV or the near-infrared, or both (data not shown). The largest divergence was found for a grating spectrograph instrument that illuminates the filter with diffuse white light (Figure 4.1). This unit yielded OD values that were significantly higher than, albeit linearly related to (with a slope of approximately 0.7), the OD measurements made with conventional dual beam spectrophotometers (Mitchell *et al*. 2000). This result indicates that the pathlength amplification (β factor) associated with this instrument is significantly different from previously published values (Table 4.1), which were derived using conventional dual beam spectrophotometers. An investigator using this type of spectrophotometer, or another design with yet a different optical configuration, must either compare filter OD spectra measurements to reference measurements on the same filters with a "conventional" spectrophotometer to derive an OD scaling function, or otherwise determine pathlength amplification factors for the instrument configuration, using methods discussed in Mitchell *et al*. (2000) and references cited therein.

4.4 PARTICLE ABSORPTION: SAMPLE FILTER PREPARATION AND ANALYSIS

The procedures described in this section are recommended for determining the spectral absorption coefficients of particles in discrete samples of natural waters. These laboratory measurements are complementary to methods for measuring *in situ* profiles of absorption, as described in Chapter 3 of this volume, and provide additional information on the partition of particle absorption by phytoplankton and other particles. Water samples are filtered and absorbance spectra of the filter, $OD_{\mathrm{fp}}(\lambda)$, are estimated for the retained particles using a laboratory spectrophotometer. After measurement, the sample filters are soaked in chemical solvents to extract, or bleach, phytoplankton pigments (Kishino *et al*., 1985; Tassan and Ferrari 1995a) then rinsed to remove the chemicals and pigments from the material retained on the filter. The $OD_{\mathrm{fd}}(\lambda)$ spectrum of the filter is then determined in the spectrophotometer to obtain the absorption component of the de-pigmented particles, which are sometimes referred to as detritus or tripton. Depending on the method used to de-pigment the samples, this fraction also includes bleached cells and phycobilipigments that are not extractable in methanol and also inorganic minerals that may be important absorbers in some water samples. The raw $OD_{\mathrm{fp}}(\lambda)$ and $OD_{\mathrm{fd}}(\lambda)$ data are used to calculate total particulate and de-pigmented absorption coefficients $a_{\mathrm{p}}(\lambda)$ and $a_{\mathrm{d}}(\lambda)$, respectively. The absorption coefficient of phytoplankton, $a_{\phi}(\lambda)$, is then calculated as the difference $a_{\mathrm{p}}(\lambda)-a_{\mathrm{d}}(\lambda)$.

Filtration

The Whatman GF/F™ filter (which is binder-free and combustible, with a nominal pore size of 0.7 μm) is recommended for particle absorption sampling. This type of filter is also recommended by (JGOFS 1991) for

various particulate and pigment analyses. Some authors have reported that particulate material less than 0.7 μm in size will not be retained by the GF/F filter, and that this fraction may contain up to 10 % or 15 % of the phytoplankton biomass as measured by chlorophyll concentration. Chavez *et al*. (1995), however, found no statistical difference between GF/F and 0.2 μm filters for chlorophyll and productivity measurements. The absorption of particles having diameters between 0.22 μm and 0.7 μm may be selectively determined by filtering the GF/F filtrate again through a 0.22 μm Millipore cellulose acetate membrane filter, and measuring its absorbance with a spectrophotometer (Ferrari and Tassan, 1996). Note that Mitchell (1990) reported pathlength amplification factors for cellulose acetate filters that are substantially different than those for GF/F filters and also described the relative difficulty of keeping cellulose acetate filters properly hydrated.

The optical transparency of the GF/F filter relative to air decreases significantly below 380 nm but many spectrophotometers can still make optical density determinations to 300 nm with these filters. The transparency of the filter also increases with hydration; so all samples must be fully - but not excessively - hydrated for proper performance of analytical procedures and accurate optical corrections. Pre-soaking GF/F filters 1 to 2 hrs before use can lead to less variability between individual filters (Bricaud and Stramski 1990). For oceanic water samples, seawater filtered through a 0.2 μm filter should be used to hydrate the filters. Freshly filtered seawater should be used since water that is left standing in clear containers may grow considerable amounts of algae over relatively short periods of time if there are any nutrients in the filtered seawater. For fresh inland water samples, purified fresh water may be used.

Glass fiber, cellulose acetate, and other strongly diffusing filters have large scattering coefficients, which increase the optical path length of photons in the measurement beam. Filtration volume V_f should be adjusted so that the optical densities of the filter samples, relative to the blank filter satisfy the criteria that $0.05 < OD_{\mathrm{fp}}(675) \le 0.25$ and $OD_{\mathrm{fp}}(440) \le 0.4 \quad OD$ (Mitchell 1990). Optical density spectra of the sample filters should be measured as soon as possible following filtration, because pigment decomposition may occur (Stramski 1990). If filters must be stored, immediately place the unfolded filters into flat tissue containers designed for liquid nitrogen storage. Liquid nitrogen storage is recommended because alternative freezing methods were shown to have more artifacts in comparison tests (Sosik, 1999).

a. Sample Filter Preparation

- Collect water samples, and maintain them in the dark at, or near, *in situ* water temperature.
- Prepare 0.2 μm filtered seawater (FSW) in sufficient volume for hydrating sample and blank filters.
- Set up and maintain the filter apparatus in dim light to minimize photodegradation of the samples.
- For each sample, place a GF/F filter onto the filtration rig. Also prepare two blank GF/F filters by soaking them in ~25 ml of 0.2 μm filtered water while mounted on the filtration funnel (with valves closed) during the sample filtration.
- Filter the samples on GF/F filters under low vacuum (~125 mm Hg).
- Filter a sufficient volume of water V_f to yield sample optical density relative to the blank filter in the range specified above. For field samples collected in the upper 100-150 m and filtered onto 25 mm GF/F filters, V_f is typically in the range 0.5 L to 5 L, depending on the *in situ* density concentration of particles.
- Do not let the preparations run dry during filtration. Turn off the vacuum to each sample as it completes filtering. Immediately place samples on a drop of 0.2 μm FSW in the appropriate container, depending on how they will be stored.
- Record the filter and filtration funnel type, the diameter D_f of the area on the filter that contains the concentrated particles, and the volume of water filtered V_f.
- Measure the absorption spectra in a spectrophotometer, or store the filters in liquid nitrogen, as soon as possible.

b. Sample Filter Storage

- If the filter samples will be analyzed immediately, store each filter in a labeled petri dish (*e.g.* Gelman™ snap-top dishes). Ensure proper hydration of the sample by placing the GF/F filter on a small drop of 0.2 μm FSW. Store each filter sample in the dark and refrigerate it (~4 deg. C) until it is to be measured in the spectrophotometer.
- If the spectrophotometric measurements will be delayed more than 24 hours following sample filtration, the filter samples should be prepared for liquid nitrogen storage. Samples should be stored in containers that allow the filter to remain flat, and which are specifically designed for immersion in liquid nitrogen (*e.g.* Fisher Histoprep™ tissue capsules). One pair of blank filters should also be prepared each day for use as the reference blank for samples collected that day. Samples may be stored in liquid nitrogen for extended periods, but it is strongly recommended to analyze them as soon as possible.
- Non-pressurized liquid nitrogen dewars generally retain liquid nitrogen for 2-4 weeks. Pressurized liquid nitrogen dewars can be rented at low cost for extended cruises (4-5 weeks) so that the sample dewars may be replenished and kept full. Care must be taken at sea, and in return shipping, to ensure that the samples are properly frozen. Samples should be shipped in liquid nitrogen dry shippers, which will maintain proper temperatures for 2 to 3 weeks, if they are properly charged and in good condition.
- Air transport of liquid nitrogen dry shippers is approved under International Air Transportation Agreement (IATA 41st Edition Section A800; US Federal Aviation Administration Dangerous Good Bulletin DGAB-98-03; August 25, 1998). That approval notwithstanding, many investigators have experienced difficulties in clearing customs, and in transport of liquid nitrogen dry shippers via commercial airfreight, or as checked baggage. The investigator should contact the carriers in advance and provide the IATA approval and FAA bulletins pertaining to liquid nitrogen dry shipper transport. If the dry shipper is to be transported as checked baggage, advanced coordination with the airline is strongly recommended to avoid confiscation of samples and delays in return shipment. When samples are shipped as checked baggage or freight, the IATA memo, DOT memo, and manufacturer's certificate should be affixed to the dry shipper to minimize potential delays.
- Temporary storage of filter samples on dry ice can be considered during transport. But maximum duration of dry ice in insulated shipping boxes is several days, so the use of liquid nitrogen dry shippers is strongly recommended.

Determination of spectral optical density of sample filters

After preparation, the optical density spectrum of each sample filter is measured using a laboratory spectrophotometer. The performance characteristics and calibration requirements of the spectrophotometer used for these measurements are described above in Section 4.3.

a. Reference Blank Spectra

With a dual beam spectrophotometer, two reference filter blanks saturated with FSW are used to measure the reference spectrum, and one is left in the reference beam during sample measurements. For typical single beam instruments, generally the reference is scanned, and then samples are placed into the beam and scanned. Most modern spectrophotometers, whether single or double beam, automatically store the instrument's reference spectrum and recorded sample spectra are automatically corrected to yield $OD_{\mathrm{fp}}(\lambda)$ relative to the reference blank filter. A new instrument reference baseline scan should be measured each time the spectrophotometer is powered up, and whenever its configuration has been changed. The baseline should also be checked regularly (every 1 hr to 2 hr) during extended periods of analysis. Frequency of baseline verification will depend on the performance and stability of each instrument and should be determined by the investigator prior to executing routine work. Uncorrected baseline drift, and changes in sorting filters or lamp source can cause systematic measurement anomalies. Wavelength accuracy and measurement precision should also be checked during the analyses (Sect. 4.3 above).

b. Spectrophotometric Measurement Procedure

- Warm up the spectrophotometer for 30 minutes.
- Measure the initial instrument baseline and wavelength calibration.
- If using frozen samples, remove the filters from the storage container and place them in petri dishes on FSW to ensure hydration. Allow the samples to thaw for approximately 5 min and then refrigerate them in the dark until each filter is ready for analysis.
- An instrument-specific sample-mounting device is recommended to hold filters against a quartz glass mounting plate. These mounts should be secure when placed in the sample compartment and hold the sample perpendicular to the illumination beam so only the filter and the quartz plate are in the beam. Usually, these mounts must be custom fabricated specifically for each different instrument.
- Clean the quartz faceplates of the mounting device with purified water and detergent if needed. Rinse them with purified water and ethanol, and dry them thoroughly using lint-free laboratory tissues.
- Set the appropriate instrument parameters according to the manufacturer's instructions.
- Mount two pre-soaked and water saturated blank filters (one for the sample beam, and one for the reference beam).
- To test for proper filter hydration, confirm that there is a drop of FSW left on the mounting plate when the filter is lifted. With the filter on the mounting plate there should be a slight sheen on the top surface of the filter, and a very narrow (~1 mm) border of water around the edges of the filter. Be careful not to use too much water, or the sample may wash away.
- Examine the back of the filter on the mounting plate to be sure that no bubbles are trapped between the filter and the quartz glass plate on the sample holder. There should be a uniform layer of water between the filter and quartz glass mounting plate. If bubbles are present, which will be obvious, pick up the filter with forceps, and replace it on the plate with a slight dragging motion across a drop of filtered seawater. Re-inspect the back of the filter and repeat the foregoing procedure until no bubbles are present. Adjust the amount of FSW as necessary to ensure proper hydration.
- Alternative mounts that expose both sides of the filter to air may be used to avoid bubbles altogether. Sample hydration is more difficult to maintain when using this type of filter mount so the investigator must develop a satisfactory procedure to ensure proper hydration of sample and reference.
- Run the instrument baseline correction using the two blanks. For most commercial units, this baseline will be automatically used as the reference to calculate $OD_{\mathrm{fp}}(\lambda)$. Immediately after the baseline correction is finished, and without touching the blank filters, run the two blanks as a sample scan to confirm that baseline performance is within acceptable tolerance over the spectral range of determination (Sect. 4.3 above). This spectrum should be flat spectrally. Baseline noise less than $\pm$ 0.005 OD is recommended. Save this scan for confirmation of instrument performance. If a spectrally flat baseline cannot be achieved over the spectral range of interest, the stored baseline must be subtracted from subsequent measurements of sample filter $OD_{\mathrm{fp}}(\lambda)$.
- If using a single beam instrument, or instruments run in the single beam mode the blank is not kept in the instrument so one does not need to rehydrate the blank reference filter regularly. Most modern single beam spectrophotometers will also automatically use the blank reference stored in memory for estimates of $OD_{\mathrm{fp}}(\lambda)$.
- Remove the blank filter from the quartz glass sample mount in the measurement beam, and replace it with a sample filter, ensuring proper hydration of the sample (see above). Measure the sample $OD_{\mathrm{fp}}(\lambda)$ spectrum, save it in a digital file, and record all relevant information.

- The blank reference filter will dry out over time, and must be hydrated regularly. If absorption signal deviates significantly from zero (more than 0.02 OD) in the infrared (750-800 nm), this often indicates a dry reference or sample filter. If using a quartz plate, check the reference filter after every 5-6 scans, and hydrate as needed. If the filters are mounted in air, hydrate the blank before every scan.

Sample Filter Preparation for De-pigmented Particle Absorption

After preparing an $a_{\mathrm{p}}(\lambda)$ filter sample and determining its $OD_{\mathrm{fp}}(\lambda)$ spectrum on the spectrophotometer, the sample should be processed to remove its pigments and determine $a_{\mathrm{d}}(\lambda)$. The shape of the $a_{\mathrm{d}}(\lambda)$ spectrum usually decreases monotonically with wavelength, following exponential form that is flatter than the shape of the soluble absorption spectrum. Since the goal is generally to get an estimate of phytoplankton absorption, if there is a residual chlorophyll *a* absorption peak in the red near 675 nm, the extraction process should be repeated to remove it. Variations of this method include use of hot or boiling methanol and varying extraction times. Use of hot methanol has risks due to flammability, and volatility. If this process is used, extra precautions must be taken.

Bleaching of the organic pigments can also be accomplished for situations with difficult to extract pigments including phycobilins or other chemically polar pigments that do not extract well in methanol. Pigment extraction in a chemical solvent, such as methanol, is a fundamentally different chemical process than bleaching the pigments using sodium hypochlorite (NaClO). Bleaching involves placing a small amount of 0.1 % active chlorine solution onto the filter, then rinsing it off with FSW. The NaClO oxidizes the pigment molecules, making their light absorption negligible. FSW rinses then remove the excess NaClO, which absorbs negligibly at wavelengths >400 nm, but absorbs strongly at shorter wavelengths. The bleaching method of pigment removal has been shown to be effective *in situ*ations where methanol cannot be used, as on cellulose membranes such as the 0.22 µm Millipore filter, or when phycobilins are present (Tassan and Ferrari 1995a; Mitchell *et al*. 2000). This procedure can also be adapted for use with particulate suspensions.

Neither methanol extraction, nor NaClO oxidation, provides an ideal means of separating particulate absorption into 'algal' and 'detrital' components. In each case, the action of the chemical agent is not well understood, and in many situations the two methods will yield very different results. The decision to apply either the bleaching, or methanol extraction, method will depend on the situation. For example, in inland waters where either cyanobacteria, or chlorophytes, are dominant, the bleaching technique is preferred, because of the presence of phycobilins and of extraction resistant algae (*e.g.* Porra 1990). In coastal oceanic waters, on the other hand, the methanol technique is preferred, because the results will be comparable to previously published results and there is no particular advantage to using bleach. In open-ocean samples (*e.g.* the Sargasso Sea), however, absorption by phycobilins is small, but present in some particulate absorption samples and in methanol-extracted filters (N.B. Nelson unpublished data). The methanol technique will provide results which are comparable to earlier studies, but with errors due to incomplete extraction and wavelength shifts in the phycobilin absorption bands.

a. Methanol Extraction method

- Replace the sample and blank filters on the filtration system. Treat blank filters exactly as if they were sample filters.
- Add 5 mL to 10 mL of 100 % methanol to each filter by gently pouring it down the sides of the filter funnel to minimize resuspension of the sample particles, and let stand for 1 min.
- Filter the methanol through the sample, turn off the vacuum, close the valves and add 10 - 15 mL of methanol.
- Allow the sample to stand in methanol for approximately 1 hr. Do not allow the filter to go dry during the extraction period. Time of extraction will vary depending on the filter load and phytoplankton species composition. Place aluminum foil over the filtration cups to minimize contamination during extraction.
- After extraction is complete, turn on the vacuum and draw the methanol and dissolved pigments through the filter. Rinse the sides of the filter tower twice with small amounts of methanol. Finally, rinse the sides of the filter tower three times with ~20 mL of 0.2 µm FSW. Also rinse the blanks with FSW after methanol extraction to minimize filter dehydration during spectrophotometric analysis.

- Pigment extraction is complete when the 675 nm chlorophyll *a* absorption peak is not present in the $OD_{\mathrm{fd}}(\lambda)$ spectrum.
- Successive, short extractions of 10 minutes can sometimes improve the pigment extraction.
- Phycobilins, and some eukaryotic pigments, will not be extracted efficiently by methanol.

b. Sodium Hypochlorite oxidation method

- Prepare NaClO solution:
- For freshwater samples: 0.1 % active chlorine in purified water (*e.g.* Milli-Q water).
- For marine samples: 0.1 % active chlorine in purified water containing 60 gl^{-1} Na_2SO_4, to match osmotic pressure of sample cells.
- The volume of 0.1% active chlorine solution needed to bleach pigments from a filter sample has been empirically shown to be approximately $3OD_{\mathrm{fp}}(440)$ mL .
- Place the sample, particle side up, on the filtration system (closed valves).
- Gently pour the solution down the sides of the filter funnel.
- Let the solution act for 5 min to 10 min, adding solution as necessary to compensate for loss through the filter.
- Cover the filtration cup with aluminum foil to prevent contamination during bleaching.
- Rinse the sample by gentle filtration of 50 mL of water (either fresh water or FSW, depending on sample source).
- Complete bleaching of the pigments is indicated by the absence of a 675 nm peak, together with a concave shape near 440 nm, in the $OD_{\mathrm{fd}}(\lambda)$ spectrum of the bleached filter. If evidence of residual pigment absorption persists, repeat the NaClO oxidation treatment, as indicated above.

Spectrophotometric Measurement of De-pigmented Optical Density Spectra

- The $OD_{\mathrm{fd}}(\lambda)$ spectrum of the de-pigmented samples should be measured in the spectrophotometer, as described above for $OD_{\mathrm{fp}}(\lambda)$.
- Note that methanol-extracted sample and blank filters will tend to dry out quickly if the methanol is not thoroughly rinsed from the filters prior to spectrophotometric measurements.
- NaClO oxidized sample and reference filters must be thoroughly rinsed with FSW (or fresh water for inland water samples) to extend the spectral range below 400 nm.

4.5 SOLUBLE ABSORPTION SAMPLE PREPARATION AND ANALYSIS

The measurement methods described in this section are used to determine $a_{\mathrm{g}}(\lambda)$, the spectral absorption coefficient spectrum of gelbstoff, often referred to as dissolved organic matter (CDOM). Water samples are collected and particulate material is removed by filtration. The absorption of the filtrate is measured, relative to purified water, using a spectrophotometer. All equipment utilized to prepare soluble absorption samples must minimize contamination by organic, or otherwise colored, material. Samples must be protected from photo-degradation during preparation and measurements. Plastic or glass filtration apparatus may be used, provided that the units are equipped with mesh filter supports made either of stainless steel or plastic, and not with ground glass frits. Glass frits tend to become clogged over time, and may cause uneven distribution on the filter, reduce the rate of filtration and may contaminate the sample filtrate.

Membrane filters with 0.2 µm pore size (*e.g*., Nuclepore™ polycarbonate filters) are recommended for this procedure. The membrane filters should be pre-soaked in 10% HCl, rinsed with 75-100 mL of freshly purified water, and rinsed again with a 75 – 100 mL of the sample before it is used. Tests with purified water have shown that all filters leach contamination that resembles soluble absorption (data not shown). Using polycarbonate membrane filters, an acid soak, pure water rinse and sample rinse minimizes this contamination. Still, we have found the sample preparation procedure increases the apparent absorption spectra of purified water that is prepared as though it were a sample when referenced to purified water drawn directly into the measuring cuvette from the pure water system. Therefore correction for this sample preparation blank is recommended.

Glass fiber filters should be avoided if possible because they have been shown to cause rather severe contamination of the filtrate in tests using purified water. For samples collected from very turbid waters, glass fiber filters have routinely been used as a pre-filter to minimize clogging of the final filtration with a membrane filter (Kowalczuk, 1999). In such cases the investigator must develop a procedure to rinse the glass fiber filter to ensure that the contamination from this method is minimized. Since situations requiring pre-filtration often coincide with large soluble absorption coefficients, the effects may be easily corrected but it is the responsibility of the investigator to demonstrate this. Careful assessment of the contamination of any method, and proper corrections must be carried out and reported.

Previously we recommended the use of amber-colored borosilicate glass bottles (*e.g*. Qorpak™ bottles), that screen ambient light, for sample preparation and to store laboratory prepared standard water. However, recent work (details not shown) indicate that the amber bottles may leach some colored material into the purified standard water that is prepared before cruises and used to assess the quality of purified water prepared at sea. Therefore we now recommend use of clear borosilicate Qorpak™ bottles (or equivalent) for sample preparations and for the preparation of the standard reference water. Prior to each experiment, all filtration apparatus and storage bottles should be thoroughly cleaned.

Purified water for soluble absorption measurements

Purified water freshly drawn from a water purification system, such as the Millipore Milli-Q, Millipore Alpha-Q, and Barnstead Nanopure units, or their equivalent, is strongly recommended for use at sea in preparing pure water for absorption reference, blanks and for equipment rinses specified in these protocols. Mitchell *et al*. (2000) compared the water-to-air baseline reference of purified water prepared with these three water purification systems. All three systems provided similar results in baseline tests relative to air at wavelengths between 300 nm and 900 nm, while small differences were found below 300 nm. It is also recommended to prepare a set of standard purified water samples prior to a field deployment as a reference to check daily for pure-water system degradation, *e.g*. due to poor quality feed water. Even though bottled purified water standards have been found to deteriorate slightly over time, especially from 250 nm to 325 nm, they provide invaluable quality control and an alternative source of reference water *in situ*ations when the purification system performance degrades dramatically.

Pre-cruise preparations

- Sample bottles (clear borosilicate Qorpak™ with polyethylene lined caps) used to collect sample filtrate or to store standard reference water need to be thoroughly cleaned in advance to remove any potential organic contaminants. Sequential soaks and rinses in dilute detergent, purified water, and 10 % HCl, followed by a final copious rinse in purified water, are recommended.
- Rinse plastic caps with 10 % HCl, twice with freshly prepared purified water (*e.g.* using a Millipore Alpha-Q system), and dry them at 70^{o} C for 4 hr to 6 hr.
- Combust bottles with aluminum foil covers at 450^{o} C for 4 hr to 6 hr.
- Fill clean, combusted bottles with fresh purified water drawn directly from the purification unit.
- Assemble the combusted bottles and clean caps. Store in the dark.
- These standards are used daily during cruises to evaluate the quality of purified water freshly prepared at sea.

- This carefully prepared standard water sometimes must be used as the reference material for actual sample analysis. If this is planned, the investigator should determine the optical density of the standard water preparations before and after a cruise relative to fresh purified water drawn directly into the quartz cuvettes. An assessment of the change in this water over time may indicate a need to use a time-dependent reference water correction.
- As a precaution, even if the investigator intends to have high quality purified water at sea, it is wise to determine the standard water optical density relative to freshly purified water before a cruise, and as a time-series to understand the quality of the purified water system used for reference.

Soluble Absorption Sample Preparation, Storage and Analysis

- Wash hands with soap and water to avoid contaminating the samples.
- Use 0.2 μm polycarbonate filters (*e.g.* Nuclepore or equivalent). Do not use irgalan black stained (low fluorescence background) polycarbonate filters for this preparation. Other membrane filters, or Sterivex cartridges, may also be used, but the investigator must then test for any contamination by the filter and ensure that no artifacts are introduced.
- The filtration system used should be equipped with control of vacuum for each individual filtration funnel and with a provision for direct filtration into clean bottles. An example of a suitable soluble absorption filtration assembly is illustrated in Mitchell *et al*. (2000).
- Pre-soak each filter for at least 15 min in 10 % HCl. Rinse the filter thoroughly with purified water. Mount the filter on a filtration funnel and filter ~100 mL of purified water through it into a sample bottle. Shake the bottle, and discard the water, pouring it over the inside of the cap to rinse it. Cover the filtration funnel with aluminum foil until ready to filter the sample.
- Collect ~200 mL of seawater into a clean sample bottle. For the blanks, use purified water drawn directly from the purification unit into 2 clean sample bottles.
- Filter ~75 mL of the samples and 1 blank directly into clean bottles at low vacuum (<120 mm Hg). Do not allow filters to go dry during sample rinsing. Shake the bottles, and discard the water.
- Filter ~75 mL of the samples into bottles. For the blank, filter ~75 mL of purified water. When finished, cap the bottles and store them until they are to be measured in the spectrophotometer.
- If the samples will be measured within 4 hr, store them in the dark at room temperature.
- If the samples will be measured 4 hr to 24 hr later, refrigerate them in the dark.
- Longer storage is not recommended, because artifacts of undocumented magnitude are known to occur. Several researchers have reported results from measurements of frozen samples, but no systematic evaluation of possible artifacts resulting from freezing has yet been reported.
- Warm refrigerated samples to room temperature before beginning optical density measurements. If it is practical to do so, control the samples and the reference water to equal temperatures during the spectrophotometric measurements. Absorption by water is strongly temperature dependent at red and near infrared wavelengths (Pegau and Zaneveld 1993).
- Qorpak bottles can be re-used at sea. After spectrophotometric analysis is completed, thoroughly rinse each bottle and its cap three times with purified water, pour in 20 mL of 10 % HCl acid, and close the cap. Before the bottle is reused, shake it well, discard the 10 % HCl, rinse the bottle and cap copiously with purified water, and fill the bottle with purified water, to be used later to rinse a new sample filter. Purified water should be drawn directly from the pure water system.

Determination of Optical Density of Soluble Absorption Preparations

- If samples have been refrigerated, allow them to warm to room temperature.

- Allow the spectrophotometer to warm up for 30 min. Confirm that the optical windows of the spectrophotometer are clean. If necessary, clean them with purified water and ethanol, sequentially, and dry them thoroughly with lint-free laboratory tissues.
- Verify the instrument's spectral characteristics and precision as described in Section 4.3.
- Wash hands with soap and water to avoid contamination
- Between use, 10 cm quartz window spectrophotometer cuvettes should be stored with purified water. For analysis, discard the purified water in the cuvettes, rinse inside and outside of cuvettes twice with 10 % HCl, twice with ethanol, then rinse them inside and outside using copious volumes of purified water. After the cuvettes have been cleaned, use laboratory tissues to handle them. Avoid contacting the cuvettes with bare-hands, and do not contaminate their optical windows by touching them.
- Fill both cuvettes with purified water drawn directly from the water preparation system. Use of purified water stored in containers is not recommended. However, if freshly purified water is not available at sea, the carefully prepared standard water in combusted bottles can be used as a reference, but the investigator must document its degradation over time relative to air (see above).
- Carefully dry the cuvettes. Bulk dry with paper towels, but dry the quartz optical windows with lint-free laboratory wipes only (*e.g.* Kimwipes™).
- Inspect cuvettes carefully, especially along their optical paths, to ensure that they are clean. Make sure there are no bubbles, floating dust, or contaminants on the optical windows, or in suspension. Looking through the cuvette against a black background can usually identify any problems in the samples. Repeat cleaning and drying procedures as needed to obtain a clean sample.
- Run an air–to-air baseline reference spectrum for the spectrophotometer. Record the digital air baseline. This spectrum should be spectrally flat, with noise less than ± 0.0005 OD.
- Place the reference cuvette in spectrophotometer and scan $OD_{\mathrm{rwa}}(\lambda)$, the optical density of purified water relative to air. Remove the reference cuvette and repeat the measurement for the sample cuvette. Store both spectra noting which file is for the cuvette to be used as reference in subsequent analyses, and which is to be used for samples. See Figure 4.2 for spectra of $OD_{\mathrm{rwa}}(\lambda)$ determined during ACE-Asia.
- Compare the spectra of $OD_{\mathrm{rwa}}(\lambda)$ determined for the reference and sample cuvettes to each other, and with a digital library of previous reference water to air optical density spectra. Ensure that the two cuvettes are well matched optically, and that both conform to tolerance of pure water relative to air. Note anomalies and plan to make any needed corrections during data processing. If anomalies are associated with poor preparation of the cuvette, repeat the preparation and run new water-to-air baseline reference scans.
- Put both reference and sample cuvettes filled with purified reference water into the spectrophotometer for a double beam unit. For a single beam unit this will be done sequentially. Run a baseline correction for purified water. After the water-to-water baseline optical density measurement is complete, record the pure water baseline as a sample, $OD_{\mathrm{rww}}(\lambda)$. This spectrum should be spectrally flat, with magnitude less than ± 0.0005 OD. Save the digital baseline spectrum. Ensure the baseline is flat and stable over time and note any anomalies. It is common for the baseline to exhibit temperature-dependent artifacts 650-800 nm. These should be minimized if possible by ensuring the purified water in the sample and reference cuvette are at the same temperature.
- If the baseline reference spectrum $OD_{\mathrm{rww}}(\lambda)$ is not flat and stable during analysis according to specifications summarized in section 4.3, the precision of any estimate of soluble absorption may be seriously questioned. It is the investigator's responsibility to ensure satisfactory performance of the instruments and use of proper methods to ensure that the final result is reasonable. Significant deviation from the specifications in section 4.3 or improper consideration of sample preparation protocols may result in estimates of soluble absorption that are not meaningful given the small magnitude of this estimate in the visible spectral region of most interest for ocean color applications.

- Remove the sample cuvette and discard the liquid. Rinse the inside of the cuvette three times with ~5 mL to 10 mL of the next sample to be measured. A copious rinse is desired, but sample volume is often limited. Several vigorously shaken small sample rinses are recommended if the volume is extremely limited.
- Fill the sample cuvette with the purified water that has been filtered as though it were a sample and record the blank spectrum, $OD_{\mathrm{bs}}(\lambda)$, relative to the reference cuvette filled directly from the purified water source..
- Repeat the rinsing for each subsequent sample. The first sample rinse for seawater samples is most important to eliminate all purified water, especially for seawater samples due to refractive index differences between fresh and salt water. Fill the cuvette with the next water sample.
- Prior to running each sample, dry the exterior of the sample cuvette carefully, and inspect it, as described above, to ensure a clean sample.
- Replace the sample cuvette in the spectrophotometer, and measure the $OD_s(\lambda)$ spectrum relative to freshly purified water. Store the digital data and record all necessary information.

4.6 DATA PROCESSING AND ANALYSIS

The protocols in this section should be followed to compute particle and soluble material absorption coefficients from the spectrophotometric OD measurements described above. The following discussion assumes that all measured $OD(\lambda)$ spectra, whether for samples, or reference blanks, have been corrected for the instrument baseline spectrum, either automatically, or by post-measurement calculations appropriate to a particular spectrophotometer configuration (see above in Section 4.3, and specific reference spectrum measurement checks in the protocols of Sections 4.4 and 4.5).

Computations for absorption coefficients of particles concentrated on filters, and for materials dissolved in water, differ primarily in the determination of optical pathlength and in the treatment of reference blanks.

Soluble Absorption Coefficients

For soluble absorption, the calculations are directly proportional to the sample optical density relative to the pure water reference after correction for the pure water blank and specification of a null absorption

$$a_g(\lambda) = \frac{2.303}{l}\Big[[OD_{\mathrm{s}}(\lambda) - OD_{\mathrm{bs}}(\lambda)] - OD_{\mathrm{null}}\Big], \tag{4.3}$$

where l is the cuvette pathlength (usually 0.1 m), $OD_{\mathrm{s}}(\lambda)$ is the optical density of the filtrate sample relative to purified water, $OD_{\mathrm{bs}}(\lambda)$ is optical density of a purified water blank treated like a sample relative to purified water (see below), and OD_{null} is the apparent residual optical density at a long visible or near infrared wavelength where absorption by dissolved materials is assumed to be zero. Note that as long as the null wavelength region is the same for sample and blank, the sample and blank spectra can be set to zero at the null wavelength independently or after they are subtracted from each other, as indicated in Equation (4.3). Equation (4.3) assumes use of a spectrophotometer that automatically references the sample and blank optical density to freshly purified water. Most modern commercial single or double beam units will compute this optical density directly relative to the reference. The user must record both raw sample and blank optical densities relative to purified water, and assess the stability of the purified water $OD_{\mathrm{rww}}(\lambda)$ reference by routine determinations of the purified water relative to air (*e.g.* $OD_{\mathrm{rwa}}(\lambda)$; Figure 4.2) and also evaluate the sample preparation methods by determining the blanks routinely (*e.g.* daily when at sea; Figure 3B).

a. Filtered pure water blank spectra

There are generally small spectral effects of the filtration and preparation procedure that cause blanks prepared from purified water to have a higher $OD_{\mathrm{bs}}(\lambda)$ at short wavelengths compared to the reference cuvette containing purified water drawn directly from the purification system. Examples of filtered blank spectra $OD_{\mathrm{bs}}(\lambda)$ for ACE-Asia where Millipore Alpha-Q water was used as the purified water source in the reference cuvette are illustrated in Figures 4.3B and 4.3D (c.f. Mitchell *et al.* 2000). The $OD_{\mathrm{bs}}(\lambda)$ spectrum should be determined, recorded and included with the data for each sample. It is recommended that the investigator carefully determine these blanks for each station, or at least once per day, during a field program, and evaluate the stability of this blank for quality control purposes. If the purified water system is performing well, and the preparation procedures are carefully implemented, the $OD_{\mathrm{bs}}(\lambda)$ sample blank offsets will generally be very consistent (Figure 4.3B). In such cases, the recommended procedure is to average $OD_{\mathrm{bs}}(\lambda)$ spectra over the entire cruise, and to then fit a smoothed exponential function over wavelength to the overall mean (the bold line in Figure 4.3B). A separate OD_{null} (see discussion below) should be determined for the averaged and smoothed $OD_{\mathrm{bs}}(\lambda)$ spectrum before it is substituted in Equation (4.3). Because the signals are small, instrument noise is a large fraction of the signal, even for high quality spectrophotometers. Therefore subtraction of an individual blank spectrum, including its noise, is strongly discouraged as this effectively doubles the noise of an already noisy signal. Instead, it is recommended that a smoothed blank be determined from many individual blank spectra provided that the investigator can demonstrate, as in Figure 4.3B that there is consistency among the population of blank spectra that are determined. The procedure of determining blanks at least each day during routine sampling provides an important quality control on the sample preparation protocols. If the blank is found to deviate considerably from the norm, the investigator should immediately determine the cause of the discrepancy.

b. Null point corrections to soluble absorption spectra

The absorption spectrum of pure water varies strongly with temperature, especially in the wavelength region between 650 nm and 750 nm, but at other wavelengths as well (Pegau and Zaneveld, 1993). To avoid temperature related measurement artifacts, the sample and reference should be maintained at the same temperature, but in practice, this is often difficult to do. If strong temperature residuals are apparent in the spectra near 750 nm, one must inspect the data to determine an appropriate wavelength range to use as a null point. For the data in Figure 4.3, it appears that assuming a null point as the average from 590-600 nm is reasonable. This assumption may not be reasonable in turbid lake, bay and coastal waters, however, where large soluble absorption values may persist into the near IR. Selection of wavelengths for null correction must be evaluated carefully for each data set, following principles discussed at more length by Mitchell *et al*. (2000).

Particle Absorption Coefficients

To compute particle absorption $a_{\mathrm{p}}(\lambda)$ in suspension from spectrophotometric $OD_{\mathrm{fp}}(\lambda)$ measured with the particles concentrated on a GF/F filter, it is necessary to appropriately adjust the optical pathlength. This includes substituting the geometric optical pathlength of the particles in suspension, and a scaling factor, β , accounting for the increase in the optical measurement path by scattering within the filter sample. The geometric absorption pathlength l_s of the filtered material in suspension is given by

$$l_s = \frac{V_{\mathrm{f}}}{A_{\mathrm{f}}}, \tag{4.4}$$

where V_{f} is the volume of water filtered and A_{f} is the clearance area of the filter calculated from the diameter D_{f} of the part of each filter that contains the particles. D_{f} should be determined very carefully on numerous individual filters using AN accurate measurement tool like a caliper that is accurate to at least 0.1 mm.

Scattering of light within the GF/F filter increases the absorption pathlength. The absorption coefficient of filtered particles must be corrected for pathlength amplification and the equivalent absorption coefficient in m^{-1} in suspension is computed as

$$a_p(\lambda) = \frac{2.303 A_{\mathrm{f}}}{\beta V_{\mathrm{f}}}\left[[OD_{\mathrm{fp}}(\lambda) - OD_{\mathrm{bf}}(\lambda)] - OD_{\mathrm{null}}\right], \tag{4.5}$$

where $OD_{\mathrm{fp}}(\lambda)$ is the measured optical density of the sample filter, $OD_{\mathrm{bf}}(\lambda)$ is the optical density of a fully hydrated blank filter, and OD_{null} is a null wavelength residual correction from the infrared where particle absorption is minimal. See also detailed discussion of null point selection in Mitchell *et al*. (2000)

a. Particle absorption blank spectra

If a spectrophotometer with automatic reference baseline correction is used, and the reference filter blank baseline is flat over the spectral range of interest, $OD_{\mathrm{bf}}(\lambda)$ does not need to be subtracted. Spectra of $OD_{\mathrm{bf}}(\lambda)$ must be determined, recorded and provided with the sample data. Properly prepared blanks generally have flat spectra relative to the reference baseline filters. If the $OD_{\mathrm{bf}}(\lambda)$ is confirmed to be flat, then it is recommended that only a null absorbance is subtracted from the $OD_{\mathrm{fp}}(\lambda)$ to compensate for baseline offsets. Subtraction of a spectrally flat baseline that varies only due to the instrument noise increases the noise of the result. If the instrument baseline cannot be maintained within the recommendations summarized in Section 4.3, the investigator should consider using a different instrument since the errors in the methods caused by using unstable instruments are difficult to control for.

b. Null point corrections to particle absorption spectra

To correct for residual offsets in the sample filter relative to the reference, and for scattering artifacts due to particle loading, it is assumed that a null absorption wavelength in the infrared can be identified. Historically, many investigators used 750 nm as the null absorption wavelength, but recent reports indicate that this wavelength is too short for some waters. It is recommended that the null wavelength be set at 800 nm (or longer), and that the investigator must examine the spectra to evaluate residual absorption structure near the null wavelength. Rather than use a single wavelength, a mean $OD_{\mathrm{fp}}(\lambda)$ in a 10 nm interval (*e.g.* 790 nm to 800 nm) may be used as the null value to minimize the introduction of noise in the null correction procedure. Mitchell *et al.* (2000) discuss, at more length, factors affecting the choice of an appropriate wavelength for estimating OD_{null}. In Case 2 waters, the definition of the null absorption is more difficult and the investigator may consider the benefits of the transmission-reflectance estimates of particle absorption (Tassan and Ferrari, 1995a).

c. Pathlength amplification corrections

To correct for the pathlength increases due to multiple scattering in the filter, the prevalent current practice is to estimate β empirically through either a quadratic or power function that may be expressed in the form

$$\beta = \left[C_1 + C_2\left[OD_{fp}(\lambda) - OD_{null}(\lambda)\right]\right]^{-1}, \tag{4.6a}$$

or

$$\beta = C_0 + C_1\left[OD_{fp}(\lambda) - OD_{null}(\lambda)\right]^{C_2}, \tag{4.6b}$$

for quadratic equation or power function fits, respectively. C_0, C_1 and C_2 are coefficients of least squares regression fits of measured data. Recommended coefficients have been reported in the literature (Table 1). The investigator should either choose published coefficients consistent with the species composition, equipment and measurement conditions for a given data set (consider the discussion in Mitchell *et al*. 2000), or independently determine

pathlength amplification factors by comparing absorption in suspension and on filters following procedures described previously (Mitchell 1990, Mitchell *et al*., 2000).

d. De-pigmented Particle and Phytoplankton Absorption Coefficients

The de-pigmented particle absorption coefficients, $a_{\mathrm{d}}(\lambda)$, may be calculated using Equation (4.5), by substituting. $OD_{\mathrm{fd}}(\lambda)$ for $OD_{\mathrm{fp}}(\lambda)$. At present it is recommended to use the same pathlength correction factor for the de-pigmented samples as for the particle absorption sample. The validity of this operational choice of β is difficult to assess, because the de-pigmented particles are created operationally from the treatment, and the relationships between their absorption on filters compared to suspensions may differ from those derived empirically for the original particles.

The spectral absorption coefficient for phytoplankton pigments can be computed as the difference between particulate and de-pigmented estimates:

$$a_{\phi}(\lambda) = a_p(\lambda) - a_d(\lambda). \tag{4.7}$$

4.7 DATA REPORTING

For purposes of data reporting and archiving, the absorption coefficients will be reported in m^{-1} and computed using the equations summarized above. Uncorrected optical density spectra for the filter samples, blank filter referenced to a blank filter, pure water referenced to air, pure water referenced to pure water and soluble absorption blank spectra must be recorded and provided so alternative algorithms could be applied to the original data. The pathlength amplification factor, a description of (or reference to) the method and the procedure for assignment of the null absorption, and any blank or spectral scattering corrections for the soluble absorption calculations must be reported.

4.9 PROTOCOL STATUS AND FUTURE DIRECTIONS

Absorption spectra for particles filtered on GF/F filters

Details of various issues related to this frequently used method for estimating particle absorption for filtered samples are not significantly changed since the summary of the NASA-sponsored Workshops found in Mitchell *et al*. (2000). It is important to address a few salient issues that are routinely asked by investigators interested in implementing the method. First, most modern dual-beam spectrophotometers that have a grating before the sample and illuminate the sample with spectrally resolved light have negligible differences (a few percent) in terms of determining the raw GF/F filter $OD_{\mathrm{fp}}(\lambda)$ of the particles relative to a properly hydrated blank filter if the protocols are carefully followed. Thus, it is not essential to determine the pathlength amplification factor, β, for each different spectrophotometer that is used as long as the investigator makes an appropriate choice of instrumentation. However, some spectrophotometers have limited spectral range, limited dynamic range, more noise and inferior stability so the investigator should evaluate the unit to be used to ensure suitability by following the recommendations in section 4.3. Second, diode-array systems that illuminate with broad-band light and then disperse the post-sample light using a spectral photodiode array may have significantly different raw OD for the filtered sample. Example OD spectra estimated for a diatom culture for various systems used at the Scripps Workshop are shown in Figure 4.1 (see also details in Mitchell *et al*. 2000). Note the Hewlett-Packard spectral diode array system has a significantly higher OD than the other instruments. An empirical relation for this offset in the range 400-700 nm is reported in Mitchell *et al*. (2000) for that specific model. The Hewlett-Packard data is reported only for wavelengths greater than 400 nm because the instrument performs poorly at short wavelengths with the glass fiber filter method. If a user chooses such optical geometry for the determination of particle absorption they should carefully assess the potential issues illustrated in Figure 4.1. We recommend that the user compare several spectrophotometers for raw optical density of properly hydrated samples relative to blank filters and ensure the unit they use does not deviate from the typical result of most systems for which amplifications factors (β) have been determined (Table 4.1). Alternatively one must determine the pathlength amplification for the

instrument of choice, a laborious and unnecessary procedure if a spectrophotometer is selected that does not cause the bias illustrated in Figure 4.1.

Absorption spectra for particles transferred to glass slides

An alternative method, developed by Allali *et al*. (1995), to estimate absorption coefficients of cultures and seawater samples is to freeze transfer the particles to transparent microscope slides, following the protocols of Hewes and Holm-Hansen (1983). The investigator must have an integrating sphere or equivalent scattered transmission accessory to implement this method. This procedure produced results comparable to the GF/F filter method in comparisons reported by Mitchell *et al*. (2000), but sufficient uncertainties remain that the GF/F method continues to be recommended for the present.

Transmission-Reflectance (T-R) Method

Tassan and Ferrari (1995a) described a modification of the light-transmission method that corrects for backscattering. This technique combines light-transmission (T) and light-reflection (R) measurements, carried out using an integrating sphere attached to a dual-beam spectrophotometer. The data analysis is performed by a theoretical model that eliminates the effect of light backscattering by the particles. At the Scripps workshop, the global error of the T-R method was comparable to the error yielded by the simpler T method for monocultures. Subsequent modifications of the T-R experimental routine (Tassan and Ferrari, 1998; Ferrari and Tassan, 1999) yielded a significant reduction of the experimental error. Tassan and Ferrari (1995) reported that for case 1 waters that have negligible inorganic particle load, the amplification factor for GF/F filters determined with the T-R methods is similar to those determined by Mitchell (1990). The T-R method is particularly suited for applications to samples containing highly scattering mineral particles that are commonly found in Case 2 waters. Despite the more complicated procedure including an instrument with an integrating sphere, this method should be considered in special circumstances, and with further development may eventually supercede the presently recommended transmission protocol.

Absorption spectra for seawater filtered through membrane filters or cartridges

For most ocean regions, the optical density of dissolved organic material, relative to purified water in a typical 10 cm pathlength cuvette, is very small in the 400-600 nm region of most interest to ocean color satellite investigations. To ensure a common frame of reference for the global data collected by diverse investigators, we recommend $OD_{\mathrm{rwa}}(\lambda)$ spectra (250-850 nm) be determined relative to air for purified water directly introduced to properly cleaned quartz cuvettes. The purpose of such spectra is to obtain an independent reference of the quality of the purified water. $OD_{\mathrm{rwa}}(\lambda)$ spectra for the sample cuvette used during ACE-Asia are shown in Figure 4.2. $OD_{\mathrm{rwa}}(\lambda)$ should be determined daily for the sample and reference cuvettes used in analyses. The investigator should keep careful records of this data and assess any bias in final estimates that may be attributed to problems with the reference water. By plotting in the range of minimal absorption by water (250-600 nm; Figure 4.2A) one can assess whether or not the reference water on a ship has seriously degraded. Production of impure water by commercial systems is a relatively common problem on ships where the feed water may have serious contamination. If the purified water system fails at sea, the investigator should use the standard water prepared prior to the cruise as the reference. Spectra of $OD_{\mathrm{rwa}}(\lambda)$ of the bottled standard water should be determined before and after a cruise for each lot of bottled standards that are prepared. This precaution is important to assist in any corrections that might be required if standard water is used as a reference, or if the purified water system degrades over time during a cruise.

There are still relatively few spectra of soluble absorption determined fresh at sea using the revised protocols recommended here. Spectra of $OD_s(\lambda)$ and $OD_{\mathrm{bs}}(\lambda)$ collected during ACE-Asia are shown in Figure 4.3. Raw optical density, relative to Millipore Alpha-Q water are shown in 3A. We routinely find small positive offsets from 600-800 nm that we feel should be compensated by subtracting a null value. Figure 4.3B illustrates $OD_{\mathrm{bs}}(\lambda)$ during ACE-Asia prepared as recommended in section 4.5, but plotted at 10x smaller scale as Figure 4.3A. The recommended procedure is to subtract a cruise (or global) mean of this blank (solid line in Figure 4.3B) from the raw sample *OD* values, and then to adjust this difference to zero at a null reference [Equation (4.3)]. The smoothed

global blank was determined by taking the mean of all blanks for each cruise we have completed since 1998, subsequently taking the mean of all cruises and lastly fitting an exponential function to the global mean after setting a null point as the average from 590-600 nm. There can be small differences in blank spectra cruise to cruise, but we do not find this to be significant relative to the overall statistics of all cruises or the variance within a single cruse. For relatively weakly absorbing samples like open oceans observed during ACE-Asia, there is negligible apparent absorption > 600 nm and there is clear evidence in 3A of uncompensated temperature effects 650-800 nm. Therefore we chose to set the null value as the mean from 590-600 nm. However, if very strong soluble absorption is present, the temperature effects 650-800 nm will be less significant, and the absorption 590-600 nm may be important. The investigator should evaluate their data to determine the best null point and report that assessment. Figure 4.3C are optical density of spectra for a 10 cm cuvette after correcting for the null value and the blank spectrum The effort to carefully determine the purified water relative to air, and blanks during each cruise will allow different investigators to inter-compare their results better, and will ensure better quality control of data collected over time. We have also determined the time-dependent change of our standard water (data not shown), and when we use that as a reference due to the failure of our purified water system at sea, we subtract a different blank than the global fit shown in Figure 4.3B.

An alternate method for preparing samples for soluble absorption allows multiple use of Sterivex sealed filtration cartridges. Use of these cartridges has been described by D'Sa *et al*. (1999) who used the method to prepare samples delivered to a capillary light guide spectrophotometer for estimating absorption by soluble material. The procedure provides high sensitivity and can be adapted to continuous flow determinations. This new method may prove useful in various applications but has not been applied extensively at this time. Evaluation of the performance of the Sterivex cartridges for sample preparation, and of light guides for spectroscopy, warrant further research.

Constraints on the estimate of soluble and particle absorption

To constrain our water sample estimates of particle and soluble absorption we have compared them to spectral estimates of the diffuse attenuation coefficient for downwelling irradiance, $K_\mathrm{d}(z,\lambda)$, determined using a free-fall radiometer during a Southern Ocean cruise (AMLR) and a western Pacific Ocean cruise (ACE-Asia). It is well known that accurate estimate of $K_\mathrm{d}(z,\lambda)$ in the upper ocean is difficult. Problems include heave of the ship, foam, bubbles, shadow, tilt, sky conditions and other influences on this apparent optical property (see more detailed discussions in other chapters of these protocols). Waters *et al.* (1990) described advantages of free-fall systems and many investigators have adopted this procedure to minimize some of the problems cited above. In 2001 we deployed our Biospherical Instruments PRR 800 system at approximately 80 stations combined between our AMLR and ACE-Asia cruises. We consider this our highest quality radiometric data set because of the free-fall deployment, the spectral range from 312-710 nm and because we acquired 4-5 separate free-fall profiles at each station to improve the confidence in our final estimate. In Figure 4.4 we show estimates of the mean cosine for spectral downwelling irradiance, $\bar{\mu}_\mathrm{d}(\lambda)$, of the upper ocean mixed layer (open symbols). Here we define $\bar{\mu}_\mathrm{d}(\lambda)$ as the ratio $[a_\mathrm{w}(\lambda)+a_\mathrm{p}(\lambda)+a_\mathrm{g}(\lambda)]/K_\mathrm{d}$. For Figure 4.4, values for pure water are estimated from Pope and Fry (1997) for 380-700 nm, Quickenden and Irvin (1980) for 300-320 and a linear interpolation between those values for 320-380 nm as recommended by Fry (2000). If the individual components are accurate, this can be considered a reasonable estimate of the mean cosine near the ocean surface (see Mobley, 1994 for detailed discussion of the mean cosine). Theoretically the values of $\bar{\mu}_\mathrm{d}(\lambda)$ should be less than 1.0 and for typical radiance distributions of the upper ocean, they should be in the range of 0.70-0.85 near the surface. For both AMLR and ACE-Asia all absorption data were determined fresh at sea with consistent methods between the two cruises. We found that in the region 500 nm to 650 nm there is little difference between the estimates of $\bar{\mu}_\mathrm{d}(\lambda)$ for the Southern Ocean and the western Pacific. However, below 500 nm, the values for ACE-Asia are near 1.0 and below 400 nm they exceed 1.0. For AMLR, values approach 1.0 for wavelengths less than 350 nm.

The ratio of $a_\mathrm{g}(\lambda)/a_\mathrm{t}(\lambda)$ where $a_\mathrm{t}=a_\mathrm{w}+a_\mathrm{p}+a_\mathrm{g}$, is also plotted in Figure 4.4 (filled symbols). The trend clearly illustrates that the soluble component dominates at short wavelength. There are several hypotheses that should be considered to understand the overestimates of $\bar{\mu}_\mathrm{d}(\lambda)$ below 400 nm. These could include underestimate of $K_\mathrm{d}(z,\lambda)$ or overestimates of any of the absorption components. A combination of these factors may prevail.

The filter radiometer in the profiler has good out of band blocking, but the spectrum of surface irradiance is rapidly changing in the region <350 nm and this may cause a red shift in the effective band center of the channels, with an associated underestimate of $K_d(z,\lambda)$. There may be small particles or colloids that pass the 0.2 μm filters causing a spectrally dependent scattering error (Aas, 2000). The particle absorption we estimate is based on Mitchell (1990), which results in higher estimates compared to some other published methods (Table 1). Also, there has not been adequate attention paid to determination of the pathlength amplification factor for the region below 400 nm. It is also possible that the values for pure water absorption are too high. The very reasonable or slightly high (by about 10-15%) values for the mean cosine of downwelling irradiance shown in Figure 4.4 for 400-600 nm indicates that the absorption methods recommended here are rather robust compared to simple estimates of diffuse attenuation coefficients. Reynolds *et al*. (2001) and Stramska *et al*. (2000) have reported reasonable closure between estimates of absorption using these methods, radiometric observations and modeling.

We have used "pure water" absorption for our estimate of $a_w(\lambda)$, and salts should in fact be added, if important, in the comparison of absorption to diffuse attenuation in Figure 4.4. Our estimate of $a_g(\lambda)$ relative to purified water will include absorption by salts, if they are significant. Salts in seawater are significant absorbers at short wavelengths. Lenoble (1956; see also Shiffrin, 1988) reported values for pure salts dissolved in purified water that indicate absorption coefficients near 300 nm comparable to the sample optical density of filtered samples relative to purified water that we routinely determine at sea in this spectral region. This UV absorption (<320 nm), relative to purified water, is generally assumed to be caused by "colored dissolved organic matter" but this may be inaccurate at these short wavelengths. Therefore one must be very cautious interpreting the apparent optical density of seawater filtrates relative to purified water for wavelengths less than 320nm. We recommend that more careful research should be carried out on the methods for soluble absorption, which appears to have a potentially dominating influence on the overestimates of $\bar{\mu}_d(\lambda)$ less than 400 nm. In particular, the influence of scattering by small particles (organic or mineral) and the role of salt absorption must be more carefully assessed.

REFERENCES

Aas, E., 2000: Spectral slope of yellow substance: problems caused by small particles. Proceedings of Ocean Optics XV, Monaco, 16-20 October, 2000.

Allali, K., A. Bricaud, M. Babin, A. Morel, and P. Chang, 1995: A new method for measuring spectral absorption coefficients of marine particulates. *Limnology and Oceanography.* **40,** 1,526-1,523

Allali, K., A. Bricaud, and H. Claustre, 1997: Spatial variations in the chlorophyll-specific absorption coefficients of phytoplankton and photosynthetically active pigments in the Equatorial Pacific. *Journal of Geophysical Research.* **102,** 12,413-12,423

Blough, N.V., O.C. Zafiriou, and J. Bonilla, 1993: Optical absorption spectra of waters from the Orinoco River outflow: terrestrial input of colored organic matter to the Caribbean. *Journal of Geophysical Research.* **98,** 2,271-2,278

Bricaud, A., A. Morel, and L. Prieur, 1981: Absorption by dissolved organic matter of the sea (yellow substance) in the UV and visible domains. *Limnology and Oceanography.* **26,** 43-53

Bricaud, A., and D. Stramski, 1990: Spectral absorption coefficients of living phytoplankton and non-algal biogenous matter: A comparison between the Peru upwelling area and the Sargasso Sea. *Limnology and Oceanography.* **35,** 562-582

Butler, W.L., 1962: Absorption of light by turbid materials. *Journal of the Optical Society of America.* **52,** 292-299

Carder, K.L., S.K. Hawes, K.S. Baker, R.C. Smith, and R.G. Steward, 1989: Remote sensing algorithms for discriminating marine humus from chlorophyll. *Limnology and Oceanography.* **30**(2), 286-298

Carder, K.L., R.G. Steward, G.R. Harvey, and P.B. Ortner, 1989: Marine humic and fulvic acids: Their effects on remote sensing of ocean chlorophyll. *Limnology and Oceanography.* **34,** 68-81

Chavez, F.P., K.R. Buck, R.R. Bidigare, D.M. Karl, D. Hebel, M. Latasa, L. Campbell, and J. Newton, 1995: On the chlorophyll *a* retention properties of glass-fiber GF/F filters. *Limnology and Oceanography.* **40(2),** 428-433

Cleveland, J.S., and A.D. Weidemann, 1993: Quantifying absorption by aquatic particles: A multiple scattering correction for glass-fiber filters. *Limnology and Oceanography.* **38,** 1321-1327

D'Sa, E.J., R.G. Steward, A. Vodacek, N.V. Blough, and D. Phinney, 1999: Determining optical absorption of colored dissolved organic matter in seawater with a liquid capillary waveguide. *Limnology and Oceanography.* **44,** 1,142-1,148

Duntley, S.Q., 1942: The optical properties of diffusing materials. *Journal of the Optical Society of America.* **32,** 61-70

Ferrari, G.M., and S. Tassan, 1996: Use of the 0.22 μm Millipore membrane for light-transmission measurements of aquatic particles. *Journal of Plankton Research.* **18,** 1,261-1,267

Ferrari, G.M, 1999: A method for removal of light absorption by phytoplankton pigments using chemical oxidation. *Journal of Phycology.* **35,** 1,090-1,098

Fry, E.S., 2000: Visible and near-ultraviolet absorption spectrum of liquid water: comments. *Applied Optics.* **39,** 2,743-2,744

Hewes, C.D., and O. Holm-Hansen, 1983: A method for recovering nanoplankton from filters for identification with the microscope: The filter-transfer-freeze (FTF) technique. *Limnology and Oceanography.* **28,** 389-394

Hoge, F.E., A. Vodacek, and N.V. Blough, 1993: Inherent optical properties of the ocean: retrieval of the absorption coefficient of chromophoric dissolved organic matter from fluorescence measurements. *Limnology and Oceanography.* **38,** 1394-1402

JGOFS, 1991: JGOFS Core Measurements Protocol. *JGOFS Report #6, Scientific Committee on Oceanic Research.* 40

Kahru, M., and B.G. Mitchell, 1998: Spectral reflectance and absorption of a massive red tide off Southern California. *Journal of Geophysical Research.* **103,** 21,601-21,609

Kalle, K., 1938: Zum problem der meerwasserfarbe. *Ann.Hydr.u.martim.Meterol.* **66,** 1.S.55-

Kiefer, D.A., R.J. Olson, and W.H. Wilson, 1979: Reflectance spectroscopy of marine phytoplankton. Part 1. Optical properties as related to age and growth rate. *Limnology and Oceanography.* **24,** 664-672

Kiefer, D.A., and J.B. SooHoo, 1982: Spectral absorption by marine particles of coastal waters of Baja California. *Limnology and Oceanography.* **27,** 492-499

Kishino, M., N. Okami, M. Takahashi, and S. Ichimura, 1986: Light utilization efficiency and quantum yield of phytoplankton in a thermally stratified sea. *Limnology and Oceanography.* **31,** 557-566

Kishino, M., N. Takahashi, N. Okami, and S. Ichimura, 1985: Estimation of the spectral absorption coefficients of phytoplankton in the sea. *Bulletin of Marine Science.* **37,** 634-642

Kou, L., D. Labrie and P. Chylek, 1993: Refractive indices of water and ice in the 0.65 to 2.5 μm spectral range, *Appl. Opt.*, **32:** 3531-3540.

Lenoble, J., 1956: L'absorption du rayonment ultraviolet par les ions presents dans la Mer. *Revue d'Optique.* **35** (10), 526-531

Mitchell, B.G. and D. A. Kiefer, 1988a: Chlorophyll *a* specific absorption and fluorescence excitation spectra for light-limited phytoplankton. *Deep-Sea Research I.* **35,** 639-663

Mitchell, B.G. and D. A. Kiefer, 1988b: Variability in pigment specific particulate fluorescence and absorption spectra in the northeastern Pacific Ocean. *Deep-Sea Research I.* **35,** 665-689

Mitchell, B.G., A. Bricaud, and others, 2000: Determination of spectral absorption coefficients of particles, dissolved material and phytoplankton for discrete water samples, In: Fargion, G.S. and J.L. Mueller, [Eds.] *Ocean Optics Protocols for Satellite Ocean Color Sensor Validation, Revision 2.* NASA/TM-2000-209966, NASA Goddard Space Flight Center, Greenbelt, MD. Chapter 12, pp125-153.

Mitchell, B.G. 1990: Algorithms for determining the absorption coefficient of aquatic particulates using the quantitative filter technique (QFT).*Ocean Optics X.* 137-148

Mitchell, B.G., M. Kahru, and P.J. Flatau, 1998: Estimation of spectral values for the mean cosine of the upper ocean. SPIE, Ocean Optics XIV. **CD-ROM**.

Mitchell, B.G., and D.A. Kiefer 1984: Determination of absorption and fluorescence excitation spectra for phytoplankton. *Marine phytoplankton and productivity.* **8,** 157-169

Moore, L.R., R. Goericke, and S.W. Chisholm, 1995: Comparative physiology of *Synechococcus* and *Prochlorococcus*: influence of light and temperature on growth, pigments, fluorescence and absorptive properties. *Marine Ecology Progress Series.* **116,** 259-275

Nelson, N.B., D.A. Siegel, and A.F. Michaels, 1998: Seasonal dynamics of colored dissolved material in the Sargasso Sea. *Deep-Sea Research.* **45,** 931-957

Pegau, W.S., and J.R.V. Zaneveld, 1993: Temperature-dependent absorption of water in the red and near infrared portions of the spectrum. *Limnology and Oceanography.* **38,** 188-192

Pope, R.M., and E.S. Fry, 1997: Absorption Spectrum (380-700 nm) of Pure Water: II. Integrating Cavity Measurements. *Applied Optics.* **36,** 8,710-8,723

Preisendorfer, R.W., 1976: Hydrologic optics 1. Introduction 2. Foundations 3. Solutions 4. Imbeddings 5. Properties 6. Surfaces 1450

Quickenden, T. I. and J. A. Irvin, 1980: The ultraviolet absorption spectrum of liquid water. *Journal of Chemical Physics*, **72**, 4,416-4,428

Reynolds, R. A., D. Stramski, and B. G. Mitchell, 2001: A chlorophyll-dependent semianalytical reflectance model derived from field measurements of absorption and backscattering coefficients within the Southern Ocean. *Journal of Geophysical Research,* **106(C4)**, 7,125-7,138.

Roesler, C.S., 1998: Theoretical and experimental approaches to improve the accuracy of particulate absorption coefficients derived from the quantitative filter technique. *Limnology and Oceanography.* **43,** 1,649-1,660

Shibata, K., 1958: Spectrophotometry of intact biological materials. Absolute and relative measurments of their transmission, reflection and absorption spectra. *Journal of Biochemistry.* **45,** 599-623

Shifrin, K.S., 1988*: Physical Optics of Ocean Water*. New York, American Institute of Physics, 285

Sogandares, F.M. and E. S. Fry. 1997: Absorption spectrum (340-640 nm) of pure water. I. Photothermal measurements. *Appl. Opt*. **36**: 8699-8709.

Sosik, H.M., 1999: Storage of marine particulate samples for light-absorption measurements. *Limnology and Oceanography.* **44,** 1,139-1,141

Sosik, H.M., and B. G. Mitchell, 1991: Absorption, fluorescence and quantum yield for growth in nitrogen limited *Dunaliella tertiolecta*. *Limnology and Oceanography.* **36,** 910-921

Sosik, H.M. and B. G. Mitchell, 1995: Light absorption by phytoplankton, photosynthetic pigments, and detritus in the California Current System. *Deep-Sea Research I.* **42,** 1,717-1,748

Stramska, M., D. Stramski, B. G. Mitchell and C. D. Mobley, 2000: Estimation of the absorption and backscattering coefficients from in-water radiometric measurements. *Limnology and Oceanography*, **45(3**): 628-641.

Stramski, D., 1990: Artifacts in measuring absorption spectra of phytoplankton collected on a filter. *Limnology and Oceanography.* **35,** 1,804-1,809

Tassan, S. and G.M. Ferrari, 1995a: An alternative approach to absorption measurements of aquatic particles retained on filters. *Limnology and Oceanography.* **40,** 1,358-1,368

Tassan, S., 1995b: Proposal for the measurement of backward and total scattering by mineral particles suspended in water. *Applied Optics.* **34,** 8,345-8,353

Tassan, S., 1998: Measurement of the light absorption by aquatic particulates retained on filters: determination of the optical pathlength amplification by the "Transmittance-Reflectance" method. *Journal of Plankton Research.* **20,** 1,699-1,709

Tassan, S., G.M. Ferrari, A. Bricaud, and M. Babin, 2000: Variability of the amplification factor of light absorption by filter-retained aquatic particles in the coastal environment. *Journal of Plankton Research.* **22,** 659-668

Vodacek, A., N.V. Blough, M.D. DeGrandpre, E.T. Peltzer, and R.K. Nelson, 1996: Seasonal variation of CDOM and DOC in the Middle Atlantic Bight: Terrestrial inputs and photooxidation. *Limnology and Oceanography.* **42,** 674-686

Waters, K. J., R. C. Smith and M. R. Lewis, 1990: Avoiding ship-induced light-field perturbation in the determination of oceanic optical properties. *Oceanography*. November: 18-21

Yentsch, C.S., 1957: A non-extractive method for the quantitative estimation of chlorophyll in algal cultures. *Nature.* **179,** 1302-1304

Yentsch, C.S., 1962: Measurement of visible light absorption by particulate matter in the ocean. *Limnology and Oceanography,* **7,** 207-217

Table 4. 1. Published coefficients for determining pathlength amplification effects. The suspension optical density, OD_{sp}, computed for a GF/F filter with OD_{fp} = 0.2 is provided for comparison.

Quadratic Functions	Particle Type	C_0	C_1	C_2	OD_{sp} (0.2)
Mitchell (1990)	Mixed Cultures	--	0.392	0.655	0.105
Cleveland & Weidemann (1993)	Mixed Cultures	--	0.378	0.523	0.097
Moore *et al*. (1995)	Prochlorococcus marinus	--	0.291	0.051	0.060
Moore *et al*. (1995)	Thalassiosira weissflogii	--	0.299	0.746	0.090
Moore *et al*. (1995)	Synechococcus WH8103	--	0.304	0.450	0.080
Tassan & Ferrari (1995)	Scenedesmus obliqus	--	0.406	0.519	0.102
Nelson *et al*. (1998)	Dunaliella tertiolecta	--	0.437	0.022	0.088
Nelson *et al*. (1998)	Phaeodactylum tricornutum	--	0.294	0.587	0.082
Nelson *et al*. (1998)	Synechococcus WH7803	--	0.277	0.000	0.055
Power Functions					
Mitchell and Kiefer (1988a)	Dunaliella tertiolecta	1.3	0.540	-0.467	0.082
Bricaud and Stramski (1990)	Field samples; D. tertiolecta Cultures of Mitchell & Kiefer (1988a)	0.0	1.630	-0.220	0.086
Kahru and Mitchell (1998)	Mitchell (1990) data	0.0	1.220	-0.254	0.109
Constant					
Roesler (1998)	Assume β = 2.0	--	--	--	0.100

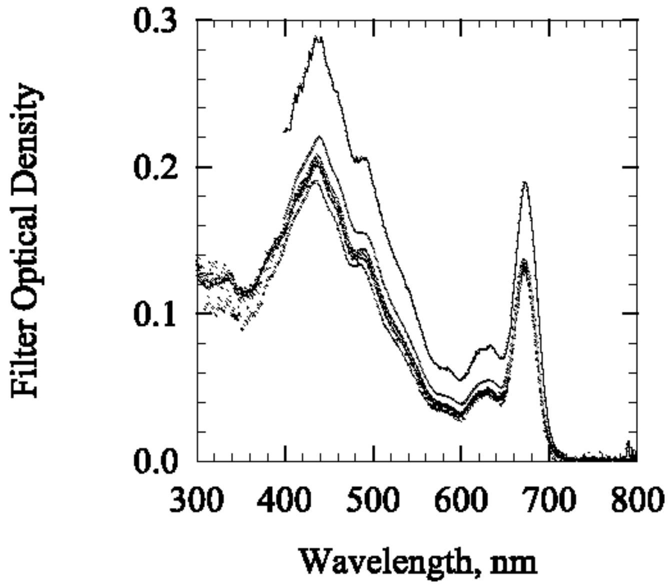

Figure 4.1: Optical density for various spectrophotometers for a diatom culture filtered onto GF/F filters. The average from 790-800 nm was used for a null value and the same volume was used for all samples. The data from the Hewlett Packard diode array system is higher than the other spectrophotometers as discussed in detail in Mitchell *et al*. (2000). Below 400 nm, the Hewlett Packard unit was too noisy for the glass fiber filter method.

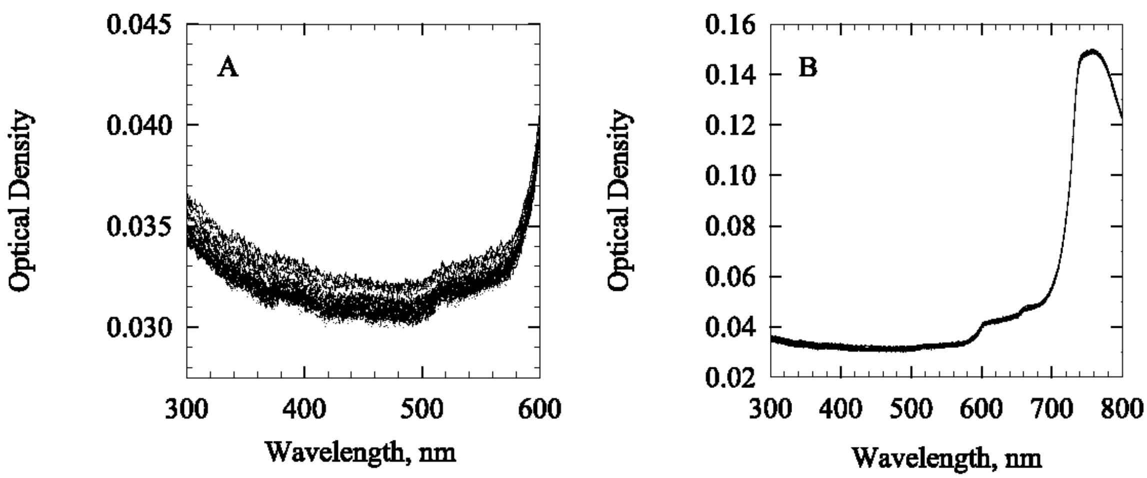

Figure 4.2: Optical density for fresh Millipore Alpha-Q water in the sample cuvette referenced to air in a dual beam spectrophotometer, $OD_{\mathrm{rwa}}(\lambda)$, determined during the ACE-Asia experiment. **A)**. $OD_{\mathrm{rwa}}(\lambda)$ plotted for the spectral range 300 nm to 600 nm. **B)**. Plotted for the spectral range 300 nm to 800 nm.

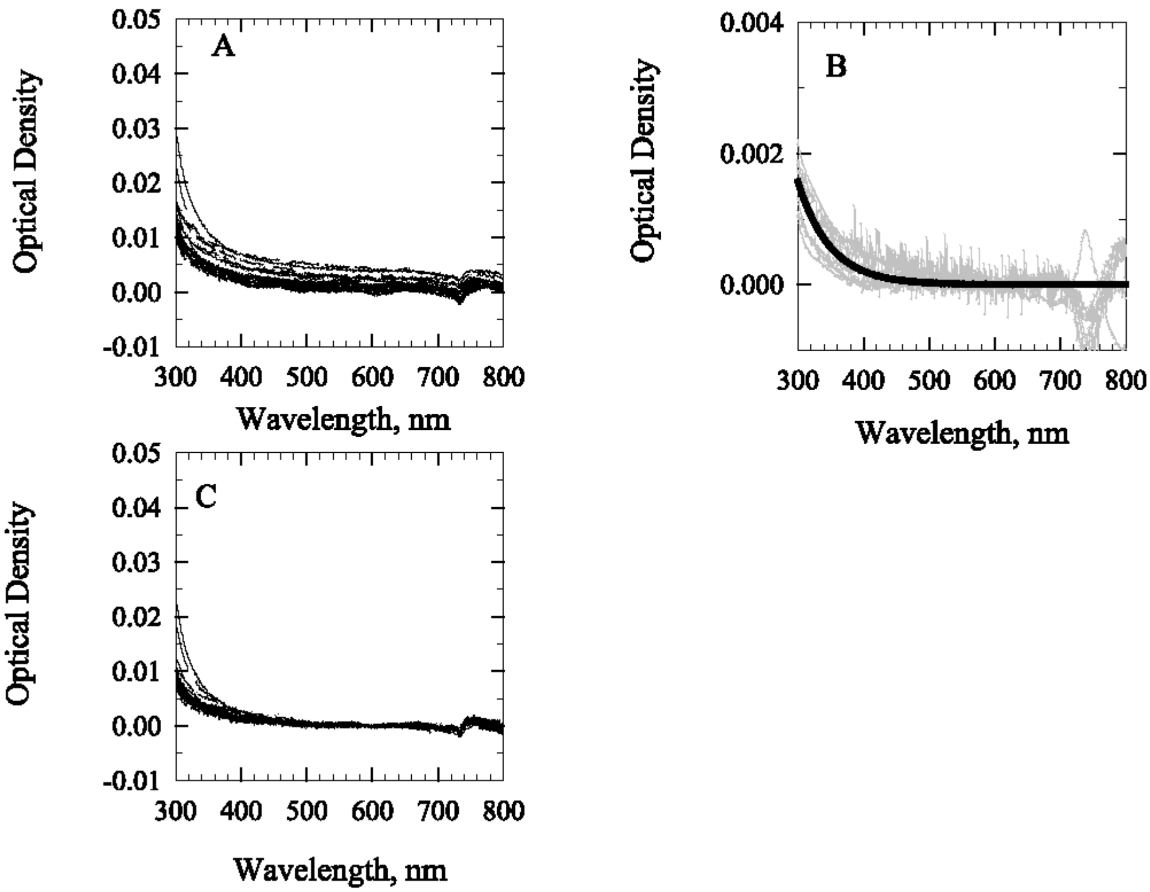

Figure 4.3: Typical results for soluble absorption determined during the ACE-Asia cruise (March – April 2001) in the western Pacific according to the protocols recommended here. **A)**. Raw optical density, $OD_{s}(\lambda)$, for samples relative to Millipore Alpha-Q water. **B)**. Blank optical density spectra, $OD_{bs}(\lambda)$ (after null offset, gray) compared to a global value (solid line). The global blank is determined by fitting an exponential function to the mean blank for more than 15 cruises from 1998-2001 where the mean for each cruise was determined as the mean of all individual blanks for each cruise. A fitted curve to a cruise or global mean for $OD_{bs}(\lambda)$ is recommended for correction of the soluble sample blank because individual spectra (gray) have significant instrument noise. Note the scale for 3B is approximately 10x smaller than the scale in 3A. **C)**. Estimates of sample optical density spectra after subtraction of the null value (average of raw values 590-600nm) and after subtraction of a global blank according to Equation (4.3). Temperature effects are evident 650-800 nm in the individual spectra.

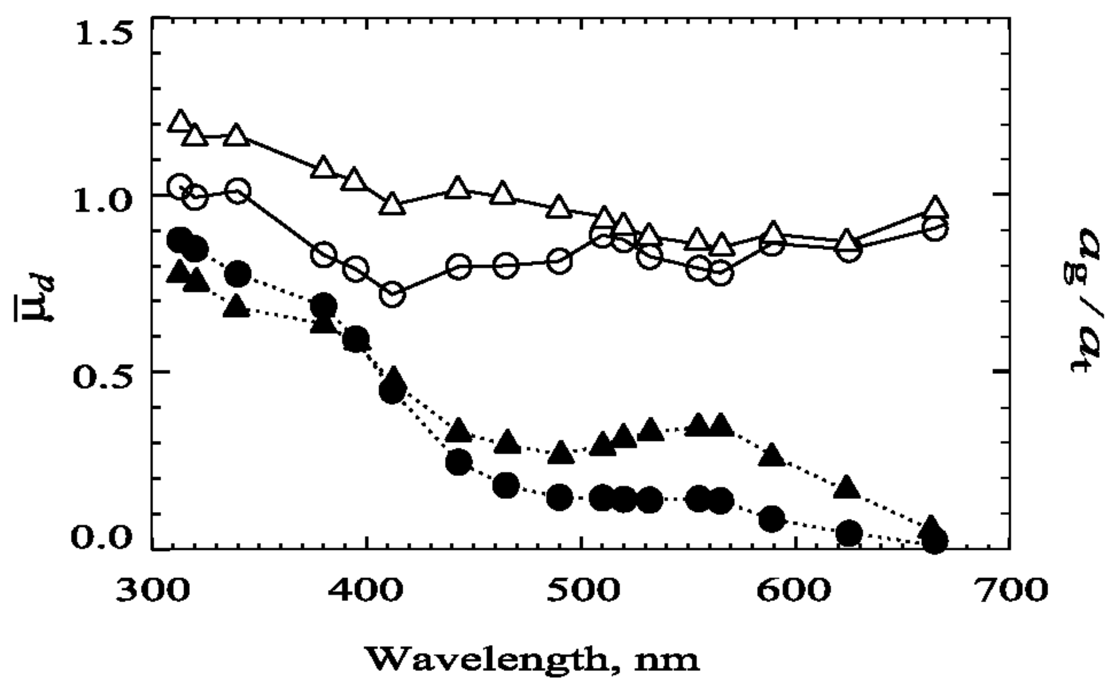

Figure 4.4: Median values for $\bar{\mu}_d(\lambda)$, the mean cosine for downwelling irradiance (open symbols, see text for definition) determined for the upper mixed layer. Values are plotted at each wavelength of the PRR 800 reflectance radiometer deployed during 2001 cruises to the Southern Ocean (AMLR) and the Western Pacific (ACE-Asia). The ratio of $a_g(\lambda)/a_t(\lambda)$ for the same data set are shown in solid symbols and plotted to the same scale. For both sets of spectra, AMLR data are circles and ACE-Asia data are triangles.

Chapter 5

Volume Scattering Function and Backscattering Coefficients: Instruments, Characterization, Field Measurements and Data Analysis Protocols

J. Ronald V. Zaneveld[1], Scott Pegau[1] and James L. Mueller[2]

[1]*College of Oceanographic and Atmospheric Sciences, Oregon State University, Corvallis*

[2]*Center for Hydro-Optics and Remote Sensing, San Diego State University, California*

5.1 INTRODUCTION

The volume scattering function (VSF) $\beta(\lambda,\psi)$ [$\mathrm{sr}^{-1}\mathrm{m}^{-1}$] and the volume absorption coefficient $a(\lambda)$ [m^{-1}] provide the most fundamental description of a medium's inherent optical properties (IOP), as all other IOP can be derived from them. In particular, the volume scattering coefficient $b(\lambda)$ and volume backscattering coefficient $b_{\mathrm{b}}(\lambda)$ may be derived by integrating $\beta(\lambda,\psi)$ over the unit sphere and backward hemisphere, respectively. In terms of determining the "complete" IOP from *in situ* measurements, a useful combination is $a(\lambda)$, the beam attenuation coefficient $c(\lambda)$, and the volume scattering phase function $\tilde{\beta}(\lambda,\psi)=\dfrac{\beta(\lambda,\psi)}{c(\lambda)-a(\lambda)}$. The reader is referred to Vol. I, Chapter 2 (Sect. 2.4) and to Chapter 1 of the present volume for further details regarding these definitions and relationships.

Knowledge of the VSF is a critical prerequisite to accurate radiative transfer modeling of remote sensing reflectance and water-leaving radiance. In Vol. III, Chapter 4 (and references cited there), it is shown that irradiance reflectance $R(\lambda)$ is approximately proportional to the ratio of the backscattering to absorption coefficients, and that upwelled radiance just beneath the sea surface is proportional to $R(\lambda)$, so that

$$L_{\mathrm{u}}\left(0^{-},\lambda,\theta,\phi\right)=E_{\mathrm{d}}\left(0^{-},\lambda\right)\frac{f}{Q}\frac{b_{\mathrm{b}}(\lambda)}{a(\lambda)}.$$

This relationship is completely general and exact, but it does not express a linear proportionality to the IOP ratio, because the factors *f* and *Q* are not simply coefficients. .They are functions, $f\left[\lambda,\left(\theta_{\mathrm{o}},\tau_{a},W\right),a(\lambda),\beta(\lambda,\Psi)\right]$ and $Q\left[\left(\lambda,\theta',\phi\right),\left(\theta_{\mathrm{o}},\tau_{\mathrm{a}},W\right),a(\lambda),\beta(\lambda,\Psi)\right]$, that account for the bidirectional nature of the ocean's reflectance; this bidirectionality may be traced directly to the shape of the VSF. Bidirectionality of remote sensing reflectance, as it arises from the VSF, is shown more explicitly in the formulation by Zaneveld (1982).

Equation (1.18) could be used directly as a basis for measuring the VSF if an instrument's source and detector were well collimated, and there were no flux losses, or FOV distortions, associated with an its optical elements. Some general angle scattering meters (Petzold 1972; Lee *et al*. 2003) are designed with a well-enough collimated beam and very small detector acceptance angle, so that equation (1.18) may be applied directly. In terms of equation (1.19), this is equivalent to assuming that the scattering response weighting function $W(\lambda,\psi,\varphi;c)$ is narrow enough to set it to unity. The General Angle Scattering Meter (GASM), built at the Scripps Institution of Oceanography's Visibility Laboratory (Petzold 1972), consists of a lamp focused into a cylindrical beam, and a narrow field of view detector mounted to swing in an arc to view the beam at many off-axis scattering angles between approximately 10^{o} and 170^{o}. Petzold (1972) reported VSF's measured for selected natural waters using the

(GASM). This reference has been widely used to describe shapes of $\tilde{\beta}(\lambda,\psi)$ in natural waters. Mobley *et al*. (2001) compared measured and modeled nadir-viewing remote sensing reflectances, using measured $c(\lambda)$ and $a(\lambda)$ with $\tilde{\beta}(\lambda,\psi)$ of different assumed shapes, including that of Petzold (1972), and the VSF measured using a general angle scattering meter of a new design (Lee *et al*., 2003); best agreement was achieved using the measured VSF. Their results showed that large systematic offsets can result if one arbitrarily assumes a scattering phase function having an incorrect backward scattering fraction. The results of Mobley *et al*. (2001) also indicated that nadir-viewing radiance reflectance is less sensitive to the detailed shape of the forward scattering lobe of $\tilde{\beta}(\lambda,\psi)$. Details of scattering at intermediate forward angles might, however, be more important for off-nadir viewing geometry (Vol. III, Ch. 4).

At present, commercially available VSF sensors[12] are designed with detector beam-spread and detector acceptance angles ranging from 10^o to 20^o Full-Width Half-Maximum (FWHM). These instruments measure the VSF, weighted as in (1.19), at one (or a few) scattering angle(s) and are typically used to determine the backscattering coefficient using the methods described below in Sect. 5.4. Although these methods depend on assumptions concerning $\tilde{\beta}(\lambda,\psi)$, determinations of $b_b(\lambda)$ from VSF profile measurements with these instruments, when combined with absorption and beam attenuation coefficients, radiometric profiles and pigment concentration measurements, have provide useful information about relationships between IOP, AOP and optically important material constituents of the water column (*e.g.* Stramska *et al*. 2000).

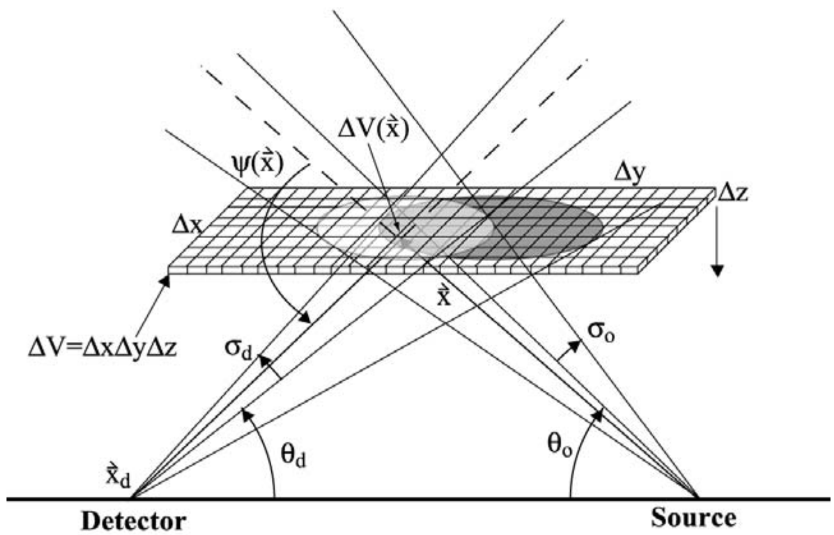

Fig. 5.1: Schematic illustration of a VSF sensor geometry used for numerical integration over the volume intersected by a source beam and detector FOV of incremental elements of the scattered radiant flux received by the detector.

[12] Certain commercial equipment, instruments, or materials are identified in this chapter to foster understanding. Such identification does not imply recommendation, or endorsement, by the National Aeronautics and Space Administration, nor does it imply that the materials or equipment identified are necessarily the best available for the purpose.

An example of a generalized source and detector arrangement to measure the VSF $\beta(\lambda,\psi)$ at a scattering angle $\psi > \frac{\pi}{2}$ is illustrated schematically in Fig. 5.1. To determine a calibration factor relating the detector response to flux scattered from the source beam into the field of view (FOV) of the detector, we must determine the sensor's response weighting function $W(\lambda,\psi,\varphi;c)$ [equation (1.19)], either explicitly, or implicitly. The explicit approach to this problem is to determine $W(\lambda,\psi,\varphi;c)$ from geometry and first principles, and then calibrate the instrument's response signals in a medium having a known VSF $\beta(\lambda,\psi)$; the detailed steps in this approach are described below in Sect. 5.2. The implicit approach (Maffione and Dana 1997) is to insert a plaque of known near-Lambertian reflectance in the position of the horizontal *xy*-plane, at distance *z* from the source-detector axis, illustrated Fig. 5.1, and record the instrument's responses as the plaque is moved vertically in small increments through the volume defined by the intersection of the source beam and detector FOV; this approach is briefly outlined in Sect. 5.3 below, but the reader is referred to Maffione and Dana (1997) for the detailed derivation and method of implementation.

For brevity, we will henceforth omit the explicit wavelength dependence of variables.

5.2 CHARACTERIZATION AND CALIBRATION OF A VSF SENSOR FROM ITS GEOMETRY AND RESPONSE TO SCATTERING BY POLYSTYRENE BEADS

Geometric Determination of W(ψ)

Figure 5.1 illustrates a source located at the origin $\bar{\mathbf{x}}_o = (0,0,0)$ and a detector located on the y-axis at position $\bar{\mathbf{x}}_d = (0,\mathrm{y}_d,0)$. As illustrated, the source beam and detector FOV are assumed to be cones with divergence angles σ_o and σ_d, respectively. At a distance z above the xy plane, a horizontal plane is shown passing through the the source beam (a nearly transparent, light-shaded ellipse) and detector FOV (a dark shaded ellipse); the intersection of the source beam and detector FOV is the intermediate gray-shaded area. The plane is divided into elemental volume elements $\Delta V = \Delta x \Delta y \Delta z$, and a particular volume element is denoted $\Delta V(\bar{\mathbf{x}})$.

The radiant flux Φ_o emitted by the source is assumed to be evenly distributed over the solid angle Ω_o, so by definition, the source radiant intensity is, by definition $I_o = \left(\frac{\Phi_o}{\Omega_o}\right)$. The flux transmitted in direction $\hat{\boldsymbol{\varepsilon}}(\bar{\mathbf{x}}) = \frac{1}{|\bar{\mathbf{x}}|}\bar{\mathbf{x}}$, where the vector length $|\bar{\mathbf{x}}| = \sqrt{\bar{\mathbf{x}}\bullet\bar{\mathbf{x}}}$, from the source to the elemental volume $\Delta V(\bar{\mathbf{x}})$ is

$$\Delta\Phi_o\left[\Delta V(\bar{\mathbf{x}});c\right] = I_o \Delta\Omega_o\left[\Delta V(\bar{\mathbf{x}})\right]\exp\left(-c|\bar{\mathbf{x}}|\right) = \Phi_o \frac{\Delta\Omega_o\left[\Delta V(\bar{\mathbf{x}})\right]}{\Omega_o}\exp\left(-c|\bar{\mathbf{x}}|\right), \tag{5.1}$$

where $\Delta\Omega_o\left[\Delta V(\bar{x})\right] = \frac{\Delta x \Delta y \left|\hat{\boldsymbol{\varepsilon}}(\bar{\mathbf{x}})\bullet\hat{\mathbf{n}}\right|}{\bar{\mathbf{x}}\bullet\bar{\mathbf{x}}}$ is the solid angle subtended at the source by the horizontal elemental area $\Delta x \Delta y$ at position $\bar{\mathbf{x}}$, and $\hat{\mathbf{n}}$ is the unit normal to the *xy*-plane (Fig. 5.1). Thus, the irradiance incident on $\Delta V(\bar{\mathbf{x}})$ is

$$E_o(\bar{\mathbf{x}};c) = \frac{\Phi_o}{\Delta x \Delta y}\left|\hat{\boldsymbol{\varepsilon}}(\bar{\mathbf{x}})\bullet\hat{\mathbf{n}}\right|\frac{\Delta\Omega_o\left[\Delta V(\bar{\mathbf{x}})\right]}{\Omega_o}\exp\left(-c|\bar{\mathbf{x}}|\right). \tag{5.2}$$

The radiant flux intensity scattered from $\Delta V(\bar{\mathbf{x}})$ in direction $\hat{\boldsymbol{\varepsilon}}(\bar{\mathbf{x}}_d - \bar{\mathbf{x}})$ toward the detector at $\bar{\mathbf{x}}_d$ is

$$I_S\left[\psi(\bar{\mathbf{x}})\right] = \beta\left[\psi(\bar{\mathbf{x}})\right]E_o(\bar{\mathbf{x}})\Delta V, \tag{5.3}$$

where the scattering angle $\psi(\bar{\mathbf{x}})$ for the incremental volume element is

$$\cos\left[\psi(\bar{\mathbf{x}})\right] = \hat{\boldsymbol{\varepsilon}}(\bar{\mathbf{x}}) \bullet \hat{\boldsymbol{\varepsilon}}(\bar{\mathbf{x}}_{\mathrm{d}} - \bar{\mathbf{x}}). \tag{5.4}$$

Combining (5.2) and (5.3), and multiplying by the flux transmittance over the pathlength $\left|(\bar{\mathbf{x}}_{\mathrm{d}} - \bar{\mathbf{x}})\right|$ leads to

$$\frac{\Delta\Phi_{\mathrm{d}}\left[\Delta V(\bar{x});c\right]}{\Phi_{\mathrm{o}}} = \beta\left[\psi(\bar{\mathbf{x}})\right]\frac{\Delta V}{\Delta x\Delta y}\left|\hat{\boldsymbol{\varepsilon}}(\bar{\mathbf{x}})\bullet\hat{\mathbf{n}}\right|\frac{\Delta\Omega_{\mathrm{o}}\left[\Delta V(\bar{\mathbf{x}})\right]\Delta\Omega_{\mathrm{d}}\left[\Delta V(\bar{\mathbf{x}})\right]}{\Omega_{\mathrm{o}}}\exp\left[-c\left(\left|\bar{\mathbf{x}}\right| + \left|(\bar{\mathbf{x}}_{\mathrm{d}} - \bar{\mathbf{x}})\right|\right)\right], \tag{5.5}$$

where the solid angle subtended by the area ΔxΔy at the detector is $\Delta\Omega_{\mathrm{d}}\left[\Delta V(\bar{x})\right] = \dfrac{\Delta x\Delta y\left|\hat{\boldsymbol{\varepsilon}}(\bar{\mathbf{x}}_{\mathrm{d}} - \bar{\mathbf{x}})\bullet\hat{\mathbf{n}}\right|}{(\bar{\mathbf{x}}_{\mathrm{d}} - \bar{\mathbf{x}})\bullet(\bar{\mathbf{x}}_{\mathrm{d}} - \bar{\mathbf{x}})}$. With reference to (1.18) through (1.20), we may now write

$$\frac{\Delta\Phi_{\mathrm{d}}\left[\Delta V(\bar{x});c\right]}{\Phi_{\mathrm{o}}} = \beta\left[\psi(\bar{\mathbf{x}})\right]W(\bar{\mathbf{x}};c), \tag{5.6}$$

and by subsitution we obtain the incremental weighting function for each volume element $\Delta V(\bar{\mathbf{x}})$ as

$$W(\bar{\mathbf{x}};c) = \frac{\Delta V}{\Delta x\Delta y}\left|\hat{\boldsymbol{\varepsilon}}(\bar{\mathbf{x}})\bullet\hat{\mathbf{n}}\right|\frac{\Delta\Omega_{\mathrm{o}}\left[\Delta V(\bar{\mathbf{x}})\right]\Delta\Omega_{\mathrm{d}}\left[\Delta V(\bar{\mathbf{x}})\right]}{\Omega_{\mathrm{o}}}\exp\left[-c\left(\left|\bar{\mathbf{x}}\right| + \left|(\bar{\mathbf{x}}_{\mathrm{d}} - \bar{\mathbf{x}})\right|\right)\right]. \tag{5.7}$$

To obtain the desired weighting function $W(\psi;c)$ for each scattering angle ψ it is necessary to sum the weights for all volume elements at which the scattering angle falls within a discrete angular interval of ψ , *i.e.*

$$W(\psi;c) = \sum_x\sum_y\sum_z W(\bar{\mathbf{x}};c)\,\delta\left[\psi,\psi(\bar{\mathbf{x}}),\Delta\psi\right] \tag{5.8}$$

where

$$\delta\left[\psi,\psi(\bar{\mathbf{x}}),\Delta\psi\right] = \begin{cases} 1; & \psi - \dfrac{\Delta\psi}{2} < \psi(\bar{\mathbf{x}}) \le \psi + \dfrac{\Delta\psi}{2} \\ 0; & \text{Otherwise} \end{cases}. \tag{5.9}$$

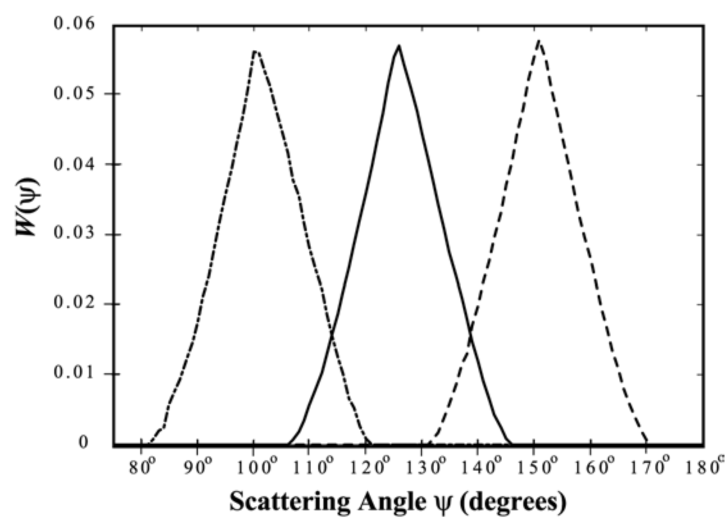

Figure 5.2: Examples of weighting functions $W(\psi)$ calculated for VSF measurements by source-detector pairs aligned at nominal scattering angles $(\bar{\psi}_1,\bar{\psi}_2,\bar{\psi}_3) = (100°,125°,150°)$ (Figs. 5.1 and 1.4).

Once the weighting functions are computed for all scattering angles ψ falling within the beam and detector FOV intersection volume, they are normalized such that

$$\sum_{\psi} W(\psi;c) = 1\,. \tag{5.10}$$

As an example, the weighting functions calculated for the WET Labs VSF-3 are illustrated in Fig. 5.2 for nominal scattering angles $(\overline{\psi}_1, \overline{\psi}_2, \overline{\psi}_3) = (100°, 125°, 150°)$. These particular, triangular source functions were derived assuming that both the source beam and detector FOV are conical about the respective centerlines illustrated in Fig. 5.1.

Generalized Weighting Functions for Arbitrary Source Beam and Detector FOV Geometries

In the above development of equations (5.1) through (5.7), it was assumed that the flux emitted by the source was uniformly distributed over a conical beam with its axis directed in direction

$$\hat{\boldsymbol{\varepsilon}}_{\mathrm{o}} = \begin{bmatrix} \sin\left(\dfrac{\pi}{2} + \theta_{\mathrm{o}}\right) \\ 0 \\ \cos\left(\dfrac{\pi}{2} + \theta_{\mathrm{o}}\right) \end{bmatrix},$$

and that the detector flux responsivity was also uniformly distributed over a conical FOV having its axis aligned in direction

$$\hat{\boldsymbol{\varepsilon}}_{\mathrm{d}} = \begin{bmatrix} -\sin\left(\dfrac{\pi}{2} + \theta_{\mathrm{d}}\right) \\ 0 \\ \cos\left(\dfrac{\pi}{2} + \theta_{\mathrm{d}}\right) \end{bmatrix}.$$

We may generalize the vector solid angle associated with the source beam as $\vec{\boldsymbol{\Omega}}_{\mathrm{o}}$, which represents the angular solid angle domain, measured relative to $\hat{\boldsymbol{\varepsilon}}_{\mathrm{o}}$, over which flux emitted by the source is non-zero. Similarly, $\vec{\boldsymbol{\Omega}}_{\mathrm{d}}$ is the solid angle domain relative to $\hat{\boldsymbol{\varepsilon}}_{\mathrm{d}}$ over which the detector's responsivity is non-zero. There are no restrictions on either the patterns of angular limits associated with $\vec{\boldsymbol{\Omega}}_{\mathrm{o}}$ and $\vec{\boldsymbol{\Omega}}_{\mathrm{d}}$, or on the relative distributions of flux within $\vec{\boldsymbol{\Omega}}_{\mathrm{o}}$, or of flux responsivity within $\vec{\boldsymbol{\Omega}}_{\mathrm{d}}$.

Real sources generally emit flux in a somewhat irregular beam pattern that typically peaks in the vicinity of $\hat{\boldsymbol{\varepsilon}}_{\mathrm{o}}$, may be relatively flat for much of its FWHM beam width, and then tends to fall sharply near the edges of the beam and gradually decay beyond the nominal FWHM limits. Detector angular responsivity FOV patterns generally exhibit similar geometric characteristics relative to $\hat{\boldsymbol{\varepsilon}}_{\mathrm{d}}$.

The flux variations within the source beam may be expressed as a normalized relative flux distribution function $h_{\mathrm{o}}\left[\hat{\boldsymbol{\varepsilon}} \in \vec{\boldsymbol{\Omega}}_{\mathrm{o}}\right]$ that takes non-zero values only in directions included in the solid angle beam pattern. Similarly, the angular response function of the the detector may be written $h_{\mathrm{d}}\left[\hat{\boldsymbol{\varepsilon}} \in \vec{\boldsymbol{\Omega}}_{\mathrm{d}}\right]$. To generalize the weighting functions to account for arbitrary source beam and detector FOV geometries, and relate the phase function to incremental detector responses $\Delta D_{\mathrm{d}}\left[\Delta V(\vec{\mathbf{x}});c\right]$:

1. Multiply the right-hand-sides of equations (5.1) and (5.2) by $h_{\mathrm{o}}\left[\hat{\boldsymbol{\varepsilon}}(\vec{\mathbf{x}}) \in \vec{\boldsymbol{\Omega}}_{\mathrm{o}}\right]$, and carry this factor through subsequent substitutions.

2. Substitute using the relationship $\Delta D_{\mathrm{d}}\left[\Delta V(\bar{\mathbf{x}});c\right] = h_{\mathrm{d}}\left[-\hat{\boldsymbol{\varepsilon}}(\bar{\mathbf{x}}_{\mathrm{d}}-\bar{\mathbf{x}}) \in \bar{\boldsymbol{\Omega}}_{\mathrm{d}}\right]\Delta\Phi_{\mathrm{d}}\left[\Delta V(\bar{\mathbf{x}});c\right]$ on the left-hand-side of (5.7) to relate $\beta\left[\psi(\bar{\mathbf{x}})\right]$ to the incremental detector response.

3. Absorb the source flux and detector responsivity distributions into the weighting function $W(\bar{\mathbf{x}};c)$ by multiplying the right-hand-side of (5.7) by the product $h_{\mathrm{o}}\left[\hat{\boldsymbol{\varepsilon}}(\bar{\mathbf{x}}) \in \bar{\boldsymbol{\Omega}}_{\mathrm{o}}\right]h_{\mathrm{d}}\left[-\hat{\boldsymbol{\varepsilon}}(\bar{\mathbf{x}}_{\mathrm{d}}-\bar{\mathbf{x}}) \in \bar{\boldsymbol{\Omega}}_{\mathrm{d}}\right]$.

The numerical implementation of the general form of (5.7) is straightforward. The more difficult aspect of obtaining generalized weighting functions is the experimental determination of the functions $h_{\mathrm{o}}\left[\hat{\boldsymbol{\varepsilon}} \in \bar{\boldsymbol{\Omega}}_{\mathrm{o}}\right]$ and $h_{\mathrm{d}}\left[\hat{\boldsymbol{\varepsilon}} \in \bar{\boldsymbol{\Omega}}_{\mathrm{d}}\right]$.

The detector FOV responsivity distribution function may be measured by mounting the detector in a rotating stage, with its entrance aperture centered on the intersection of the axis of rotation and the optical axis of a stable collimated source. The stage is rotated in small angular increments, and the detector response is recorded at each angle to measure the relative variations in response in one plane containing $\hat{\boldsymbol{\varepsilon}}_{\mathrm{d}}$. The instrument is then rotated in increments about $\hat{\boldsymbol{\varepsilon}}_{\mathrm{d}}$ and the process is repeated to map the distribution of responses in a sequence of planes adequate to resolve the full function $h_{\mathrm{d}}\left[\hat{\boldsymbol{\varepsilon}} \in \bar{\boldsymbol{\Omega}}_{\mathrm{d}}\right]$. This is essentially the same procedure used to characterize the angular FOV of field radiometers (Vol. II, Ch. 3).

The inverse of the above setup may be used to map the flux distribution of the source beam. The instrument is mounted with the source aligned with the optical and rotation axes, and a narrow FOV detector is substituted for the collimated source. The stage is rotated through a suitable angular range to map out flux variations in a plane through $\hat{\boldsymbol{\varepsilon}}_{\mathrm{o}}$, and the instrument is rotated about $\hat{\boldsymbol{\varepsilon}}_{\mathrm{o}}$ and the process repeated to measure flux distributions in a sequence of planes. If the temporal stability of flux output by the source is in question, a second detector may be mounted to monitor the source output from a fixed off-axis direction relative to $\hat{\boldsymbol{\varepsilon}}_{\mathrm{o}}$, *i.e.* by mounting it on an extension to the rotational stage.

Whether one must go to the trouble to determine the beam and FOV weighting functions more accurately than can be modeled from simple geometric elements of the optical design depends on the shape of the VSF in the region to be measured. The detailed behaviour of the outer edges of the two distribution functions are not important factors in determing the weighting functions for measurements of the VSF of pure water, or of a particulate VSF at scattering angles near, or greater than, 90^{o} (Figs. 1.2 and 1.3). Therefore, relatively simple approximations to $h_{\mathrm{o}}\left[\hat{\boldsymbol{\varepsilon}} \in \bar{\boldsymbol{\Omega}}_{\mathrm{o}}\right]$ and $h_{\mathrm{d}}\left[\hat{\boldsymbol{\varepsilon}} \in \bar{\boldsymbol{\Omega}}_{\mathrm{d}}\right]$ should be completely adequate for the commercial backscattering instruments mentioned above. Conversely, the angular breadth and details of the beam and FOV distribution functions both become increasingly more critical when one wishes to measure the VSF at decreasing angles in the forward direction.

Dependence of the Weighting Functions on the Beam Attenuation Coefficient c

The effect of the beam attenuation coefficient on the weighting function $W(\bar{\mathbf{x}};c)$ for each volume element is explicitly represented in (5.7) by the transmittance over the combined pathlength from the source to the volume element at $\bar{\mathbf{x}}$ and from there to the source location. The transmittance term is integrated into each angular weighting function $W(\psi;c)$ determined using (5.8). Strictly speaking, near-forward scattered light still enters $\Delta V(\bar{\mathbf{x}})$ and can be scattered to the detector (see also the discussion of transmissometer acceptance angles in Chapter 2), but we will neglect this complication in the present discussion. The ratios of integrated weighting functions $\frac{\int W(\psi;c)\sin\psi d\psi}{\int W(\psi;c=0)\sin\psi d\psi}$ are compared against increasing beam attenuation coefficient *c* for the three ECO-VSF weighting functions illustrated in Fig. 5.2. These functions are clearly log-linear, and should we choose to represent the weighting function exclusively using $W(\psi;c=0)$, it would be a simple matter to adjust the results for c dependence. This dependence may either be applied as a correction to the weighting function, or by a

transmittance function of the form $\overline{\beta}_{\mathrm{p}}(\lambda,\overline{\psi};c)=\overline{\beta}_{\mathrm{p}}(\lambda,\overline{\psi})\exp\left[cr_{\mathrm{eff}}(\overline{\psi})\right]$, where $\overline{\beta}_{\mathrm{p}}(\lambda,\overline{\psi})$ is the measured VSF using $W(\psi;c=0)$ (see below) and $r_{\mathrm{eff}}(\overline{\psi})$ is an effective net pathlength for the particular scattering angle measurement.

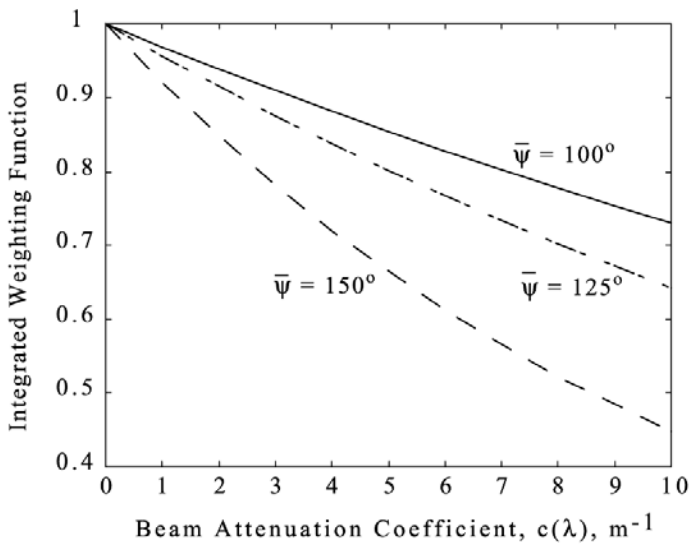

Fig. 5.3: Dependence of the integrated weighting functions $\int W(\psi;c)\sin\psi d\psi$ on the beam attenuation coefficient for the 3 ECO-VSF weighting functions of Fig. 5.2.

Calibration with Polystyrene Spheres

In this approach, a sample of polystyrene microsphere beads must be obtained and prepared for use in the calibration procedure. The following procedures are recommended:

1. Assume the bead diameters D_{p} in the sample are distributed as a Gaussian probability density function (pdf) $p(D_{\mathrm{p}})$ with the mean $\overline{D}_{\mathrm{p}}$ and standard deviation S_{D} provided by the manufacturer; normalize the pdf to unit area.
   a. It is good practice to occasionally verify the reported mean diameter and standard deviation using a Coulter Counter, or other particle size counting device, for randomly selected samples received from a manufacturer.
2. Calculate the refractive index of the polystyrene spheres relative to pure water

$$n_{\mathrm{p}}(\lambda)=\frac{n_{\mathrm{p}}^{\mathrm{air}}(\lambda)}{n_{\mathrm{w}}(\lambda)}, \tag{5.11}$$

where the particle refractive index relative to air is determined according to a relationship provided by the manufacturer, *e.g.* from Duke Scientific as

$$n_{\mathrm{p}}^{air}(\lambda)=1.5663+0.00785\lambda^{-2}+0.000334\lambda^{-4},\ \lambda \text{ in } \mu\text{m}, \tag{5.12}$$

and the refractive index of water relative to air is (Austin and Halikas 1976)

$$n_{\mathrm{w}}(\lambda)=1.325147+\frac{6.6096}{\lambda-137.1924},\ \lambda \text{ in nm}. \tag{5.13}$$

Note carefully the different wavelength units in the empirical equations (5.12) and (5.13).

3. Calculate the particle scattering phase function for each diameter D_p, in 500 equally spaced intervals spanning ± 3 standard deviations about the mean diameter (*i.e.* $\Delta D_p = \frac{6S_D}{500}$), using a Mie (1908) scattering model code (*e.g.* Bohren and Huffman 1983; other coding implementations are also available at various web sites). The Mie scattering intensity functions should be calculated at angle intervals $\Delta\psi$ matching those at which the weighting functions $W(\psi;c)$ were resolved [equations (5.8) and (5.9)]. It is important that the selected angle increment adequately resolves variations in $\tilde{\beta}_{ps}(\lambda,\psi;D_p)$ for the narrow size distributions typically used in this application; an interval $\Delta\psi \le 0.5°$ is recommended.

4. Determine the phase function for the sample polydispersion by numerical quadrature of the convolution integral

$$\tilde{\beta}_{ps}(\lambda,\psi) = \int \tilde{\beta}_{ps}(\lambda,\psi;D_p)p(D_p)dD_p = \sum_{n=-250}^{250} w_n \tilde{\beta}_{ps}(\lambda,\psi;\bar{D}_p + n\Delta D_p)\,p(\bar{D}_p + n\Delta D_p)\Delta D_p \qquad (5.14)$$

where w_n are the weighting coefficients of the selected numerical quadrature algorithm (*e.g.* the composite Simpson formula).

5. To obtain the weighted phase function to be measured by the sensor, divide both sides of (1.19) by $b(\lambda)$ and numerically approximate the integral equation as

$$\bar{\tilde{\beta}}_{ps}(\lambda,\bar{\psi}) = \sum_{n=-\frac{N_{\Delta\psi}}{2}}^{\frac{N_{\Delta\psi}}{2}} w_n \tilde{\beta}_{ps}(\lambda,\bar{\psi}+n\Delta\psi)W(\bar{\psi}+n\Delta\psi;c)\sin\psi\Delta\psi\,, \qquad (5.15)$$

where again w_n are the quadrature weighting coefficients.

6. Measure and record the instrument's dark offset response $V_{dark}(\bar{\psi})$ by pointing the source and detector at a black velvet cloth, at a distance of approximately 2 m in a completely dark room.

7. Prepare a volume of filtered optically pure water, using the procedures described in Chapter 3.

8. Using an ac-9, calibrate it using the freshly prepared pure water (Chapters 2 and 3).

9. Immerse the VSF sensor in the pure water volume and record its response $V_w(\bar{\psi}) - V_{dark}(\bar{\psi})$.

10. Add a sufficient amount of the polystyrene microsphere bead sample to increase the instrument's response to approximately the maximum level desired for the calibration run.

    a. Label this bead concentration as C0 and record the VSF sensor response $V_{C0}(\bar{\psi})$.

    b. Measure $a_{C0}(\lambda)$ and $c_{C0}(\lambda)$, relative to the pure water calibration offsets, using the ac-9 for bead concentration C0. Determine $b_{ps}^{C0}(\lambda) = c_{C0}(\lambda) - a_{C0}(\lambda)$, including scattering and temperature corrections to the ac-9 measurements (Chapter 3).

11. Add pure water to dilute the sequence to bead concentration C1 and record the VSF response signal $V_{C1}(\bar{\psi})$, and repeat this step several times to obtain N+1 VSF response signal $V_{C0}(\bar{\psi}),\ldots,V_{CN}(\bar{\psi})$ corresponding to N+1 bead concentrations. It is not necessary to determine either the absolute, or relative bead concentrations, so dilution volumes of pure water need not be measured. At each dilution concentration Cn, repeat steps 10a and 10b.

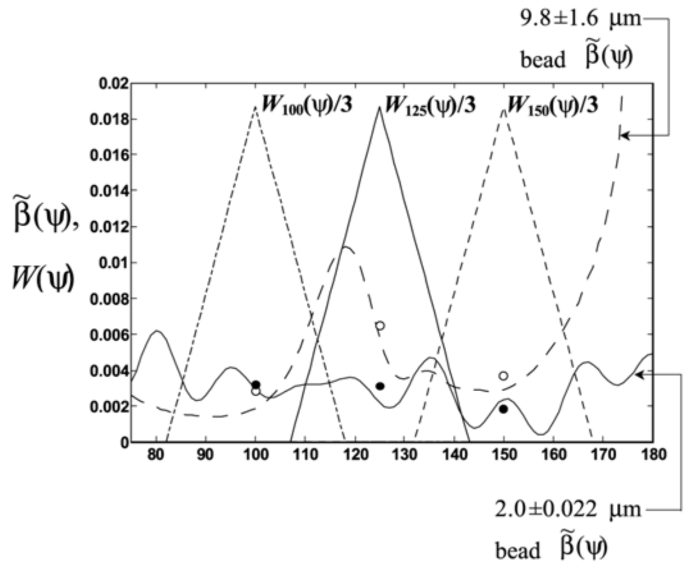

Figure 5.4: Examples of phase functions $\tilde{\beta}_{ps}(\lambda,\psi)$ calculated using Mie theory for polydispersions of polystyrene microsphere beads having mean diameters of 2 µm (solid line) and 9.8 µm (dashed line), and in both cases relatively small standard deviations. The open and closed circles show the corresponding weighted phase functions $\bar{\tilde{\beta}}_{ps}(\lambda,\bar{\psi})$ calculated by convolving each phase function with the ECO-VSF weighting functions $W(\psi)$ illustrated in Fig. 5.2.

The response calibration factor for a given bead concentration C0 to CN is determined as

$$F_{Cn}(\bar{\psi}) = \frac{b_{ps}^{Cn}(\lambda)\bar{\tilde{\beta}}_{ps}(\lambda,\bar{\psi})}{V_{Cn}(\bar{\psi}) - V_{w}(\bar{\psi}) - V_{dark}(\bar{\psi})} \tag{5.16}$$

where the polystrene sphere phase function $\bar{\tilde{\beta}}_{ps}(\lambda,\bar{\psi})$ is determined from (5.15). If necessary, the coefficient for each Cn is adjusted for dependence on the beam attenuation coefficient, and the sample is averaged to obtain the linear calibration coefficient $F(\bar{\psi})$. Given VSF measurements $V_{m}(\bar{\psi})$ in an unknown natural water mass, the weighted VSF for particles is calculated as

$$\bar{\beta}_{p}(\lambda,\bar{\psi}) = F(\bar{\psi})\left[V_{m}(\bar{\psi}) - V_{w}(\bar{\psi}) - V_{dark}(\bar{\psi})\right]. \tag{5.17}$$

5.3 CHARACTERIZATION and CALIBRATION OF A VSF SENSOR USING A REFLECTING PLAQUE

Maffione and Dana (1997) approach the calibration of a VSF sensor by inserting a horizontal plaque of assumed Lambertian reflectance $\frac{\rho}{\pi}$ into the position of the xy-plane illustrated in Fig. 5.1. Substituting this reflectance for the VSF in (5.6) and integrating over x and y yields the equation

$$\frac{\Phi_{d\rho}[\Delta z; c]}{\Phi_{o}} = \frac{\rho}{\pi}\int_{x}\int_{y}\left|\hat{\boldsymbol{\varepsilon}}(\hat{\mathbf{x}}_{\mathbf{d}} - \hat{\mathbf{x}})\bullet\hat{\mathbf{n}}\right| W(\bar{\mathbf{x}}; c)dxdy = \frac{\rho}{\pi}W_{\rho}(z; c), \tag{5.18}$$

representing the total flux reflected from the plaque into the FOV of the detector. If the plaque is moved continuously over z the integral of (5.18) yields the total relative flux reflected from the plaque to the detector from the volume intersection of the source beam and detector FOV as

$$\frac{\Phi_{d\rho}[c]}{\Phi_o} = \frac{\rho}{\pi}\int_z W_\rho(z;c)\,dz \,. \tag{5.19}$$

A similar integration of (5.1) yields

$$\frac{\Phi_{d\beta}[c]}{\Phi_o} = \int_z\int_x\int_y \beta(\psi(\bar{\mathbf{x}}))W(\bar{\mathbf{x}};c)dxdydz = \beta(\psi^*)\int_z W(z;c)\,dz \tag{5.20}$$

where the angle ψ^* is selected so that the equality holds; the mean value theorem assures that this must be true for at least one scattering angle. Taking the ratio of (5.10) and (5.20) and solving for $\beta(\psi^*)$ yields the result

$$\beta(\psi^*) = \frac{\rho}{\pi}\frac{\Phi_{d\beta}[c]}{\Phi_{d\rho}[c]}\frac{\int_z W_\rho(z;c)\,dz}{\int_z W(z;c)\,dz} \,. \tag{5.21}$$

We refer the reader to Maffione and Dana (1997) for the derivation of the unknown terms in (5.21) from the plaque integral and differential measurements, and defer further comparative analysis and description of this method and the explicit approach of Section 5.2 for a future revision to this chapter.

5.4 METHODS FOR THE DETERMINATION OF THE BACKSCATTERING COEFFICIENT FROM VSF MEASUREMENTS AT ONE OR MORE SCATTERING ANGLES

If the complete VSF is measured at fine angular resolution using a general angle scattering meter, then it is straightforward to integrate it over the backward hemisphere to determine $b_b(\lambda)$ directly.

Determination of $b_b(\lambda)$ from VSF Measurements at Three or More Angles

The approach used to determine $b_b(\lambda)$ from measurements of $\overline{\beta}(\lambda,\psi_i,\varphi)$; at $i = 1,2,\ldots,\mathrm{N}$ angles, *e.g.* using a WET Labs VSF-3, is to fit a polynomial to the N+1 values $2\pi\overline{\beta}(\lambda,\psi_i,\varphi)\sin\psi_i$ derived from the N measurements and the endpoint $2\pi\beta(\lambda,\pi,\bullet)\sin\pi \equiv 0$ and integrate it from $\frac{\pi}{2}$ to π (following Beardsley and Zaneveld 1969).

Determination of $b_b(\lambda)$ from VSF Measurements at Only One Angle

Oishi (1990) used Mie scattering calculations and VSF observations to determine $\beta^n(\lambda,\psi)$ and $b_b^n(\lambda)$ for polydispersions of spheres having different size distributions similar to those observed for marine hydrosols. He invoked the mean value theorem to observe, from the definition of $b_b(\lambda)$, that for each n<u>th</u> polydispersion phase function $\tilde{\beta}^n(\lambda,\psi)$ there must be at least one angle ψ_n^* for which

$$b_b^n(\lambda) = 2\pi\beta^n(\lambda,\Psi_n^*)\int_{\frac{\pi}{2}}^{\pi}\sin\Psi d\Psi = 2\pi\beta^n(\lambda,\Psi_n^*).^{13} \tag{5.22}$$

Oishi (1990) then futher observed that for a selected common reference angle ψ^*, he could determine an approximate linear estimate of the backscattering coefficient for each polydispersion as

[13] Recalling that $\beta(\lambda,\psi) = b(\lambda)\tilde{\beta}(\lambda,\psi)$ [Vol. I, Ch. 2, Sect. 2.4].

$$\hat{b}_{\mathrm{b}}^{n}(\lambda) \approx 2\pi\chi(\Psi^{*})\beta^{n}(\lambda,\Psi^{*}), \tag{5.23}$$

where the coefficient $\chi(\Psi^{*})$ is selected to minimize the uncertainty

$$U(\Psi^{*}) = \sqrt{\frac{\sum_{n=1}^{\mathrm{N}}\left[b_{\mathrm{b}}^{n}(\lambda) - \hat{b}_{\mathrm{b}}^{n}(\lambda)\right]^{2}}{\mathrm{N}}}. \tag{5.24}$$

By varying ψ^{*}, Oishi found that the minimum overall uncertainty for the ensemble of N size distributions occurred at $\psi^{*} = 120°$, with $\chi(120°) = 1.14$.

Boss and Pegau (2001) separated the VSF and backscattering coefficient as

$$\begin{aligned} \beta(\lambda,\Psi) &= \beta_{\mathrm{w}}(\lambda,\Psi) + \beta_{\mathrm{p}}(\lambda,\Psi) \text{ and} \\ b(\lambda) &= b_{\mathrm{w}}(\lambda) + b_{\mathrm{b}}(\lambda), \end{aligned} \tag{5.25}$$

where the subscripts "p" and "w" designate contributions due to particles and water, respectively. The scaling factor $\chi(\Psi^{*})$ is correspondingly partitioned as

$$\chi(\Psi^{*}) = \chi_{\mathrm{p}}(\Psi^{*})\frac{\beta_{\mathrm{p}}(\lambda,\Psi^{*})}{\beta(\lambda,\Psi^{*})} + \chi_{\mathrm{w}}(\Psi^{*})\frac{\beta_{\mathrm{w}}(\lambda,\Psi^{*})}{\beta(\lambda,\Psi^{*})}. \tag{5.26}$$

Analyses similar to those of Oishi (1990) and Maffione and Dana (1997), but in this partitioned framework, led Boss and Pegau (2001) to conclude that $\chi(\Psi^{*}) = \chi_{\mathrm{p}}(\Psi^{*}) = \chi_{\mathrm{w}}(\Psi^{*}) \cong 1.1$ only when $\Psi^{*} = 117° \pm 3°$, consistent with the results of Oishi (1990). For measurements at other scattering angles, they recommend modifying Equation (4.6) to correct for the water scattering contribution as

$$\hat{b}_{b}(\lambda) = 2\pi\chi_{\mathrm{p}}(\Psi^{*})\left[\beta(\lambda,\Psi^{*}) - \beta_{\mathrm{w}}(\lambda,\Psi^{*})\right] + b_{\mathrm{bw}}(\lambda). \tag{5.27}$$

They provide equations for estimating $\beta_{\mathrm{w}}(\lambda,\Psi)$ and $b_{\mathrm{w}}(\lambda)$, based on the theoretical equations and experimental results of Morel (1974), and tabulate estimates of $\chi_{\mathrm{p}}(\Psi^{*})$ in the range $90° \leq \Psi^{*} \leq 170°$.

REFERENCES

Beardsley, G.F. and J.R.V. Zaneveld, 1969: Theoretical dependence of the near-asymptotic apparent optical properties of sea water. *J. Opt. Soc. Amer*. 59: 373-377.

Bohren, C.F., and D.R. Huffman, 1983: *Absorption and Scattering of Light by Small Particles*, Wiley, New York, 530pp

Boss, E. and W.S. Pegau, 2001: Relationship of light scattering at an angle in the backward direction to the backscattering coefficient. *Appl. Opt.,* **40:** 5503-5507.

Mie, G., 1908: Beitrage zur Optic truber Medien, speziell kolloidalen Metallosungen, *Ann. Phys*., **25:** 377-442.

Maffione, R.A. and D.R. Dana, 1997: Instruments and methods for measuring the backward-scattering coefficient of ocean waters. *Appl. Opt*. **36**: 6057-6067.

Mobley, C.D., L.K. Sundman, and E. Boss, 2002. Phase function effects on oceanic light fields. *Appl. Opt.*, **41**(6): 1035-1050.

Oishi, T., 1990. Significant relation between the backward scattering coefficient of sea water and the scatterance at 120 degrees. *Appl. Opt.*, *29(31)*: 4658-4665.

Petzold, T.J., 1972. Volume scattering functions for selected ocean waters. Contract No. N62269-71-C-0676, UCSD, SIO Ref. 72-78.

Stramska, M., D. Stramski, B.G. Mitchell and C.D. Mobley. 2000: Estimation of the absorption and backscattering coefficients from in-water radiometric measurements. *Limnol. Oceanogr*., **45**: 628-641.

Zaneveld, J.R.V., 1982: Remotely sensed reflectance and is dependence on vertical structure: a theoretical derivation. *Appl. Opt*., **21(22):** 4146-4150.

Appendix D

NASA/TM-2003-21621/Rev-Vol V

Ocean Optics Protocols For Satellite Ocean Color Sensor Validation, Revision 4, Volume V:

Biogeochemical and Bio-Optical Measurements and Data Analysis Protocols

James L. Mueller, Giulietta S. Fargion and Charles R. McClain, Editors
J. L. Mueller, R. R. Bidigare, C. Trees, J. Dore, D. Karl, and L. Van Heukelem, Authors.

National Aeronautical and
Space administration

Goddard Space Flight Space Center
Greenbelt, Maryland 20771

January 2003

NASA/TM-2003-

Ocean Optics Protocols For Satellite Ocean Color Sensor Validation, Revision 4, Volume V:

Biogeochemical and Bio-Optical Measurements and Data Analysis Protocols

James L. Mueller, CHORS, San Diego State University, San Diego, California
Giulietta S. Fargion, Science Applications International Corporation, Beltsville, Maryland
Charles R. McClain, Goddard Space Flight Center, Greenbelt, Maryland

J. L. Mueller, and C. Trees
CHORS, San Diego State University, San Diego, California
R. R. Bidigare, D. M. Karl and J. Dore
Department of Oceanography, University of Hawaii, Hawaii
L. Van Heukelem
University of Maryland Center for Environmental Science, Maryland

National Aeronautical and
Space administration

Goddard Space Flight Space Center
Greenbelt, Maryland 20771

January 2003

Preface

This document stipulates protocols for measuring bio-optical and radiometric data for the Sensor Intercomparison and Merger for Biological and Interdisciplinary Oceanic Studies (SIMBIOS) Project activities and algorithm development. The document is organized into 7 separate volumes as:

Ocean Optics Protocols for Satellite Ocean Color Sensor Validation, Revision 4

Volume I: Introduction, Background and Conventions
Volume II: Instrument Specifications, Characterization and Calibration
Volume III: Radiometric Measurements and Data Analysis Methods
Volume IV: Inherent Optical Properties: Instruments, Characterization, Field Measurements and Data Analysis Protocols
Volume V: Biogeochemical and Bio-Optical Measurements and Data Analysis Methods
Volume VI: Special Topics in Ocean Optics Protocols
Volume VII: Appendices

The earlier version of *Ocean Optics Protocols for Satellite Ocean Color Sensor Validation*, *Revision 3* (Mueller and Fargion 2002, Volumes 1 and 2) is entirely superseded by the seven Volumes of Revision 4 listed above.

The new multi-volume format for publishing the ocean optics protocols is intended to allow timely future revisions to be made reflecting important evolution of instruments and methods in some areas, without reissuing the entire document. Over the years, as existing protocols were revised, or expanded for clarification, and new protocol topics were added, the ocean optics protocol document has grown from 45pp (Mueller and Austin 1992) to 308pp in Revision 3 (Mueller and Fargion 2002). This rate of growth continues in Revision 4. The writing and editorial tasks needed to publish each revised version of the protocol manual as a single document has become progressively more difficult as its size increases. Chapters that change but little, must nevertheless be rewritten for each revision to reflect relatively minor changes in, *e.g*., cross-referencing and to maintain self-contained consistency in the protocol manual. More critically, as it grows bigger, the book becomes more difficult to use by its intended audience. A massive new protocol manual is difficult for a reader to peruse thoroughly enough to stay current with and apply important new material and revisions it may contain. Many people simply find it too time consuming to keep up with changing protocols presented in this format - which may explain why some relatively recent technical reports and journal articles cite Mueller and Austin (1995), rather than the then current, more correct protocol document. It is hoped that the new format will improve community access to current protocols by stabilizing those volumes and chapters that do not change significantly over periods of several years, and introducing most new major revisions as new chapters to be added to an existing volume without revision of its previous contents.

The relationships between the Revision 4 chapters of each protocol volume and those of Revision 3 (Mueller and Fargion 2002), and the topics new chapters, are briefly summarized below:

Volume I: This volume covers perspectives on ocean color research and validation (Chapter 1), fundamental definitions, terminology, relationships and conventions used throughout the protocol document (Chapter 2), requirements for specific *in situ* observations (Chapter 3), and general protocols for field measurements, metadata, logbooks, sampling strategies, and data archival (Chapter 4). Chapters 1, 2 and 3 of Volume I correspond directly to Chapters 1, 2 and 3 of Revision 3 with no substantive changes. Two new variables, Particulate Organic Carbon (POC) and Particle Size Distribution (PSD) have been added to Tables 3.1 and 3.2 and the related discussion in Section 3.4; protocols covering these measurements will be added in a subsequent revision to Volume V (see below). Chapter 4 of Volume I combines material from Chapter 9 of Revision 3 with a brief summary of SeaBASS policy and archival requirements (detailed SeaBASS information in Chapter 18 and Appendix B of Revision 3 has been separated from the optics protocols).

Volume II: The chapters of this volume review instrument performance characteristics required for *in situ* observations to support validation (Chapter 1), detailed instrument specifications and underlying rationale (Chapter 2) and protocols for instrument calibration and characterization standards and methods (Chapters 3 through 5). Chapters 1 through 5 of Volume II correspond directly to Revision 3 chapters 4 through 8, respectively, with only minor modifications.

Volume III: The chapters of this volume briefly review methods used in the field to make the *in situ* radiometric measurements for ocean color validation, together with methods of analyzing the data (Chapter 1),

detailed measurement and data analysis protocols for in-water radiometric profiles (Chapter 2), above water measurements of remote sensing reflectance (Chapter III-3), determinations of exact normalized water-leaving radiance (Chapter 4), and atmospheric radiometric measurements to determine aerosol optical thickness and sky radiance distributions (Chapter 5). Chapter 1 is adapted from relevant portions of Chapter 9 in Revision 3. Chapter 2 of Volume III corresponds to Chapter 10 of Revision 3, and Chapters 3 through 5 to Revision 3 Chapters 12 through 14, respectively. Aside from reorganization, there are no changes in the protocols presented in this volume.

Volume IV: This volume includes a chapter reviewing the scope of inherent optical properties (IOP) measurements (Chapter 1), followed by 4 chapters giving detailed calibration, measurement and analysis protocols for the beam attenuation coefficient (Chapter 2), the volume absorption coefficient measured *in situ* (Chapter 3), laboratory measurements of the volume absorption coefficients from discrete filtered seawater samples (Chapter 4), and *in situ* measurements of the volume scattering function, including determinations of the backscattering coefficient (Chapter 5). Chapter 4 of Volume IV is a slightly revised version of Chapter 15 in Revision 3, while the remaining chapters of this volume are entirely new contributions to the ocean optics protocols. These new chapters may be significantly revised in the future, given the rapidly developing state-of-the-art in IOP measurement instruments and methods.

Volume V: The overview chapter (Chapter 1) briefly reviews biogeochemical and bio-optical measurements, and points to literature covering methods for measuring these variables; some of the material in this overview is drawn from Chapter 9 of Revision 3. Detailed protocols for HPLC measurement of phytoplankton pigment concentrations are given in Chapter 2, which differs from Chapter 16 of Revision 3 only by its specification of a new solvent program. Chapter 3 gives protocols for Fluorometric measurement of chlorophyll *a* concentration, and is not significantly changed from Chapter 17of Revision 3. New chapters covering protocols for measuring, Phycoerythrin concentrations, Particle Size Distribution (PSD) and Particulate Organic Carbon (POC) concentrations are likely future additions to this volume.

Volume VI: This volume gathers chapters covering more specialized topics in the ocean optics protocols. Chapter 1 introduces these special topics in the context of the overall protocols. Chapter 2 is a reformatted, but otherwise unchanged, version of Chapter 11 in Revision 3 describing specialized protocols used for radiometric measurements associated with the Marine Optical Buoy (MOBY) ocean color vicarious calibration observatory. The remaining chapters are new in Revision 4 and cover protocols for radiometric and bio-optical measurements from moored and drifting buoys (Chapter 3), ocean color measurements from aircraft (Chapter 4), and methods and results using LASER sources for stray-light characterization and correction of the MOBY spectrographs (Chapter 5). In the next few years, it is likely that most new additions to the protocols will appear as chapters added to this volume.

Volume VII: This volume collects appendices of useful information. Appendix A is an updated version of Appendix A in Revision 3 summarizing characteristics of past, present and future satellite ocean color missions. Appendix B is the List of Acronyms used in the report and is an updated version of Appenix C in Revision 3. Similarly, Appendix C, the list of Frequently Used Symbols, is an updated version of Appendix D from Rev. 3. The SeaBASS file format information given in Appendix B of Revision 3 has been removed from the protocols and is promulgated separately by the SIMBIOS Project.

In the Revision 4 multi-volume format of the ocean optics protocols, Volumes I, II and III are unlikely to require significant changes for several years. The chapters of Volume IV may require near term revisions to reflect the rapidly evolving state-of-the-art in measurements of inherent optical properties, particularly concerning instruments and methods for measuring the Volume Scattering Function of seawater. It is anticipated that new chapters will be also be added to Volumes V and VI in Revision 5 (2003).

This technical report is not meant as a substitute for scientific literature. Instead, it will provide a ready and responsive vehicle for the multitude of technical reports issued by an operational Project. The contributions are published as submitted, after only minor editing to correct obvious grammatical or clerical errors.

Table of Contents

Chapter 1

Overview of Biogeochemical Measurements and Data Analysis in Ocean Color Research

James L. Mueller

Center for Hydro-Optics and Remote Sensing, San Diego State University, California

1.1 INTRODUCTION

A total of 9 biogeochemical and bio-optical observations are listed in Tables 3.1 and 3.2. Phytoplankton pigment concentrations determined by the HPLC method, and fluorometric chlorophyll *a* and pheopigment concentrations are ***required*** measurements for which detailed protocols are described in Chapters 2 and 3, respectively. Observation of chlorophyll *a* fluorescence intensity *in situ* is listed as highly desired, and protocols for its measurement and data analysis are also included in Chapter 3. Six additional biogeochemical observations are listed as ***specialized measurements***. These include concentrations of Phycobiliprotein (Phycoerythrin), and suspended particulate measurements including *Coccolith* concentrations, total Suspended Particulate Matter (SPM), Particulate Organic Carbon (POC), Particulate Organic Nitrogen (PON, and Particle Size Distribution (PSD). Methods of measurement and data analysis for these specialized observations, most of which are related to applications of ocean color image data to ocean process studies, are reviewed briefly in the present chapter.

1.2 PHYTOPLANKTON PIGMENT CONCENTRATIONS

High Performance Liquid Chromatography (HPLC) Measurements and Analysis (Chapter 2)

Mueller and Austin (1995) simply adopted the JGOFS HPLC protocols for measuring phytoplankton pigment concentrations by reference (UNESCO 1994), and supplemented them with some brief instructions on sampling and sample handling procedures. Although this approach embraced protocol documentation describing a complete methodology, and represented a community consensus, the lack of a comprehensive end-to-end protocol statement has proved to be a source of confusion and debate within the ocean color community. Furthermore, the JGOFS protocols (UNESCO 1994) specified that pigment concentrations should be reported in units of pigment mass per mass of seawater (ng Kg^{-1}), rather than in units of pigment mass per volume of seawater (either μg L^{-1}, or mg m^{-3}). The use of volumetric concentrations is critical because radiative transfer in the ocean, and absorption by pigments, are volumetric processes. One could use the mass concentration values preferred by JGOFS, but it would be essential to supplement them with densities computed from CTD data, and make the conversion to volumetric concentrations. Therefore, a complete set of protocols for HPLC measurement of phytoplankton pigment concentrations was added as Chapter 13 of Revision 2.0 to the Ocean Optics Protocols (Fargion and Mueller 2000), updated as Chapter 16 of Revision 3 (Mueller and Fargion 2002), and updated here again as Chapter 2 of the present volume. Chapter 2 provides complete protocols for obtaining water samples, filtering them, freezing the filtered samples in liquid nitrogen, sample handling and storage, extraction, HPLC calibrations and measurements, data analysis and quality control. A new HPLC solvent program in Chapter 2 replaces that specified in the previous version of the protocols (Bidegare *et al*. 2002).

Fluorometric Measurement of Chlorophyll a Concentration (Chapter 3)

For reasons similar to those described above for HPLC pigment measurements, it was decided that the protocols for fluorometric measurement of the concentrations of chlorophyll *a* and phaeopigments were too briefly abstracted in Mueller and Austin (1995). Therefore, new detailed protocols for this measurement were added as Chapter 14 to Revision 2 (Fargion and Mueller 2000), updated as Chapter 17 of Revision 3 (Mueller and Fargion 2002), and reproduced here without significant change as Chapter 3. Chapter 3 provides complete protocols for obtaining water samples, filtering them, freezing the filtered samples in liquid nitrogen, sample handling and storage, extraction, fluorometer calibrations and measurements, data analysis and quality control.

In addition, Chapter 3 discusses geographic and temporal variability in the relationship between fluorometric chlorophyll concentrations and combined concentrations of total chlorophyll pigments determined by the HPLC methods (Chapter 2). It is both easier and less expensive to measure chlorophyll *a* and pheopigment concentrations using the fluorometric method, which has the added advantage of allowing shipboard analyses at sea during lengthy cruises. When these data are used for remote sensing algorithm development or validation, however, regional and temporal (*i.e.* cruise-to-cruise) dispersions and/or biases may be introduced unless the fluorometric data are first statistically adjusted (on a local basis) to agree with HPLC determinations of the concentration of total chlorophylls. A cost-effective strategy is to acquire, on each cruise, a majority of filtered pigment samples for fluorometric chlorophyll *a* and pheopigment analysis, supplemented by a smaller number of replicate samples for HPLC pigment analysis. The HPLC replicates should provide a representative distribution over geographic location, depth and time during a cruise, and will be used to determine a local regression relationship between the two measurements. This approach is now required for pigment data submitted for SeaBASS archival and SIMBIOS validation analysis.

Phycoerythrin and other Phycobiliproteins

$R_{RS}(\lambda)$ may be enhanced by fluorescence by phycoerythrin (PE) in a band near 565 nm (*e.g.* Hoge *et al*. 1998; Wood *et al*. 1999). The detection from aircraft of laser-induced phycoerythrin fluorescence is already well established (Hoge *et al*. 1998). It is more difficult to detect and quantify solar induced phycoerythrin fluorescence, but some work has been done in that area as well (Morel *et al*. 1993; Morel 1997; Hoge *et al*. 1999; Subramaniam *et al*. 1999).

Various phycoerythrins differ from one another in chromophore composition. All phycoerythrins contain phycoerythrobilin chromophores [PEB; maximum $a(\lambda)$ near $\lambda \sim 550$ nm]; many others also contain phycourobilin chromophores [PUB; maximum $a(\lambda)$ near $\lambda \sim 500$ nm], which extends the range of wavelengths absorbed by the pigment molecule into the blue regions of the spectrum. The ratio of PUB:PEB chromophores in the PE pigments synthesized by different *Synechococcus* strains greatly affects the absorption spectrum of the whole cells (Wood *et al*. 1985). Clearly, the dependence of $a(\lambda)$ on the PUB:PEB ratio of phycoerythrin will affect also $R_{RS}(\lambda)$ in water masses dominated by cyanobacteria. The PUB:PEB ratio for the PE in a given water mass may be characterized using scanning fluorescence spectroscopy (Wood *et al*., 1999; Wyman, 1992).

The measurement of phycoerythrin is not yet as routine, nor as accurate, as the measurements of chlorophylls and carotenoids. The techniques introduced by Stewart and Farmer (1984) work well for measuring biliproteins in freshwater and estuarine species, but are less successful for natural populations of marine species. Wyman (1992) reported a linear relationship between the *in vivo* fluorescence emission intensity of PE measured in the presence of glycerol and the PE content of *Synechococcus* strain WH7803. Scanning spectral fluorescence measurements have been used to estimate PE concentration of extracted bulk samples (Vernet *et al*., 1990). Nevertheless, there are few direct measurements of separated PE proteins from natural samples. High Performance Capillary Electrophoresis (HPCE) is a powerful analytical tool currently used in clinical, biochemical, pharmaceutical, forensic, and environmental research. In HPCE, high voltages (typically 10-30 KV) are used to separate molecules rapidly in narrow-bore (25-100 μm), fused-silica capillaries based on differences in the charge-to-mass ratio of the analytes. HPCE is an automated analytical separation system with reduced analysis times and on-line quantification of compounds, ideally suited to the separation and quantification of water-soluble proteins (like phycobilins) from seawater. HPCE methods for separation analyses of phycoerythrin from cyanobacterial cultures and natural samples are currently under development and may be included in a future revision to the ocean optics protocols (C. Kinkade, Pers. Comm.).

1.3 *IN SITU* CHLOROPHYLL *a* FLUORESCENCE

Protocols for measuring and analyzing profiles of *in situ* fluorescence by chlorophyll *a*, $F(z)$ (Table 3.1 in Chapter 3, Volume I) are described in Chapter 3. When measured together with $c(z,660)$ profiles (Chapter 2, Volume IV), the structure of $F(z)$ provides valuable guidance for selecting depths of water samples, analyses of structure in $K(z,\lambda)$ derived from radiometric profiles, and various aspects of quality control analysis. It is often useful to digitally record one-minute averages of $F(z, lat, lon)$ in water pumped from a near-surface depth ($z \sim 3$ m) to measure horizontal variability while underway steaming between stations, especially in water masses where mesoscale and sub-mesoscale variability is strong (Section 4.2, Chapter 4, Vol. I). If supplemented by frequent

fluorometric chlorophyll *a* samples filtered from the flow-through system, the alongtrack profile of $F(z, lat, lon)$ can be "calibrated" in units of chlorophyll *a* concentration (mg m^{-3}).

1.4 SUSPENDED PARTICLES

Suspended Particulate Matter

All total suspended particulate material (SPM) dry weight (mg L^{-1}) will be determined gravimetrically as outlined in Strickland and Parsons (1972)[1]. In general, samples are filtered through preweighed 0.4 µm polycarbonate filters. The filters are washed with three 2.5 mL - 5.0 mL aliquots of DIW and immediately dried, either in an oven at 75^{o} C, or in a dessicator. The filters are then reweighed in a laboratory, back on shore, using an electrobalance with at least seven digits of precision.

Particulate Organic Carbon and Particulate Organic Nitrogen

Protocols for measuring concentrations in seawater of Particulate Organic Carbon (POC) and Particulate Organic Nitrogen (PON), as specified for JGOFS (UNESCO 1994, Chapter 15), are also adopted here. The units of POC and PON are $\mu\mathrm{g\,C\,Kg}^{-1}$ and $\mu\mathrm{g\,N\,Kg}^{-1}$, respectively. Therefore, it is mandatory that each of thes measurements be accompanied by Conductivity, Temperature and Pressure measurements so that the density of seawater $\left[\mathrm{Kg\ m}^{-3}\right]$ may be calculated.

Particle Size Distributions

Particle size distributions can potentially provide important information about the shape of the volume scattering function, which strongly influences the bidirectional aspects of remote-sensing reflectance (Chapter 4 of Volume III and, *e.g.*, Morel and Gentili 1996). Particle size distributions have been measured for many years using Coulter Counters and related to IOP, including $c(\lambda)$ (*e.g.* Kitchen *et al*. 1982). More recently, several investigators have used the Spectrix Particle Size Analyzer to measure particle size distributions (see, *e.g*., Chapter 2, Vol. VI). Protocols for measurements and analyses of particle size distributions are not included in this version of the ocean optics protocols, but should be written and added to a future revision of this protocol volume.

Coccolith Concentrations

Concentrations of coccoliths, calcium carbonate ($CaCO_3$) platelets detached from coccolithophorids (sp.), are measured as cell counts [number density per unit volume] using a microscope with polarization optics (Balch *et al*. 1991). An epifluorescence microscope is used to count plated and naked intact cells, before and after the coccoliths are dissolved by acidification. Also measured, before and after acidification, are the Volume Scattering Function (VSF) values at three angles, from which the volume specific backscattering coefficient for coccoliths is determined by subtraction (Voss *et al*. 1998).

1.5 FUTURE DIRECTIONS

Future additions to this volume include chapters providing detailed prototolc for Phycoerythrin measurement and data analysis, measurements and analyses of coccolith concentrations, and methods for measurement and analyses of SPM, PSD, and the organic suspended particulate fractions POC and PON.

REFERENCES

Balch, W.M., P.M. Holligan, S.G. Ackleson, and K.J. Voss, 1991: Biological and optical properties of mesoscale coccolithophore blooms in the Gulf of Maine. *Limnol. Oceanogr*., **36:** 629-643.

[1] In some previous versions of the Ocean Optics Protocols (Mueller and Austin 1992, 1995; Fargion and Mueller 2000), it was incorrectly stated that suitable protocols were part of the JGOFS core measurements protocols (UNESCO 1994). The JGOFS protocols do not include SPM measurements of the type specified here.

Bidegare, R.R., L. Van Heukelem, and C.C. Trees, 2002: HPLC phytoplankton pigments: sampling, laboratory methods, and quality assurance procedures. Chapter 17 in *Ocean Optics Protocols for Satellite Ocean Color Sensor Validation, Revision 3*, Mueller J.L. and G.S. Fargion [Eds.], NASA TM 2002-210004, NASA Goddard Space Flight Center, Greenbelt, Maryland, pp258-268.

Fargion, G.S. and J.L. Mueller, 2000: *Ocean Optics Protocols for Satellite Ocean Color Sensor Validation, Revision 2*, NASA TM 2001-209955, NASA Goddard Space Flight Center, Greenbelt, Maryland, 184 pp.

Hoge, F. E., C. W. Wright, P. E. Lyon, R. N. Swift, and J. Yungel. 1999: Satellite retrival of the absorption coefficient of phytoplankton phycoerythrin pigment: Theory and feasibility status. MODIS ATBD document 27.

Kitchen, J.C., J.R.V. Zaneveld and H. Pak, 1982: Effect of particle size distribution and chloropyll content on beam attenuation spectra. *Appl. Opt.*, **21**: 3913-3918.

Morel, A. 1997: Consequences of a Synechococcus bloom upon the optical properties of oceanic (case 1) waters. *Limnol. Oceanogr*., **42**: 1746-1754.

Morel, A., Y.H. Ahn, F. Partensky, D. Vaulot, and H. Claustre. 1993: *Prochlorococcus* and *Synechococcus*: A comparative study of their optical properties in relation to their size and pigmentation. *J. Mar. Res*., **51**: 617-647.

Mueller, J.L., and R.W. Austin, 1995: Ocean Optics Protocols for SeaWiFS Validation, Revision 1. *NASA Tech. Memo. 104566, Vol.* ***25,*** S.B. Hooker, E.R. Firestone and J.G. Acker, Eds., NASA Goddard Space Flight Center, Greenbelt, Maryland, 67 pp.

Mueller, J.L. and G.S. Fargion, 2002: *Ocean Optics Protocols for Satellite Ocean Color Sensor Validation, Revision 3*, NASA TM 2002-210004, NASA Goddard Space Flight Center, Greenbelt, Maryland, 184 pp.

Stewart, D.E. and F.H. Farmer. 1984: Extraction, identification, and quantification of phycobiliprotein pigments from phototrophic plankton. *Limnol. Oceanogr.,* **29**: 392-397.

Strickland, J.D.H., and T.R. Parsons, 1972: *A Practical Handbook of Sea Water Analysis,* Fisheries Research Board of Canada, 310 pp.

Subramaniam, A., E. J. Carpenter, and P. G. Falkowski, 1999: Bio-optical properties of the marine diazotrophic cyanobacteria Trichodesmium spp. II. A reflectance model for remote sensing. *Limnol. Oceanogr*., 44: 618-627.

UNESCO, 1994: Protocols for the Joint Global Ocean Flux Study (JGOFS) Core Measurements, Manuals and Guides **29**: 170pp

Vernet, M., B.G. Mitchell, and O. Holm-Hansen: 1990: Adaptation of *Synechococcus in situ* determined by variability in intracellular phycoerythrin-543 at a coastal station off the Southern California coast, USA. *Mar. Ecol. Prog. Ser*., **63**: 9-16.

Voss, K.J., W.M. Balch and K.A. Kilpatrick, 1998,. Scattering and attenuation properties of *Emiliania huxleyi* cells and their detached coccoliths. . Limnol. Oceangr., **43**(5): 870-876.

Wood, A.M., P.K. Horan, K. Muirhead, D. Phinney, C.M. Yentsch, and J.M. Waterbury, 1985: Discrimination between types of pigments in marine *Synechococcus* by scanning spectroscopy, epifluorescence microscopy, and flow cytometry. *Limnol. and Oceanogr.*, **30**: 1303-1315.

Wood, A.M., M. Lipsen and P. Coble, 1999: Fluorescence based characterization of phycoerythrin-containing cyanobacterial communities in the Arabian Sea during the Notheast and early Southwest Monsoon (1994-1995). *Deep-Sea Res. II*, **46**: 1769-1790.

Wyman, M. 1992: An in vivo method for the estimation of phycoerythrin concentrations in marine cyanobacteria (*Synechococcus* spp.). *Limnol. Oceangr*., **37**: 1300-1306.

Chapter 2

HPLC Phytoplankton Pigments: Sampling, Laboratory Methods, and Quality Assurance Procedures

Robert R. Bidigare[1], Laurie Van Heukelem[2] and Charles C. Trees[3]

[1] *Department of Oceanography, University of Hawaii, Hawaii*

[2]*Horn Point Environmental Laboratory, University of Maryland, Maryland*

[3]*Center for Hydro-Optics and Remote Sensing, San Diego State University, California*

2.1 INTRODUCTION

Marine phytoplankton utilize chlorophyll *a* as their major light harvesting pigment for photosynthesis. Other accessory pigment compounds, such as chlorophylls *b* and *c*, carotenoids and phycobiliproteins, also play a significant role in photosynthesis by extending the organism's optical collection window, thereby improving absorption efficiencies and adaptation capabilities. The important chlorophyll degradation products found in the aquatic environment are the chlorophyllides, phaeophorbides, and phaeophytins. The presence, or absence, of the various photosynthetic pigments is used to separate the major algal groups, and to map the chemotaxonomic composition of phytoplankton in the oceans.

The unique optical properties of chlorophyll *a* have been used to develop spectrophotometric (Jeffrey and Humphrey 1975) and fluorometric (Holm-Hansen *et al.* 1965) measurement techniques. With the commercial availability of fluorometers for routine measurements of chlorophyll *a*, this pigment became a universal parameter in biological oceanography for estimating phytoplankton biomass and productivity. These optical methods can significantly under- or overestimate chlorophyll *a* concentrations, because of the overlap of the absorption and fluorescence bands of co-occurring chlorophylls *b* and *c*, chlorophyll degradation products, and accessory pigments (Trees *et al*. 1985; Smith *et al.* 1987; Hoepffner and Sathyendranath 1992; Bianchi *et al.* 1995; Tester *et al*. 1995).

The application of HPLC to phytoplankton pigment analysis has lowered the uncertainty for measuring chlorophyll *a* and pheopigments, as well as the accessory pigments, since compounds are physically separated and individually quantified. HPLC has provided oceanographers with a powerful tool for studying the processes affecting the phytoplankton pigment pool. Pigment distribution is useful for quantitative assessment of phytoplankton community composition, phytoplankton growth rate and zooplankton grazing activity.

For low uncertainty determinations of chlorophylls *a*, *b*, and *c*, chlorophyll degradation products, and carotenoid pigments, HPLC techniques are recommended. It should be noted, however, that the reverse-phase C_{18} HPLC method recommended by the Scientific Committee on Oceanographic Research (SCOR) (Wright *et al*. 1991) is not capable of separating monovinyl chlorophyll *a* from divinyl chlorophyll *a*, nor monovinyl chlorophyll *b* from divinyl chlorophyll *b*. This method, therefore, only provides concentration *estimates* for these co-eluting pigment pairs; methods for optically resolving monovinyl chlorophyll *a* and divinyl chlorophyll *a* are given below.

Divinyl chlorophyll *a*, the major photosynthetic pigment found in *Prochlorococcus,* accounts for 10 % to 60 % of the total chlorophyll *a* in subtropical and tropical oceanic waters (Goericke and Repeta 1993; Letelier *et al.* 1993; Andersen *et al.* 1996; Bidigare and Ondrusek 1996; Gibb *et al.* 2000). Divinyl chlorophyll *a* is spectrally different from *normal* (monovinyl) chlorophyll *a* and its presence results in a significant overestimation of total chlorophyll *a* concentration as determined by the conventional HPLC methods (Goericke and Repeta 1993; Letelier *et al.* 1993; Latasa *et al.* 1996). To avoid these errors, it is recommended that monovinyl and divinyl chlorophyll *a* be spectrally resolved, or chromatographically separated, to obtain an unbiased determination of total chlorophyll *a* for ground-truthing satellite ocean color algorithms and imagery. Total chlorophyll *a*, TChl *a*, is the sum of divinyl chlorophyll *a*, monovinyl chlorophyll *a*, chlorophyllide *a*, and chlorophyll *a* epimers and allomers. These co-eluting chlorophyll species can be resolved spectrally following C_{18} HPLC chromatography (Wright *et al.* 1991) and quantified using dichromatic equations at 436 nm and 450 nm (Latasa *et al.* 1996). Alternatively, these two chlorophyll species can be separated chromatographically and individually quantified using C_8 HPLC techniques (see below).

The protocols specified below for HPLC pigment analyses follow closely those prescribed in the *JGOFS Core Measurement Protocols* (UNESCO 1994). Both sets of protocols include:

1. Use of Whatman GF/F glass fiber filters, approximately 0.7 μm pore size;
2. Extraction in aqueous acetone; and
3. Calibration with standards.

The present protocols differ from the JGOFS protocols in one critical respect. Absorption of light in seawater, or any other medium, is a volumetric process, even though the volume absorption coefficient may vary with the density of the medium. For ocean color and optical analyses, therefore, the concentrations in seawater of all phytoplankton pigments shall be expressed in units of mass per unit volume of seawater (μg L^{-1} or mg m^{-3}). This differs from the JGOFS protocols, which specify that concentrations in seawater of all phytoplankton pigments should be expressed in ng Kg^{-1}.

In addition to HPLC analyses, it is recommended that the standard fluorometric methodology used for measuring chlorophylls and pheopigments (Holm-Hansen *et al.* 1965, Strickland and Parson 1972) also be applied to the same extracted pigment samples used for HPLC analysis. Protocols for fluorometric measurements of chlorophyll *a* and pheopigments are given here in Chapter 3 of the present volume. For a more in depth review of guidelines for measuring phytoplankton pigments in oceanography see Jeffrey *et al.* (1997)

2.2 SAMPLING PROTOCOLS FOR PHYTOPLANKTON PIGMENTS

Water Samples

Water samples should be taken using, *e.g*., Niskin bottles at the site of, and simultaneously with, the surface in-water upwelled radiance and reflectance measurements, and at depth increments sufficient to resolve variability within at least the top optical depth. The $K(z,\lambda)$, profiles over this layer will be used to compute optically weighted, near-surface pigment concentration for bio-optical algorithm development (Gordon and Clark 1980).

When possible, samples should be acquired at several depths distributed throughout the upper 200 m of the water column [or in turbid water, up to seven diffuse attenuation depths, *i.e.* $\ln(E(z,\lambda)/E(z,\lambda))=7$, to provide a basis for relating fluorescence signals to pigment mass concentrations.

Samples should be filtered as soon as possible after collection. If processing must be delayed for more than an hour, hold the samples on ice, or in a freezer at 4°C, and protect them from exposure to light. For delays longer than several hours, the samples should be stored in liquid nitrogen. Use opaque sample bottles, because even brief exposure to light during sampling and/or storage might alter pigment values.

Filtration

Whatman GF/F glass fiber filters, with approximately 0.7 μm pore size, are preferred for removing phytoplankton from water. The glass fibers assist in breaking the cells during grinding, accommodate larger sample volumes, and do not form precipitates after acidification. Twenty-five mm diameter GF/F glass fiber filters should be used with vacuum (7-8 inches of mercury) or positive pressure (1-2 psi). Positive pressure filtration is recommended, because it filters larger volumes of water at reduced filtration times. The only problem with vacuum filtration is that unobservable air leaks may occur around the filtration holder, and as a result the pressure gradient across the filter is much less than what is indicated on the vacuum gauge. When positive filtration is used, any leakage around the filter holder results in observable dripping water.

Inert membrane filters, such as polyester filters, may be used when size fraction filtration is required. When this is done, it is recommended to also filter a replicate sample through a GF/F to determine the total concentration. Summing the various size-fractionated concentrations may not produce an accurate estimate of the total, because of the potential for cell disruption during filtration.

There has been an ongoing discussion of filter types and retention efficiencies for natural samples. Phinney and Yentsch (1985) showed the inadequacy of GF/F filters for retaining chlorophyll *a* in oligotrophic waters, as did Dickson and Wheeler (1993) for samples from the North Pacific. In response to Dickson and Wheeler (1993),

Chavez *et al.* (1995) compared samples collected in the Pacific Ocean using GF/F and 0.2 μm membrane filters with small filtered volumes (100 mL to 540 mL). Their results showed a very close agreement between the two filter types, with GF/F filters having only a slightly positive 5 % bias.

Filtration volume can directly affect the retention efficiency for GF/F filters. Particles can be retained by filters through a variety of ways, such as filter sieving, filter adsorption, electrostatic and van der Waals attractions (Brock, 1983). When water flows through the pores of a Nuclepore filter, streamlines are formed that can align small particles longitudinally, with the result that cell diameter becomes important with these filters. It is known, on the other hand, that Whatman GF/F filters can retain particles much smaller than their rated pore size. Generally, at small volumes (100 mL to 300 mL) filter adsorption, and electrostatic and van der Waals attractions are important, whereas at larger volumes (>2,000 mL) sieving dominates. This has been tested in oligotrophic waters off Hawaii in which small (<500 mL) and large volumes (> 2 L to 4 L) retained similar amounts of chlorophyll *a* on the two types of filters, whereas for intermediate sample volumes the GF/F filters showed lower concentrations. During several cruises off the Hawaiian Islands, differences in retention efficiencies were found for GF/F filters to be a function of sample volume; large sample volumes (2 L and 4 L) retained about 18 % more chlorophyll *a* than replicate 1 L samples.

Filtration volumes are usually limited by the concentration of particles present in each sample. For HPLC analysis it is important to filter as large a volume as possible, so as to accurately measure most of the major pigments. A qualitative check to determine whether a large enough volume has been filtered is to count the number of accessory pigments (chlorophylls b, c_1, c_2, c_3, and carotenoids) quantified, excluding chlorophyll degradation products (Trees *et al*. 2000). Most algal groups (excluding phycobiliprotein-containing groups) contain at least *four* HPLC-measurable accessory pigments (see Jeffrey *et al*. 1997). Therefore, pigment samples that do not meet this minimum accessory pigment criterion may have detection limit problems related to low signal-to-noise ratios for the HPLC detectors and/or inadequate concentration techniques (*e.g.* low filtration volumes). It is generally recommended that the following volumes be filtered for HPLC pigment analyses: 3 L to 4 L for oligotrophic waters, 1 L to 2 L for mesotrophic waters, and 0.5 L to 1 L for eutrophic waters.

It is recommended to not pre-filter seawater samples to remove large zooplankton and particles, because this practice may exclude pigment-containing colonial and chain-forming phytoplankton, such as diatoms and *Trichodesmium* sp. Forceps may be used to remove large zooplankton from the GF/Fs following filtration.

Sample Handling and Storage

Samples should be filtered as quickly as possible after collection and stored immediately in liquid nitrogen. Liquid nitrogen is the best method for storing samples with minimum degradation for short, as well as, longer storage times (*e.g.* 1 year). Placing samples in liquid nitrogen also assists in pigment extraction by weakening the cell wall and membrane during this rapid temperature change. Ultra-cold freezers (-90 ^{o}C) can be used for storage, although they have not been tested for longer than 60 days (Jeffrey *et al*. 1997). Conventional deep freezers should not be used for storing samples more than 20 hours before transferring them to an ultra-cold freezer, or liquid nitrogen. Again, storage of samples in liquid nitrogen immediately after filtration is the preferred method.

Samples should be folded in half with the filtered halves facing in. This eliminates problems of rubbing particles off the filter during placement in sample containers and storage.

It is strongly recommended to use aluminum foil wrappings for sample containers. This simple, but effective, container is both inexpensive and easy to use. Cut small pieces of heavy-duty aluminum foil into approximately 4 cm squares. Fold each piece in half, and using a fine-point permanent marker, write a short sample identifier (*e.g.* first letter of the cruise and a sequential sample number) on the foil. Writing on the folded foil, prior to placement of the filter, both avoids puncturing the foil with the marking pen, and improves the legibility of the sample identifier. Place the folded filter in the aluminum foil. Fold the three open sides to form an envelope that is only slightly larger than the folded filter (~3 cm x 1.5 cm).

The use of foil containers minimizes the size requirement of the storage container. It is also acceptable to use either cryogenic tubes, or HistoPrep tissue capsules, but they occupy more storage volume per sample, and they are more expensive than aluminum foil. If fluorometric analysis is to be done soon after collection, it is still recommended to place the samples in liquid nitrogen to assist in pigment extraction, and on removal from the liquid nitrogen to place them immediately in chilled 90 % acetone.

Recordkeeping

Information regarding sample identification should be logged in a laboratory notebook with the analyst's initials. For each filter sample record the sample identifier (as written on the sample container), station number for the cruise, water volume filtered (V_{FILT}) in mL, and depth of the water sample, together with the date, time, latitude, and longitude of the bottle cast during which the sample was acquired.

2.3 LABORATORY METHODS FOR HPLC PHYTOPLANKTON PIGMENT ANALYSIS

Internal Standard and Solvent Preparation

In addition to daily calibration of the HPLC system with external standards, an internal standard (*e.g.* canthaxanthin) should be used to determine the extraction volume. It is important to verify that the internal standard employed is not a *naturally* occurring analyte in the field samples to be analyzed by HPLC. Canthaxanthin is recommended as an internal standard because it has a restricted distribution in ocean waters, and it is readily available in high purity from commercial sources. For additional background on the use of internal standards see Snyder and Kirkland (1979). The internal standard should be added to the sample prior to extraction and used to correct for the addition of GF/F filter-retained seawater and sample volume changes during extraction. When new external and internal standards are prepared they should be verified against previous standards and a standard reference solution if available. An internal standard with an HPLC peak removed from those of all the pigments, canthaxanthin, is added at a fixed concentration to the HPLC-grade acetone solvent used to extract the pigments from the filtered samples. A sample of canthaxanthin spiked acetone solvent is injected into the HPLC system and its peak area $A_{\mathrm{STD}}^{\mathrm{Cantha}}$ is recorded to provide a baseline internal standard for monitoring the solvent concentration in each extracted sample.

Extraction

Filters are removed from the liquid nitrogen, briefly thawed (~1 min), and placed in glass centrifuge tubes for extraction in acetone. Three mL HPLC-grade acetone is added to each tube, followed by the addition of a fixed volume of internal standard (typically 50 μL canthaxanthin in acetone). Alternatively, canthaxanthin spiked HPLC-grade acetone solvent may be prepared in advance, in a batch large enough for all samples, and 3 mL is added to each tube in a single step. Since GF/F filters retain a significant amount of seawater following filtration (ca. 0.2 mL per 25 mm filter), the final acetone concentration in the pigment extracts is ~ 94 % (acetone:water, by volume); by measuring the canthaxanthin peak area $A_{\mathrm{STD}}^{\mathrm{Cantha}}$ for each sample, the ratio $A_{\mathrm{STD}}^{\mathrm{Cantha}} \big/ A_{\mathrm{Sample}}^{\mathrm{Cantha}}$ may be used to adjust for sample to sample variations in the extraction volume.

Samples are disrupted by sonication, placed in a freezer, and allowed to extract at 0^{o}C for 24 h. Alternatively, the cells can be mechanically disrupted using a glass/Teflon tissue grinder and allowed to extract at 0^{o}C for 24 h. If after disrupting the cells, it is necessary to rinse the tissue grinder, or mortar and pestle, then a known volume of 90 % acetone, measured using a Class A volumetric pipette, should be used. The ease with which the pigments are removed from the cells varies considerably with different phytoplankton. In all cases, freezing the sample filters in liquid nitrogen improves extraction efficiency.

Prior to analysis, pigment extracts are vortexed and centrifuged to minimize cellular debris. To remove fine glass fiber and cellular debris from the extract, as well as enhance the life expectancy of the HPLC column, filter the extract through 13 mm PTFE (polytetrafluoroethylene) membrane syringe filters (0.2 μm pore size). The use of Nylon filters is not recommended as they may bind certain hydrophobic pigments.

Apparatus

The HPLC system consists of solvent pumps, sample injector, guard and analytical columns, absorption (and fluorescence) detector, and a computer. A temperature-controlled autosampler is optional, but highly recommended, to chill the samples chilled prior to injection and to reduce uncertainties during sample preparation and injection. A variety of companies manufacture HPLC systems (*e.g.* Agilent Technologies, Beckman, ThermoQuest, Waters

Associates). For a review of hardware and software requirements for measuring chlorophylls and their degradation products, as well as carotenoids, see Jeffrey *et al.* (1997).

HPLC Eluants and Gradient Programs

There are several currently recognized HPLC methods for separating chlorophylls, chlorophyll derivatives and taxonomically important carotenoids. The C_{18} method of Wright *et al.* (1991) is recommended by SCOR and separates more than 50 chlorophylls, carotenoids, and their derivatives using a ternary gradient system. This HPLC method is described in detail below. The separation of the various pigments requires about 30 minutes. Prior to injection, 1000 µL of the aqueous acetone pigment extract is diluted with 300 µL HPLC-grade water to increase the affinity of pigments for the column during the loading step. This procedure results in sharper peaks, allowing greater loading than can be obtained with undiluted samples.

This method does not separate monovinyl and divinyl chlorophylls *a* and *b*. The presence of divinyl chlorophylls *a* and *b*, can cause errors if they are not separated either physically on the column, or by a channels ratio method from the monovinyl forms. Latasa *et al.* (1996) showed that the use of a single response factor (only for monovinyl chlorophyll *a*) could result in a 15 % to 25 % overestimation of total chlorophyll *a* concentration if divinyl chlorophyll *a* was present in significant concentrations. Although monovinyl and divinyl chlorophyll *a* co-elute, each compound absorbs differently at 436 nm and 450 nm and it is therefore possible to deconvolve the absorption signals due to these pigments (Latasa *et al.* 1996).

Alternatively, these two chlorophyll species can be separated chromatographically and individually quantified using the C_8 HPLC techniques described by Goericke and Repeta (1993) and Van Heukelem and Thomas (2001). The latter technique uses a two solvent system and elevated column temperature to achieve desired separations.

Regardless of the method or column-packing material used (C_{18} or C_8), it is important that HPLC performance be validated before and during use. This would include validation that resolution between peaks is acceptable, or when peaks are not chromatographically resolved, that equations based on spectral deconvolution are possible in order to quantify relative proportions of each pigment in a co-eluting pair.

Determination of Algal Chlorophyll and Carotenoid Pigments by HPLC (Wright et al. 1991):

a. Equipment and reagents:

1. *Reagents*: HPLC grade acetone (for pigment extraction); HPLC-grade water, methanol, acetonitrile and ethyl acetate; 0.5 M ammonium acetate aq. (pH = 7.2); and BHT (2,6-di-tert-butyl-p-cresol, Sigma Chemical Co.).
2. *High-pressure injector valve* equipped with a 200µL sample loop.
3. *Guard-column* (50 mm x 4.6 mm, ODS-2 Spherisorb C_{18} packing material, 5 µm particle size) for extending the life of the primary column.
4. *Reverse-phase HPLC column* with end capping (250 mm x 4.6 mm, 5 µm particle size, ODS-2 Spherisorb C_{18} column).
5. *Variable wavelength or filter absorbance detector* with low volume flow through cell. Detection wavelengths are 436 nm and 450 nm.
6. *Data recording device*: a strip chart recorder, or preferably, an electronic integrator and computer equipped with hardware and software for chromatographic data analysis.
7. *Glass syringe (500 µL) or HPLC autosampler.*
8. *HPLC Solvents*: solvent A (80:20, by volume; methanol:0.5 M ammonium acetate aq., pH=7.2; 0.01 % BHT, w:v), solvent B (87.5:12.5, by volume; acetonitrile:water; 0.01 % BHT, w:v) and solvent C (ethyl acetate). Solvents A and B contain BHT to prevent the formation of chlorophyll *a* allomers. Use HPLC-grade solvents. Measure volumes before mixing. Filter solvents through a solvent resistant 0.4 µm filter before use, and degas with helium, or an in-line vacuum degassing system, during analysis.

9. *Calibration standards*: Chlorophylls *a* and *b* and β, and β-carotene can be purchased from Sigma Chemical Co. (St. Louis, MO 63178, USA). Other pigment standards can be purchased from the International Agency for ^{14}C Determination, VKI Water Quality Institute, Agern Allé 11, DK-2970 HØrsholm, Denmark. The concentrations of all standards in the appropriate solvents should be determined, using a monochromator-based spectrophotometer, prior to calibration of the HPLC system (Latasa *et al.* 1999). Spectrophotometric readings should be made at a bandwidth ≤ 2 nm and the optical density (*OD*) of the pigment standards should range between 0.2 to 0.8 OD units at λ_{max} (Marker *et al.* 1980). The recommended extinction coefficients for the various phytoplankton pigments can be found in Appendix E of Jeffrey *et al.* (1997). Absorbance is measured in a 1 cm cuvette at the peak wavelength λ_{max}, and at 750 nm to correct for light scattering.

10. Concentrations of the standards are calculated as

$$C^i_{\mathrm{STD}} = \frac{10^6[A^i(\lambda^i{}_{\mathrm{max}}) - A^i(750)]}{bE^i_{\mathrm{1cm}}}, \tag{2.1}$$

where C^i_{STD} is the concentration (µg L^{-1}) of the standard for pigment *i*, $A^i\left(\lambda^i{}_{\mathrm{max}}\right)$ and $A^i(750)$ are absorbances at $\lambda^i{}_{\mathrm{max}}$ and 750 nm, respectively, *b* is the pathlength of the cuvette (cm), and E^i_{1cm} is the weight-specific absorption coefficient (L g^{-1} cm^{-1}) of pigment *i*. Values for $\lambda^i{}_{\mathrm{max}}$ and E^i_{1cm} are given in Appendix E of Jeffrey *et al.* (1997). Standards stored under nitrogen in the dark at -20^{o}C do not change appreciably over a one-month period, provided that they are stored in containers proven to prevent evaporation (*e.g.* glass or Teflon bottles/vials).

b. Procedure:

1. Set up and equilibrate the HPLC system with eluant A at a flow rate of 1 mL min^{-1}.

2. Calibrate the HPLC system using working standards prepared, on the day of use, by diluting the primary standard with the appropriate solvent (Jeffrey *et al.* 1997, Appendix E). When preparing calibration standards, one should only use dilution devices for which the precision and uncertainty have been validated with the solvent to be measured. Prepare at least 5 concentrations (µg L^{-1}) of working standards for each pigment spanning the concentration range appropriate for the samples to be analyzed.

3. For each working standard, mix 1000 µL with 300 µL of distilled water, shake, and equilibrate for 5 min prior to injection (diluting the standards and sample extracts with water increases the affinity of pigments for the column in the loading step, resulting in an improved separation of the more polar pigments). Rinse the sample syringe twice with 300 µL of the diluted working standard and draw 500 µL of the working standard into the syringe for injection. Place the syringe in the injector valve, overfilling the 200 µL sample loop 2.5-fold. To check for possible interferences in the extraction solvent and/or filter, prepare a blank by extracting a glass fiber filter in 90 % acetone, mixing 1000 µL of the 90 % acetone filter extract and 300 µL distilled water, and injecting the mixture onto the HPLC system. For each pigment *i*, plot absorbance peak areas (arbitrary system units) against working standard pigment masses (concentrations multiplied by injection volume). The HPLC system response factor F^i (area µg^{-1}) for pigment *i* is calculated as the slope of the regression of the peak areas of the parent pigment (plus areas of peaks for structurally-related isomers if present) against the pigment masses of the injected working standards (µg). Structurally related isomers (*e.g.* chlorophyll *a* allomer) contribute to the absorption signal of the standards and disregarding them will result in the over-estimation of analytes in sample extracts (Bidigare 1991).

4. Prepare pigment samples for injection by mixing a 1000 µL portion of the aqueous acetone pigment extract and 300 µL distilled water, shake, and equilibrate for 5 min prior to injection. Inject the sample onto the HPLC column. Samples that are pre-mixed with distilled water (or other injection buffer) should not be allowed to reside in autosampler compartments for extended durations, because hydrophobic pigments will precipitate out of solution (Mantoura *et al*. 1997).

For additional information regarding HPLC method implementation and injection conditions see Wright and Mantoura (1997).

5. Following injection of the sample onto the HPLC system, use the following solvent system program to separate the chlorophyll and carotenoid pigments: 0.0' (90%A, 10%B), 1.0' (100%B), 11.0' (78%B, 22%C), 27.5' (10%B, 90%C), 29.0' (100%B), and 30.0' (100%B). Degas solvents with helium or an in-line vacuum degassing system during analysis. It should be noted that method performance varies significantly between HPLC systems because of differences in dwell volume, equilibration time, and injection conditions. It is, therefore, recommended that analysts validate that desired peak separations are attained for pigment pairs of interest by calculating the peak resolution indices R_s as

$$R_s = \frac{2\left(t_{R2} - t_{R1}\right)}{w_{B1} + w_{B2}}, \tag{2.2}$$

where t_{R1} and t_{R2} are the retention times (min) of peaks 1 and 2, and w_{B1} and w_{B2} are the widths (min) of peaks 1 and 2 at their respective bases (Wright 1997). Peak separation values $R_s < 1.0$ are insufficient for accurate quantification of peak areas (Wright 1997).

6. Peak identities are routinely determined by comparing the retention times of sample peaks with those of pure standards. Peak identities can be confirmed spectrophotometrically by collecting eluting peaks from the column outlet (or directly with an on-line diode array spectrophotometer). Absorption maxima for the various phytoplankton pigments can be found in Part IV of Jeffrey *et al.* (1997).

7. Calculate individual pigment concentrations as

$$C^i_{\mathrm{Sample}} = \frac{A^i_{\mathrm{Sample}} V_{\mathrm{Extracted}} A^{\mathrm{Cantha}}_{\mathrm{STD}}}{F^i V_{\mathrm{Injected}} V_{\mathrm{Sample}} A^{\mathrm{Cantha}}_{\mathrm{Sample}}}, \tag{2.3}$$

where C^i_{Sample} is the individual pigment concentration (μg L^{-1}), A^i_{Sample} is the area of individual pigment peak for a sample injection, $V_{\mathrm{Extracted}}$ is the volume extracted (mL, to nearest 0.1 mL), V_{Injected} is the volume injected (mL, measured to the nearest 0.001 mL), V_{Sample} is the sample volume filtered (L, measured to the nearest 0.001 L), and the other coefficients are defined above.

8. This method is designed for the separation of chlorophyll and carotenoid pigments, but it is also capable of separating the major chlorophyll breakdown products.

9. The uncertainty of the HPLC method was assessed by performing triplicate injections of a mixture of phytoplankton and plant extracts; coefficients of variation (standard deviation/mean x 100 %) ranged from 0.6 % to 6.0 %. The use of an appropriate internal standard, such as canthaxanthin, will decrease the uncertainty.

2.4 QUALITY ASSURANCE PROCEDURES

Quality assurance procedures outlined here should be routinely employed to insure accurate, precise and representative results.

As a means of monitoring an instrument's performance, individual pigment response factors (F^i) should be charted as functions of time (Clesceri *et al.* 1998). These quality control graphs should be retained with the data analysis logbooks to document the quality of each data set.

A selected number of samples should be analyzed in duplicate (or triplicate) to assess representativeness and uncertainty in the method and instrumentation. In multi-ship/investigator studies, replicate samples should be collected and archived for future intercalibration checks.

Fortified samples should be analyzed as part of the quality assurance effort. Fortified samples are prepared in duplicate by spiking a sample with known quantities of the analytes of interest at concentrations within the range

expected in the samples. Fortified samples are used to assess the method's uncertainty in the presence of a typical sample matrix.

The method detection limit (*MDL*) for the analytes of interest can be determined by measuring seven replicate standard injections (Glaser *et al* 1981). The standard deviation S_c of the seven replicate measurements is calculated, and the *MDL* is computed as

$$MDL = t\left(6, 0.99\right) S_c . \qquad (2.4)$$

where $t\left(6, 0.99\right)$ is the Student's t value for a one-tailed test at the 99 % confidence level, with (N-1)=6 degrees of freedom. For this particular sample size (N=7) and the 99% confidence level, $t\left(6, 0.99\right) = 3.707$ (Abramowitz and Segun 1968, Table 26.10).

System and spiked blanks should be routinely analyzed. A system blank consists of a filter, reagents, and the glassware and hardware utilized in the analytical scheme. The system blank is quantified under identical instrumental conditions as the samples and is analyzed by appropriate quantitative methods. The system blank may not contain any of the analytes of interest above the *MDL* or corrective action must be taken. A spiked blank is defined as a system blank plus an authentic external standard containing the analytes of interest. Each set of samples should be accompanied by a spiked blank and is quantified under the same instrumental conditions as the samples.

2.5 PROTOCOL STATUS AND FUTURE DIRECTIONS FOR RESEARCH

Recent studies have identified the presence of novel bacterial phototrophs in coastal and oceanic waters. These include proteorhodopsin-containing *Bacteria* (Béjà *et al.* 2000, 2001) and aerobic anoxygenic phototrophic *Bacteria* (Kolber *et al.* 2000, 2001). Sequence analysis of BAC clone libraries prepared from Monterey Bay, Station ALOHA and the Southern Ocean revealed that numerous uncultivated members of the γ-*Proteobacteria* contain genes that code for proteorhodopsin. This membrane-bound pigment contains *trans*-retinal, absorbs at blue-green to green wavelengths, and functions as a light-driven proton pump. In an unrelated study, Kolber *et al.* (2000) used an infrared fast repetition rate (IRFRR) fluorometer to document the widespread occurrence of aerobic anoxygenic phototrophs (AAPs) in the world oceans. These microbes possess low amounts of bacteriochlorophyll *a* (λ_{max} = 358 nm, 581 nm and 771 nm) and unusually high levels of bacteriocarotenoids (λ_{max} = 454 nm, 465 nm, 482 nm and 514 nm). They require molecular oxygen for growth. One of us (RRB) has initiated HPLC pigment analysis of these latter clones and retinal-related compounds to determine if the Wright *et al.* (1991) method can be used for their separation and quantification.

REFERENCES

Abramowitz, A. and I.A. Segun, 1968: Handbook of Mathematical Functions, Dover, New York (5th Printing), 1046pp.

Andersen, R.A., R.R. Bidigare, M.D. Keller, and M. Latasa, 1996: A comparison of HPLC pigment signatures and electron microscopic observations for oligotrophic waters of the North Atlantic and Pacific Oceans. *Deep-Sea Res. II*, **43**, 517-537.

Béjà O, L. Aravind, E. V. Koonin, M. T. Suzuki, A. Hadd, L. P. Nguyen, S. B. Jovanovich, C. M. Gates, R. A. Feldman, J. L. Spudich, E. N. Spudich, and E. F. DeLong, 2000: Bacterial rhodopsin: Evidence for a new type of phototrophy in the sea. *Science*, **289**, 1902-1906.

Béjà, O., E. N. Spudich, J. L. Spudich, M. LeClerc, and E. F. DeLong, 2001: Proteorhodopsin phototrophy in the ocean. *Nature*, **411**, 786-789.

Bianchi, T. S., C. Lambert, and D. C. Biggs. 1995: Distribution of chlorophyll *a* and pheopigments in the northwestern Gulf of Mexico: a comparison between fluorometric and high-performance liquid chromatography measurements. *Bull. Mar. Science* **56** ,25-32.

Bidigare, R.R., 1991: Analysis of algal chlorophylls and carotenoids. In: *Marine Particles: Analysis and Characterization*, D.C. Hurd and D.W. Spencer, Eds., Am. Geophys. Union, Washington, DC, 119-123.

Bidigare, R.R., and M.E. Ondrusek, 1996: Spatial and temporal variability of phytoplankton pigment distributions in the central equatorial Pacific Ocean. *Deep-Sea Res. II*, **43**, 809-833.

Brock, T.D., 1983: *Membrane filtration: a user's guide and reference manual*. Science Tech., Madison, WI, 381 pp.

Chavez, F., K.R. Buck, R.R. Bidigare, D.M. Karl, D. Hebel, M. Latasa, L. Campbell, and J. Newton, 1995: On the chlorophyll *a* retention properties of glass-fiber GF/F filters. *Limnol. Oceanogr*., **40**, 428-433.

Clesceri, L.S., A.E. Greenberg, and A.D. Eaton (editors), 1998: Part 10000, Biological Examination, Section 1020 B. *in* Standard Methods for the Examination of Water and Wastewater. 20th ed. Balitmore (MD): American Public Health Association, American Water Works Association, Water Environment Federation.

Dickson, M.-L., and P.A. Wheller, 1993: Chlorophyll *a* concentrations in the North Pacific: Does a latitudinal gradient exist? *Limnol. Oceanogr*., **38**, 1813-1818.

Gibb, S.W, R.G. Barlow, D.G. Cummings, N.W. Rees, C.C. Trees, P. Holligan and D. Suggett, 2000: Surface phytoplankton pigment distribution in the Atlantic: an assessment of basin scale variability between 50^{o}N and 50^{o}S. Progress in Oceanography, **45** (3-4), 329-368.

Glaser, J.A., D.L. Foerst, G.D. McKee, S.A. Quave, and W.L. Budde, 1981: Trace analyses for wastewaters. *Environ. Sci. Technol.,* **15**, 1426-1435.

Goericke, R., and D.J. Repeta, 1993: Chlorophylls *a* and *b* and divinyl chlorophylls *a* and *b* in the open subtropical North Atlantic Ocean. *Mar. Ecol. Prog. Ser*., **101**, 307-313.

Gordon, H.R., and D.K. Clark, 1980: Remote sensing optical properties of a stratified ocean: an improved interpretation. *Appl. Optics*, **19**, 3,428-3,430.

Hoepffner, N., and S. Sathyendranath, 1992: Bio-optical characteristics of coastal waters: absorption spectra of phytoplankton and pigment distribution in the western North Atlantic. *Limnol. Oceanogr.* **37**,1660-1679.

Holm-Hansen, O., C.J. Lorenzen, R.W. Holmes, and J.D.H. Strickland, 1965: Fluorometric determination of chlorophyll. *J. du Cons. Intl. Pour l'Expl. de la Mer.,***30**, 3-15.

Jeffrey, S.W., and G.F. Humphrey, 1975: New spectrophotometric equations for determining chlorophylls *a*, *b*, c_1 and c_2 in higher plants, algae and natural phytoplankton. *Biochem. Physiol. Pflanzen*, **167**, 191-194.

Jeffrey, S.W., R.F.C. Mantoura, and S.W. Wright (eds.), 1997: *Phytoplankton Pigments in Oceanography*, Monographs on Oceanographic Methodology, UNESCO, 661 pp.

Kolber, Z. S., C. L. Van Dover, R. A. Niederman, and P. G. Falkowski, 2000: Bacterial photosynthesis in surface waters of the open ocean. *Nature*, **407**, 177-179.

Kolber, Z. S., F. G. Plumley, A. S. Lang, J. T. Beatty, R. E. Blankenship, C. L. VanDover, C. Vetriani, M. Koblizek, C. Rathgeber, and P. G. Falkowski, 2001: Contribution of aerobic photoheterotrophic bacteria to the carbon cycle in the ocean. *Science*, **292**, 2492-2495.

Latasa, M., R. R. Bidigare, M. E. Ondrusek, and M. C. Kennicutt II, 1996: HPLC analysis of algal pigments: A comparison exercise among laboratories and recommendations for improved analytical performance. *Mar. Chem*., ***51***, 315-324.

Latasa, M., R. R. Bidigare, M. E. Ondrusek, and M. C. Kennicutt II, 1999: On the measurement of pigment concentrations by monochromator and diode-array spectrophotometers. *Mar. Chem.,* **66**, 253-254.

Letelier, R.M., R.R. Bidigare, D.V. Hebel, M.E. Ondrusek, C.D. Winn, and D.M. Karl, 1993: Temporal variability of phytoplankton community structure at the U.S.-JGOFS time-series Station ALOHA (22^{0}45'N, 158^{0}W) based on HPLC pigment analysis. *Limnol. Oceanogr*., **38**, 1,420-1,437.

Mantoura, R.F.C., R.G. Barlow and E.J.H. Head, 1997: Simple isocratic HPLC methods for chlorophylls and their degradation products. Ch. 11 *in* Jeffrey, S.W., R.F.C. Mantoura, and S.W. Wright (editors), Phytoplankton pigment in oceanography: guidelines to modern methods. Vol. 10, Monographs on oceanographic methodology. UNESCO Publishing, 661 pp.

Marker, A.F.H., E.A. Nusch, H. Rai and B. Riemann, 1980: The measurement of photosynthetic pigments in freshwaters and standardization of methods: conclusion and recommendations. Arch. Hydrobiol. Beih. Ergebn. Limnol. **14**: 91-106.

Phinney, D.A., C.S. Yentsch, 1985: A novel phytoplankton chlorophyll technique: Toward automated analysis. *J. Plankton Res*., **7**, 633-642.

Smith, R. C., R. R. Bidigare, B. B. Prezelin, K. S. Baker, and J. M. Brooks, 1987: Optical characterization of primary productivity across a coastal front. *Mar. Biol*. **96**, 575-591.

Snyder, L.R. and Kirkland, J.J, 1979: Quantitative and trace analysis. In: Introduction to modern liquid chromatography, John Wiley and Sons, New York, 541-574.

Strickland, J.D.H., and T.R. Parsons, 1972: *A Practical Handbook of Sea Water Analysis,* Fisheries Research Board of Canada, 310 pp.

Tester, P. A., M. E. Geesey, C. Guo, H. W. Paerl, and D. F. Millie, 1995: Evaluating phytoplankton dynamics in the Newport River estuary (North Caroline, USA) by HPLC-derived pigment profiles. *Mar. Ecol. Prog. Ser*. **124**, 237-245.

Trees, C.C., M.C. Kennicutt II, and J.M. Brooks, 1985: Errors associated with the standard fluorometric determination of chlorophylls and pheopigments. *Mar. Chem*., **17**, 1-12.

Trees, C.C., D.C. Clark, R.R. Bidigare, M.E. Ondrusek and J.L. Mueller, 2000. Accessory pigments versus chlorophyll *a* concentrations within he euphotic zone: a ubiquitous relationship. *Limnol. Oceanogr.*, **45**(5): 1130-1143.

UNESCO, 1994: Protocols for the Joint Global Ocean Flux Study (JGOFS) Core Measurements, Manual and Guides **29**, 170pp.

Van Heukelem, L. and C.S. Thomas, 2001: Computer-assisted high-performance liquid chromatography method development with applications to the isolation and analysis of phytoplankton pigments. *J. Crom. A*. **910**:31-49.

Wright, S.W., S.W. Jeffrey, R.F.C. Mantoura, C.A. Llewellyn, T. Bjornland, D. Repeta, and N. Welschmeyer, 1991: Improved HPLC method for the analysis of chlorophylls and carotenoids from marine phytoplankton. *Mar. Ecol. Prog. Ser.,* **77**, 183-196.

Wright, S.W., 1997: Summary of terms and equations used to evaluate HPLC chromatograms. Appendix H *in* Jeffrey, S.W., R.F.C. Mantoura, and S.W. Wright (editors), Phytoplankton pigment in oceanography: guidelines to modern methods. Vol. **10**, Monographs on oceanographic methodology. UNESCO Publishing, 661 pp.

Wright, S.W., and R.F.C. Mantoura, 1997: Guidelines for selecting and setting up an HPLC system and laboratory. Ch. 15 *in* Jeffrey, S.W., R.F.C. Mantoura, and S.W. Wright (editors), Phytoplankton pigment in oceanography: guidelines to modern methods. Vol. **10**, Monographs on oceanographic methodology. UNESCO Publishing, 661 pp.

Chapter 3

Fluorometric Chlorophyll *a*: Sampling, Laboratory Methods, and Data Analysis Protocols

Charles C. Trees[1], Robert R. Bidigare[2], David M. Karl[2] Laurie Van Heukelem[3] and John Dore[2]

[1]*Center for Hydro-Optics & Remote Sensing, San Diego State University, California*
[2] *Department of Oceanography, University of Hawaii, Hawaii*
[3]*Horn Point Laboratory, University of Maryland Center for Environmental Science, Horn Point, Maryland*

3.1 INTRODUCTION

In addition to HPLC analyses, it is recommended that the standard fluorometric methodology used for measuring chlorophylls and pheopigments also be applied to (i) the same extracted pigment samples used for HPLC analysis, and (ii) additional independent samples. Analysis of fluorometric chlorophyll *a* concentration is a far simpler procedure than HPLC analysis, especially at sea. On a given research cruise, therefore, it is economically feasible to acquire and process many more fluorometric than HPLC samples and to statistically relate fluorometric and HPLC chlorophyll *a* concentrations using linear regression analysis. This additional analysis will also enable a direct link to the historical bio-optical algorithms and database development during the CZCS validation experiments.

Protocols for fluorometric determination of the concentrations of chlorophyll and pheopigments were developed initially by Yentsch and Menzel (1963) and Holm-Hansen *et al.* (1965), and are described in detail by Strickland and Parsons (1972). Holm-Hansen *et al*. (1965) and Strickland and Parsons (1972) used first principles of fluorescence spectroscopy to derive these fluorometric equations. The equation proposed by Yentsch and Menzel (1963) is only indirectly linked to first principles, through debatable assumptions, and its use is not recommended. Although these measurements have been shown to contain errors as compared to HPLC determinations (Trees *et al*. 1985; Smith *et al*. 1987; Hoepffner and Sathyendranath 1992; Bianchi *et al*. 1995; Tester *et al*. 1995), the CZCS phytoplankton pigment concentration algorithms were based on them entirely. The SeaWiFS protocols for this analysis will be those given in Strickland and Parsons (1972) as updated by this chapter.

Pigment databases generally show a log-normal distribution, which is consistent with that proposed by Campbell (1995) for bio-optical properties. Therefore, it is appropriate to perform log-linear regressions on HPLC determined total chlorophyll *a* (chlorophyllide *a*, chlorophyll *a* epimer, chlorophyll *a* allomer, monovinyl chlorophyll *a* and divinyl chlorophyll *a*) and fluorometrically determined chlorophyll *a*, using model I regressions. Standard Model I regressions were selected because HPLC determined total chlorophyll *a* concentrations are to be predicted from fluorometrically determined chlorophyll [Model I regressions are appropriate for both predictions and determining functional relationships, whereas Model II regressions should not be used to predict values of y given x (page 543, Sokal and Rohlf 1995)].

Examples of regression models predicting log HPLC total chlorophyll *a* (following Chapter 2 HPLC protocols) from log fluorometric chlorophyll *a* are shown in Figures 3.1, 3.2, and 3.3 for three cruises in different geographic areas. In each example, the regression slopes are significantly different from a one-to-one relationship, although for the Gulf of California (GoCAL November 1996, Figure 3.3) the slope is close to unity. One-to-one ratios have also been found for other geographic areas, but not necessarily during all seasons. Therefore, the relationship (slope and offset) between HPLC total chlorophyll *a* and fluorometric chlorophyll *a* must be determined for a selected number of samples for each cruise, so that a cruise-specific scaling factor can be applied to other fluorometric samples.

The protocols specified below for fluorometric chlorophyll *a* analyses follow closely those prescribed in the *JGOFS Core Measurement Protocols* (UNESCO 1994), but they differ in one important respect. Absorption of light in seawater, or any other medium, is a volumetric process, even though the volume absorption coefficient may

vary with the density of the medium. For ocean color and optical analyses, therefore, the concentration of chlorophyll *a* shall be expressed in units of mass per unit volume of seawater, either in $\mu g\ L^{-1}$, or $mg\ m^{-3}$. This differs from the JGOFS protocols, which specify that concentrations in seawater of chlorophyll a and pheopigments should be expressed in $\mu g\ kg^{-1}$.

3.2 SAMPLE ACQUISITION AND STORAGE

Water samples should be taken using, *e.g.*, Niskin bottles at the site of, and simultaneously with, the surface in-water upwelled radiance and reflectance measurements, and at depth increments sufficient to resolve variability within at least the top optical depth.

The K(z), profiles over this layer will be used to compute optically weighted, near-surface pigment concentration for bio-optical algorithm development (Gordon and Clark 1980). When possible, samples should also be acquired at several depths distributed throughout the upper 200 m of the water column [or in turbid water, up to seven diffuse attenuation depths, *i.e.* ln(E(0)/E(z))=7, to provide a basis for relating fluorescence signals to pigment mass concentration.

Samples should be filtered as soon as possible after collection. If processing must be delayed for more than an hour, hold the samples on ice, or in a freezer at $4^{o}C$, and protect them from exposure to light. For delays longer than several hours, the samples should be stored in liquid nitrogen. Use opaque sample bottles, because even brief exposure to light during sampling and/or storage might alter pigment values.

Filtration

Whatman GF/F glass fiber filters, with approximately 0.7 μm pore size, are preferred for removing phytoplankton from water. The glass fibers assist in breaking the cells during grinding and no precipitate forms after acidification. Twenty-five mm diameter GF/F glass fiber filters should be used with a vacuum or positive pressure with a pressure differential equivalent to 180-200 mm of mercury. Large filtration volumes are not required, because of the increased sensitivity of the fluorescence measurement.

Inert membrane filters, such as polyester filters, may be used when size fraction filtration is required. When this is done, it is recommended to also filter a replicate sample through a GF/F to determine the total concentration. Summing the various size-fractionated concentrations may not produce an accurate estimate of the total, because of the potential for cell disruption during filtration.

There has been an ongoing discussion on filter types and retention efficiencies for natural samples. Phinney & Yentsch (1985) showed the inadequacy of GF/F filters for retaining chlorophyll *a* in oligotrophic waters, as did Dickson and Wheeler (1993) for samples from the North Pacific. In response to Dickson and Wheeler (1993), Chavez *et al*. (1995) compared samples collected in the Pacific Ocean using GF/F and 0.2 μm membrane filters with small filtered volumes (100-540 mL). Their results for small volumes showed a very close agreement between the two filter types with GF/F filters having only a slightly positive 5% bias.

Filtration volume can directly affect the retention efficiency for GF/F filters. Particles can be retained by filters through a variety of ways, such as filter sieving, filter adsorption, electrostatic and van der Waals attractions (Brock, 1983). When water flows through the pores of a Nuclepore filter, streamlines are formed that can align small particles longitudinally, with the result that cell diameter becomes important with these filters. It is known, on the other hand, that Whatman GF/F filters can retain particles much smaller than their rated pore size. Generally, at small volumes (100-300 mL) filter adsorption, and electrostatic and van der Waals attractions are important, whereas at larger volumes (> 2,000 mL) sieving dominates. This has been tested in oligotrophic waters off Hawaii in which small (< 500 mL) and large volumes (> 2-4 liters) retained similar amounts of chlorophyll *a* on the two types of filters, whereas for intermediate sample volumes the GF/F filters showed lower concentrations. As a general rule, it is recommended that the following volumes be filtered for these water types: 0.5-1.0 liter for oligotrophic, 0.2-0.5 liter for mesotrophic, and 0.1 liter and less for eutrophic water.

It is recommended to not pre-filter seawater samples to remove large zooplankton and particles, because this practice may exclude pigment-containing colonial and chain-forming phytoplankton, such as diatoms and *Trichodesmium* sp. Forceps should be used to remove large zooplankton from the GF/Fs following filtration.

Sample Handling, and Storage

Samples should be filtered as quickly as possible after collection, and the filters stored immediately in liquid nitrogen. Liquid nitrogen is the best method for storing filter samples with minimum degradation for short, as well as, longer storage times (*e.g.* 1 year). Placing samples in liquid nitrogen also assists in pigment extraction by weakening the cell wall and membrane during this rapid temperature change. Ultra-cold freezers (-90^{o}C) can be used for storage, although they have not been tested for longer than 60 days (Jeffrey *et al*. 1997). Conventional deep freezers should not be used for storing samples more than 20 hours before transferring them to an ultra-cold freezer, or liquid nitrogen.

Again, storage of samples in liquid nitrogen immediately after filtration is the preferred method. The addition of $MgCO_3$ at the end of the filtration process to stabilize chlorophyll has not been used for many years as a routine oceanographic method, because of the uncertainty in pigment absorption by $MgCO_3$.

If samples are to be stored for any length of time prior to fluorometric analysis, they should be folded in half with the filtered halves facing in. This eliminates problems of rubbing particles off the filter during placement in sample containers and storage.

It is strongly recommended to use aluminum foil wrappings for sample containers. This simple, but effective, container is both inexpensive and easy to use. Cut small pieces of heavy-duty aluminum foil into approximately 4 cm squares. Fold each piece in half, and using a fine-point permanent marker, write a short sample identifier (*e.g.* first letter of the cruise and a sequential sample number) on the foil. Writing on the folded foil, prior to placement of the filter, both avoids puncturing the foil with the marking pen, and improves the legibility of the sample identifier. Place the folded filter in the aluminum foil. Fold the three open sides to form an envelope that is only slightly larger than the folded filter (~3cm x 1.5cm).

The use of foil containers minimizes the size requirement of the storage container. It is also acceptable to use either cryogenic tubes, or HistoPrep tissue capsules, but they occupy more storage volume per sample, and they are more expensive than aluminum foil. If fluorometric analysis is to be done soon after collection, it is still recommended to place the samples in liquid nitrogen to assist in pigment extraction, and on removal from the liquid nitrogen toplace them immediately in chilled 90% acetone.

Recordkeeping

Information regarding sample identification should be logged in a laboratory notebook with the analyst's initials. For each filter sample record the sample identifier (as written on the sample container), station number for the cruise, water volume filtered (V_{FILT}) in mL, and depth of the water sample, together with the date, time, latitude, and longitude of the bottle cast during which the sample was acquired.

3.3 LABORATORY METHODS FOR FLUOROMETRIC DETERMINATION OF CHL. *a* AND PHEOPIGMENT CONCENTRATIONS

Chlorophyll and pheopigments can be determined using either a Turner Designs (or Sequoia) fluorometers equipped with the standard light sources and Corning excitation and emission filters, following the manufacture's recommendation for measuring extracted chlorophyll. The fluorometric instrument should be warmed-up for at least 30 to 45 minutes prior to making measurements.

Because of the acidification requirement for the standard fluorometric method (Holm-Hansen *et al.* 1965), differences in excitation and emission wavelength bands between fluorometers can produce uncertainties (Trees *et al.* 1985). The sensitivity with which a particular instrument is able to differentiate between chlorophyll and pheopigment is a function of the excitation wavelength. This effect is measured during calibration of the fluorometer and is called the tau factor (τ). Saijo and Nishizawa (1969) have shown that τ can vary from 1 to 11.5, depending upon the excitation wavelength (in the range between 410 nm and 440 nm). For example, a comparison between a Turner Designs (Model 10-005R) analog fluorometer and a Turner Designs (Model 10-AU-005) digital fluorometer showed statistically significant differences for 42 oceanic samples (slope = 1.06), even though both were calibrated with exactly the same standards (Figure 3.4). The departure from a unit slope is attributable to differences in the excitation bands for the two fluorometers.

Fluorometer Calibrations

Bench fluorometers used to measure concentrations of extracted chlorophyll and pheopigments should be calibrated using authentic chlorophyll *a* standards, as prescribed also in the HPLC Protocols (Chapter 2). Chlorophyll *a* standards can be purchased from Sigma Chemical Co. (St. Louis, MO 63178, USA).

If a fluorometer has been shipped for a cruise, or if it has been unused for several weeks, it is strongly recommended that it be recalibrated with an authentic chlorophyll *a* standard. The use of solid standards, like those provided by Turner Designs and other manufacturers, can only provide a check for instrumental drift. They cannot be used as primary pigment standards. However, the solid standard should be used at frequent intervals during each day's analyses to monitor instrument drift.

The concentration of the chlorophyll *a* standard, in the appropriate solvent, must be determined using a monochromator-based spectrophotometer prior to calibrating the fluorometer. The recommended extinction coefficients for chlorophyll *a* in several solvents can be found in Appendix E of Jeffrey et al. (1997). Absorbance is measured in a 1 cm cuvette at the peak wavelength λ_{max}, and at 750 nm to correct for light scattering. The bandwidth of the spectrophotometer should be between 0.5 and 2 μm, with the standard concentration being such that the absorbance falls between 0.1 and 1.0 optical density units (Clesceri *et al.*, 1998a). The concentration of the standard is calculated as

$$C_{\mathrm{STD}} = \frac{10^6[A(\lambda_{\max}) - A(750)]}{bE_{1\mathrm{cm}}}, \tag{3.1}$$

where C_{STD} is the concentration (μg L^{-1}) of the chlorophyll *a* standard, $A(\lambda_{\max})$ and $A(750)$ are absorbances at $\lambda_{\max}$ and 750 nm, *b* is the pathlength of cuvette (cm), and $E_{1\mathrm{cm}}$ is the specific absorption coefficient (L g^{-1} cm^{-1}) of chlorophyll *a* in 90% acetone. For 90% acetone $E_{1\mathrm{cm}}$ =87.67 L g^{-1} cm^{-1}, and for 100% acetone $E_{1\mathrm{cm}}$ =88.15 L g^{-1} cm^{-1}, when applied to the absorption measured at the peak wavelength $\lambda_{\max}$ (Jeffrey *et al.* 1997, Appendix E). The peak wavelength $\lambda_{\max}$ must be determined by inspection of the measured spectrum, because its location may shift due to interactions between the particular solvent and mixture of pigment compounds in each sample. Standards stored under nitrogen in the dark at -20°C do not change appreciably over a one-month period, provided that they are stored in containers proven to prevent evaporation (*e.g.* glass or Teflon bottles/vials).

The stock chlorophyll *a* standard, with its concentration measured on a spectrophotometer as described above, should be diluted using calibrated gas-tight syringes, and Class A volumetric pipettes and flasks. The minimum number of dilutions of the stock standard for calibrating a fluorometer depends on whether it is a digital model (Turner Designs 10-AU-005), or it is an analog model with a mechanical mode for changing sensitivity (*e.g.* Turner Designs 10-005). A minimum of 5 dilutions is required for calibrating a digital fluorometer. Analog fluorometers with a variety of door settings, such as the Turner Designs Model 10-005, must be calibrated for each door setting using at least three standard concentrations per door. The diluted standard pigment concentrations used in calibrating the fluorometer must bracket the range of concentrations found in the samples being analyzed.

Each diluted chlorophyll *a* standard is placed in the fluorometer and the signal (F_b) is recorded, after waiting a short period of time (60 seconds) for it to stabilize. The standard is removed and diluted HCL acid (2 drops of 5 %, or 1 drop of 10 %, both concentrations by volume) is added and mixed within the test tube. The tube is then placed back into the fluorometer, and after stabilization, the acidified fluorescence signal (F_a) is recorded. Following acidification of the chlorophyll *a* standard, the fluorescence signal stabilizes relatively quickly. This is not the case for natural samples that contain a mixture of pigment compounds, however, and stabilization time may vary from sample to sample. Stabilization time has to be the same for both pigment standards and for natural samples. To minimize this source of uncertainty, and to standardize this measurement technique, it is recommended that both acidified natural sample and acidified pigment standards be allowed to react with the acid for one minute prior to recording the acidified fluorescence signal (F_a). Two drops of 5 % (by volume) hydrochloric acid is added to each of the pigment standards and natural samples. Once the acid is added, the sample in the test tube should be mixed by inverting the tube several times, using parafilm as a stopper. All fluorometric measurements for both pigment standards and natural samples should be carried out at room temperature. A 90 % (by volume) acetone blank (Blk_b) and an acidified acetone blank (Blk_a) should also be measured, even though the acidified blank (Blk_a) is frequently found to be equal to the non-acidified blank (Blk_b). The fluorometer's sensitivity to pheopigments, τ, is calculated as

$$\tau = \frac{F_{\mathrm{b}} - Blk_{\mathrm{b}}}{F_{\mathrm{a}} - Blk_{\mathrm{a}}}, \tag{3.2}$$

and is averaged over all concentrations of the chlorophyll *a* standard. For the mechanical door model fluorometers, data from the higher gain door settings will often become noisy and computed τ values will begin to decrease. These data should be excluded from the average. The fluorometer's response factor, F_{R} (μg L^{-1} per fluorescence signal), is determined as the slope of the simple linear regression equation

$$C_{\mathrm{STD}} = F_{\mathrm{R}}\left(F_{\mathrm{b}} - Blk_{\mathrm{b}}\right), \tag{3.3}$$

calculated for the sample of diluted concentrations of the pigment standard, and forcing a zero intercept. With a digital fluorometer, the regression analysis is applied to the data from the entire 5, or more, concentrations and a single F_R factor is determined for the instrument. With a mechanical fluorometer, the regression is applied to the data from the 3, or more, concentrations of the standard, and a separate F_R factor is determined, for each door setting. As a means of monitoring an instrument's performance, F_R factors from successive calibrations should be charted as functions of time (Clesceri *et al.*, 1998b). These quality control graphs should be retained with the data analysis logbooks to document the quality of each data set for which that fluorometer is used.

Solvent Preparation.

It is recommended that 90 % acetone (by volume) be used to extract pigments for the fluorometric analysis. Richard and Thompson (1952) were the first to propose 90 % acetone as a solvent to extract pigments from marine phytoplankton. Their results indicated improved extraction efficiencies, and also showed that the procedure minimized the activity of the naturally occurring chlorophyllase enzyme, which degrades the pigment. With a graduated cylinder, make up 90 % acetone by first pouring in distilled water, followed by 100 % acetone. Using volumetric pipettes, or auto-pipettes, accurately measure 8 mL to 10 mL of 90 % acetone and place it in a centrifuge tube. Record this volume as V_{EXT}. A number of such tubes containing acetone are then stored in a freezer and individually removed as filter samples are collected. Pre-chilling the solvent in this way reduces the possibility of temperature induced pigment degradation.

Extraction

Filters are removed from liquid nitrogen and placed in the chilled centrifuge tubes for extraction in V_{EXT} mL of 90% acetone. Samples are disrupted by sonication, placed in a freezer, and allowed to extract at 0^{o}C for 24 h. Alternatively, the cells can be mechanically disrupted using a glass/Teflon tissue grinder and allowed to extract at 0^{o}C for 24 h. If after disrupting the cells, it is necessary to rinse the tissue grinder, or mortar and pestle, then a known volume of 90% acetone, measured using a Class A volumetric pipette, should be used. The ease at which the pigments are removed from the cells varies considerably with different phytoplankton. In all cases, freezing the sample filters in liquid nitrogen improves extraction efficiency. Prior to analysis, pigment extracts are swirled into a vortex to remove particles from the sides of the tube, and then centrifuged to minimize cellular debris.

Measurement

Following the same measurement procedure described above under *Fluorometer Calibration*, each extracted sample is placed in the fluorometer and its non-acidified and acidified responses, Fb and Fa, are measured and recorded. The concentration of chlorophyll [Chl] (μg L^{-1}) in the sample is calculated as

$$\left[Chl\right] = \left(F_{\mathrm{b}} - F_{\mathrm{a}} - Blk_{\mathrm{b}} + Blk_{\mathrm{a}}\right)\frac{\tau}{\tau - 1}F_{\mathrm{R}}\frac{V_{\mathrm{EXT}}}{V_{\mathrm{FILT}}}, \tag{3.4}$$

and pheopigments concentration [Pheo] (μg L^{-1}) as

$$\left[Pheo\right] = \left\{\left(F_{\mathrm{a}} - Blk_{\mathrm{a}}\right)\tau - \left(F_{\mathrm{b}} - Blk_{\mathrm{b}}\right)\right\}\frac{\tau}{\tau - 1}F_{\mathrm{R}}\frac{V_{\mathrm{EXT}}}{V_{\mathrm{FILT}}}, \tag{3.5}$$

where volumes extracted V_{EXT} and filtered V_{FILT} are in mL. Pheopigment concentrations determined using the standard fluorometric method of Holm-Hansen *et al.* (1965) have not been reported in published articles for many years. This is based on the fact that (i) there is always a residual amount of pheopigments in all natural samples (Smith and Baker, 1978; 25% of the summed chlorophyll plus pheopigment), (ii) pheopigment concentrations are

overestimated in the presence of chlorophyll *b* (Lorenzen and Jeffrey, 1980; Vernet and Lorenzen, 1987), and (iii) HPLC measured pheopigments, generally contribute very little to the chlorophyll *a* pigment pool (*e.g.*, Hallegraeff, 1981; Everitt *et al.*, 1990; and Bricaud *et al.*, 1995). Trees *et al.* (2000a) assembled an extensive HPLC pigment database (5,617 samples) extending over a decade of sampling and analysis, and including a variety of environments ranging from freshwater to marine, oligotrophic to eutrophic, and tropical to polar, and found that the average pheopigment to chlorophyll *a* ratio was only 0.037. This global scale result emphasizes the problems associated with estimating pheopigments using the standard fluorometric method.

3.4 *In Situ* CHLOROPHYLL a FLUORESCENCE PROFILES

An *in situ* fluorometer should be employed to measure a continuous profile of chlorophyll fluorescence. The fluorometer should be mounted on the same underwater package as the water sampler, ideally together with a CTD, transmissometer and other inherent optical properties (IOP) sensors. In some cases it may be desirable to also include a radiometer on this package, if shading effects associated with the package and/or ship are not significant.

In situ fluorometers produce nearly continuous profiles of artificially stimulated fluorescence. Fluorometer data (in volts) should be corrected by subtracting an offset, determined by shading the instrument on deck. These unscaled fluorescence responses are adequate to provide guidance in K-profile analysis and interpretation.

To produce vertical continuous profiles of pigment concentration, HPLC-derived pigment concentrations from water samples taken at discrete depths may be interpolated, with the aid of *in situ* fluorescence profiles. These *fluorescence interpolated* profiles should then be used with $K_d(z,\lambda)$ profiles to compute the optically weighted average pigment concentration over the top attenuation length (Gordon and Clark 1980).

The A/D channel used to acquire and record signal voltages from the *in situ* fluorometer must be calibrated, and its temperature-dependent response to known voltage inputs characterized. The range dependent A/D bias coefficients should be determined at approximately 5^0 C intervals over the range from 0-25^0 C to characterize the temperature sensitivity of the data acquisition system.

Zero fluorescence offsets should be measured on deck before and after each cast; the optical windows should be shaded to avoid contamination of the zero offset value by ambient light. Before each cast, the fluorometer windows should be cleaned following the manufacturer's instructions.

3.5 PROTOCOL STATUS AND FUTURE DIRECTIONS FOR RESEARCH

In order to minimize interferences caused by the overlapping excitation and emission wavebands of chlorophylls *a, b, c* and pheopigments, Turner Designs (Sunnyvale, CA) manufactures the multi-spectral fluorometer TD-700. This instrument was recently tested using samples collected at the US JGOFS Hawaii Ocean Time-series Station ALOHA (22.75^{0}N, 158^{0}W). A set of replicate monthly (May - Dec 2000) pigment samples collected between the surface and 175 m were analyzed by HPLC using the protocols described in Chapter 2. Duplicate samples were subsequently analyzed in 100% acetone with the TD-700 using the manufacturer's calibration. The results of these comparisons are illustrated in Figures 3.5, 3.6 and 3.7 for chlorophylls *a*, *b*, and *c*, respectively. The Model I regression equations predicting each HPLC pigment (in mg m^{-3}) from the equivalent TD700 estimate are:

- HPLC Chl *a* = 0.729[TD-700 Chl *a*] + 0.0144; (r^2 = 0.894).
- HPLC Chl *b* = 0.607[TD-700 Chl *b*] – 0.0163; (r^2 = 0.816).
- HPLC Chl *c* = 1.083[TD-700 Chl *c*] – 0.00249; (r^2 = 0.906).

These equations differ significantly from a one-to-one relationship. The present comparisons differ also from those published in Trees *et al*. (2000a), although care must be used in this comparison since the concentrations were expressed there in ng L^{-1} (which accounts for the factor of 10^{-3} differences in the respective offset coefficients). These results call into question the stability of the fluorometer. It is also evident that the equations provided by the manufacturer must be verified with HPLC data, and that these calibration relationships should be reviewed frequently.

It is interesting and noteworthy that the TD-700 fluorometer did not detect pheopigments in any of the samples analyzed.

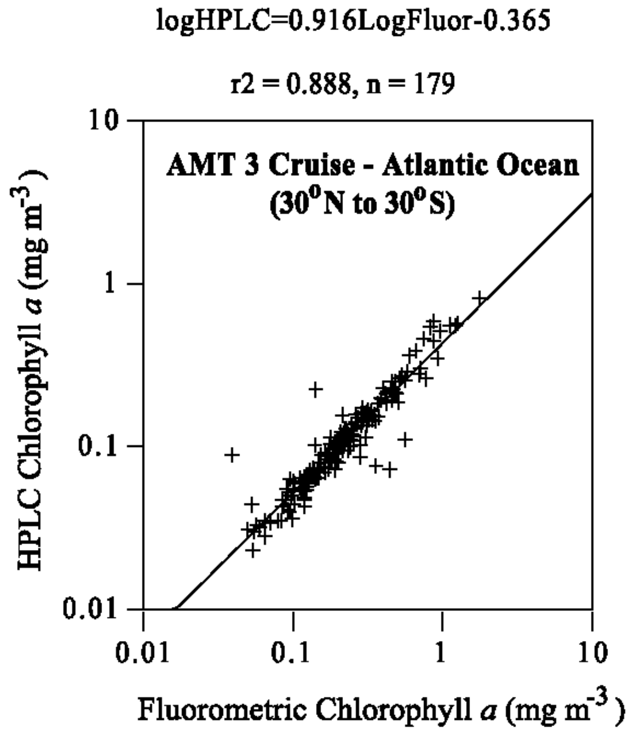

Figure 3.1: Comparisons between fluorometrically determined chlorophyll and HPLC determined total chlorophyll a (chlorophyllide a, chlorophyll a epimer, chlorophyll a allomer, monovinyl chlorophyll a, and divinyl chlorophyll a) from samples collected during Atlantic Meridional Transect 3 cruise (30°N to 30°S, October 1996).

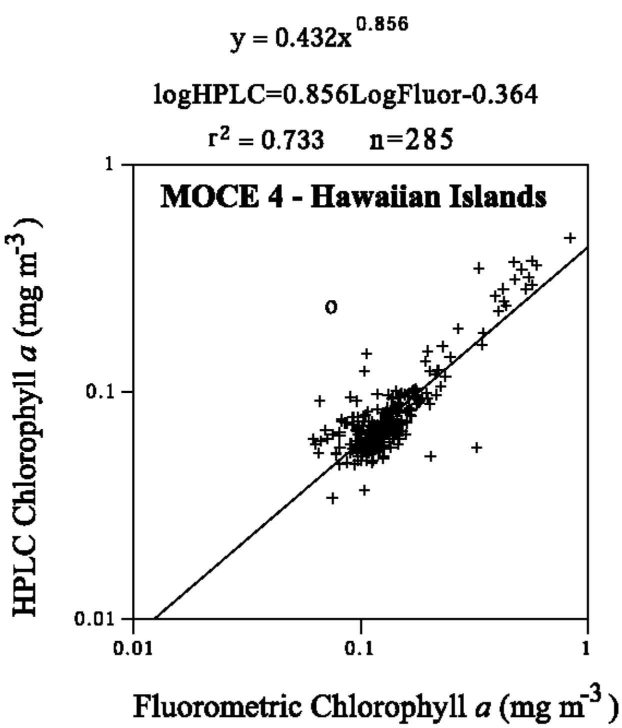

Figure 3.2: Same as Figure 3.1 for data collected during the Marine Optical Characterization Experiment (MOCE) 4 cruise.

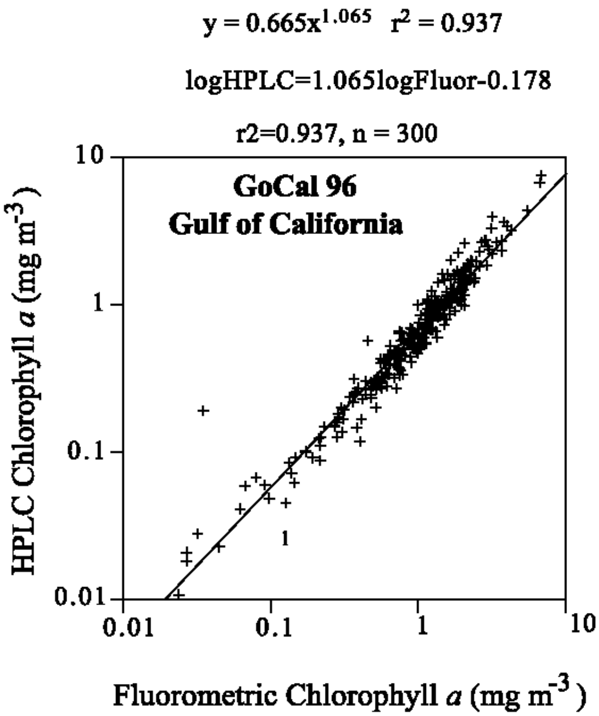

Figure 3.3: Same as Figure 3.1 for data collected during the Gulf of California cruise (Gulf of California, November 1996).

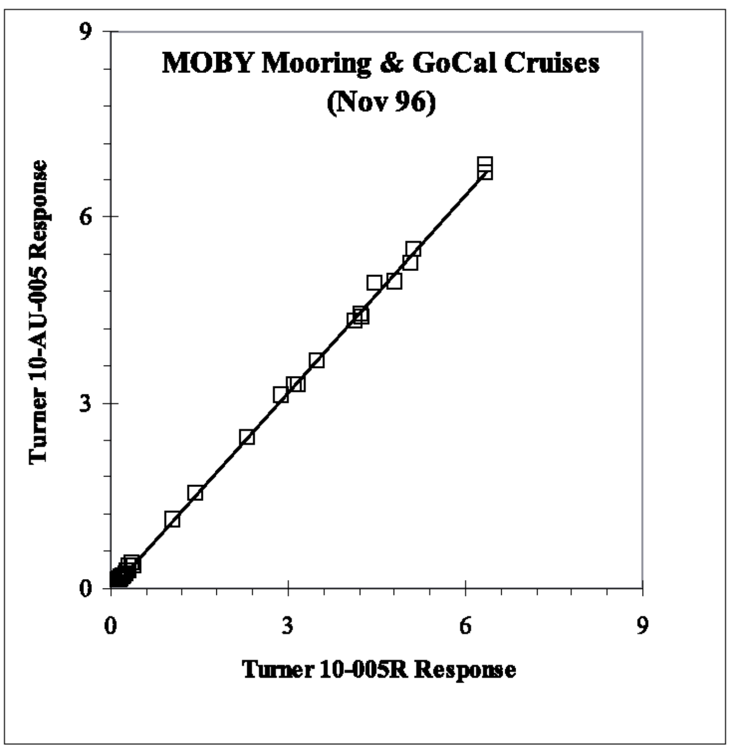

Figure 3.4: Comparison of fluorometrically determined chlorophyll a using the VisLab Turner Fluorometer (10-005R) and the Moss Landing Marine Laboratory Turner Fluorometer (10-AU-005). Samples were analyzed from a MOBY Nov 96 cruise and a Gulf of California cruise (Mueller, Nov 96).

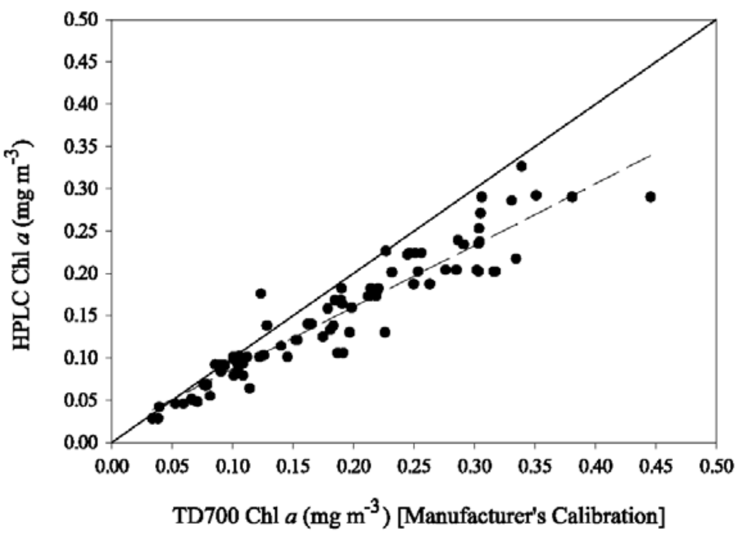

Figure 3.5. Comparison between chlorophyll a determined by the TD700 equation supplied by the manufacturer and that measured by HPLC methods.

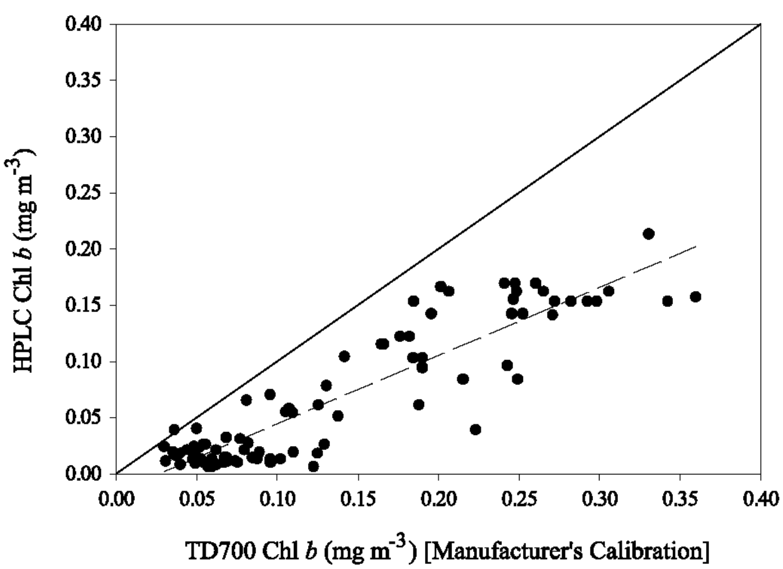

Figure 3.6: Same as Figure 3.5 for chlorophyll b.

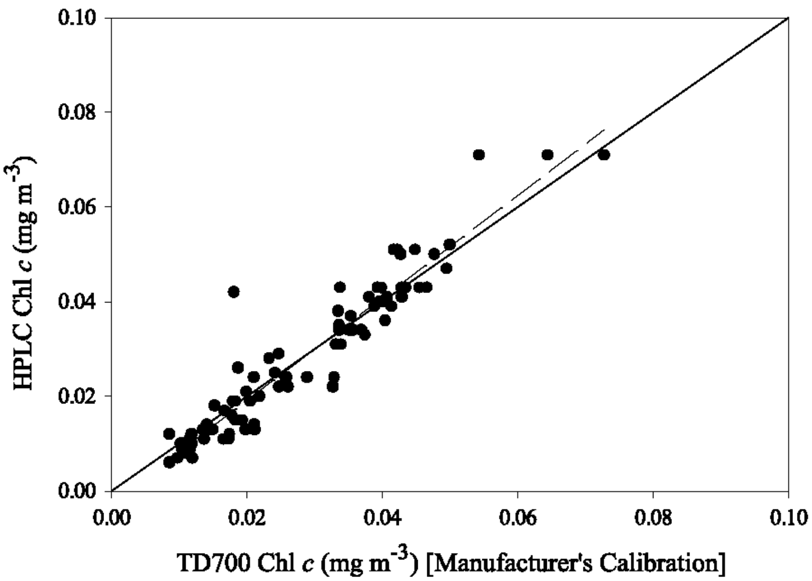

Figure 3.7: Same as Figure 3.5 for chlorophyll c.

REFERENCES

Bianchi, T. S., C. Lambert, and D. C. Biggs. 1995: Distribution of chlorophyll *a* and pheopigments in the northwestern Gulf of Mexico: a comparison between fluorometric and high-performance liquid chromatography measurements. *Bull. Mar. Science,* **56,** 25-32.

Brock, T.D., 1983: *Membrane filtration: a user's guide and reference manual.* Science Tech., Madison, WI, 381 pp.

Campbell, J.W. 1995: The lognormal distribution as a model for bio-optical variability in the sea. J. Geophys Res., **100**, 13237-13254.

Chavez, F., K.R. Buck, R.R. Bidigare, D.M. Karl, D. Hebel, M. Latasa, L. Campbell, and J. Newton, 1995: On the chlorophyll *a* retention properties of glass-fiber GF/F filters. *Limnol. Oceanogr.*, **40**, 428-433.

Clesceri, L.S., A.E. Greenberg and A.D. Eaton (eds), 1998a: Part 10000, Biological Examination, Section 10200 H. in Standard Methods for the Examination of Water and Wastewater. 20th ed. Baltimore (MD): American Public Health Association, American Water Works Association, Water Environment Federation.

Clesceri, L.S., A.E. Greenberg and A.D. Eaton (eds), 1998b: Part 10000, Biological Examination, Section 10200 **B**. in Standard Methods for the Examination of Water and Wastewater. 20th ed. Baltimore (MD): American Public Health Association, American Water Works Association, Water Environment Federation.

Dickson, M.-L., and P.A. Weeller, 1993: Chlorophyll *a* concentrations in the North Pacific: Does a latitudinal gradient exist? *Limnol. Oceanogr.*, **38**, 1813-1818.

Gordon, H.R., and D.K. Clark, 1980: Remote sensing optical properties of a stratified ocean: an improved interpretation. *Appl. Optics*, **19**, 3,428--3,430.

Hoepffner, N., and S. Sathyendranath. 1992: Bio-optical characteristics of coastal waters: absorption spectra of phytoplankton and pigment distribution in the western North Atlantic. *Limnol. Oceanogr.* **37:** 1660-1679.

Holm-Hansen, O., C.J. Lorenzen, R.W. Holmes, and J.D.H. Strickland, 1965: Fluorometric determination of chlorophyll. *J. du Cons. Intl. Pour l'Expl. de la Mer.,***30**, 3-15.

Jeffrey, S.W., R.F.C. Mantoura, and S.W. Wright (eds.), 1997: *Phytoplankton Pigments in Oceanography*, Monographs on Oceanographic Methodology, UNESCO, 661 pp.

Lorenzen, C.J. and S.W. Jeffrey. 1980: *Determination of Chlorophyll in Seawater.* UNESCO Technical Papers in Marine Science, Vol. **35**, UNESCO, 20 pp.

Phinney, D.A. and C.S. Yentsch, 1985: A novel phytoplankton chlorophyll technique: Toward automated analysis. *J. Plankton Res*., **7**, 633-642.

Richards, F.A. and T.G. Thompson. 1952: The estimation and characterization of plankton populations by pigment analysis. II. A spectrophotometric method for the estimation of plankton pigments. *J. Mar. Res*., **11**, 156-172.

Saijo, Y. and S. Nishizawa. 1969: Excitation spectra in the fluorometric determination of chlorophyll a and phaeophytin *a*. *Mar Biol,*. **2**, 135-136.

Smith, R. C., and K. S. Baker. 1978: The bio-optical state of ocean waters and remote sensing. *Limnol. Oceanogr*., **23**, 247-259.

Smith, R. C., R. R. Bidigare, B. B. Prezelin, K. S. Baker, and J. M. Brooks. 1987: Optical characterization of primary productivity across a coastal front. *Mar. Biol*. **96:** 575-591.

Strickland, J.D.H., and T.R. Parsons, 1972: *A Practical Handbook of Sea Water Analysis,* Fisheries Research Board of Canada, 310 pp.

Tester, P. A., M. E. Geesey, C. Guo, H. W. Paerl, and D. F. Millie, 1995: Evaluating phytoplankton dynamics in the Newport River estuary (North Caroline, USA) by HPLC-derived pigment profiles. *Mar. Ecol. Prog. Ser*. **124,** 237-245.

Trees, C.C., R.R. Bidigare, D.M. Karl and L. Van Heukelem, 2000a: Fluorometric chlorophyll a: sampling, laboratory methods, and data analysis protocols, Chapter 14 in: Fargion, G.S. and J.L. Mueller (Eds.) *Ocean Optics Protocols for Satellite Ocean Color Sensor Validation*. NASA/TM-2000-209966, NASA Goddard Space Flight Center, Greenbelt, MD. pp 162-169.

Trees, C.C., D.K. Clark, R.R. Bidigare, M.E. Ondrusek, and J.L. Mueller. 2000: Accessory pigments versus chlorophyll a concentrations within the euphotic zone: a ubiquitous relationship. *Limnol. Oceanogr.*, **45**(5): 1130-1143.

Trees, C.C., M.C. Kennicutt II, and J.M. Brooks, 1985: Errors associated with the standard fluorometric determination of chlorophylls and pheopigments. *Mar. Chem*., **17**, 1-12.

UNESCO, 1994: Protocols for the Joint Global Ocean Flux Study (JGOFS) Core Measurements, Manual and Guides 29, 170pp.

Vernet, M., and C. J. Lorenzen. 1987: The presence of chlorophyll b and the estimation of pheopigments in marine phytoplankton. J. Plankton Re*s.,* **9**, 255-265.

Yentsch, C.S., and D.W. Menzel, 1963: A method for the determination of phytoplankton, chlorophyll, and phaeophytin by fluorescence. *Deep-Sea Res.,* **10**, 221-231.

Appendix E

LI-1400 DataLogger PAR Measurements

Standard Operating Procedures

Overview

The LI-1400 DataLogger and calibrated quantum sensors provide the capability to quantify Photosynthetically Active Radiation (PAR) both above and below the water surface. The 'air' sensor remains above the water and quantifies downwelling radiance from the sun each time a discrete measurement is taken; this is most often used to normalize readings taken over several minutes to a constant downwelling value. The 'underwater' sensor is deployed on a frame that is lowered into the water. This sensor is generally used to measure a profile of in-water irradiance versus depth so as to estimate the diffuse attenuation coefficient (K_d), a measure of the rate at which photosynthetically active radiation is attenuated as it passes down through the water-column.

In general, the attenuation of light is exponential versus depth. To obtain K_d from a series of light readings with depth, a series of measurements at at least 8 depths is desired (in shallow waters this may not be possible). One obtains K_d by making a linear regression of sample depth versus ln (PAR) and calculating 1/(slope of the regression). Additional information of interest includes the percent of surface radiation reaching the bottom.

Estimates of K_d are considered robust if the r^2 of the regression is >0.95 (generally >0.98). The precision of the method is estimated by taking 3 complete profiles sequentially and calculating the standard error (SE) of the measurement. The SE should be less than 10%.

Before First Sampling of the Day

1. Insure that the sensors are securely attached to their frames and confirm that the calibrations factors stored in the DataLogger are correct for the sensors in use.
2. Hook up the Underwater BNC connector to Channel I1 labeled "underwater".
3. Hook up the Air BNC connector to Channel I2 labeled "air".
4. Turn the DataLogger 'ON'.
5. Under View, press 'ENTER' to view new data.
6. The first view should say "I1I" which corresponds to the underwater connector. "I2I" corresponds to the air connector.
7. Switch to view I2I, take the cap off of the air sensor, check the reading then cover the sensor with your hand to confirm the reading changes (the reading should decrease with a decrease in light).
8. Switch to view I1I, take the protective covering off of the underwater sensor, check the reading and then cover the sensor with your hand to confirm the reading changes (again the reading should decrease).

At Each Station

1. Turn on the DataLogger.
2. Take out the respective data sheet for the site. Record the time when the underwater sensor is put in the water.
3. Lower the sensor to 10cm. Allow the reading to stabilize (1-2 seconds) and then press 'ENTER'. This logs the data into the DataLogger. Cross off 10cm (and each subsequent depth for which you log data into the DataLogger) on the data sheet.
4. Lower the sensor to the next depth. In shallow areas, record measurements every 25cm as marked on the cable. In deep and/or clearer water areas the sensor can be lowered every 50cm. At least 6-8 depths should be recorded in the DataLogger for each station.
5. When (If) the sensor reaches bottom, write the bottom depth (approximate using the depth markers) on the datasheet and press 'ENTER' to log data into the DataLogger. You do not need to go to the bottom if you have >10 good readings; if the DataLogger is showing light readings less than 0.5 or if the sensor begins to stream out in strong currents.
6. Raise the underwater sensor out of the water and put the protective cover on. Put the cap on the air sensor also. Turn the DataLogger 'OFF' until reaching the next station.

At End of Sampling

1. Unplug the BNC connectors from the LI-1400.
2. Rinse underwater sensor, frame and cable with freshwater and let dry before storage.

Download Data to Excel in the Laboratory

1. After returning to the lab the data should be retrieved from the DataLogger.
2. Attach the DataLogger to the computer using the serial cable.
3. Open the LI-1400 program and then turn the DataLogger on.
4. Under the remote menu click on 'CONNECT'. Under the connect window, type '2' next to com port number and click 'CONNECT'.
5. Under the remote menu click 'RECEIVE DATA'. Save the data on the computer.
6. Open Microsoft Excel and then open the file you just saved. The file is a delimited file and click 'FINISH'.
7. Download LiCor Data into a new Excel file and **Save As** GBSWMP Raw Light Profile (MMDDYY) where the MMDDYY represents the sampling date.
8. Once you are certain that you have successfully downloaded and saved the data the data in the DataLogger should be cleared from memory. This can be done 2 ways:
    a. On the DataLogger, press the 'FCT' key. Arrow to the right twice till clear memory is in the window. Arrow down to clear all, down to date, down to time, and down to clear memory yes/no. Confirm that "clear memory yes" is in the window and then press 'ENTER'. (This may not clear the memory).
    b. In the LI-1400 program, under the remote menu click 'CLEAR DATABASE'. In the clear database window confirm that all is chosen then click 'OK'.

9. Under the remote menu click 'DISCONNECT'. Unplug the DataLogger from the computer, turn it off, make sure that there is no dirt or salt on it and put it away.

Data Processing

1. **Open** _GBSWMP Light Profile Master_ Excel File and **Save As** _GBSWMP Light Attenuation (MMDDYY)_

2. Cut and paste the raw light data into the appropriate rows/columns in the _GBSWMP Light Attenuation (MMDDYY)_ file making sure to separate each station as indicated by the station labels in column A.

3. Edit the depths Column E so that they reflect the correct depths at which each of the readings at a particular station was taken.

4. Run individual regression analyses for each of the light profiles as follows (using APL as an example):

   a. Click on **Tools**, **Data Analysis**, **Regression**
   b. Select 'Input Y Range' as the range of measured Depth [m] in Column E
   c. Select 'Input X Range' as the range of calculated Quantum [LN] in Column H
   d. Select 'Output Range' as the Yellow Shaded Block in Column J
   e. Select 'OK'; this should insert the regression statistics to the right of the data [Note: Do not include data for which the Quantum [Raw Water] data is < 0.1]
   f. Save File (intermediate save so as to not lose data)

5. At this point, the Diffuse Attenuation Coefficients ($\mathbf{K_d}$) should have been calculated for each station at which you did the regression. $\mathbf{K_d}$ = 1/x-coefficient from the regression. For Great Bay, values of $\mathbf{K_d}$ should range from -0.5 (clear) to -6.0 (very turbid).

6. QA/QC: Examine the regression output data:

   a. Acceptable regressions must have an $R^2 > 0.95$ and, for stations with an optimal number of sample depths (>8) should have an $R^2 > 0.98$.
   b. Examine the Quantum [Raw Water] data. These data should show a continuous decrease with depth except for the odd cases where the Quantum [Air] data increased significantly from the preceding reading (e.g. the passing of a cloud). Highlight any questionable reading by applying an 'Orange' fill to the cells in question.

7. In the event that the $R^2 < 0.95$ and there is a data point at the top or bottom of the profile that is clearly bad (these are the most likely places for this to occur because of surface reflection or sediment resuspension) you may choose to run the regression again omitting the suspect data. In such cases it is imperative that you make a notation in Column I, just below the $\mathbf{K_d}$ calculation block.

Appendix F

Standard Operating Procedure for EPA Water Quality Project

1. Navigate to station (use attached maps) and note station, date, time, location and water depth below.

2. Measure water temperature, salinity and PAR and record on field sheet below

3. Sample collection: Plunge inverted bottle below surface at approximately 0.5 m. Care must be taken to avoid sampling the very surface layer. Right sample bottle underwater and allow bottle to partially fill and cap underwater. Remove from water, shake and empty. Repeat for three rinses total. Completely fill bottle with same protocol above.

4. Store on ice in dark until delivered to processing team at JEL.

Contact cell numbers:	Ru Morrison	603 957 0998
	Tom Gregory	808 294 0265
	Mike Novak	603 828 5240

Your Name and affiliation: ____

Station	Date	Time (local)	Lat	Lon	Temp (°C)	Salinity (psu)	Water Depth / Comments

PAR Measurements

Station: ______________________ Start Time (local) : __________ End Time : ___________

Depth (m)	Surface PAR (units:__________________)	PAR at depth (units:__________________)

Station: ______________________ Start Time (local) : __________ End Time : ___________

Depth (m)	Surface PAR (units:__________________)	PAR at depth (units:__________________)

Station: ______________________ Start Time (local) : __________ End Time : ___________

Depth (m)	Surface PAR (units:__________________)	PAR at depth (units:__________________)

Station: ______________________ Start Time (local) : ___________ End Time : ____________

Depth (m)	Surface PAR (units:__________________)	PAR at depth (units:__________________)

Station: ______________________ Start Time (local) : ___________ End Time : ____________

Depth (m)	Surface PAR (units:__________________)	PAR at depth (units:__________________)

Station: ______________________ Start Time (local) : ___________ End Time : ____________

Depth (m)	Surface PAR (units:__________________)	PAR at depth (units:__________________)

Additional Comments:

USING MOORED ARRAYS AND HYPERSPECTRAL AERIAL IMAGERY TO DEVELOP NUTRIENT CRITERIA FOR NEW HAMPSHIRE'S ESTUARIES

Quality Assurance Project Plan Addendum

Purpose: The New Hampshire Estuaries Project collected hyperspectral imagery and water quality data from the Great Bay Estuary in 2007. Data were collected under the referenced approved QAPP. After the data were collected, the NHEP and other researchers at the University of New Hampshire received funding from EPA to conduct additional analyses with the hyperspectral imagery data. No new data will be collected for this project. The purpose of this addendum to the original QAPP is to document the additional analyses that will be conducted using the hyperspectral imagery data.

Project Description

A. General Summary Statement of Project Goal & Justification

Increasing nitrogen concentrations (Figure 1) and declining eelgrass beds in Great Bay (Figure 2) are clear indicators of impending problems for NH's estuaries (NHEP, 2006). The NH Department of Environmental Services (DES) is responsible for developing nutrient criteria for NH's estuaries. DES, in collaboration with the New Hampshire Estuaries Project (NHEP), began this process with the formation of a workgroup in 2005. The NHEP Coastal Scientist, a DES employee, is coordinating the work to undertake this process, with input from the workgroup. Information from the workgroup meetings is available at www.nhep.unh.edu/programs/nutrient.htm. This workgroup adopted eelgrass survival as the water quality target for nutrient criteria development for NH's estuaries.

In 2007, the New Hampshire Estuaries Project (NHEP) received a 104(b)(3) grant from the U.S. Environmental Protection Agency to collect water quality information including that from hyper-spectral imagery data of the Great Bay Estuary (EPA Grant Award X7-97167001). The expected outcome of this research will support the development of numeric nutrient criteria for NH's estuaries. The NHEP has successfully collected the data and will prepare the final report by the deadline of June 30, 2008. Recommendations for numeric nutrient criteria are planned for December 31, 2008.

Preliminary analysis of the data revealed an opportunity to contribute to the development numeric nutrient criteria. Analysis of the data showed that phytoplankton, as measured by suspended chlorophyll-*a*, only accounts for 8% of the light attenuation in the estuary. This finding does not support a hypothesis that nitrogen enrichment is causing phytoplankton blooms which reduce water clarity to any great degree. Therefore, the NHEP is proposing research to test the hypothesis that, alternatively, the eutrophication response to nutrient increases in the Great Bay has been the proliferation of nuisance macroalgae, which has reduced the amount of area where eelgrass can reestablish from seed (i.e., the potential eelgrass habitat). The hyper-

spectral imagery collected in August and October 2007 will be used to map eelgrass and nuisance macroalgae throughout the estuary. The distribution of nuisance macroalgae will be compared to areas where historic eelgrass beds have been lost to determine whether nuisance macroalgae correlates with eelgrass loss in the Great Bay Estuary. The research outputs will contribute to the development of numeric nutrient criteria for NH's estuaries. The research will benefit other states in New England because eutrophication responses in Great Bay can be used as a model for other northern, macrotidal estuaries.

Figure 1: Dissolved inorganic nitrogen concentrations in Great Bay (NHEP, 2006)

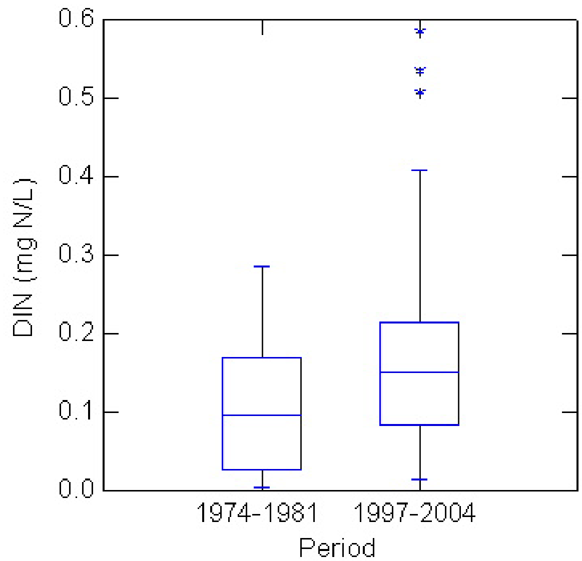

Figure 2: Eelgrass cover and biomass in Great Bay (NHEP, 2006)

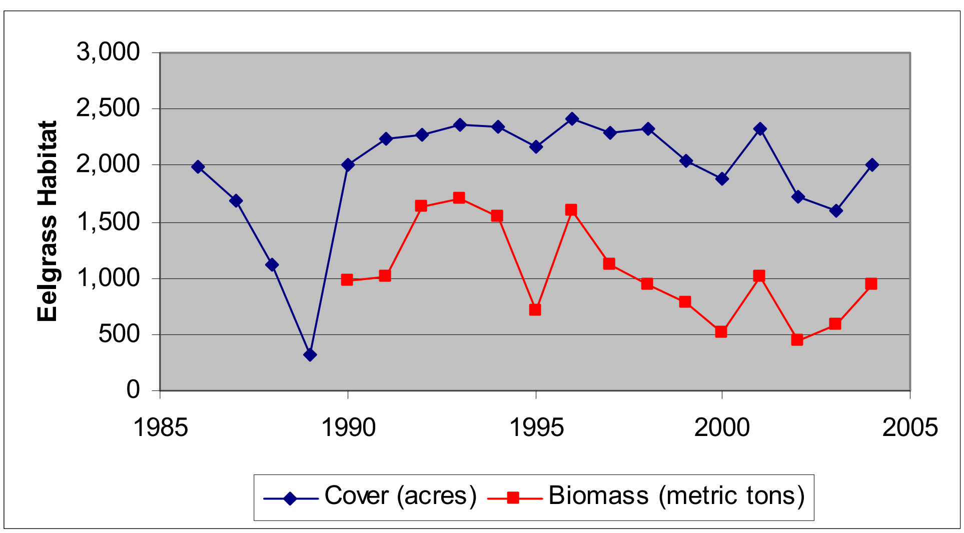

B. Project Description

Who: The project will be completed by the NHEP, researchers at the University of New Hampshire (UNH), and the NH Department of Environmental Services (DES). The NHEP is part of EPA's National Estuary Program, and is coordinating the nutrient criteria development process through its Technical Advisory Committee. The NHEP's latest "State of the Estuaries" report highlighted declines in eelgrass beds and increases in nitrogen concentrations in Great Bay. The NHEP Director will manage the funds and will assign staff and committee meeting time to this project. The NHEP will coordinate with UNH researchers from the Center for Coastal and Ocean Mapping (CCOM), Coastal Ocean Observing Center (COOC), and the Jackson Estuarine Laboratory (JEL) to conduct the technical tasks of the project. The results of the project will be integrated into the nutrient criteria development process and ultimately provided to DES, which is responsible for developing nutrient criteria in NH's estuaries.

The project team will be:
Jennifer Hunter (NHEP) – Project/grant manager
Shachak Peeri, Ph.D. (UNH/CCOM) – Analysis of hyper-spectral imagery
Ru Morrison, Ph.D. (UNH/COOC) – Optical properties measurements
Arthur Mathieson, Ph.D. (UNH/JEL) – Macroalgae species and distribution
Fred Short, Ph.D. (UNH/JEL) – Eelgrass distribution and estuarine ecology
Phil Trowbridge, P.E. (NHEP/DES) – Data synthesis and nutrient criteria development

What: Maps of eelgrass and nuisance macroalgae cover in the Great Bay Estuary from hyper-spectral imagery collected in August 2007 and October 2007. Nuisance macroalgal cover (multiple *Ulva* species, *Gracilaria* [e.g. *G. tikvahiae*], epiphytic red algae [e.g., ceramialean red algae] and detached/entangled *Chaetomorpha* populations) has not been quantified throughout the estuary using a standard, synoptic method. The hyper-spectral imagery collected in August 2007 and October 2007 provides an opportunity to map the nuisance macroalgae and eelgrass cover in the estuary using standardized methods. GIS software will be used to summarize the total coverage of eelgrass and the different species of nuisance macroalgae in different zones of the estuary. The results will be compared to maps of areas where historic eelgrass beds have been lost to determine whether nuisance macroalgae correlates with eelgrass loss in the Great Bay Estuary. The data will also be useful to compare the dominant macroalgae species in the Great Bay, which has large intertidal areas, and the lower estuary, which does not.

Where: The project will be completed in the Great Bay Estuary system of NH and Maine (Figure 3). The hyper-spectral imagery covers most of the Great Bay Estuary: Great Bay, Little Bay, Upper Piscataqua River, Lower Piscataqua River (to the I-95 bridge), Salmon Falls River, Cocheco River, Bellamy River, Oyster River, Lamprey River, Squamscott River, and the Winnicut River. The area covered by the hyper-spectral imagery is approximately 200 square kilometers.

Figure 3: The Great Bay Estuary

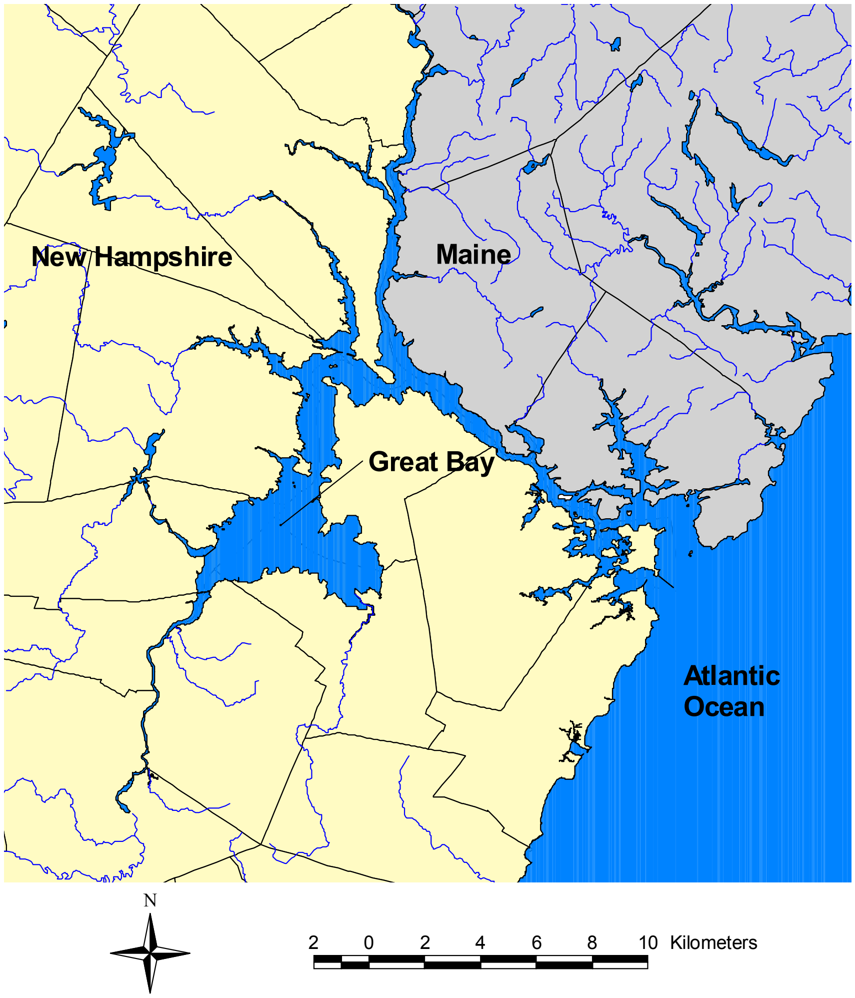

When: Project will commence on July 1, 2008; and will end by December 31, 2008. DES has set a deadline of December 31, 2008 for delivering recommendations to the Water Quality Standards Advisory Committee on the formulation of numeric nutrient criteria for NH's estuaries. Information on impairments of eelgrass beds due to nuisance macroalgae must be provided before this deadline. Therefore, the summary report for the project will be due by September 30, 2008. Deliverables related to presentations, data management, and outreach will be completed between October 1, 2008 and December 31, 2008.

Why: Nitrogen concentration in Great Bay have increased by 59% in the past 25 years (NHEP, 2006). Since the 1940s, 29% of the historic eelgrass cover has been lost. Nitrogen loading rates in Great Bay (182 kg/ha/yr) are higher than estuaries for which dramatic eelgrass loss has occurred (>60 kg/ha/yr) (Hauxwell et al., 2003). However, observations by the UNH Ocean Observing Center in 2007 show that phytoplankton only accounts for 8% of the total light attenuation in the bay. While there is evidence for nitrogen enrichment in the estuary, the expected response of high phytoplankton blooms has not been observed due to the light-limited water column environment caused by suspended sediments and rapid water column mixing.

Thus, the contribution of phytoplankton blooms to decreased water clarity is unexpectedly low. Instead, eelgrass takes up a large portion of nitrogen from the water column in Great Bay, but as nitrogen levels have risen, researchers have observed a proliferation of green and red nuisance macroalgae. Macroalgae can eliminate potential eelgrass habitat when it forms dense mats on the sediment (Short and Burdick 1996), but evidence of this interaction is limited to the upper intertidal areas of Great Bay. The hypothesis of this research is that the eutrophication response in the Great Bay has been the proliferation of nuisance macroalgae, which has reduced the amount of area where eelgrass can reestablish from seed (i.e., the potential eelgrass habitat).

How: The NHEP (with EPA funding) obtained high-quality hyper-spectral imagery of the Great Bay Estuary at low tide in August 2007 and October 2007 (Figure 4). The imagery consisted of radiance, reflectance, and georeference in 64 spectral bands between 390 nm and 950 nm with a 2.5 m resolution. The delivered data was provided in ENVI readable format, which will be the main processing software for this study. ENVI (the Environment for Visualizing Images) is an image processing software package. ENVI provides comprehensive data visualization and analysis for multiband and hyperspectral data imagery.

UNH will use remote sensing techniques to isolate eelgrass and green and red macroalgal areas in the estuary. The remote sensing sub-tasks are described below:

- Endmember collection- A spectrum representing a spectrally "pure" feature (e.g, vegetation, soil, etc.) is defined as a spectral endmember. Following the review of field observations from 2007 and *in situ* measurements, candidate locations will be identified in the hyperspectral imagery and endmember will be created of the macroalgae areas and of bottoms without macroalgae present (pure background). Macroalgal does not remain permanent in one location and does not usually create a dense bed representing just one species macroalgae, like eelgrass beds. Therefore, UNH will use the regions with most dense macroalgal patches as the best available endmember that can be produced (purest feature available).
- Endmember analysis- The endmembers collected will be analyzed according to macroalgal type and bottom mineral type. Distinct features along the specra will be used in order to discriminate between the different endmembers.
- Classification- Following the characteristics of the different endmembers a classification technique will be chosen and applied to the data. The product will be a thematic map that each class will represent a macroalgal density.
- Data export- The classification results will be exported to a vector format that is compliant with the GIS environment (shapfile polygons).

A similar project was able to map macroalgae species in the Venice Lagoon (Alberotanza et al., 2006).

No human subjects or research animals will be used for this study.

Figure 4: Area of hyperspectral imagery collection

C. Deliverables and Schedule

1. Summary Report – due 9/30/08
The summary report will contain methods, results, maps, and interpretation. Specifically, the report will contain the following items.

a) Maps of eelgrass and nuisance macroalgae (multiple *Ulva* species, *Gracilaria* [e.g. *G. tikvahiae*], epiphytic red algae [e.g., ceramialean red algae] and detached/entangled

Chaetomorpha populations) in Great Bay, Little Bay, Piscataqua River and contiguous tidal tributaries in August 2007 and October 2007;
b) Calculations of the total cover of eelgrass and the different species of nuisance macroalgae in the NHEP eelgrass assessment zones (e.g., Great Bay, Little Bay, Oyster River, etc.) in August 2007 and October 2007;
c) Maps showing the distribution of nuisance macroalgae in August 2007 and October 2007 compared to the areas where eelgrass has been lost relative to baseline conditions from the Great Bay Estuarine Restoration Compendium (1949-1981);
d) Calculations of the how much of the area of former eelgrass beds was covered by nuisance macroalgae in August 2007 and October 2007.

2. Transfer of GIS files to New Hampshire GRANIT Repository – due 12/31/08
GIS files of eelgrass and nuisance macroalgae distributions will be converted to ESRI shapefiles with FGDC metadata. The files will be transferred to the New Hampshire GRANIT repository at UNH, from which they will be made available to the public.

3. Presentations on results to NH nutrient criteria work group – due by 12/31/08
Progress on the project will be presented to the NHEP Technical Advisory Committee at a meeting in the fall of 2008.

<u>E. Cost</u>
The total cost of the project will be $14,798. An itemized budget is attached.

References

Alberotanza L et al. 2006. Classification of submerged aquatic vegetation of the Venice lagoon using MIVIS airborne data. *Annals of Geophysics*, **49**(1): 271-276.

Hauxwell et al. 2003. Eelgrass *Zostera marina* loss in temperate estuaries: relationship to land-derived nitrogen loads and effect of light limitation imposed by algae. *Marine Ecology Progress Series*, **247**: 59-73.

NHEP. 2004. Monitoring Plan. New Hampshire Estuaries Project, University of New Hampshire, Durham, NH. June 30, 2004. Available at: www.nhep.unh.edu/resources/pdf/nhepmonitoringplan-nhep-04.pdf

NHEP. 2006. State of the Estuaries. New Hampshire Estuaries Project, University of New Hampshire, Durham, NH. Available at www.nhep.unh.edu.

Short FT and Burdick DM. 1996. Quantifying eelgrass habitat loss in relation to housing development and nitrogen loading in Waquoit Bay, Massachusetts. *Estuaries*, **19**:730-739.